

Bulletin 43
(Part 1 of 4 Parts)

THE SHOCK AND VIBRATION BULLETIN

Part 1
Invited Papers, Submarine Shock Testing,
Shock Analysis, Shock Testing

JUNE 1973

A Publication of
THE SHOCK AND VIBRATION
INFORMATION CENTER
Naval Research Laboratory, Washington, D.C.



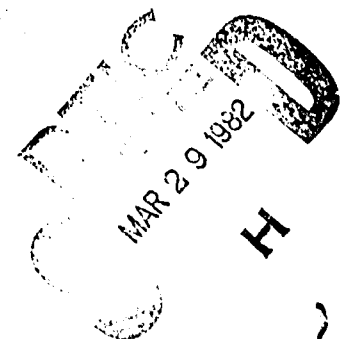
Office of
The Director of Defense
Research and Engineering

This document has been approved for public release and sale; its distribution is unlimited.

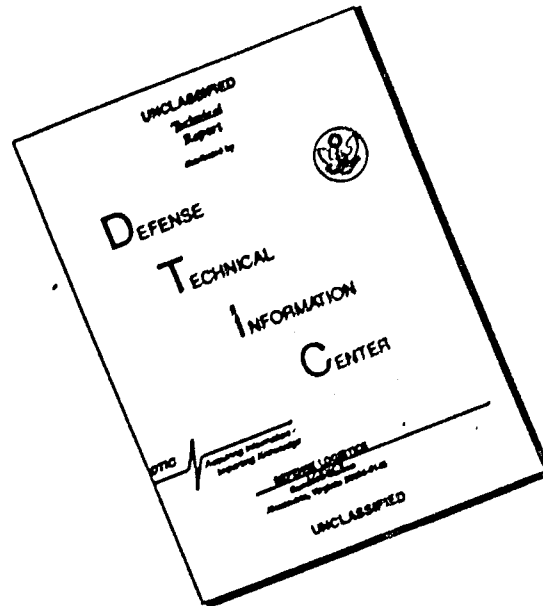
82 03 26 008

ADA 112527

DTIC FILE COPY



DISCLAIMER NOTICE



THIS DOCUMENT IS BEST QUALITY AVAILABLE. THE COPY FURNISHED TO DTIC CONTAINED A SIGNIFICANT NUMBER OF PAGES WHICH DO NOT REPRODUCE LEGIBLY.

SYMPOSIUM MANAGEMENT

THE SHOCK AND VIBRATION INFORMATION CENTER

Robert O. Belsheim, Director
Henry C. Pusey, Coordinator
Edward H. Schell, Coordinator
Rudolph H. Volin, Coordinator

Bulletin Production

Graphic Arts Branch, Technical Information Division,
Naval Research Laboratory

Bulletin 43
(Part 1 of 4 Parts)

THE SHOCK AND VIBRATION BULLETIN

JUNE 1973

A Publication of
THE SHOCK AND VIBRATION
INFORMATION CENTER
Naval Research Laboratory, Washington, D.C.

The 43rd Symposium on Shock and Vibration was held at the Asilomar Conference Grounds, Pacific Grove, California, on 5-7 December 1972. The U.S. Army, Fort Ord, was host.

Office of
The Director of Defense
Research and Engineering

DISTRIBUTION STATEMENT A
Approved for public release;
Distribution Unlimited

CONTENTS

PAPERS APPEARING IN PART I

REMARKS	1
Dr. Elias Klein, ret., Sarasota, Florida	

Invited Papers

A QUARTER CENTURY OF PROGRESS	3
Mr. Dwight C. Kennard, Consultant, Traverse City, Michigan	
FORMER SHOCK	9
Dr. Donald E. Marlowe, Vice President for Administration, Catholic University, Washington, D. C.	
THE ARMY'S BIG FIVE AND RDTE PROGRAM THRUSTS.	13
Major General John R. Guthrie, Deputy Commanding General for Materiel Acquisition, Army Materiel Command Headquarters, Washington, D. C.	

Submarine Shock Testing

UNDERWATER EXPLOSION TESTS WITH THE SWEDISH FULL-SCALE TEST SECTION "STÅLMYGGAN". PART I: TEST SECTION WITH OBJECTS AND MEASURING POINTS, ARRANGEMENTS AND DIMENSIONAL MEASUREMENTS.	19
H. Nilsson, Kockums Mekaniska Verkstads AB, Naval Department, Malmö, Sweden	
UNDERWATER EXPLOSION TESTS WITH THE SWEDISH FULL-SCALE SUBMARINE TEST SECTION "STÅLMYGGAN": RECORDING AND DATA REDUCTION SYSTEM	31
L. Westin and A. Henningson, Military Electronics Laboratory, Stockholm, Sweden	
UNDERWATER EXPLOSION TEST WITH THE SWEDISH FULL SCALE SUBMARINE TEST SECTION "STÅLMYGGAN": PART III. INTERPRETATION OF RESULTS OF SHOCK MEASUREMENTS,	43
K. Spång, IFM-AKUSTIKBYRÅN AB, Stockholm, Sweden	

Shock Analysis

SHOCK ANALYSIS ERRORS IN THE PRESENCE OF VIBRATION	55
C. T. Morrow, Advanced Technology Center, Inc., Dallas, Texas	
APPROXIMATE RESPONSE SPECTRA OF DECAYING SINUSOIDS	61
A. E. Galef, TRW Systems, Inc., Redondo Beach, California	
STEADY-STATE MOTIONS OF ORBITAL CABLE PLOWS,	67
M. Senator and L. J. Scerbö, Bell Laboratories, Whippany, New Jersey	

TRANSIENT MOTIONS OF ORBITAL CABLE PLOWS.	83
L. J. Scerbo and M. Senator, Bell Laboratories, Whippany, New Jersey	
SHOCK WAVE INDUCED TRANSIENT PRESSURE ENVIRONMENT ABOUT THE SPRINT II MISSILE CAUSED BY LAUNCH CELL EJECTION.	95
A. J. Culotta, Martin Marietta Aerospace Corporation, Orlando, Florida	

Shock Testing

DIGITAL CONTROL TECHNIQUE FOR SEISMIC SIMULATION.	109
G. C. Kao, K. Y. Chang, and W. W. Holbrook, Wyle Laboratories, Huntsville, Alabama	
PYROTECHNIC SHOCK SIMULATION USING THE RESPONSE PLATE APPROACH.	119
C. L. Thomas, Honeywell Inc., Aerospace Division, St. Petersburg, Florida	
TEST METHOD TO QUALIFY ELECTRONIC COMPONENTS IN SHOCK AND SUSTAINED ACCELERATIONS.	127
R. K. Melzer, Sperry Univac, St. Paul, Minnesota	
THE USE OF SHAKER-OPTIMIZED PERIODIC TRANSIENTS IN MATCHING FIELD SHOCK SPECTRA.	139
D. O. Smallwood, Sandia Laboratories, Albuquerque, New Mexico and A. F. Witte, Kaman Sciences, Colorado Springs, Colorado	
A TRANSIENT VIBRATION TEST TECHNIQUE USING LEAST FAVORABLE RESPONSES.	151
D. O. Smallwood, Sandia Laboratories, Albuquerque, New Mexico	

PAPERS APPEARING IN PART 2

Structural Analysis

APPROXIMATE METHOD FOR CALCULATING THE RESPONSE OF EMPLACEMENT STRUCTURES SUBJECTED TO GROUND SHOCK FROM UNDERGROUND NUCLEAR DETONATIONS
M. Hartzman, University of California, Lawrence Livermore Laboratory, Livermore, California
VIBRATION ANALYSIS OF STRUCTURAL SYSTEMS USING VIRTUAL SUBSTRUCTURES
A. Berman, Kaman Aerospace Corporation, Bloomfield, Connecticut
MULTI-DEGREE-OF-FREEDOM ELASTIC SYSTEMS HAVING MULTIPLE CLEARANCES
R. C. Winfrey, Burroughs Corporation, Westlake Village, California
RESPONSE BOUNDS FOR STRUCTURES WITH INCOMPLETELY PRESCRIBED LOADING
W. D. Pilkey, University of Virginia, Charlottesville, Virginia and A. J. Kalinowski, IIT Research Institute, Chicago, Illinois
NONLINEAR VIBRATIONS OF MULTILAYER SANDWICH PLATES
R. M. Shahin, Gibbs & Hill, Inc., New York, New York
A DIGITAL COMPUTER PROGRAM FOR AIRCRAFT RUNWAY ROUGHNESS STUDIES
T. G. Gerardi and A. K. Lohwasser, Air Force Flight Dynamics Laboratory, Wright-Patterson AFB, Ohio
AN ALGORITHM FOR SEMI-INVERSE ANALYSIS OF NONLINEAR DYNAMIC SYSTEMS
R. L. Eshleman and T. M. Scopelite, IIT Research Institute, Chicago, Illinois

GUNFIRE-INDUCED VIBRATION ON THE A-7E AIRPLANE
T. W. Elliott, Naval Missile Center, Point Mugu, California

APPLICATIONS OF STRAIN GAGES TO BALLISTIC PROBLEMS
P. D. Flynn, Frankford Arsenal, Philadelphia, Pennsylvania

STRESS WAVE MEASUREMENT TECHNIQUE
A. J. Kalinowski, IIT Research Institute, Chicago, Illinois

Design Techniques

MAXIMIZATION AND MINIMIZATION OF DYNAMIC LOAD FACTORS
G. J. O'Hara, Naval Research Laboratory, Washington, D. C.

THE REDUCTION OF HELICOPTER VIBRATION AND NOISE PROBLEMS BY THE
ELIMINATION OF THE BLADE TIP VORTEX
R. P. White, Jr., Rochester Applied Science Associates, Inc., Rochester, New York

MATHEMATICAL MODEL OF A TYPICAL FLOATING SHOCK PLATFORM SUBJECTED TO
UNDERWATER EXPLOSIONS
R. P. Brooks and B. C. McNaught, Naval Air Engineering Center,
Philadelphia, Pennsylvania

EXCITATION, RESPONSE, AND FATIGUE LIFE ESTIMATION FOR STRUCTURAL
DESIGN OF EXTERNALLY BLOWN FLAPS
E. E. Ungar, Bolt, Beranek and Newman, Inc., Cambridge, Massachusetts

DETUNING AS A MECHANICAL DESIGN APPROACH
C. T. Morrow, Advanced Technology Center, Inc., Dallas, Texas

EARTHQUAKE RESPONSE OF SHOCK-MOUNTED COMMUNICATIONS EQUIPMENT
N. J. DeCapua, G. Nevrucean and E. F. Witt, Bell Laboratories, Whippany, New Jersey

THE REDUCTION OF IMPACT INDUCED PRESSURES IN FUEL TANKS
P. J. Torvik and J. W. Clark, Air Force Institute of Technology,
Wright-Patterson AFB, Ohio

A TREATMENT OF A NON-STATIONARY RANDOM PROCESS - LOAD TRANSFER AT SEA
H. S. Zwibel and D. A. Davis, Naval Civil Engineering Laboratory, Port Hueneme,
California

CRITERIA DEVELOPMENT OF JK-1 AND JK-2 CARGO RESTRAINT SYSTEMS
R. Kennedy, MTMTS-Army Transportation Engineering Agency, Newport News,
Virginia

PAPERS APPEARING IN PART 3

Skylab

SKYLAB VIBROACOUSTIC TESTING - AN OVERVIEW
G. M. Mosely, Teledyne-Brown Engineering, Huntsville, Alabama

SKYLAB VIBRATION AND ACOUSTIC STRUCTURAL TEST SYSTEMS
J. D. Johnston, Jr., NASA, Manned Spacecraft Center, Houston, Texas and
D. L. Knittle, Northrop Services Inc., Houston, Texas

ORBITAL WORKSHOP VIBROACOUSTIC TEST PROGRAM

W. H. Keller and E. Yoshida, McDonnell Douglas Astronautics Company,
Huntington Beach, California

SKYLAB PAYLOAD ASSEMBLY - VIBROACOUSTIC TEST PROGRAM

P. Rader, Martin Marietta Corporation, Denver, Colorado and J. Macpherson,
Marshall Space Flight Center, Huntsville, Alabama

**DEVELOPMENT OF AN AUTOMATIC MODAL TUNING AND ANALYSIS SYSTEM FOR
PERFORMING SKYLAB MODAL SURVEYS**

R. A. Salyer, TRW Systems, Redondo Beach, California, E. J. Jung, Jr., NASA,
Manned Spacecraft Center, Houston, Texas, S. L. Huggins and B. L. Stephens,
Northrop Services, Inc., Houston, Texas

SKYLAB MODAL SURVEY TESTING

J. J. Nichols, NASA Marshall Space Flight Center, Huntsville, Alabama, R. E. Hull
and B. I. Bejmuk, Martin Marietta Corporation, Denver, Colorado

**USE OF GENERALIZED MASS CONTRIBUTIONS IN CORRELATION OF TEST AND
ANALYTICAL VIBRATION MODES**

R. E. Hull and B. I. Bejmuk, Martin Marietta Corporation, Denver, Colorado and
J. J. Nichols, NASA, Marshall Space Flight Center, Huntsville, Alabama

**VIBRATION AND ACOUSTIC TESTS OF THE RECONFIGURED APOLLO SERVICE
MODULE ADAPTED FOR SKYLAB MISSIONS**

R. A. Colonna, NASA, Manned Spacecraft Center, Houston, Texas, D. E. Newbrough,
General Electric Company, Houston, Texas and J. R. West, Jr., North American
Rockwell Corporation, Downey, California

Vibration Testing and Analysis

**THE EFFECTIVENESS OF ENVIRONMENT ACCEPTANCE TESTING ON THE APOLLO
SPACECRAFT PROGRAM**

R. W. Peverley, The Boeing Company, Houston, Texas

ON THE DEVELOPMENT OF PASSENGER VIBRATION RIDE ACCEPTANCE CRITERIA

S. A. Clevenson and J. D. Leatherwood, NASA Langley Research Center,
Hampton, Virginia

CAPTIVE FLIGHT ACOUSTIC TEST CRITERIA FOR AIRCRAFT STORES

A. H. Burkhard, Air Force Flight Dynamics Laboratory, Wright-Patterson AFB, Ohio

**AIRCRAFT EQUIPMENT RANDOM VIBRATION TEST CRITERIA BASED ON VIBRATIONS
INDUCED BY TURBULENT AIRFLOW ACROSS AIRCRAFT EXTERNAL SURFACES**

J. F. Dreher, Air Force Flight Dynamics Laboratory, Wright-Patterson AFB, Ohio

**AIRCRAFT EQUIPMENT RANDOM VIBRATION TEST CRITERIA BASED ON VIBRATION
INDUCED BY JET AND FAN ENGINE EXHAUST NOISE**

J. H. Wafford, Aeronautical Systems Division, and J. F. Dreher, Air Force Flight
Dynamics Laboratory, Wright-Patterson AFB, Ohio

THEORETICAL AND PRACTICAL ASPECTS OF MULTIPLE-ACTUATOR SHAKER CONTROL

D. K. Fisher, University of California, Lawrence Livermore Laboratory,
Livermore, California

**GROUND VIBRATION SURVEY AS A MEANS OF ELIMINATING POTENTIAL IN-FLIGHT
COMPONENT FAILURES**

J. A. Hutchinson and R. N. Hancock, Vought Aeronautics Company, Dallas, Texas

PROBABILITY DENSITY FUNCTIONS OF MEASURED DATA

R. G. Merkle and R. E. Thaller, Air Force Flight Dynamics Laboratory, Wright-Patterson AFB, Ohio

PAPERS APPEARING IN PART 4

Prediction and Experimental Techniques

A SIMPLIFIED NONLINEAR METHOD FOR ESTIMATING THE FATIGUE LIFE OF ACOUSTICALLY EXCITED PANELS

M. B. McGrath, P. J. Jones and S. R. Tomer, Martin Marietta Corporation, Denver, Colorado

STUDIES ON THE DYNAMIC IMPACT OF JET ENGINE BLADES

C. T. Sun, Iowa State University, Ames, Iowa, and R. L. Sierakowski, Air Force Materials Laboratory, Wright-Patterson AFB, Ohio

A TIME DOMAIN MODAL VIBRATION TEST TECHNIQUE

S. R. Ibrahim and E. C. Mikulcik, University of Calgary, Calgary, Alberta, Canada

NATURAL FREQUENCIES AND DAMPING OF FULL-SCALE HYDROFOILS BY "PLUCK TEST" METHODS

J. R. Peoples, Naval Ship Research and Development Center, Bethesda, Maryland

ON THE THEORY AND PRACTICE OF STRUCTURAL RESONANCE TESTING

C. C. Ni, Naval Research Laboratory, Washington, D. C.

ELEVATION OF GRANULAR MATERIAL BY VIBRATION

M. Paz and Vicharn Vivekaphirat, University of Louisville, Louisville, Kentucky

Isolation and Damping

GROUND TESTS OF AN ACTIVE VIBRATION ISOLATION SYSTEM FOR A FULL-SCALE HELICOPTER

B. R. Hanks and W. J. Snyder, NASA, Langley Research Center, Hampton, Virginia

A FULL-SCALE EXPERIMENTAL STUDY OF HELICOPTER ROTOR ISOLATION

R. Jones, Kaman Aerospace Corporation, Bloomfield, Connecticut

DECOUPLING THE THREE TRANSLATIONAL MODES FROM THE THREE ROTATIONAL MODES OF A RIGID BODY SUPPORTED BY FOUR CORNER-LOCATED ISOLATORS

T. F. Derby, Barry Division Barry Wright Corporation, Watertown, Massachusetts

SHOCK MITIGATION SYSTEM SUBJECTED TO THIRTEEN FEET OF GROUND MOTION — CANNIKIN EVENT

E. C. Jackson, University of California, Lawrence Livermore Laboratory, Livermore, California

THE ACTIVE DAMPER — A NEW CONCEPT FOR SHOCK AND VIBRATION CONTROL

M. J. Crosby, Lord Corporation, Erie, Pennsylvania, and D. C. Karnopp, University of California, Davis, California

VIBRATION CHARACTERISTICS OF SKIN-STRINGER STRUCTURES

J. P. Henderson, Air Force Materials Laboratory, Wright-Patterson AFB, Ohio

MATERIALS FOR VIBRATION CONTROL IN ENGINEERING

A. D. Nashif, University of Dayton, Research Institute, Dayton, Ohio

VISCOELASTIC EPOXY SHEAR DAMPING CHARACTERISTICS

C. V. Stahle, A. T. Tweedie and T. M. Gresko, General Electric Company,
Philadelphia, Pennsylvania

VISCOELASTIC DAMPING IN FREE VIBRATIONS OF LAMINATES

S. Srinivas, NASA, Langley Research Center, Hampton, Virginia

OPTIMUM PASSIVE SHOCK ISOLATION FOR UNDERGROUND PROTECTIVE STRUCTURES

D. L. Platus, Mechanics Research Inc., Los Angeles, California

INFLUENCE OF AN ABSORBER ON MACHINE TOOL VIBRATION

O. Susolik, The Timken Company, Canton, Ohio

REMARKS

Elias Klein,* Ph.D.
Sarasota, Florida

(U) Prior to 1940 little consideration was given to the phenomena of Shock and Vibration in military operations. Damage caused by explosive or vibratory forces was repaired by trail and error. By the end of World War II repair shops in many parts of the world recognized and took up the problem. But there was no coordinated effort. Recognizing the need, the Navy Department early in 1946 established at the Naval Research Laboratory one unit devoted to basic research in shock and vibration and another to act as a "centralizing activity" for the collection, correlation and dissemination of all information on this subject. Later, the function came under the jurisdiction of the research and development board, and finally under the Office of the Assistant Secretary of Defense for research and engineering. All interested service agencies participated, and the function was linked with the preparedness effort. The Centralizing activity carried out its part in several ways:

1. By keeping engineers and scientists informed of developments in the field through periodic symposia on subjects which appeared urgent and timely.

2. By compiling surveys, inventories and summaries of current live research in different areas bearing upon an immediate problem. This centered the focus on whatever was being done in the Department of Defense.

3. By providing consultative services to contractors of the Department of Defense.

(U) Needless to say, the centralizing activity grew and expanded. Its prosperity attested to it as a success story.

(U) As we approach the second quarter century of operation, I would like to offer suggestions on the changes or emphasis which could be made if I had it to do again. Here are a few that come to mind.

- a. Eliminate prejudice in problems as well as humans.
- b. Develop motivation for interpersonal cooperation among co-workers.
- c. Correct the mistake of wasting time.

This overview also points to the conclusion that in this day of problems faced by the human race, as for example in pollution, a centralizing activity can be a method for correlating the attack. Concerted effort and cooperation, exchange of information rather than competition, would bring successful solutions sooner.

* Dr. Klein was a main driving force at the inception of the Shock and Vibration Technical Symposia in 1947. Until his retirement in 1958 he planned and directed the Shock and Vibration Symposia and the other related activities of his office. Since the 43rd Shock and Vibration Symposium in Monterey, California was held during the 25th Anniversary year of these Symposia SVIC had arranged for Dr. Klein to record these remarks. They were heard as part of the opening session chaired by Dr. W.W. Mutch, who was Head of the Shock and Vibration Center from 1958 until his retirement in 1972.

INVITED PAPERS

A QUARTER CENTURY OF PROGRESS

Dwight C. Kennard, Jr.
Consultant
Traverse City, Michigan

INTRODUCTION

(U) A quarter century, I am sure, seems like forever to the younger set. I have lived through the quarter century that followed World War II, but even to me it seems incredibly longer when reminiscing about the events of that period. Many will agree that in no other comparable period have there been more changes and perhaps more progress that seem to make time stretch like a rubber band.

(U) Twenty-five years ago we were still emerging from the devastation of World War II. The charter of the newly formed United Nations at long last raised our hopes that never again would there be another war between nations. Hardly anyone took Wernher VonBraun's crackpot ideas seriously about the feasibility of space flight and he was regarded then simply as the captured German scientist who developed the V2 Rocket. New cars were equipped with wooden planks in place of bumpers because of material shortages. There were no passenger jet airplanes. The B-50 and B-36 were our first-line bombers. Neighborhood parties were in vogue for watching TV programs in the one home on the block fortunate enough to have a set. Even the young males visited the barber shop every other week.

NEED FOR COMMUNICATION IN SHOCK AND VIBRATION TECHNOLOGY

(U) We had managed to come through the war with a shock and vibration technology that resided with only a few isolated individuals and groups primarily in the three military services but interservice coordination was practically nil. Shock and Vibration was not generally recognized as a technology or at best it was considered a kind of unimportant off-beat idiosyncrasy. The technique of the shock and vibration engineer often revolved around a kind of enlightened "cut and try" procedure.

"SOMETHING MUST BE DONE"

(U) Then into this scene came the eternally youthful and perceptive Dr. Elias Klein,

a scientist at the Naval Research Laboratory. He said "something must be done" to consolidate ideas and to coordinate shock and vibration technology along more scientific lines. With characteristic vigor, foresight and determination, he became instrumental in bringing about a recognition by the Navy that no longer could it afford to deprecate the importance of this technology. In one problem alone, that of transporting World War II military equipment, it was found that more than half arrived at the scene of operations in a damaged and unusable condition due to handling and transportation-induced shock and vibration.

(U) This tremendous waste was just part of the price of neglecting the effects of shock and vibration. Facts were coming to light that showed compounding costs from malfunctions of equipment improperly designed for shock and vibration, excessive maintenance and repair, and unreliability of systems under combat and/or service conditions.

THE NAVY ACTS

(U) Yes, it was agreed that something must be done, so early in 1946 the Chief of Naval Operations through the Office of Naval Research, established a unit at the Naval Research Laboratory to conduct basic research in shock and vibration, and another unit "to act as a center for the collection, correlation, and dissemination of all available information on this subject". Thus for the first three years, the newly created Centralizing Activity for Shock and Vibration was sponsored by the Navy alone, certainly a tribute to its foresight and progressive attitude. This action, of course, was in keeping with the Naval tradition of promoting applied sciences which a quarter century earlier in 1923 led to the establishment of the Naval Research Laboratory as recommended by Thomas A. Edison.

(U) Then in 1949, the Research and Development Board of the Department of Defense

took over jurisdiction for operating the Centralizing Activity although it was destined even to this day to remain at the Naval Research Laboratory and to be operated and manned by that Laboratory.

INTERSERVICE TECHNICAL GROUP/TECHNICAL ADVISORY GROUP

(U) To involve the other services in the Centralizing Activity, a planning council composed of technical representatives from the three armed services was established, known as the Interservice Technical Group for Shock and Vibration (ITG). It was my privilege to serve as one of the Air Force members for 13 years and for the last three years of that period (1959-62) to serve as chairman. This group now is known as the Technical Advisory Group for Shock and Vibration (TAG) and is composed of four representatives each from the Air Force, Navy, Army, and the National Aeronautics and Space Administration. Also there is one representative from the Defense Nuclear Agency. Dr. Mutch served as chairman of this group from 1962 until his recent retirement as the Director of the Shock and Vibration Information Center. Mr. J. R. Sullivan, NAVSEC, is the current chairman.

DEVELOPING THE MISSION AND MODUS OPERANDI OF THE SHOCK AND VIBRATION SYMPOSIA

(U) The original mission assigned by the Chief of Naval Operations to the Centralizing Activity in 1946 still stands as the mission being performed by the Shock and Vibration Information Center today and that is: "to act as a center for the collection, correlation and dissemination of all available information on this subject". Quoting Dr. Klein concerning methods of carrying out this mission, he said in 1957: "The most fruitful method has been the periodic symposia on subjects which appeared urgent and timely in light of current defense programs". I think that statement applies as well in 1972 as it did 15 years ago.

(U) From inception there has been an underlying question about the symposia which might be paraphrased as: "What purpose can be served by the DOD-organized Shock and Vibration Symposia that could not be served better by appropriate technical societies?" Certainly this is a legitimate question but to pose it indicates a basic misconception of the functions performed over the years by the symposia. From the start, the symposia were carefully planned and conceived so as not to intrude into areas which could be served better by technical societies. At that time none of the technical societies were organized to give specific attention or recognition to shock and vibration as a field of technology. The Steering Committee (ITG) felt that one of its major goals would be to encourage the technical societies to set up

their own specific programs and to change their organizations so as to give shock and vibration technologists a recognized niche on a par with other specialized areas provided by a particular technical society. This goal has been achieved during the succeeding years by several technical societies who have organized their own vibration or shock and vibration technical committees *eg.* ASME, SAE, IFS, SESA, ASA. ASME holds biennial vibration conferences and various other technical societies hold vibration sessions at their National meetings.

(U) Aside from encouraging technical society activity in shock and vibration technology, the symposia have been organized and conceived to perform a different function than normally performed by the typical technical society. The symposia have been designed to provide up-to-the-minute information on current work in progress. Hence, papers may describe projects that are not yet completed but which are of sufficient interest to benefit others working on similar problems. Novel and innovative ideas often appear even prior to final verification. Papers sometimes evoke brainstorming sessions in the subsequent formal and informal discussion periods where the possible solution to a knotty problem may emerge.

(U) Staff members of the Shock and Vibration Information Center and sometimes the TAG members travel throughout the USA and Europe to visit organizations doing work in shock and vibration. During these visits, workers, projects, and progress in the field are noted. Where appropriate, individuals and organizations are encouraged and/or invited to present their results and describe their projects at a subsequent symposium. The net result is that papers are accepted on current work, involving short lead times for selection and review. This practice is in contrast to that of the typical technical society where papers are selected generally from completed projects or phases after long reviews with lead times possibly 18 months or more before publication. This should not be construed as a criticism of the highly selective approach typically practiced by technical societies because it is important to have their kind of refereed and reviewed papers too. The point is, there is a need for both the Shock and Vibration Symposia to summarize current work, as well as the technical societies to document the more formal, sophisticated, and conclusive work.

(U) I understand that a new policy is being adopted by the Information Center which will impose a more stringent procedure for review, referee, and selection of Symposium papers to be included in the "Bulletin" published following each symposium. Until now there has been a liberal publication policy that permitted practically all papers

presented at the Symposium to be included in the "Bulletin". It is commendable to try to raise the quality of papers included in the "Bulletin", but it must be done with great care so as not to inhibit the spontaneity of contributors which has been the hallmark of the Shock and Vibration Symposia. I would like to inject a note of caution and a warning that if the selection process dampens the motivation for presenting up-to-the-minute information on current work in progress then the "raison d'etre" for these Symposia will be gone. If this should be allowed to happen, then there would be little justification for continuing the Shock and Vibration Center since its function would be indistinguishable from that of the Technical societies.

(U) Another aspect of the Shock and Vibration Symposium which distinguishes it from the traditional function of the technical societies is the handling and publication of classified papers. With the symposia under DOD sponsorship, it is far more feasible to control presentation and publication of classified material than it would be for a technical society. Often this DOD Symposium provides the only outlet for a scientist working in classified areas to present and publish the results of his work and to exchange technical ideas concerning scientific problems.

(U) A matter closely related to the encouragement of technical society activity in shock and vibration technology, has been the development of standards in the United States Standards Institute, International Standards Organization, and the International Electrochemical Commission. It is interesting to note that many persons who have been most active in the Shock and Vibration Symposia also have been active in these standardization projects as well as in the various technical societies. This multiplicity of involvement assures an informal type of coordination and explains the absence of excessive duplication. Typically the last five chairmen of the USASI S2 Committee on "Mechanical Vibration and Shock" (Trent, Vigness, Muster, Kennard, Bouche) also served as members and/or chairmen of the "Vibration Technical Committee" of the Acoustical Society of America and have all been active participants in the Shock and Vibration Symposia. Each of these individuals have also served variously in similar capacities in the ASME, IFS, SFSA and international standardization.

(U) The Shock and Vibration Symposia on several occasions were planned and organized to help resolve specific technical problems. By getting workers together concerning a mutual problem area to describe their work and to discuss points of common interest, the state of the art was more clearly defined and possible approaches to a solution became

more apparent. One example took place in 1950 at the start of the Korean War. Large quantities of war material were arriving at battle areas in an unusable condition due to damage in transit. This was having disastrous consequences in the conduct of the war. In Dr. Klein's words: "When this situation came to the notice of the Interservice Technical Group, a nation-wide symposium was soon organized to discuss ways and means for reducing damage to military shipments. The railroads, the trucking industry, the airlines, and maritime groups were invited to help in this emergency. Several hundred engineers, packaging designers, and operating personnel from government and commercial agencies were assembled to formulate an answer to the question: 'What can be done now to safeguard military shipments from shock and vibration damage?'"

(U) "Two symposia on loading damage were held in 1950 and they served a very useful purpose. The prevailing deficiencies in the handling and transportation of cargo were promptly recognized, and definite cooperative recommendations were made with a view of immediately increasing safety in transit. To help implement the improvements discussed at these meetings, an offer was made on behalf of the government by the Centralizing Activity to provide any carrier system with the best available technical knowledge in the field of shock and vibration which would be amicable to the problem at hand. In addition, we offered guidance to any common carrier in the use of modern instrumentation for evaluating and improving the chances of an equipment's safe arrival. Certain computer facilities and data reduction procedures were made available to these organizations to expedite their results and to put them into practice. The Naval Research Laboratory processed some measurements for a railroad company which accepted our offer. This aspect of quantitative railroad technology represented a new approach to the problems of the transportation industry.

(U) "Out of these transportation symposia also came some long-range projects to benefit both civilian and military shipments."

PROFILES OF PROGRESS

(U) We often hear such statements as, "the production of scientific information doubles every ten years." It is interesting to note that this is happening in the output of the Shock and Vibration Symposia if one considers each published technical paper as a unit of production. By referring to Table I it can be seen that during the first decade (Symposia 1 through 24, 1947-1957) 412 papers were produced. During the second decade (Symposia 25 through 36, 1957-1967) 789 papers were produced with a 1.9 factor of increase. We now are half way through the third decade and the number of papers produced, including the 43rd Symposium, amounts to 744 with a 0.64

factor of increase relative to the entire second decade. So if we continue the same production rate for the next five years, the number of papers produced during the third decade will be about double that produced during the second decade.

(U) Table I also shows significant data concerning participation in the Symposia. During the twenty-five year period a total of 2181 individual authors have participated in preparing 1945 papers for the forty-three Symposia. In contemplating the audiences who have listened to these 1945 papers and the readers who have studied the subsequent published versions, one gains some idea of the immense dimension taken on by this means of communication among scientific workers.

(U) There have been many trend-setting papers which represent milestones of progress. It would be foolhardy for any one person to enumerate these because each individual would have his own opinion based upon particular interests and problem areas. However, in consultation with the Shock and Vibration Information Center staff, it is apparent that a few memorable papers stand out as typical of the many milestones which are too numerous to mention individually:

"Vibration Problems in the V2 and Similar Guided Missiles" presented in 1949 at the 14th Symposium by Werner VonBraun. This paper was a preview of the forthcoming challenge that would be faced by shock and vibration technologists in developing rockets for the space program.

"Shortcomings of Present Methods of Measuring and Simulating Vibration" presented in 1953 at the 21st Symposium by C.T. Morrow and R.B. Mucimore. This paper "shook up" constituents of the Shock and Vibration Symposia and set off a controversy over sinusoidal and random vibration concepts that was to continue for many years.

"A Novel High-and Low-Temperature Horizontal-Vibration Test Fixture" presented in 1957 at the 25th Symposium by W.O. Hansen. This paper introduced the "slip table". Many variations since have been developed based on this first published data.

"A Method for Predicting Environmental Vibration Levels in Jet-Powered Vehicles" presented in 1960 at the 28th Symposium by P.T. Mahaffey and K.W. Smith. This paper set forth a prediction technique that has been used widely and modified to fit other situations.

"Simulating Flight Environment Shock on an Electrodynmic Shaker" presented in

1963 at the 33rd Symposium by G.W. Painter and H.J. Parry. This paper presented the first of several methods of synthesizing shock motion on a shaker from a given spectrum and helped solve missile shock testing problems involving pyrotechnic separation devices used for staging and other actuations.

"Elementary Considerations of Shock Spectra" presented in 1964 at the 34th Symposium by Irwin Vigness. This was a tutorial paper which clarified widely misunderstood concepts of shock spectra.

"Transient Waveform Control of Electromagnetic Vibration Test Equipment" presented in 1969 at the 40th Symposium by J.D. Favour, J.M. LeBrun, and J.P. Young. This paper won the Irwin Vigness memorial award of the Institute of Environmental Sciences. It represents a newer trend for using computer facilities to control a shaker in reproducing the time history of a motion parameter involving application of Fourier integral techniques.

(U) The foregoing is only a partial list to illustrate the point that there have been many papers presented at these symposia that have been of special interest and/or have been influential in setting trends in dealing with particular problem areas.

THE SHOCK AND VIBRATION INFORMATION CENTER

(U) Although this paper primarily deals with the Shock and Vibration Symposia, it must be noted that the Shock and Vibration Information Center provides many additional services. The Symposia proceedings are published in "The Shock and Vibration Bulletin"; nine state-of-the-art monographs have been published on specific aspects of shock and vibration technology; "The Shock and Vibration Digest" is published monthly; a direct information service is provided to answer inquiries for technical information.

(U) At this point I would like to pay special tribute to the people who have administered the Shock and Vibration Centralizing Activity/Information Center over the years: to Dr. Elias Klein for his perseverance, wisdom, and foresight in conceiving, establishing, and nurturing his idea to a successful status; to Dr. W.W. Mutch who with enthusiasm, dedication, and innovation caused the activity to grow to its present importance and stature; and to Dr. Robert Relsheim who recently had the courage to accept the challenge of leading the Shock and Vibration Information Center to new levels of attainment and usefulness.

(U) A great deal of credit also goes to the Shock and Vibration Information Center Technical Staff, each of whom have established

reputations for their individual contributions in specific areas: Henry C. Pusey—Packaging and Transportation; Rudolph H. Volin—Vibration and Test Equipment; and Edward H. Schell—Shock and Fragility. We can be proud of the competence of each of these individuals and grateful for their dedication in providing the outstanding service that so many have come to rely on and perhaps too often to take for granted.

(U) In conclusion, it is this fine group of people who will be bringing about new developments to assure continued growth, improvement, and increased efficiency of the services performed by the Shock and Vibration Information Center. I do not wish to steal their thunder by revealing plans for the future, but we can all be assured that the tradition of success and service that has been so firmly established will be reaching new levels of achievement as the third decade of service continues to unfold.

TABLE I

Record of Papers Produced and Authors Participating in the Shock and Vibration Symposia

SYMPOSIUM NO.	AUTHORS	NEW AUTHORS	PAPERS	TIME PERIOD
1 - 24	393	393	412	FIRST DECADE 1947-57
25 - 36	1121	1070	789	SECOND DECADE 1957-67
37 - 43	949	718	744	THIRD HALF DECADE 1967-72
TOTALS	2463	2181	1945	QUARTER CENTURY

FORMER SHOCK

Donald E. Marlowe, Ph.D
Catholic University
Washington, D. C.

(U) When Dr. Belsheim invited me to speak to the 25th anniversary meeting of the Shock and Vibration Symposium, he reminded me that I had been one of the earliest contributors to the Symposium, and that perhaps my memories of those early days would be an amusing and informative introduction to the anniversary. His instructions were "Tell it like it was." While preparing this paper, it seemed wise to cite even earlier experiences, as they too illuminated the former state of theory and experiment in the field of applied mechanics. Although it is somewhat dismaying to recognize that my engineering studies have now extended for nearly forty years, I will plagiarize Allen Toffler's famous book, and call this paper "Former Shock".

(U) I must confess that my early education was as a Civil/Structural engineer, and at that time, moving load calculation was the epitome of dynamic analysis. Iterative methods (the Hardy Cross method) were just making their appearances. Differential equations was an elective subject in all engineering curricula. My own break with this educational tradition began with my employment as a demonstration assistant in a physics department. In this job I was guided by an excellent experimental physicist (Wm. Baker), and I learned much about the difficulties of good laboratory work, something about the sources and propagation of errors, and, above all, about that marvelous journal, Physics Abstracts. From the Abstracts, I learned something about photoelasticity, and did an undergraduate thesis on "Photoelastic Analysis of a Gravity Dam," using gelatin models. The stimulation provided by this little project was worth much more than the analysis itself.

(U) My new interest in mechanics inevitably drew me to Ann Arbor, as a graduate student, where S. Timoshenko was the keeper of the flame. (His biography is must reading for every worker in Mechanics). When I arrived, there were less than a dozen Mechanics majors, Timo had fled to Stanford, though he did return to Michigan each summer, as did most of his first generation of students.

Although I had elected Differential Equations as an undergraduate, my mathematical foundation needed extensive repair, and while this was underway, I turned again to laboratory work, largely as an assistant to Lawrence Maugh, whose modest research support in studies of rigid frames enabled me to keep the wolf from the door and simultaneously introduced me to the reciprocal theorem. He also introduced me to the terrors of experiments whose output consists of small differences between large numbers. These were the days when the principal tools of strain measurement were the travelling microscope, the Huggenburger and Ackerman strain gages and the Michelson interferometer.

(U) I owe to Jesse Ormondroyd the diversion of my interests to structural dynamics. He had just finished work on the Mount Palomar telescope (a very slow dynamics, indeed); my own mathematical background had been somewhat repaired, so I went into Jesse's courses on dynamics, vibrations and above all, analysis of transients. Feedback concepts had not yet reached Ann Arbor.

(U) The Michigan mechanics department was enthusiastic about research courses (probably because there were too few students for many formally organized courses), so I plunged through a series of projects which gave me additional experience in photoelasticity, mechanical strain measurement, physical optics, and error analysis. I also discovered the existence of electricity, a phenomena which my education had kept carefully hidden from me until that time. It's true that in reading about prior research on gravity dam stresses (Physics Abstracts, again), I had come across the Bureau of Reclamation practice of burying lengths of resistance wire in dams, as a way of measuring concrete shrinkage; but since the gage lengths were a foot, and I was mostly working with models, I had quickly dismissed this as a useful strain gage.

(U) But the Michigan laboratory had, shoved away in one corner, a Peter's Telemeter

gage. No one had used it for years. After Ormondroyd suggested I try to make some dynamic strain measurements with it, I quickly learned the cause of its neglect. The Telemeter was a carbon pile gage, much like the old style telephone receiver, and, due to erratic packing of the carbon resistance column, was a very temperamental beast. Even static measurements required working in the laboratory in the old South Engineering building from midnight to six a.m. (with my new wife as research assistant), hours when all extraneous influences of temperature, vibration, etc. were minimized. Dynamic measurements were a real nightmare, and not just because of the midnight hours we were working. The Telemeter was my introduction to electrical measurements, and with it I learned to appreciate the inherent instability of D.C. amplifiers. However, the useful gage length had shrunk from a foot to an inch, but unfortunately at the expense of a great increase in inertia. I also learned, under the tutelage of A.D. Moore, of Michigan's EE Department, how to restrain a string oscillograph. Moore was truly amazed—I was the first student from Mechanics, to his knowledge, who had ever set foot in the EE Department, so he spent quite a bit of time with me, even letting me learn to use the department's newest acquisition—its first cathode ray oscillograph.

(U) In the summer of 1939, Stan Filion from MIT spent the summer in Ann Arbor. He had been working with Ruge at MIT on a resistance wire strain gauge in which the wire was multiply folded, so that gauge lengths of an inch (with little inertia) seemed possible. He had brought a roll of commercial nicrome wire with him, and as the department's leading (and only) electrical expert, I spent that summer learning to manufacture the prototypes of the modern gage. It didn't occur to us to cement them to the specimen—we clamped the ends to the specimen (as in mechanical strain gages), and then worried as to what precisely was the active length of the gage. Under the direction of Maugh and Ormondroyd, I made many electrical strain measurements, both static and dynamic, over the next two years, but the advent of World War II put an end to this leisurely approach to research.

(U) Ralph Bennett had activated his reserve Navy commission in 1940, and had been assigned to the Naval Ordnance Laboratory to direct work on naval influence mines, which had appeared during the Battle of Britain. He asked his old friend, A.D. Moore, to help him recruit an engineering team, and Moore, knowing my interest in instrumentation and measurement, persuaded me to go to Washington for a year or two. (Thirty-two years later, I'm still in Washington.)

(U) At NOL we quickly identified all of the ship's influences which could possibly activate a mine (no other was ever discovered),

and I was quickly at work under Shirley Quimby (Mr.) (even though once listed in Who's Who in American Women) on problems of resonance in hydraulically loaded diaphragms (as usual, Lamb had already set up the basic equations). One possible method of detecting diaphragm movement was the resistance wire strain gage, so most of my experimental effort went into detection circuitry. Unfortunately, such hydrophones were very sharply tuned, and thus unsuitable for the broad noise spectrum distributed by ship traffic. However, the strain gage did offer a time dependent signal, with the potential of great discrimination, so work on it continued. I was asked to participate in development of underwater explosion gages, and in a few weeks was reasonably familiar with the vagaries of copper ball crusher gages, piezoelectric gages and cable noise. This work brought me into a close relationship with Royal Weller, probably the most ingenious person with whom I have ever associated. Roy's restless mind focused on the aerodynamic design of mines, and before I knew it, I was measuring the aerodynamic coefficients of bombs and mines, using (again after midnight) the underwater facilities of the old Taylor Model Basin, as wind-tunnel time had become absolutely unavailable, due to the WWII "50,000 airplanes" program. I learned a lot of fluid mechanics under conditions of great urgency, saved only by Goldstein's "Modern Developments" which had just appeared. I learned the hard way that most data on drag of streamlined bodies, published prior to 1935, was wrong, due to the so-called "horizontal buoyance" effect of early wind tunnels.

(U) From aerodynamic coefficients to underwater ballistics was a short step, indeed. Naval aerial mines flew very badly, and the shock of water impact was very damaging to their delicate influence fuses. Several ad hoc solutions, such as cushioning, only seemed to make matters worse, so we undertook to try to really understand the water entry phenomenon. My prior technical history had given me many of the tools to tackle the problem. Underwater explosion gages, mechanical and electrical; measurements in fluid mechanics, dynamic analysis; familiarity with vacuum tube technology; etc., all were useful in the search. Our initial understanding of the shock problem on water impact was largely based on observations of functioning (or non-functioning) of water impact bomb fuses, and no good data existed. NACA had done some theoretical work on impact of airplane floats. I came across a single photo of a British "Hedgehog" riding in its hydrodynamic cavity, and with my own bias towards model measurements, we quickly designed and built the first water entry tank in the U.S. Our photographic equipment was an old Mitchell high speed (128 frames/sec.) movie camera, and only the advent of the Fastax camera made it possible to get meaningful data. (Remember, the old problem of small differences between large numbers.)

With this equipment we determined dynamic drag coefficients, and we miniaturized copper ball crusher gages for both field and model measurements of peak shocks. We also learned much about the response of crusher gages to transient shocks, and developed the pre-loading techniques which made these data meaningful. Simultaneously, we developed laboratory equipment for shock simulation; drop testers, air guns and standard input testers which could be correlated with field tests and greatly speed up laboratory tests of delicate instruments. Two developments seem to have been particularly sophisticated; the use of yielding metal as an energy absorber, and the use of the 54 foot tides in Nova Scotia to simplify recovery, from underwater, of field tested ordnance.

(U) Even with better understanding of shock patterns, the inherent delicacy of influence mechanisms required us to resort to parachutes, but there was an insistent service demand for a free fall mine, at water entry speeds in excess of 1000 ft/sec. This led to a careful restudy of the initial shock wave occurring at water entry, as well as the more sustained "drag" shock, and also required sophisticated changes to the laboratory simulation devices. Many members of the S & V Symposium--L. Fisher, J. Armstrong, R. Ayres, J. New and many others--pushed this research forward. An XHAM was, in fact, successfully developed, but with some limitations. Recent military actions in Southeast Asia awakened many memories for me.

(U) The failure of torpedo exploders to fire upon impact, or of influence exploders to fire on transit, led to urgent assignments in that area of ordnance, and the members of the team which had been engaged in mine warfare tackled these new, but similar, problems of torpedoes. For myself, it was my first introduction to feedback control theory, and my experience in measuring aerodynamic coefficients stood me in good stead. We were still only reluctant electronikers--I remember carrying a card proclaiming me a member of the "Committee for Electronics without Vacuum Tubes", little realizing the prophetic content of that name. Problems associated with the water entry of aircraft launched torpedoes quickly brought us in touch with the Division 6-OSRD group at Cal Tech., who had experience with many of the shock phenomena which we had regarded as our private property--we had many fruitful exchanges, and I have the fondest memories of that period of collaboration with F. Lindvall, L. Slichter, D. Hudson, H. Wayland, R. Knapp and many others. Morris Dam, the torpedo launching setup, was, in fact, the genesis of our own Hwassee Dam launching rig for anti-submarine weapons. Torpedo studies, of course, led us into target impact studies, a branch of shock measurement not present in many other undersea

weapons.

(U) This period also reintroduced me to the subject of underwater explosion damage. Until this time, as an ordnance engineer, I had been interested in plate rupture; any damage less than this seemed hardly worth while. The relatively small charges carried by some homing torpedoes made equipment damage from explosions an important topic, and we soon became aware of the extensive work in this area by groups at NRL and DTMB.

(U) It should be noted that, prior to 1947, practically all of our technical information on ordnance shock was obtained either by field testing (which depended on the recovery of ordnance, and was usually go--no go testing), or by use of internal recorders (which were themselves subject to shock). The securing and analysis of shock data was a slow and tedious process, with many unproductive experiments. Almost as much development effort went into recovery devices and internal recorders as into the ordnance itself. The first telemetered shock record I ever saw was in 1947, when a single channel of information was radioed from an impacting bomb which trailed a small transmitter at the end of a cable. Wm. Pabst and M. Schuyler kept us conscious of the vital importance of good statistical design of experiments (a service which often had to be thrust upon us). I recall that, in May of 1947, I reported to this S & V Symposium on our intention to measure accelerations in projectiles, by radiating information from an antenna in the nose of the projectile.

(U) My recollection may be faulty, but I believe the first S & V Symposia were intended to draw together those persons interested in equipment damage from underwater shock, and that Dr. Klein and his associates may have felt that they had opened Pandora's Box when respondents flocked in from all parts of DOD, with their peculiar problems of water impact, projectile firings, railroad car bumpings, luggage handling, etc. Truly, there was no physical phenomenon more common to all types of military hardware than shock and vibration. Our group worked very hard in the immediate post-war years developing the concept of environmental simulation, beginning with shock and vibration simulation, and consolidating with it much of the rather random temperature, humidity, etc., testing which we had always carried on. We were fortunate, at that time, to be able to design the excellent simulation laboratory in the new Whiteoak establishment.

(U) I believe that many of you are aware of my interest in the history of technology. In its origin in the Renaissance, the history of technology was identical with the history of mechanics. Our philosophical ancestors were Galileo, Toricelli, and Leonardo. While

fully recognizing the sharp discontinuity in technological history caused by the advent of Electronics, it seems accurate to state that no field has been more influential in providing the underpinnings of modern civilization than that of Mechanics. I was fortunate to have practiced much of my active engineering career during one period of great engineering advances, both in theory and experiment. As today's engineers attempt even more difficult advances, particularly in these days when mankind must seek a new level of accommodation with nature, I predict that our historical concerns with shock, vibration, reliability, damage, stress and strain, and all the rest, will continue to provide the insights which will make possible a better and safer world in which to live.

THE ARMY'S BIG FIVE AND RDTE PROGRAM THRUSTS

Major General John R. Guthrie
Deputy Commanding General for Material Acquisition
US Army Material Command
Washington, D.C.

INTRODUCTION

I am honored to have been selected to represent the Department of the Army as your keynote speaker for this year's Shock and Vibration Symposium. I am doubly honored to have been selected to address this meeting which marks the 25th Anniversary of the Shock and Vibration Information Center. I offer the Army's congratulations on your well known success in these fields of endeavor and thank you for your outstanding support to the United States Army. The interest of the Department of the Army in Shock and Vibration studies and research is indicated by the funding support we provide to the Shock and Vibration Information Center and the four technical consultants we have assigned to assist the Chief of the Center, Dr. Belsheim and his staff.

At your annual symposium in 1971 your host was the Navy and the keynote speaker, Admiral Mason, spoke on "Ships of the Future." I believe it is appropriate, therefore, that I address you on the subjects of "The Army's Big Five and RDTE Program Thrusts." Since I am responsible within AMC for material acquisition this is a subject of daily concern to me and one that I hope you will find interesting.

A couple of years ago - during the preparation of the Fiscal 1971 budget - the Army staff became concerned with ordering its hardware priorities. The Army, like any large establishment, has always had a variety of priority systems - to identify the relative importance of its R&D tasks, to use in maintaining goals or to meet distribution requirements. But in the summer of 1969, looking forward to the possible lean postwar years ahead, it became apparent to those in the Army staff concerned with budgeting and programming that a determination had to be made of those hardware items or categories which were most essential to our combat forces if they were to be competitive in the next 10 to 15 years. The principle here was to build a fence around the items once they were selected to protect them in each annual budget exercise. After

much careful deliberation involving assessments of the threat, the state-of-the-art, and the prospective fiscal climate there emerged what was known as the "Big Eight" which has now been reduced to the "Big Five" which are as follows.

1. Main Battle Tank (MBT)
2. Advanced Attack Helicopter
3. Utility Helicopter (UTTAS)
4. Mechanized Infantry Combat Vehicle (MICV)
5. SAM-D Air Defense Missile System

Main Battle Tank (MBT) (Figure 1)

The former Main Battle Tank XM803 was terminated by Congress, primarily because it was going to cost in excess of \$1 million per copy. Instead, \$20 million were allocated to build two new prototype tanks. In other words, we were to start over and come up with a less expensive tank.

As a result, the Army revised its future tank requirements and has prepared a new development program. We are now seeking approval from OSD to issue a Request for Proposal (RFP) to industry with the objective of contracting for the Validation Phase of our development program before the end of fiscal year 1973. We intend to select two contractors, each of which will build one prototype and some test rigs during the competitive validation phase. The Army will then select a winner from these two for continued engineering development and limited production.

The name of the game is to go low-risk, but there are several danger areas. The schedule is seven years from start to limited production if we go the competitive route. There is no room for lost time, for strikes or other slippages. As the song of the 1930's put it - "There may be trouble ahead, but let's face the music and dance." I am sure you are all familiar with the shock and vibration problems of combat vehicles. The effect of travel over rough terrain and the shock from

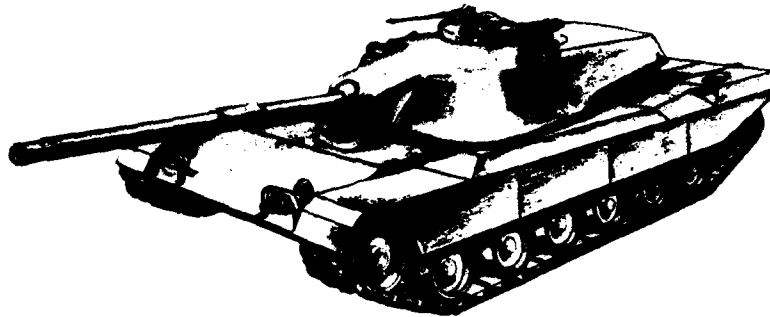


Fig. 1 - Main Battle Tank (Conceptual).



Fig. 2 - Advance Attack Helicopter.

firing the main armament is felt by all subsystems, in particular the communications, ranging, fire control and night vision systems.

Specially designed helmets are required to protect the occupant and to permit communication in the environment of noise and vibration. The noise level inside a tank during combat operations requires special design of protective equipment to make it bearable for the crew.

Advance Attack Helicopter (Figure 2)

An ancient proverb says trouble arrives on wings and leaves on foot. The originator of that must have had the Army's Advanced Attack Helicopter program in mind.

For some time, the Army has stated that one of its top priority development programs is a new attack helicopter and until very recently, this was the CHEYENNE. The Army cancelled that program in August, after determining (1) the cost of the bird was going to be so high that either Congress wouldn't let us produce it or we couldn't buy enough of the aircraft to fill out the requirements; (2) the appearance of two possibly lower cost alternative aircraft; (3) a revision in the aircraft requirement based on experience, studies, and computer simulation. These studies indicate that all three aircraft tested: The CHEYENNE, the Sikorsky Black Hawk, and the Bell KING COBRA, did not meet our latest requirements, and product improvement for each one would be uneconomical. A new program was determined to be necessary and Congress has approved minimal funding for this program.

Utility Helicopter (UTTAS) (Figure 3)

The good old Hueys, the workhorse helicopter of Vietnam, are just that, good but rapidly getting old. They were developed with technology of the late 1950s and early 60s, and the state of the art in helicopters has advanced considerably since then. By the 1980s they will be basically 20-year old technology. Therefore, we have started development on its replacement for the 1980 timeframe. The program is currently called UTTAS (Utility Tactical Transport Aircraft System).

We completed an engine competition for the UTTAS in December 1971, with the award going to General Electric. This past August we awarded competitive prototype airframe contracts to Boeing Vertol and Sikorsky. The contracts call for each company to provide three flyable aircraft, with an Army option to raise the number to 5 or 6. The current schedule provides for the prototype evaluation by September 1976, and a limited production contract award to the winner in April 1977.

But here, too, there is a problem area. The Army wanted six flyable aircraft of each contractor, to obtain maximum data in a given period of time. The Senate Armed Services Committee Report restricted us to three each.

There is hope that additional funding will be provided in next years budget.

If ever there was an area that needs support from shock, vibration and acoustic experts these helicopters qualify. The UTTAS and the new attack helicopter will both employ the latest design techniques to reduce the adverse noise and vibration effects. Redesign of rotor blades will greatly reduce noise. A significant breakthrough in this area is the use of swept tips on the blades to better control the shock wave pattern. Both of these aircraft are expected to be relatively silent when compared to the present COBRA, HUEY, or CHINOOK. The number of rotor blades employed has also been found to be a significant factor in vibration problems. Four rotor blades appear to be better than two primarily because this raises the passing frequency (the frequency at which each blade passes over the fuselage). The low frequency passes of the 2-bladed rotor excite similar frequencies in the aircraft structure and these are more difficult for the crew to withstand than higher frequencies. It is important that the rotor and the aircraft structure be detuned to arrive at vibrations in a frequency range that the crew and the aircraft can best endure. This will be a critical design factor in all new helicopters.

Mechanized Infantry Combat Vehicle (MICV) (Figure 4)

We are preparing to enter engineering development of a successor to the M113 Armored Personnel Carrier. It is called the MICV - for Mechanized Infantry Combat Vehicle.

It is a new type vehicle to the US Army, and results from the Infantry's decision in 1963 to change its doctrine to allow commanders the option to fight from within their personnel carriers.

Studies showed that upgrading or product improving the M113 could not provide a key essential, sufficient mobility, to allow the carrier to accompany the future Main Battle Tank across country. The technique to achieve this will probably be a tube over bar suspension system that permits greater torsion and greater wheel travel than conventional systems. It is a proven component.

We have received authority (and we believe the necessary funds in the FY73 appropriation) to begin building the first prototype vehicles early next calendar year. A special board evaluated bids from the three potential contractors: FMC, Chrysler, and Pacific Car and Foundry. The contract was awarded to FMC. A single contractor was selected rather than several competitive contractors since the components to be used on MICV, with the exception of the gun, are already proven components.

The gun is to be the BUSHMASTER - a new stabilized automatic weapon now undergoing a



Fig. 3 - Utility Helicopter (UTTAS).

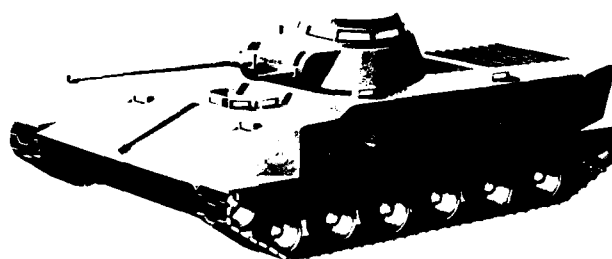


Fig. 4 - Mechanized Infantry Combat Vehicle (MICV).

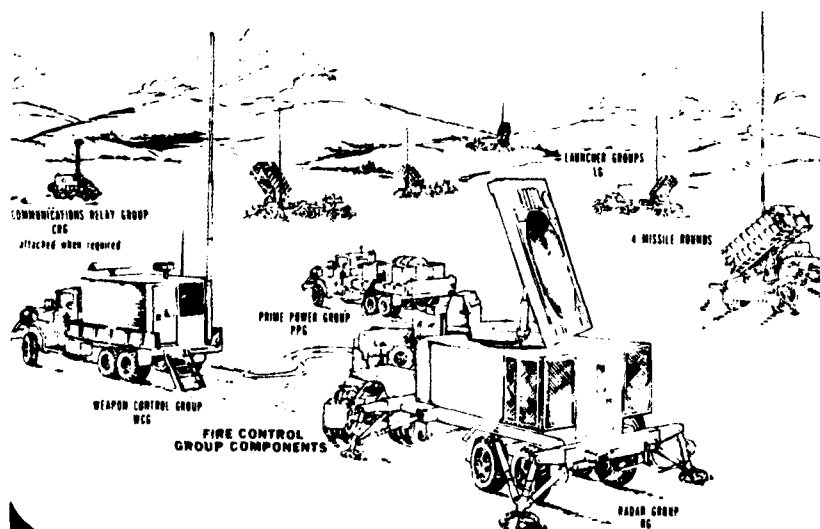


Fig. 5 - Air Defense Missile System (SAM-D).

competitive development effort by several contractors. It will be in the caliber range of 20-30mm and considerably more effective and more armor penetrating than current guns.

The shock and vibration problems of the MICV are similar to the Main Battle Tank and there will be unique problems associated with the 20-30mm automatic weapons. Combat vehicles in general have been described by some as having a built-in self-destruct capability. This is a very apt description. Wherever a threaded fastener is used on these vehicles - be they on wheeled or to a certain extent tracked vehicles - there is an almost certainty that over a period of time they will work loose. This problem can be attacked in two ways. One is to design the springs and tires so that the vibration body is damped and the energy absorbed at these points. The other is to use self-locking threaded fasteners, or those with fine threads, which are expensive solutions and which complicates the maintenance function. The XM746, Heavy Equipment Transporter is a good example. Much design effort and testing has been devoted to improving the springs, tires and shock absorbers to dampen the vibration and absorb road shock energy. Fasteners have been working loose in the axle cover plates, axle carriers, wheel lugs, door striker - you name it - and there has been a problem. On our M60 series tanks there has been trouble with both welded and bolted brackets and locks for the driver hatch. A great deal of assistance is still needed in these areas for the design of future vehicles and the improvement of current ones.

Air Defense Missile System (SAM-D) (Figure 5)

SAM-D is the Army's advanced surface-to-air missile system being developed to provide air defense for the Field Army in the 1980s. It will replace both the Hercules and Hawk systems and it could also be used to complement the defense in CONUS.

SAM-D evolved from studies dating back to 1960. The program was officially renamed SAM-D in October 1964. Advanced development began in 1967 and lasted for 4½ years. We are presently in the engineering development phase. SAM-D will have increased fire power through its multiple target engagement capability. The NIKE HERCULES and Improved HAWK fire units have the capability of engaging only one target at a time, whereas a SAM-D fire unit is capable of engaging many targets simultaneously. SAM-D will be mobile, have short reaction time, be highly effective in an ECM environment, and be able to survive on the future battlefield. The system will be complemented by improved short range air defense systems, such as STINGER (REDEYE II) and VULCAN/CHAPARRAL, to provide overall air defense of a theater of operations. Advanced automation and improved reliability and maintainability techniques will result in lower personnel requirements and operating costs compared to the HERCULES and HAWK systems which it will replace.

The question of SAM-D survivability has been raised relative to its single multifunction phased array radar. The SAM-D radar performs the functions now requiring ten radars in the HERCULES and HAWK systems. The HERCULES and HAWK systems, with several rapidly rotating radar antennas, and the closeness of missile launchers to the radars, results in a very distinct signature on the battlefield. The SAM-D radar antenna does not rotate and can be easily camouflaged. Its launchers can be located at a much further distance thus reducing its signature as a SAM site and making it more difficult to be detected, thereby reducing its vulnerability. Its mobility permits frequent redeployment which reduces its being targeted.

RDTE Program Thrust Areas

In addition to these specific hardware development programs the Commander of AMC has, in coordination with the Commodity Commands, reviewed all of our on-going research and development programs to determine those areas where the greatest possibility for breakthroughs exist and those that are most urgently needed to meet future threats. These have been identified as RDTE program thrusts or major thrusts. It is our intent to provide our highest priority and fullest funding in these specific areas.

These thrusts fall into seven major categories, as follows:

1. Munitions
2. Weapons
3. Electronics and Communications
4. Missiles
5. Air Mobility
6. Tanks and Automotive
7. Mobility Equipment

This breakout follows the functional organization of our Commodity Commands as you would expect. Let me discuss then briefly the areas we intend to emphasize and exploit within each of these categories.

Munitions

In munitions a prime concern is improved anti-tank munitions. As the ability to penetrate armor has improved so has the penetration resistance of the armored vehicles. New techniques are being developed constantly to improve armor plate and to defeat the shaped charge. Looking ahead to the future we must assume that these protective capabilities will increase and anti-tank munitions must keep pace. A second area of concern is the need for improved warning and protective devices against chemical and biological agents. A third area is the requirement for mass scatterable mines. In the environment of future battlefields featuring highly mobile ground forces it is necessary that mine fields be laid in a hurry.

Weapons

In the field of weapons several specific future requirements exist that deserve high priority. The first is the need for an improved infantry anti-tank weapon and the second is the need for a low altitude air defense gun.

Emphasis in artillery is upon soft recoil to reduce the shock of firing. Another area of special emphasis is upon aircraft weaponization and this field has many shock and vibration factors to consider.

Electronics and Communications

Electronics and Communications will focus upon more secure communications, weapons detection and location, and night vision. Night vision systems encounter severe shock and vibration problems when mounted upon crew served weapons, combat vehicles and helicopters.

Missiles

In the missile area, development is urgently needed in the fields of terminal homing, high energy lasers and free rockets. Equipment and subsystems associated with missiles must endure severe shock and sometimes vibration environments.

Air Mobility

The field of air mobility is also singled out for special attention. Our aircraft must be safer and be more survivable on the battlefield. Improvements are needed in the propulsion systems to increase the power to weight ratio and decrease fuel consumption. This relates also to the rotors and other systems which must be improved. Overall, the maintainability and reliability of aircraft must be improved and careful consideration must be given to the fatigue factors introduced by shock and vibration.

Tanks and Automotive

Our tank and automotive system must also be improved. We need improved armor protection and a reduction in the signatures of our equipment whether it be the optical, radiation or acoustic signature. Their propulsion problems are similar to those of aircraft reduced weight, increased power, longer range and, in today's environment, reduced pollution.

Mobility Equipment

Here there are three more areas being emphasized. These are camouflage, improved electric power generation, and mine detection and neutralization. Your attention is invited to electric power generators. Those using gasoline or diesel drive sources are particularly susceptible to adverse shock and vibration factors.

Program Management

All of you have no doubt heard some of the complaints that were hurled against the Defense Department's Materiel Acquisition System - involving such things as cost overruns, delays, failure of systems to perform, etc. Whether or not any or all of these were justified is after the fact. The name of the game of the past 18 months has been "change the system". Well, there are certain things that can be changed and certain things that cannot. Pregnancy takes nine months, no matter how many men you put on the job. So it is with the acquisition process that extends from concept formulation till its death. Our recent management changes are designed to give major programs a gestation period of about six years. Whether it is a practical goal in all cases remains to be seen but it is an objective that we will certainly attempt to meet.

It is difficult to think of any significant military system within the Army that does not require serious consideration of shock, vibration and/or noise factors. Your organization serves as the focal point and scientific information center for the services in these critical areas and your assistance in the future is as necessary as it has been in the past if we are to field effective military hardware.

This then is a summary of our major hardware programs and RDTE thrusts and an insight into the management changes being made. It has been a pleasure to address you and I wish you success in your symposium and another 25 years of outstanding service and support to the Department of Defense.

SUBMARINE SHOCK TESTING

UNDERWATER EXPLOSION TESTS WITH THE SWEDISH FULL-SCALE TEST
SECTION 'STÅLMYGGAN'. PART I: TEST SECTION WITH OBJECTS AND
MEASURING POINTS, ARRANGEMENTS AND DIMENSIONAL MEASUREMENTS

Herbert Nilsson
Kockums Mekaniska Verkstads AB
Naval Department
Malmö, Sweden

The Royal Swedish Navy carried out underwater explosion tests against the full-scale test section 'Stålmyggan' during Spring 1972.

The tests were performed in order to obtain:-

Basic data for design shock spectra for submarine equipment, with regard to item weights, internal or external mounting etc.

Pressure wave distribution in tanks and internal piping.

Effects on hull welds from built-in imperfections.

Permanent deformations of the hull.

The test section, 8 m in length and 6 m in diameter with ballast tanks fore and aft, was designed to resemble the mid-section of a submarine.

The test section was fitted out with measuring gear for various shock parameters and also with various test objects.

BACKGROUND

Previous Swedish Standards regarding the shock resistance of submarines were based on assigning each part of the submarine to a specific shock class, and each shock class being allocated fixed design values known as Shock Numbers.

From the mid-sixties a number of explosion tests against submarines and sections of submarines have been carried out in Sweden, where shock parameters have been measured electronically, mostly by means of piezo-resistive accelerometers.

The results from these experiments have been used for establishing new shock standards based on shock spectrum theories. Based on these studies each shock class has been allocated a specific design shock spectrum.

In order to obtain improved grounds for these standards it was decided in 1970 to carry out a further set of explosion tests.

In addition to measuring various shock parameters, materials and structures intended for the next type of R.Sw.N. submarines, should be shock tested.

In order to gain experiences from welding a new type of steel intended for submarines, a scale 1:1 section of a submarine was constructed. This was subsequently used for the explosion tests and was hence fitted out with test objects and measuring gear.

The test section was christened 'Stålmyggan' ('Mighty Mosquito').

The tests were carried out in April and May 1972 by the R.Sw.N.

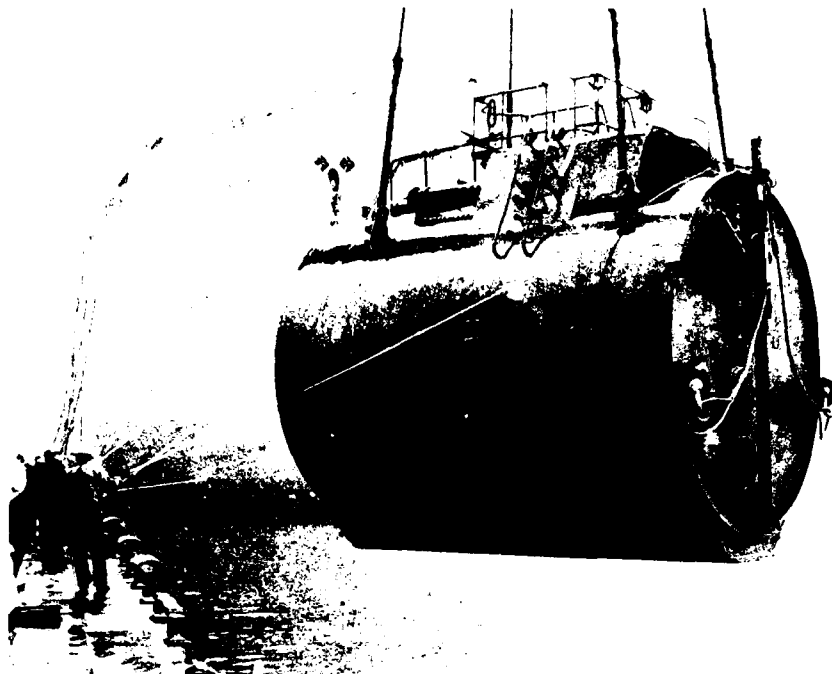


Fig. 1 - 'Stålmyggan' being launched.

MANAGEMENT

The R.Sw.N. appointed Kockums Mekaniska Verkstads AB (Kockums' Engineering Works Co. Ltd.) in Malmö to design and construct the 'Stålmyggan'.

The explosion tests were supervised by the R.Sw.N. in cooperation with Kockums Mekaniska Verkstads AB (KMV), Försvarets Tekniska Laboratorium (Military Electronics Laboratory) (FTL), Stockholm, and Akustikbyrån AB (AKB) (Noise, Vibration and Shock Consultants), Stockholm.

COSTS

	Sw. Kr.	US \$
Hull section including development of manufacturing methods	1,100,000.-	245,000.-
Additional work and outfit for converting the hull section to a test section	980,000.-	210,000.-
Development of measuring methods and subsequent measurements	170,000.-	40,000.-
Blasting tests and analysis (including equipment and personnel)	365,000.-	80,000.-
Total approx.	2,600,000.-	575,000.-

GOALS

When planning the explosion tests against the 'Stålmyggen' the following results were aimed at:-

General

Shocks corresponding to the requirements for Swedish submarines should be attained.

Measuring Methods

Further development of methods for calculating shock spectra from shock acceleration measurements.

Development of methods for measuring shock accelerations and fast strain rates.

Shocks

Obtaining basic data for design shock spectra for submarine equipment with regard to item weights, internal or external mounting etc.

Confirmation of assumed shock class subdivisions.

Pressure

Investigations of hydrodynamic shock pressure propagation in tanks and internal piping.

Determination of design pressures for externally mounted items.

Hull

Investigation of the shock resistance of various hull designs.

Confirmation of the suitability of a new steel quality for submarine hulls.

Investigation of built-in hull defects.

Parts and Components

Determination of shock deformations of the hull and of displacements of shock isolated parts and items.

Explosion testing of various system components for submarines.

Design Methods

Confirmation of calculation methods for shock resistance design.

RESULTS

Available results from acceleration measurements are discussed in Part III of this Report. However, certain results mainly concerning the hull structure are discussed in Part I below.

ARRANGEMENT OF TEST AREA

Test Area

A protected place in the Swedish archipelago was chosen as test area.

Preparations

The 'Stålmyggen' was secured between buoys as shown in Figure 2.

The 'Stålmyggen' was controlled by means of filling and draining the external ballast tanks using compressed air from a shore supply.

Buoyancy

The amount of water in the internal ballast tanks was adjusted to produce a buoyancy of approx. 1.5 tons with the external tanks filled.

An external ballast weight of approx. 2 tons was suspended underneath the 'Stålmyggen'. On filling the external tanks the 'Stålmyggen' sank until the external ballast weight touched the bottom. The diving depth of the 'Stålmyggen' could hence be set by simply adjusting the lengths of the wire ropes carrying the external ballast.

Explosion Distances

The charges were suspended from buoys and the distance to the 'Stålmyggen' was set by tying the charges to the 'Stålmyggen' mooring wire ropes.

Transfer of Signals

Signals from the various sensors were taken from the 'Stålmyggen' to a shore-based measuring centre by means of cables suspended above water between buoys.

STÅLMYGGAN

"MIGHTY MOSQUITO"

Securing and Mooring Arrangements

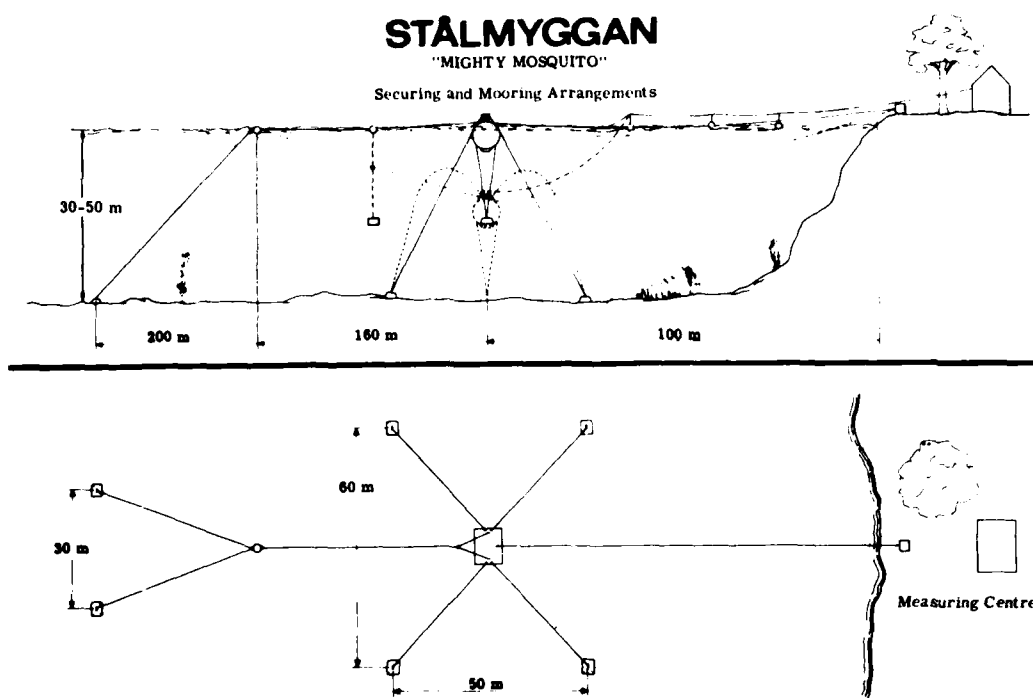


Fig. 2 - Mooring Plan.

EXPLOSION SCHEDULE

Twentyone charges, each consisting of 100 kgs 'Hexotonal', were detonated around and above the 'Stålmyggan', see Figure 3.

'Hexotonal' is developed from TNT and produces a pressure wave impulse which is approx. 30 percent higher than that of TNT.

The explosion distances were chosen to obtain a severity corresponding to the requirements for R.Sw.N. submarines.

HULL TEST SECTION

General

The hull test section 'Stålmyggan' was designed to resemble the mid-section of a modern Swedish submarine. The section was built to enable production methods for a new submarine steel to be tested and for carrying out full scale explosion test against it.

Hence there are included frames, bulkheads, shear plates, external keel, casing, access hatch, torpedo tube parts etc. See Figure 4.

Ballast tanks are fitted fore and aft, with openings to the sea as well as connections for compressed air controlling the 'Stålmyggan'.

Inside the 'Stålmyggan' there are internal ballast tanks which, however, have no connection with the sea. The tank top forms the platform.

The construction of the 'Stålmyggan' and its main dimensions are shown in Figure 5. Its total weight was 120 tons.

Steel

The 'Stålmyggan' is built of a carbon-manganese steel, grain-refined with vanadium and niobium. The yield point is approx. 430 N/mm².

This steel quality will be used for the next type of R.Sw.N. submarines.

The steel analysis is as follows (in percent):-

C	0.20	V	0.10
Mn	1.60	P	0.030
Si	1.45	S	0.030
Nb	0.035	N	0.020

The schematic diagram shows a mechanical assembly with several components labeled with numbers 6 through 16. On the left, there are three vertical pins labeled 7, 8, and 13. Below them are horizontal dimension lines indicating distances of $2D$, $\sqrt{2}D$, and D . A central rectangular component has a pin labeled 12 at its bottom center and another pin labeled 16 above it, with a vertical distance R between them. To the right of this component is a horizontal row of four pins labeled 12, 9, 6, and K 1 from left to right.

Certain cracks and slag enclosures have been left on purpose in bulkhead and hull plating joints. See Figure 8.

General Results

One interesting result was also that an ordinary fillet weld between frames and hull proved completely satisfactory.

R.S.W.N. Acceptance Standard for submarines will be modified accordingly.

The 'Stålmygga' was fitted with a number of test objects, intended for R.S.w.N. submarines, see Figure 9.

Other items have been designed to comply with existing standards and the tests should confirm the validity of the design methods. With regard to this, only small safety factors had been employed.

DIMENSIONAL MEASUREMENTS

As the design of the 'Stålmygga' closely resembles a modern R.S.W.N. submarine,

Design Principles

Hence different bulkhead thicknesses, different stiffening methods, different stiffener connections, different placing of shear plates and so on have been used.

The weld joints between frame webs and hull plating have been carried out with varying degrees of penetration, i.e. from a double bevel groove with full penetration to a normal fillet weld. See Figure 7.

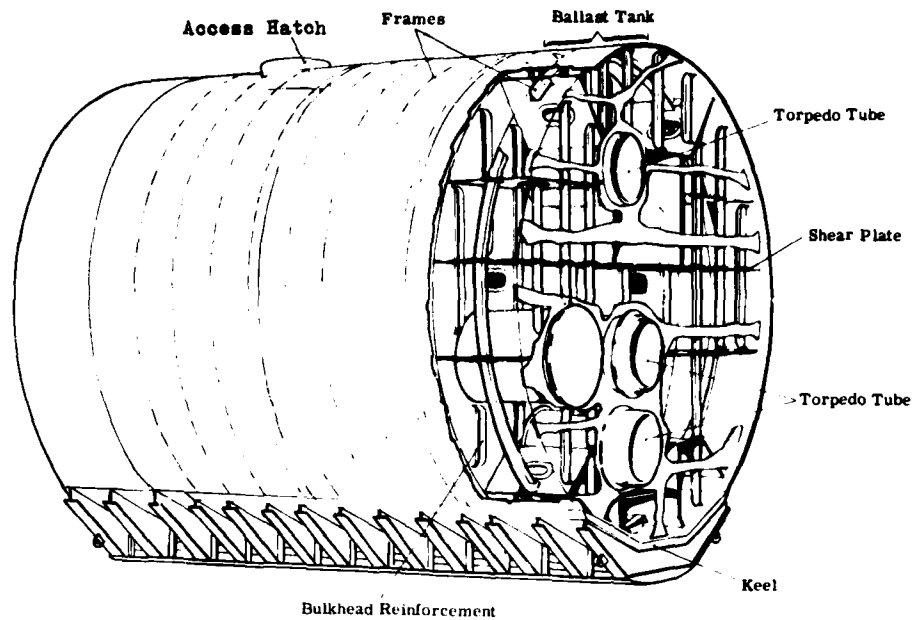


Fig. 4 - 'Stålmyggen'.

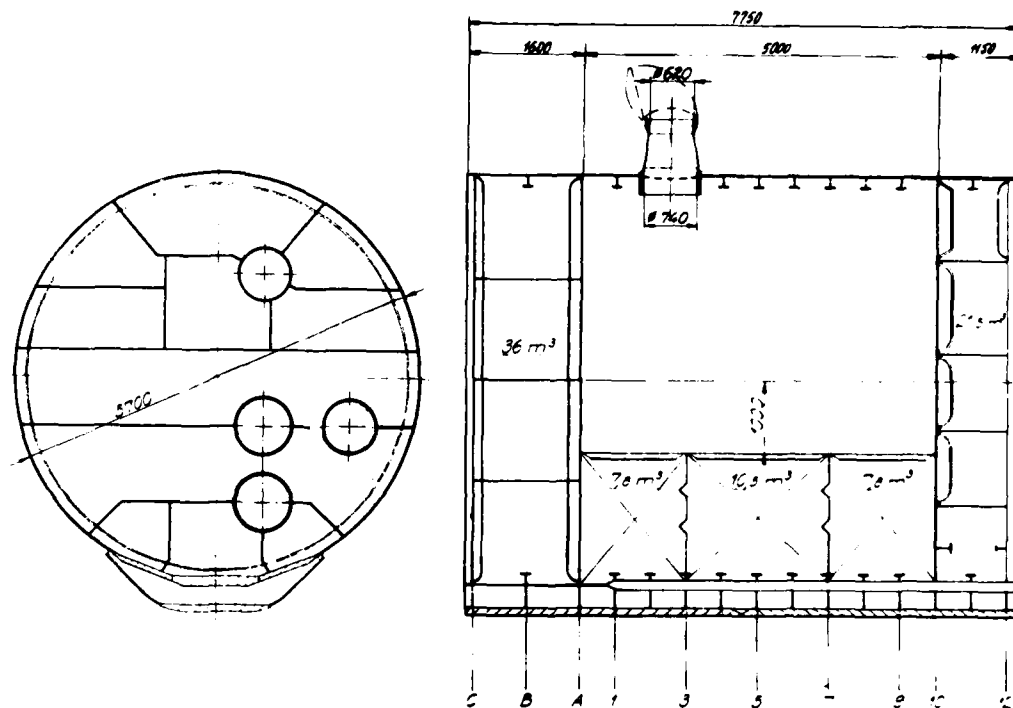


Fig. 5 - 'Stålmyggen'. Main Dimensions.

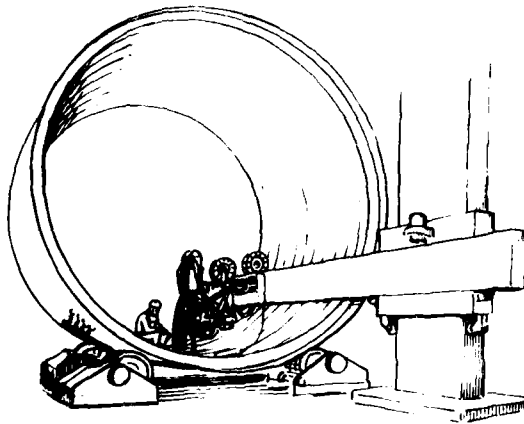


Fig. 6 - Machine Welding.

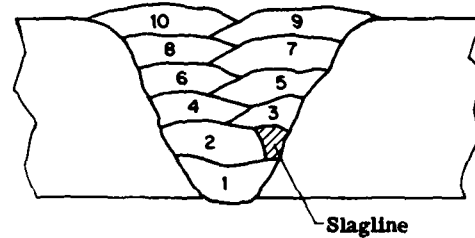


Fig. 8 - Weld Defects in Hull.

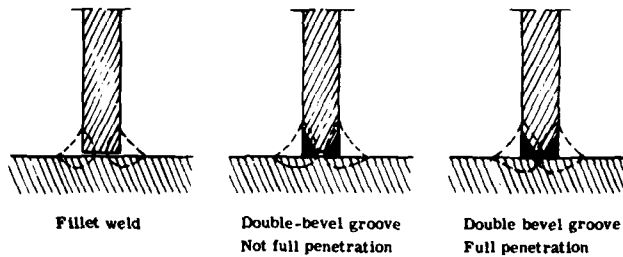


Fig. 7 - Weld between Web and Plating.

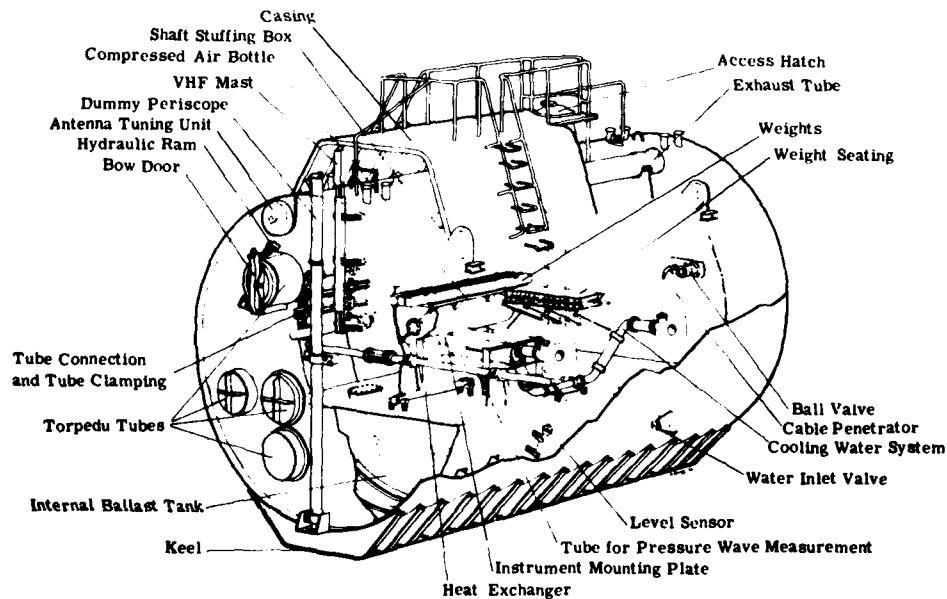


Fig. 9 - 'Stålmyggen' with Test Objects.

permanent deformations of hull and certain objects were measured, such as access hatch and torpedo tubes.

Displacement of shock isolated items was measured by means of soft plastic cones ('Alstick').

Measuring Areas

The hull plating was measured with regard to buckling and out-of-roundness between frames.

The frames were measured with regard to out-of-roundness and warping.

The bulkheads were measured between stiffeners and shear plates.

Torpedo tubes, access hatch, exhaust tubes and hatch covers were measured with regard to shock deformations.

Measuring Methods

Wires

Hull plating, bulkheads and frames were measured between a number (30-50) of fixed points by means of inside calipers. A system of nylon wires stretched internally were used as reference levels. See Figure 10.

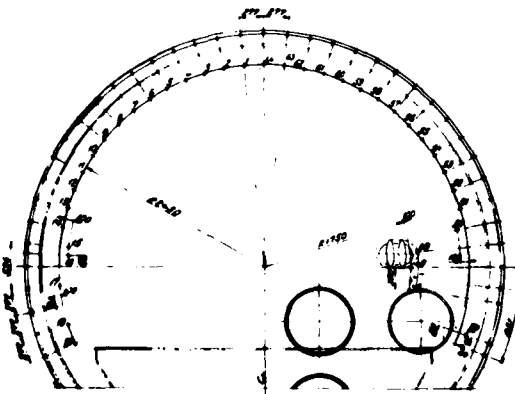


Fig. 10 - Hull Plating Measuring Points.

Chord Instrument

Additionally for measuring the hull plating a wheel-mounted chord instrument was used. This was moved along the hull plating (externally) and the variations in height of arch were measured.

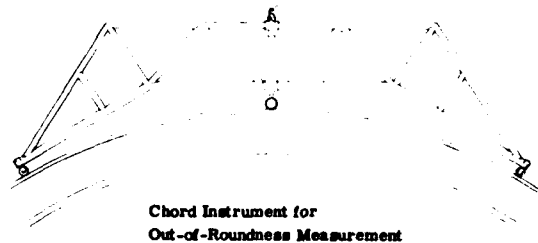


Fig. 11 - Chord Instrument for Out-of-Roundness Measurement.

Ruler

Torpedo tubes and access hatch were measured by means of rulers fitted with dial indicators.

Accuracies

Accuracies for the different methods are as follows:-

Wires	plus or minus	1 mm
Chord Instrument	" " "	0.1 "
Rulers	" " "	0.3 "

General Results

Dimensional measurements on bulkheads and hull plating show how the amount of deformation depends on the distance to the explosion.

The hull plating deformation pattern is related to the distance to a bulkhead, to the presence of heavy masses in the plating such as pads and to circumferential welds.

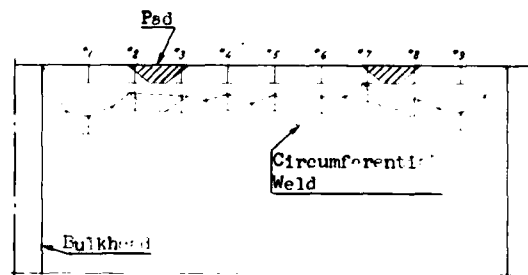


Fig. 12 - Examples of Plastic Deformations as measured during Blasting Tests against 'Stålmyggen'. N.B. Original dimensions and deformations are not referred to the same scale.

The deformation of air-filled tubes depends on the tube dimensions.

MEASURED SHOCK PARAMETERS

General

The following shock parameters were recorded during the tests:-

- (i) Shock accelerations in different directions at 19 points dispersed between hull and test objects, internally and externally;
- (ii) Hydrodynamic shock pressures at 12 points situated on the hull plating, outside the hull and in piping;
- (iii) Elongation at 19 points inside the hull plating and in piping.

Goals

Acceleration measurements were intended for:-

- (i) Determining shock spectra for various component positions;
- (ii) Investigation of the influence of heavy masses on shock spectra;
- (iii) Investigation of the influence from the pressure wave acting on external bulkheads;
- (iv) Investigation of circumferential oscillations in the hull;
- (v) Determining the rigid body movement.

Pressure measurements were intended for:-

- (i) Determining the total pressure impulse at certain points;
- (ii) Determining the pressure wave amplitude and duration versus distance to detonation;
- (iii) Determining the pressure wave amplitude and duration and its propagation properties in tube systems;
- (iv) Checking the uniformity of the detonating charges.

Elongation measurements were intended for:-

- (i) Determining the plastic and elastic elongation versus time in certain places on the hull and in tube systems;

(ii) Determining stresses in certain parts of the hull subjected to pressure waves;

(iii) Investigation of local stresses around built-in hull defects.

Results

The results presented in Part III are based on the above measurements.

ACCELERATION MEASURING POINTS

The measuring directions were defined by a coordinate system, see Figure 13.

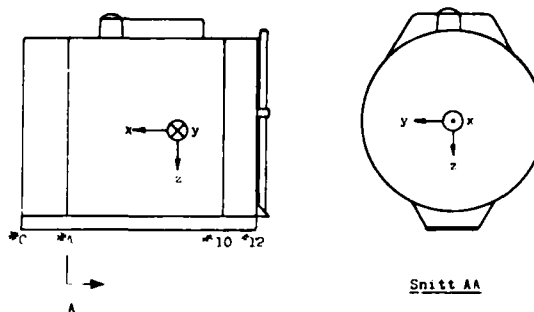


Fig. 13 - Measuring Coordinates.

In hull areas having light mass loading measurements were made according to the table below:- (See Figure 14.)

No.	Test Object	Measuring Directions
A1	VHF mast, top	x, y, z
A2	Ditto, mounting point	x, y, z
A3	Dummy periscope, top	x, y, z
A4	Bulkhead of water-filled tank	x
A5		
A6	Frames	y, z
A7		
A8	Circular torpedo tube	x, y, z
A9	Circular torpedo tube	z
A10	Bulkhead	y, z

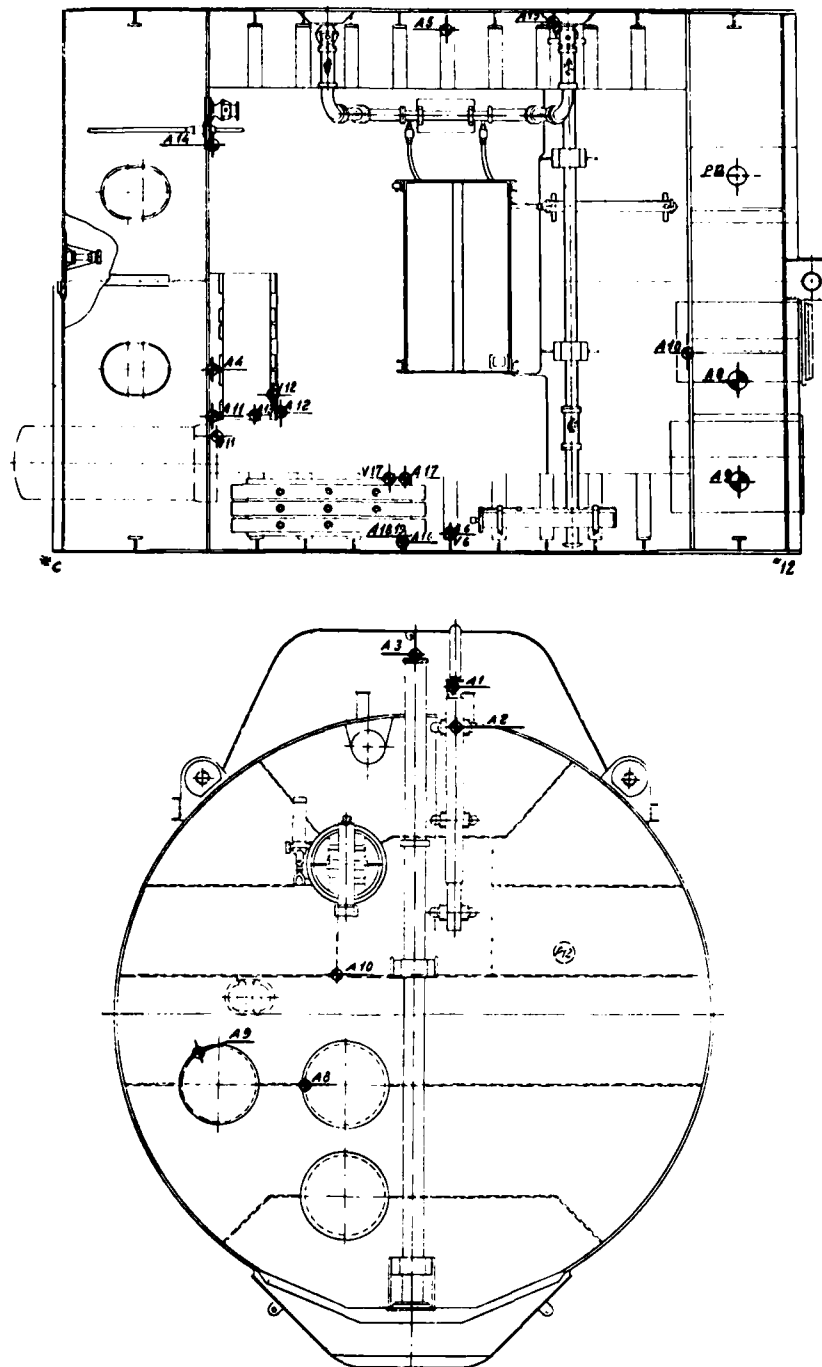


Fig. 14 - Location of some Measuring Points.

In hull areas having heavy mass loading measurements were made as follows:- (See Figure 14.)

No.	Test Object	Measuring Directions
A11	Seating base on plating	x, y, z
A12	Seating for shock isolated item	x, y, z
A13	Shock isolated item	x, y, z
A14	Bulkhead pad	x, y, z
A15	Hull plating pad	x, y, z
A16	Frame adjacent to seating	x, y, z
A17	Seating welded to hull plating	x, y, z
A18	Frame adjacent to mass	y, z
A19	loaded seating	

The 'Stålmyggan' rigid body movement should be determined by means of the results from the following acceleration measuring points:-

Movement	along the x-axis from A8
"	" " y- " " A10
"	" " z- " " A10
Rotation	around the x-axis from A5 + A6
"	" " y- " " A10 + A4
"	" " z- " " A10 + A4

PRESSURE MEASUREMENTS

Hydrodynamic shock pressures were measured at 12 measuring points, in internal pipe systems connected to the sea, in a ballast tank and in external points.

Pipe Systems

Figure 15 shows the measuring points in one of the internal pipe systems of the 'Stålmyggan'.

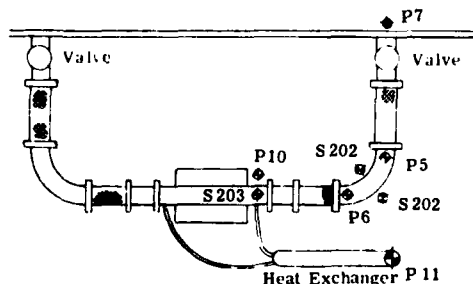


Fig. 15 - Location of Pressure Sensors and Strain Gauges in Pipe Systems.

Ballast Tank

The shock pressure was measured at measuring point P12. The sensor was fitted at various distances from bulkhead No. 10.

Outside the Hull Plating

Pressure measurements were made at one measuring point (P8) located between the hull and the explosion charge and at another measuring point (P9) close to the hull.

Results

Pipe Systems

Where the pressure wave had passed through rubber hoses and pipe bends pressure pulses with comparatively high peak pressure were measured. Elongation measurements in these places also showed that these pulses deformed the piping plastically.

Ballast Tank

Pressure measurements in the ballast tank showed that on passing a bulkhead surrounded by water the peak pressure of the pulse was reduced and its duration increased. Thus the bulkhead showed not to be completely transparent to the pressure wave.

Outside Pressure Hull

Results from measurements of external pressures are used in Part III.

ELONGATION MEASUREMENTS

Pipe Systems

Strain gauges were fitted in pipe bends and in straight pipe pieces. Elongations due to the pressure wave were recorded, see Figure 15, as described above.

Hull

Strain gauges were fitted on faultless hull parts as well as in places where various welding defects had been built-in or left untouched. See Figure 16.

Strain versus time was recorded as was remaining elongation after blasting, i.e. dynamic measurements and static measurements respectively.

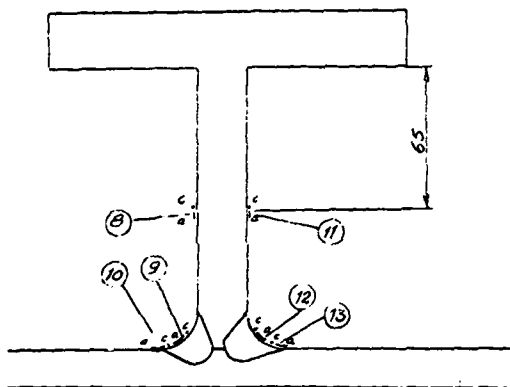


Fig. 16 - Strain Gauge Location of an Imperfectly Penetrating Weld.

Results

Strain rate hardening was found to be fairly common and stress levels up to the order of twice the static yield strength were measured in points where no local plastic deformation could be detected.

NOTE: Discussion on this paper follows paper by Mr. Spang.

UNDERWATER EXPLOSION TESTS WITH THE SWEDISH FULL-SCALE SUBMARINE
TEST SECTION "STÅLMYGGAN": RECORDING AND DATA REDUCTION SYSTEM

L Westin and A Henningson
Military Electronics Laboratory
Stockholm, Sweden

For measurements made at the underwater explosion test with the test section "Stålmyggan" piezoresistive accelerometers, strain gages and pressure gages were used. With respect to the dynamic limitation of the recording system the signal from the accelerometer was split into one low-frequency signal and one high-frequency signal. The shock spectra from the two signals overlapped each other accurately in a medium frequency range. The accelerometers were protected from damage at explosions from the shortest distances by means of mechanical filters. All acceleration signal were digitized for further analysis in a digital computer.

INTRODUCTION

The measurement programme at the "Stålmyggan"-tests in 1972 was more extensive than the measurement programmes at earlier Swedish underwater explosion tests. A measurement system was developed which in certain essential respects differed from systems used at earlier tests. As concerns the acceleration measurements, for example, high requirements were put on the resolution in the high-frequency as well as in the low-frequency range as shock spectrum analysis was to be performed within the frequency range 1 cps - 3,000 cps. When studying the results from earlier underwater explosion tests it appeared that the available tape recording systems did not satisfy the dynamic range requirements of severe measurement locations. In order to get satisfactory measurement accuracy in the whole frequency range, the accelerometer signals were split into one high-frequency and one low-frequency

signal in a manner described below.

Pressure gages and different types of capsules intended for accelerometers in severe measurement locations were designed. The pressure gages were so designed, that the dynamic pressure could be measured in the centre line of pipes, between bulkheads in ballast tanks and in the orifice of hull valves. For accelerometers located outboard, special water-tight capsules were designed and accelerometers in locations where very high acceleration levels were to be expected were mounted on mechanical filters.

DESCRIPTION OF THE MEASUREMENT SYSTEM

In figure 1 a basic block schema for the shock measurements is presented. Figure 2 shows the block diagram of the measurement system. Amplifiers, filters and calibration relays were placed on a shock-isolated table inside the test body. The measurement sig-

nals were transmitted to the land station where tape recorders and other recording equipment were placed. (See preceeding paper by Herbert Nilsson for further details.)

ACCELERATION MEASUREMENTS

In order to obtain acceptable frequency response for low frequencies and to minimize zero shifts in the accelerometer signals a piezoresistive accelerometer - Endevco, type 2261 M6 - was used.

The accelerometers were mounted on fine-grinded cubic steel heads, 39 mm in side (figure 3).

The problem with the dynamic range limitation in the tape recorder system was solved by splitting the output signal from the measurement amplifier into two signals; one high-frequency (HF) signal and one low-frequency (LF) signal (figure 2 and 4). These two signals were treated in different ways. The gain of the measurement amplifier was adjusted so that the HF-signal could be transmitted and recorded without further adjustment. The LF-signal, on the other hand, was lowpass-filtered and further amplified before transmission to the tape recorders in the land station. The slope of the filters used at this process was 12 db/octave and the 3 db cut-off frequency was 150 cps.

At severe measurement locations the accelerometers were mounted on mechanical filters in which way excitation of the transducer resonance (figure 5) was avoided. The resonant frequency of these shock mounts was about 12,000 cps with an amplification of 2.5 to 3 at resonance.

At an early stage in the test program, signals from accelerometers mounted on mechanical filters were compared to signals from normally mounted accelerometers. The

results from these comparative tests are presented below.

Before and after each detonation the measurement system was calibrated by introducing shunt resistances in the measuring bridge of the amplifier, thereby simulating an acceleration.

PRESSURE MEASUREMENTS

A block diagram of a pressure measuring channel is shown in figure 6. Different types of transducers and associated electronics were examined. A piezoelectric crystal fabricated by Crystal Research was found suitable. The crystal (1/8 inch tourmaline crystal) was connected to the end of a coaxial cable and then embedded in polyurethane (figure 7). By this arrangement the crystal was mechanically isolated from the walls of the pipes and could easily be installed in the centre line of pipes. The amplifier used was Endevco Charge Amplifier, type 2760.

In order to avoid distorsion of the measurement signals owing to the big capacitance of the signal cable, the signals had to be low-pass filtered and amplified before transmission to the land station. The cut-off frequency of the RC-filters used was 60,000 cps.

STRAIN MEASUREMENTS

The block diagram of a strain measuring channel is shown in figure 8.

For measuring strains a gage fabricated by Tokyo Sokki was used.

THE LAND STATION

The instrumentation in the land station included three analog tape recorders, each with 14 channels, one time code generator,

calibration switches and an oscillograph. The FM-systems of the tape recorders were used and the recording speed was 60 inches per second which implies that the frequency range d-c to 20,000 cps was covered. To be able to compare the data on all recorded channels at a given instant and to correlate these data with external events, a common time code signal was recorded on the magnetic tapes. The carrier frequency of the code used (Irig Format A) is 10,000 cps which gives a resolution of 0.1 millisecond. This code also could be used for controlling the digitalization process which was performed in a digital computer.

One additional channel was used for spoken information.

ROUTINES OF ANALYSIS

Immediately after each detonation the shock signals were transcribed from magnetic tape to oscillographic form. When analyzing the oscillograph records, errors in the measurement system could be detected at an early stage.

ACCELERATION MEASUREMENTS AND SHOCK SPECTRUM ANALYSIS

In order to make further analysis of the acceleration shock signals in digital computer possible, the analog signals on the magnetic tapes had to be converted to digital form. This analog to digital conversion was performed at a computer station, located at the Research Laboratory of the Swedish National Defence, immediately after each test.

Before A/D-conversion the signals were lowpass-filtered. The HF-signals were filtered at 3,000 cps and the LF-signals at 300 cps. The signals were then digitized with the frequencies 25,000 cps and 5,000 cps respectively.

PRESSURE AND STRAIN MEASUREMENTS

The shock signals from these measurements have all been transformed from magnetic tape to oscillographic form.

RESULTS OF TESTS ON THE MEASUREMENT SYSTEM

For controlling the reproducibility in the acceleration measurements, two accelerometers were installed opposite each other on the same cubic stud. Analysis of computed shock spectra shows, (figure 9 and 10) that the reproducibility is good in both the high-frequency and low-frequency range. In the high-frequency range, however, some deviations can be observed for frequencies above 2,000 cps.

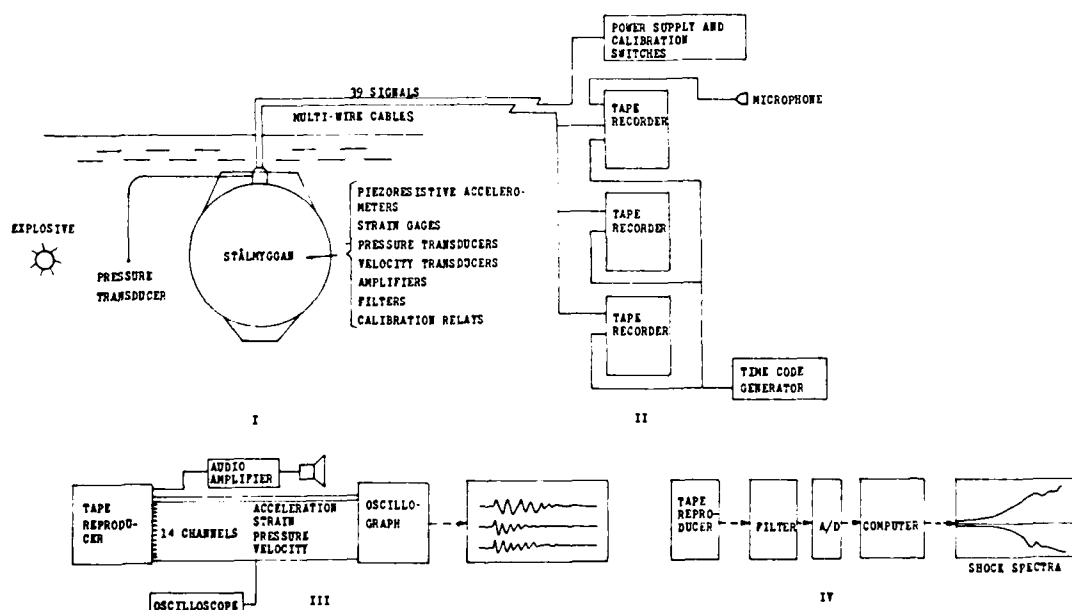
The mechanical filters were controlled in a similar manner. As before, two accelerometers were installed opposite each other on the same cubic stud; one of the accelerometers being installed on a mechanical filter. The deviations observed lie within the limits determined by the reproducibility in the measurements. In figure 11, time histories of signals recorded as described above are shown. The corresponding shock spectra are presented in figure 12 and 13.

The analysis time in computing shock response spectra was 50 msec for the HF-signals and 500 msec for the LF-signals.

The low-pass filtering process and the dynamic range limitations of the tape recorders mean that some frequency ranges in the shock spectrum analysis are less reliable. For frequencies below about 70 cps, for example, the HF-analysis gives too high levels as the measurement signals are hidden in noise and hum. In the range 70-100 cps the HF- and LF-analysis give coincident values. For higher frequencies the LF-analysis becomes uncertain as phase delay and

filter damping affects the shock spectrum.
The influence of the analysis time on the shock spectrum can be observed in figure 14.

Extensive tests with different sampling frequencies show that stable results for the LF and the HF analyses were obtained at sampling frequencies of 5000 cps and 20,000 cps respectively. Figure 15 demonstrates the influence of a greater sampling rate on the calculated shock spectra; it suggests that the sampling rates employed for routine analyses are acceptable.



Section I includes the shock target and the items installed within it; section II the recording station, section III the reproducing station on the test site and section IV the computer station

Figure 1 - Basic block scheme for the measurements

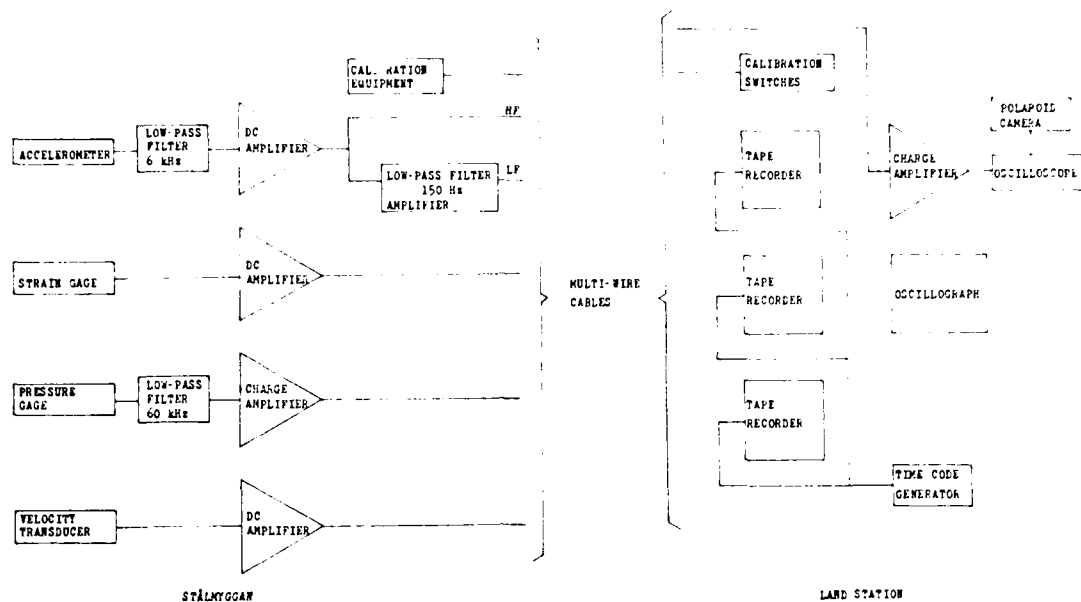


Figure 2 - Block diagram of the measurement system



Figure 3 - Accelerometers mounted on cubic stud. The accelerometer to the left is mounted on a mechanical filter

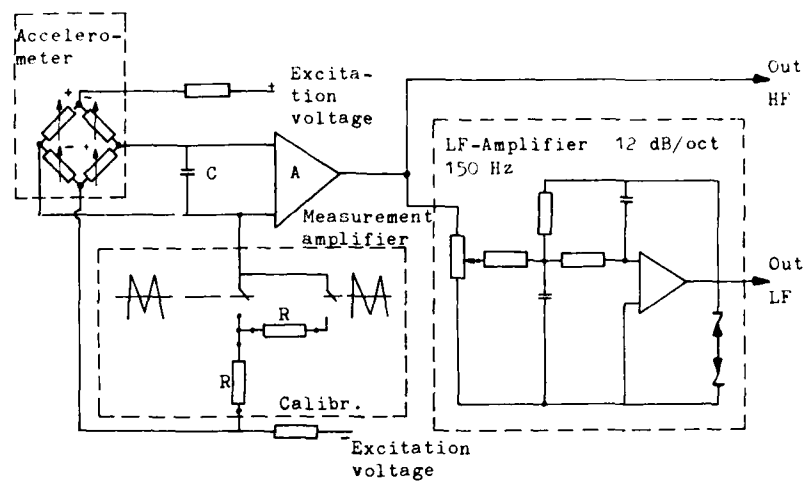


Figure 4 - Block diagram of acceleration-measuring channel

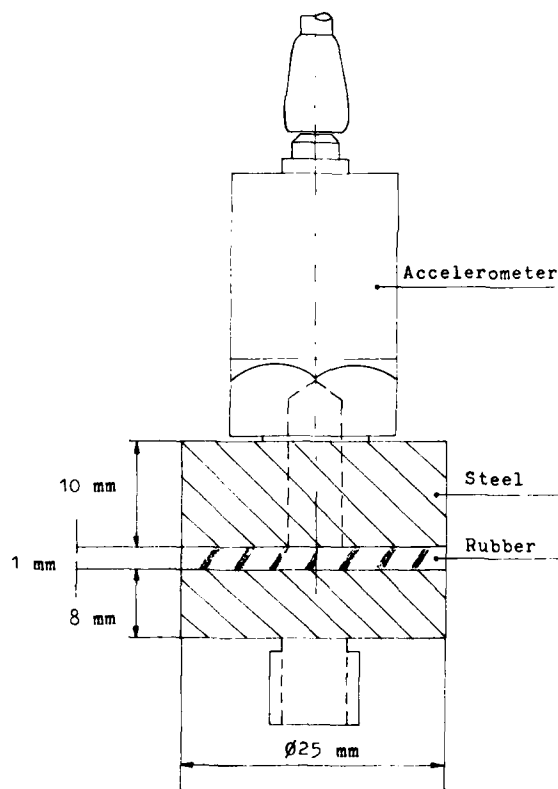


Figure 5 - Mechanical filter

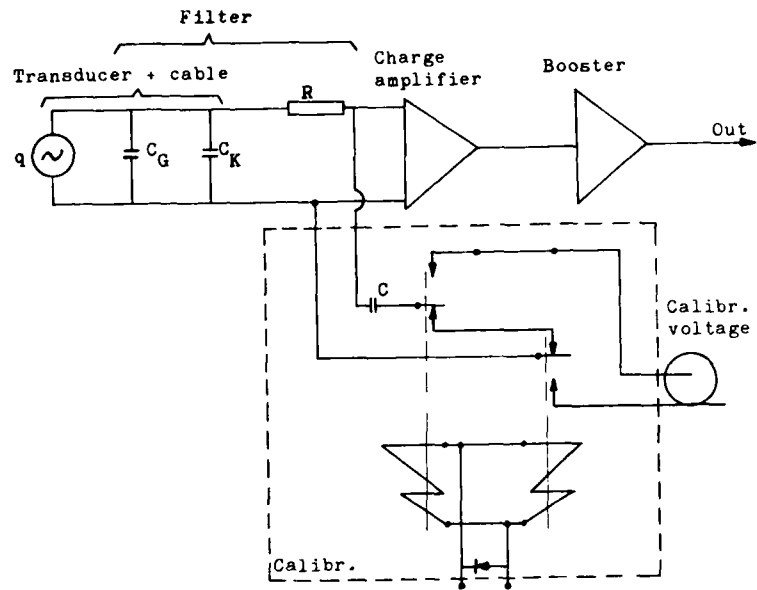


Figure 6 - Block diagram of pressure-measuring channel

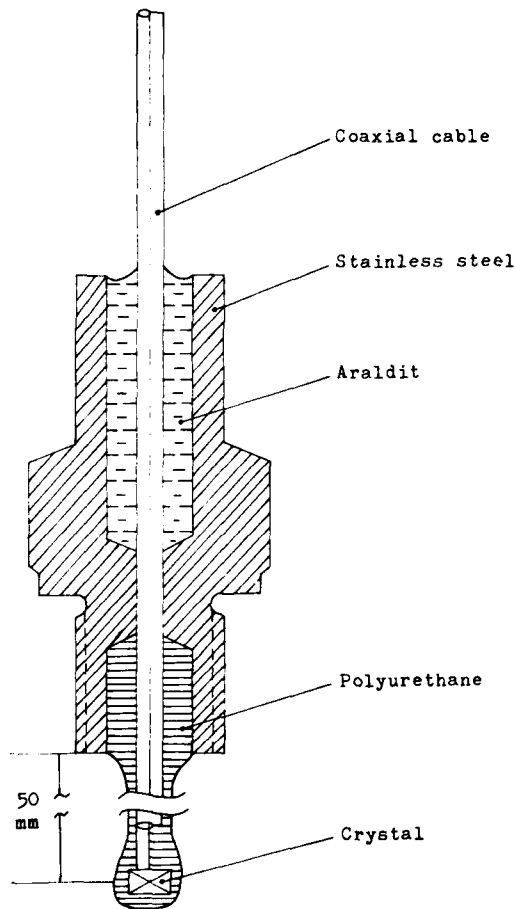


Figure 7 - Pressure transducer

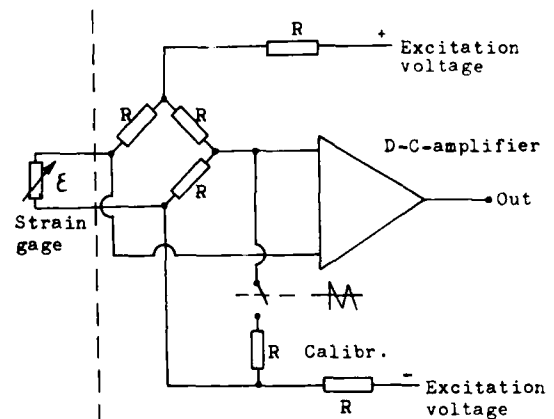


Figure 8 - Block diagram of strain-measuring channel

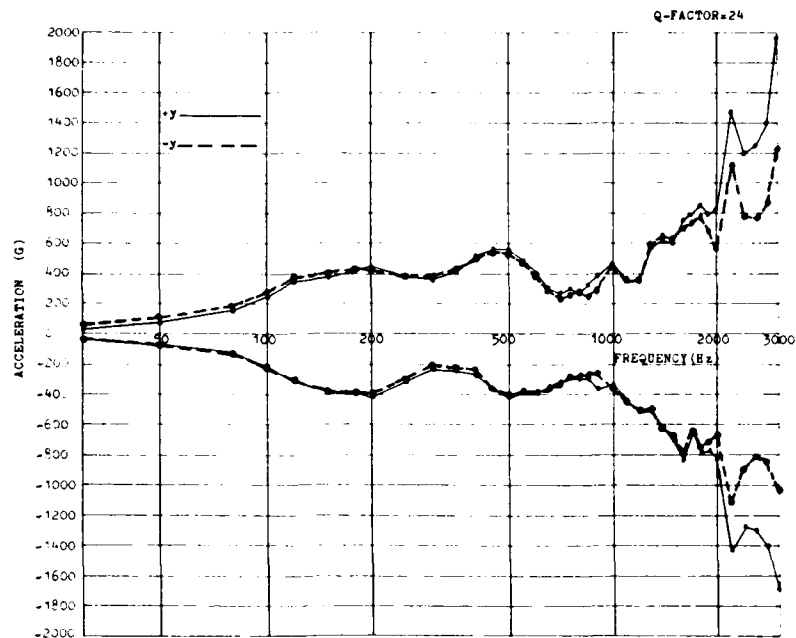


Figure 9 - Shock spectra within the high frequency range

Measurement direction: +y Measuring point: 11
 Shot direction: y

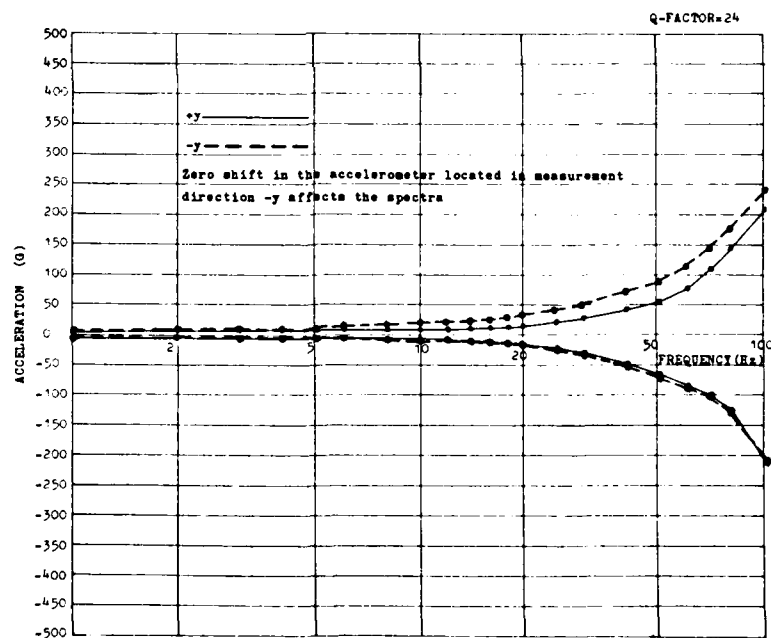


Figure 10 - Shock spectra within the low frequency range

Measurement direction: +y Measuring point: 11
 Shot direction: y

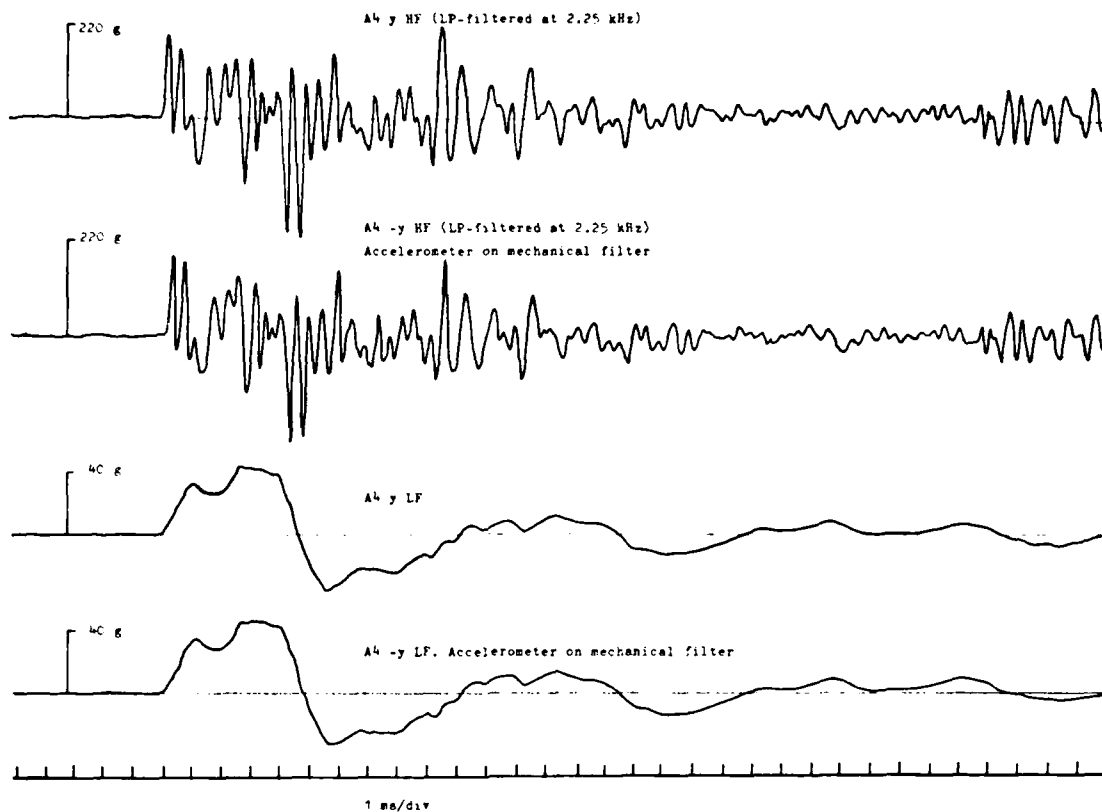


Figure 11 - LF and HF acceleration-time histories

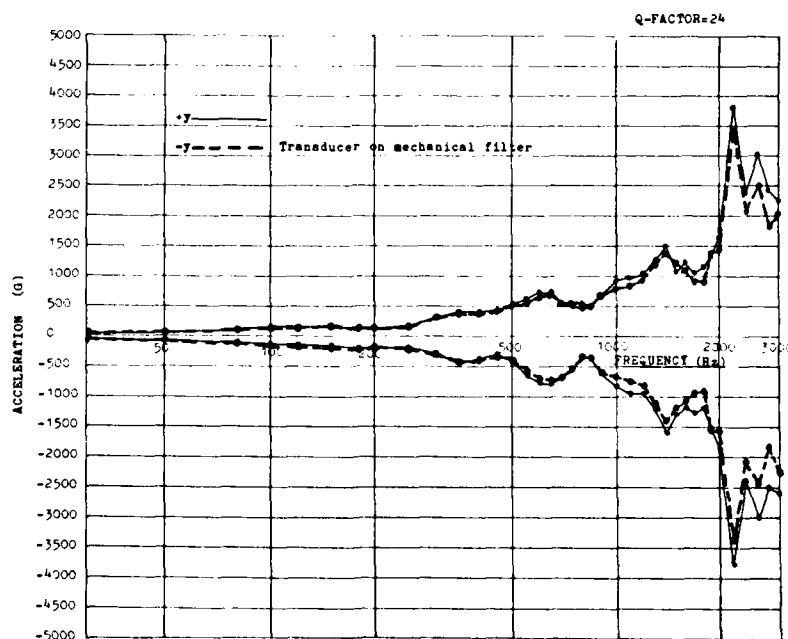


Figure 12 - Shock spectra within the high frequency range
 Measuring point: 4
 Measurement direction: y Shot direction: y

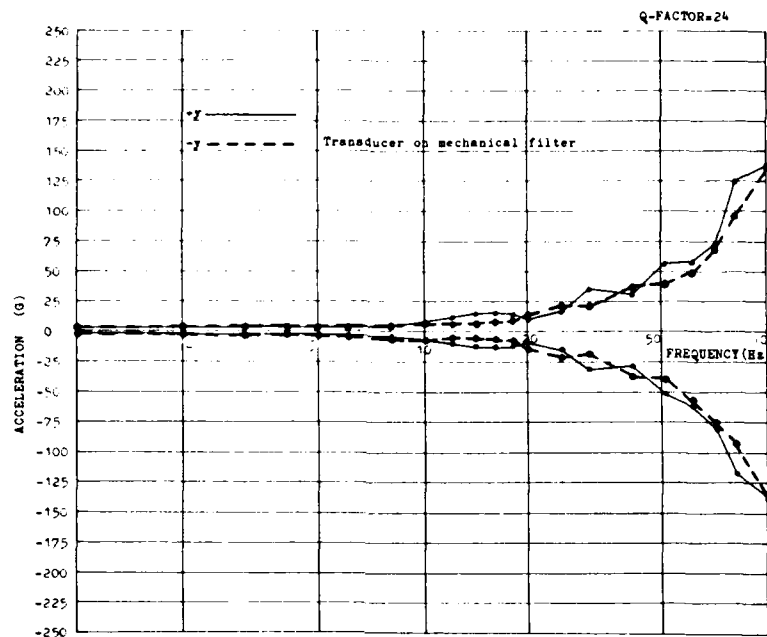


Figure 13 - Shock spectra within the low frequency range

Measuring point: 4
Measurement direction: +y Shot direction: y

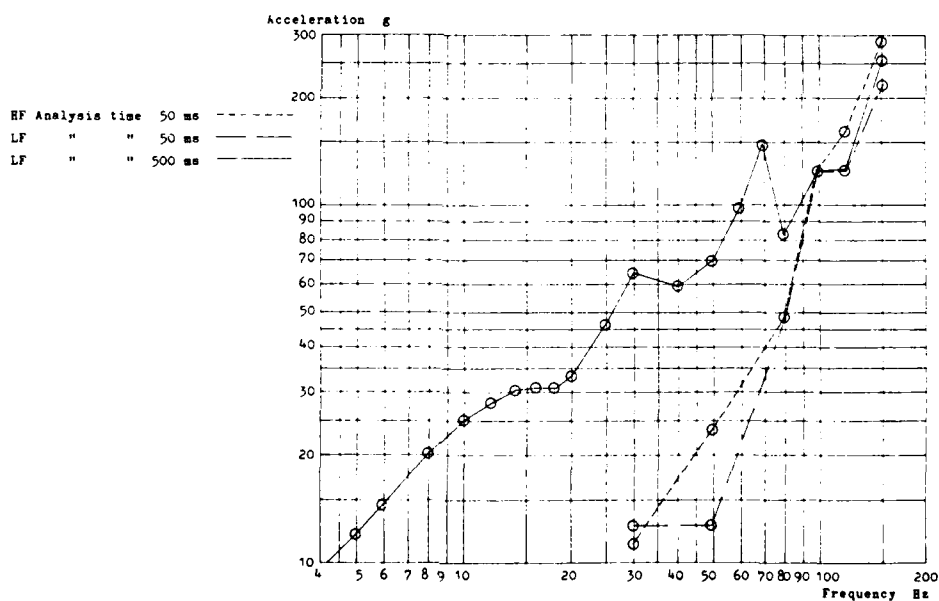


Figure 14 - Measuring point A5 z

Positive shock spectra

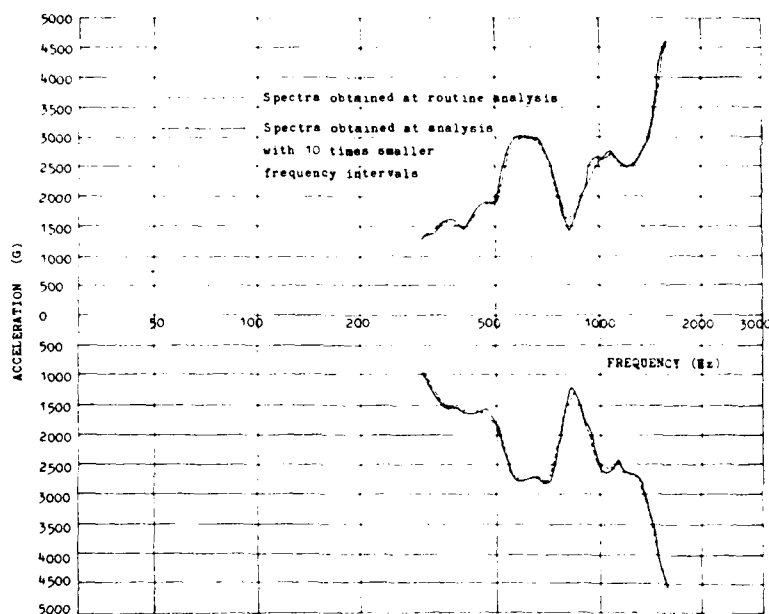


Figure 15 - Shock spectra within the high frequency range
The diagram shows what effect the number of calculation points have on the shock spectra

NOTE: Discussion on this paper follows the paper by Mr. Spang.

UNDERWATER EXPLOSION TEST WITH THE SWEDISH FULL SCALE SUBMARINE TEST SECTION "STÄLMYGGAN": PART III. INTERPRETATION OF RESULTS OF SHOCK MEASUREMENTS

Kjell Spång
IFM-AKUSTIKBYRÅN AB
Stockholm, Sweden

The results of shock measurements made at the underwater explosion test with the test section "Stålmyggan" are discussed together with the methods used for transformation of measured shocks into design parameters. A brief description of the Swedish submarine shock specification is included and the correlation between the results of the measurements and the shock specification is shown to be reasonably good. The influence of the component mass on the shock level, however, seems to be slightly overestimated in the shock specification.

INTRODUCTION

The results of the shock measurements described in the preceding paper by Lennart Westin have been studied in relation to design levels used in Swedish submarine shock specification. Some results of general nature are discussed in this paper in relation to

- general correlation between shock spectra from shocks recorded and corresponding design spectra used in the shock specification
- influence of the component mass on the shock levels in supporting structures for rigidly and flexibly mounted components
- origin of shocks encountered in outboard devices
- variation of pressure and shock levels with explosion distance

GENERAL CONTENT OF THE SUBMARINE SHOCK SPECIFICATION

The following résumé of the Swedish submarine shock design specification is intended to give a broad picture of its basic approach. A full description is outside the scope of this paper.

The shock specification divides the

components into four severity classes, depending on the type of structure to which the component is attached. The shock severity also varies with the direction of mounting in relation to the mounting structure (parallel to, perpendicular to).

Class 0, 1 and 2 relate to components mounted to parts of the ship hull, bulkheads, interior parts (class 2) etc., whilst class 3 relates to components mounted to secondary structures, e.g. big instrument panels. In class 3 the shock analysis is made on the complete component/secondary structure system, using the shock severity of the class relevant to the secondary structure as input. Shock design levels are therefore given only for class 0, 1 and 2, where 0 relates to components mounted to the outer hull and 2 to the inner parts.

A. Severities applicable to design of rigidly mounted components including mounting devices

A static acceleration for design purposes is given as a function of frequency, related to fundamental modes (fixed-base frequencies) of the component, approximated to a simple system of masses and stiffnesses (figure 1).

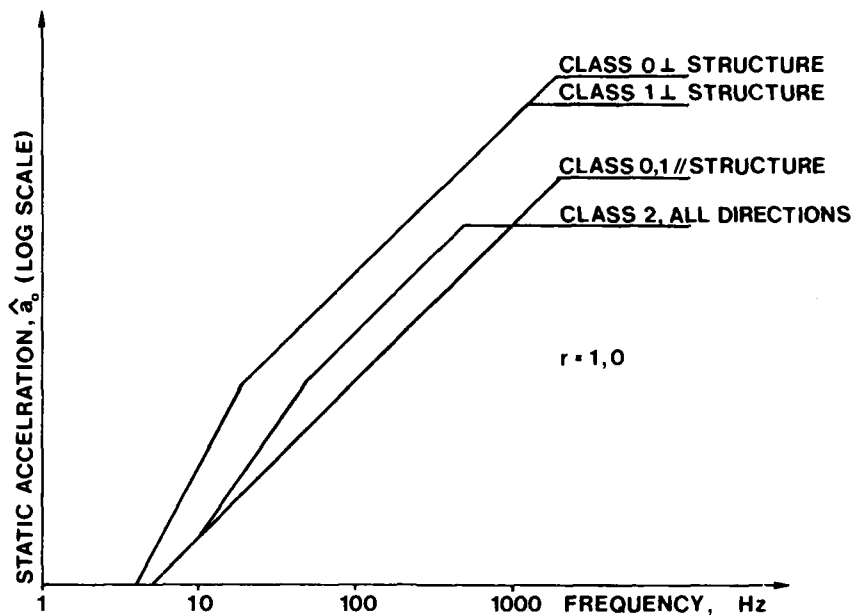


Figure 1. Static acceleration levels for design purposes

The shock encountered in a structure, when the ship is subjected to an underwater explosion, depends on the relationships between the mechanical characteristics of the structure and the mechanical characteristics (masses, stiffnesses) of the components loading the structure. The design levels must therefore depend on these factors. A reduction factor $r(f)$ is used, which is based on simplified assumptions of these relationships. The static acceleration for design, $a(f)$, is achieved from figure 1 as

$$\hat{a}(f) = r(f) \cdot \hat{a}_0(f) \quad (1)$$

B. Severities applicable to design of shock isolated components including mounting devices

For components in class 0 and 1 parallel to the structure and class 2 earlier measurements have indicated that the low frequency response (shock isolation frequencies) can be considered proportional to a certain velocity u_0 with a value independent of frequency. The shock specification therefore defines a velocity u_0 , from which the velocity used for arriving at the severity for a component is achieved as

$$\hat{u}(f) = r(f) \cdot \hat{u}_0 \quad (2)$$

The acceleration of the component is then

$$\hat{a}(f) = 2\pi f \cdot \hat{u} \quad (3)$$

where f is the mounting frequency.

This is valid for the simple case where the movement of the component is primarily translational and the shock isolators are linear. If this can not be assumed a more complicated analysis has to be applied.

For components mounted perpendicular to the outer hull structure (class 0 and 1) the deformation of the structure must be taken into account.

The acceleration level is then (for the simple case considered above):

$$\hat{a}(f) = (2\pi f)^2 \cdot \max(s, \delta_{total}) \quad (4)$$

$$\text{where } s = \sqrt{\delta_{static}^2 + \frac{\hat{u}^2}{(2\pi f)^2}}$$

δ_{static} = static deformation of the structure (residual)

δ_{total} = total deformation of the structure

C. Shock testing severities

The shock testing is based on subjecting the component to a shock, the shock spectrum of which covers the design spectrum in figure 1, multiplied by the appropriate reduction factor $r(f)$.

TRANSFORMATION OF MEASURED SHOCKS INTO DESIGN PARAMETERS

An object with the underwater explosion test with "STALMYGGAN" was to compare the design spectra in figure 1 and the low frequency design values with the characteristics of the shocks, measured in corresponding component positions. This comparison was based on analysis of acceleration shock spectra, defined according to IEC Publication 68-2-27A (reference 2):

The acceleration shock spectrum can be regarded as the maximum acceleration responses to a given shock excitation of (undamped) mass-spring systems as a function of the frequencies of the systems. Only first order shock spectra have been considered where the mass-spring systems are unidirectional linear one-deg-of-freedom systems.

The shock spectrum analysis was made in a digital computer after digitalisation of the acceleration-time history. The Q-value (magnification factor

at resonance) for the mass-spring system was chosen to 25 in the analysis (damped system), based on measurements of Q-values for some typical submarine components.

As shown in reference 3 the shock spectra derived from measurements relates to design levels only at frequencies corresponding to resonances (fixed-base frequencies) of the component mounted close to the measuring point in the structure. Such frequencies are normally found as valleys in the measured shock spectra. Efforts are therefore made in the evaluation of the measured data to correlate the valleys to fixed-base frequencies of components mounted in the structure and to find a suitable model for the mechanical system involved.

The design shock spectrum values thus obtained are plotted vs frequency for each measuring point and for each explosion distance. The value plotted is divided by the reduction factor r , applicable to the component and structure considered. An acceleration-frequency curve proportional to the curve for the actual class given in figure 1 is then fitted to the values plotted.

Figure 2 shows results for two measuring points in class 1 perpendicular to the structure.

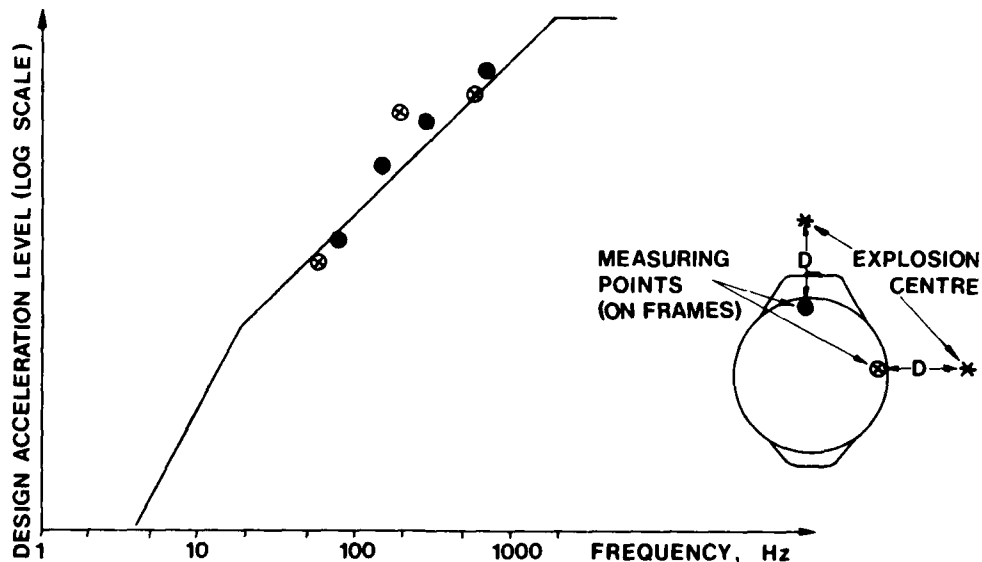


Figure 2. Equivalent design values from two measuring points compared to the design level for class 11 structure

The principle for determination of equivalent velocity values \hat{u}_0 , applicable to design of shock isolated components, is illustrated in figure 3 (valid for components in class 0 and 1 // structure and class 2).

The $\hat{u}_0 \cdot 2\pi f$ -curve with the best fit to the measured shock spectrum at low frequencies (below 15 Hz) is determined. The equivalent velocity $\hat{u}_0 = \hat{a} / 2\pi f$ thus defines a velocity from which the acceleration on the component is given as $\hat{a}_0 = 2\pi f \cdot \hat{u}_0$. Note that this velocity does not necessarily equals the maximum velocity of the shock.

200 kg and 1 200 kg) was about half of the masses of the seating involved. Figure 4 shows the resulting shock spectra

The rigidly mounted heavy masses appear to have one fundamental frequency (fixed-base frequency) at about 100 Hz, another close to 200 Hz and a third in the region of 400 Hz. Figure 4 a shows that the shock spectrum has been depressed at these frequencies and the corresponding design shock spectrum levels become significantly lower than for the case of light masses.

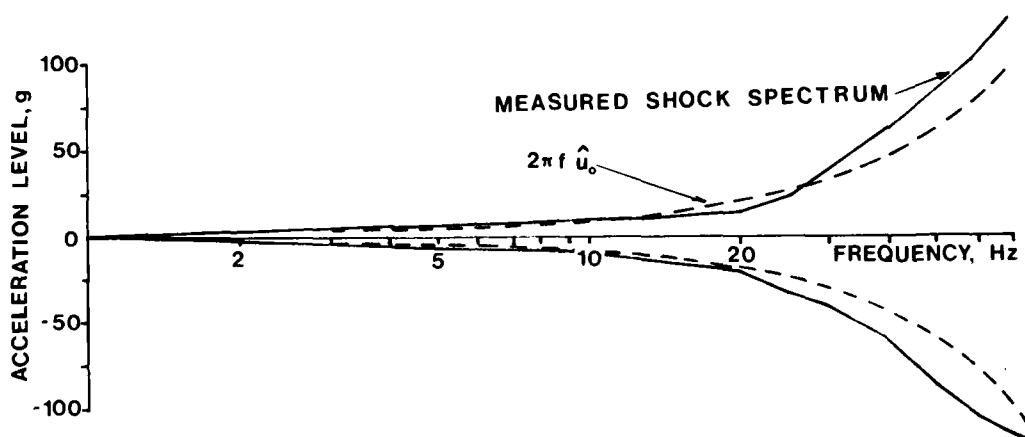


Figure 3. Principle for determination of u_0

STUDY OF THE INFLUENCE OF A COMPONENT MASS ON THE SHOCK SPECTRUM AND DESIGN SHOCK SPECTRUM LEVELS

In order to study the relationships between component mass and shock levels, seatings were loaded with variable masses at the same explosion distance and charge weight. This was done with masses rigidly mounted to the seating as well as with masses shock isolated from the seating. The mass variation (between

A comparison between the depression achieved and the theoretically calculated depression at fixed-base frequencies used in the Swedish shock specification, shows that the theoretical calculation tends to overestimate the magnitude of the depression.

As can be shown also theoretically the influence of mass on the shock level of an elastically mounted component is small (not detectable), see figure 4b.

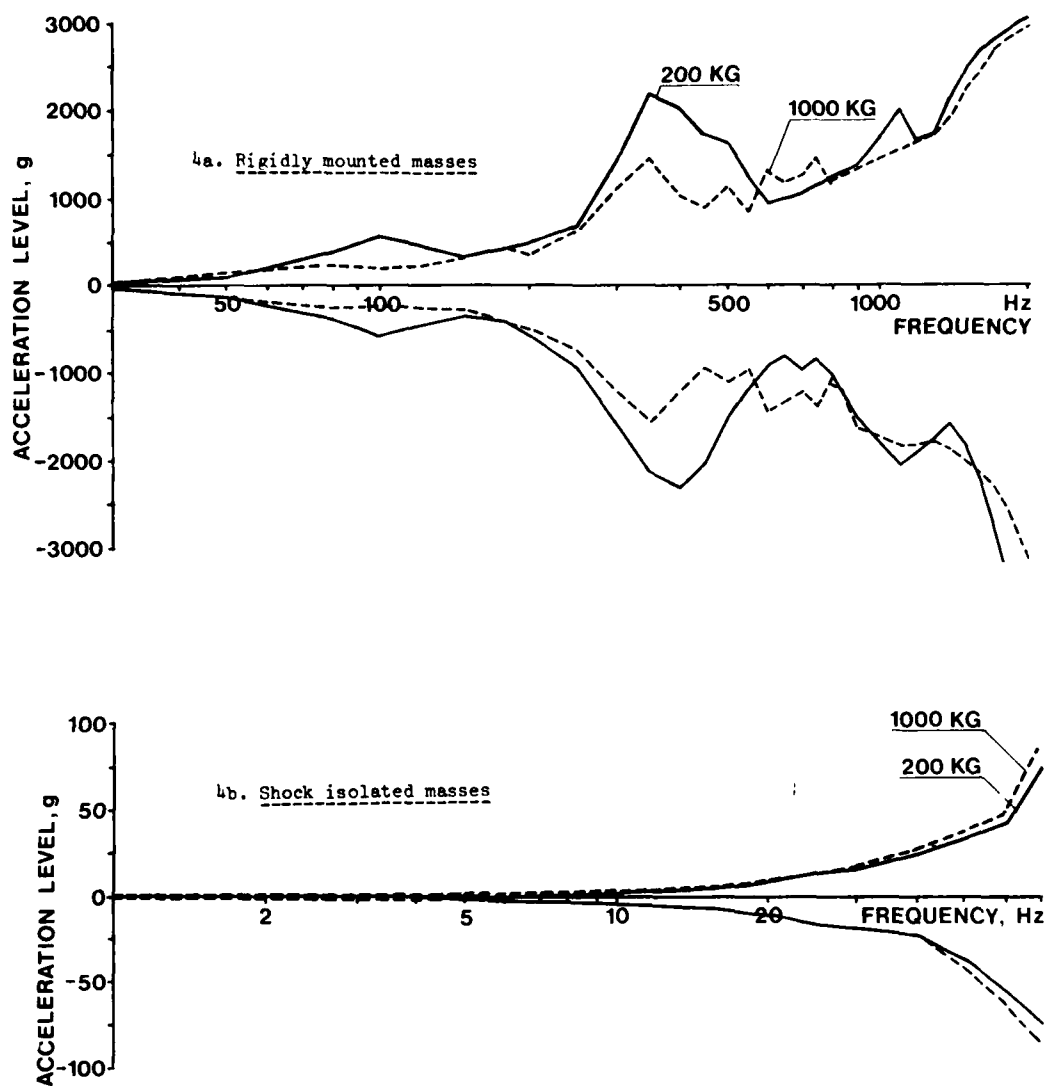


Figure 4. Shock spectra for different mass loads

SHOCK LEVELS IN AN OUTBOARD COMPONENT

Measurements were made in an outboard antenna, mounted to the end section of the hull via shock isolators (figure 5). A comparison was made between the shock spectrum measured in the antenna and the shock spectrum measured in the mounting point on the hull, see figure 5.

It is obvious that the part of the shock coming from the hull structure via the mounting is negligible compared to the effect of the shock wave directly hitting the antenna.

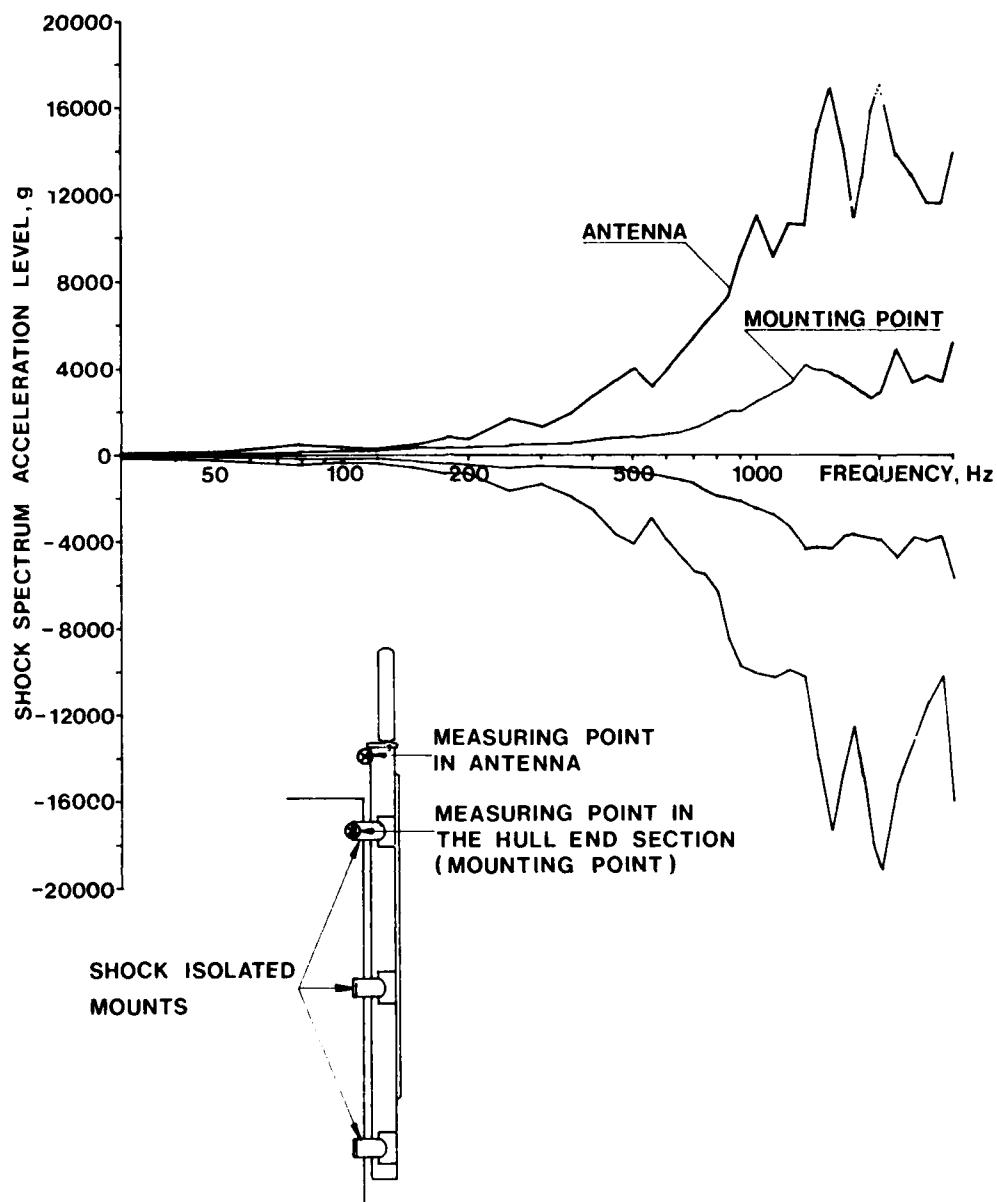


Figure 5. Comparison of shock spectra from point in antenna and from the mounting point of the antenna

DEPENDENCE OF PRESSURES AND SHOCK LEVELS ON EXPLOSION DISTANCE

Pressure peak levels

The pressure peak level of the primary shock wave hitting the ship hull is normally supposed to be proportional

to $1/R$, where R is the distance between the explosion centre and the point of the hull considered.

Figure 6 shows pressure peak levels measured in the water at a distance of one metre from the hull of the test section as a function of explosion dis-

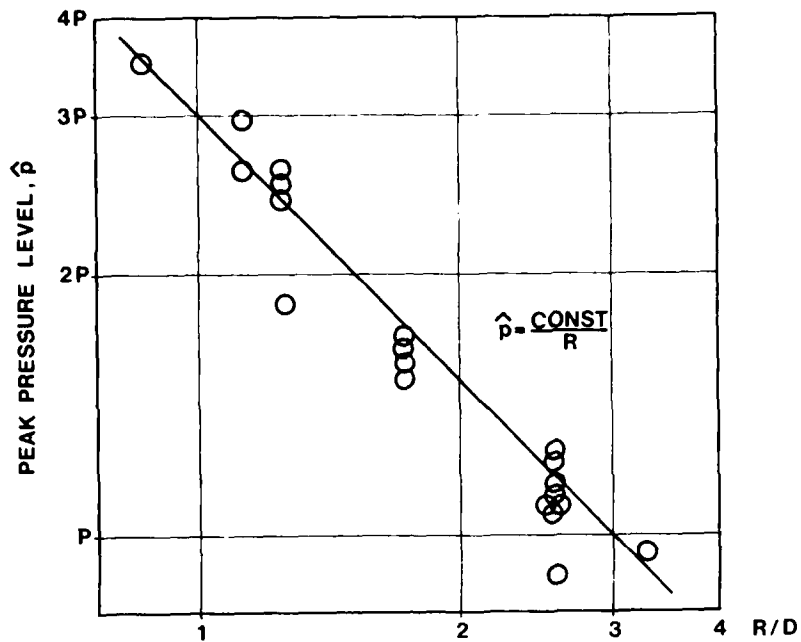


Figure 6. Pressure peak level as a function of explosion distance

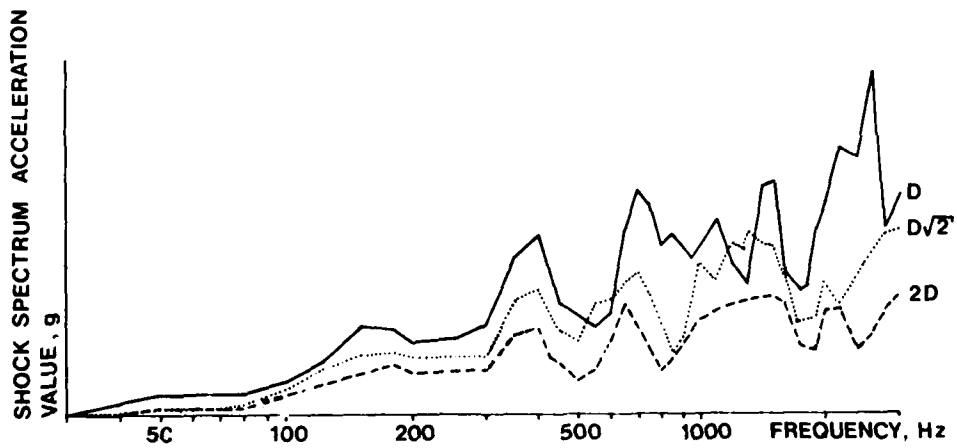


Figure 7. Shock spectra for shocks encountered in an inner structure at explosions from different distances D , $D/\sqrt{2}$, $2D$.

tance. The charge weight has been kept constant. The curve $\hat{p} \cdot R = \text{constant}$ has been drawn for comparison and it is shown that the peak levels measured follow the $1/R$ law reasonably well.

Shock levels

Figure 7 shows shock spectra for shocks measured in a typical inner structure at three different explosion distances. Comparisons of this kind give an idea of how the shock level depends on the explosion distance.

The explosion distance dependence can be more systematically evaluated if the design shock spectrum values for a given shock measurement are approximated to curves proportional to the design curves given in figure 1. The shocks may then be denoted by the corresponding acceleration level in the upper frequency range (plateau level). The dependence of explosion distance on this value for different measuring points is shown in figure 8.

It is shown that the shock level is

reasonably proportional to $1/R$.

CONCLUSIONS

The results of the shock measurements on "Stålmyggen" may be summarized as follows:

- there is a reasonably good correlation between the shape and level of the design spectra used in the submarine shock specification and the equivalent design shock spectrum values achieved from the measurements
- the influence of the component mass on the shock level in supporting structure was significant for a rigidly mounted beam. A simple theoretical calculation seems, however, to overestimate the mass influence on the shock level
- the influence of the component mass on the shock level in supporting structure was not significant for a flexibly mounted beam

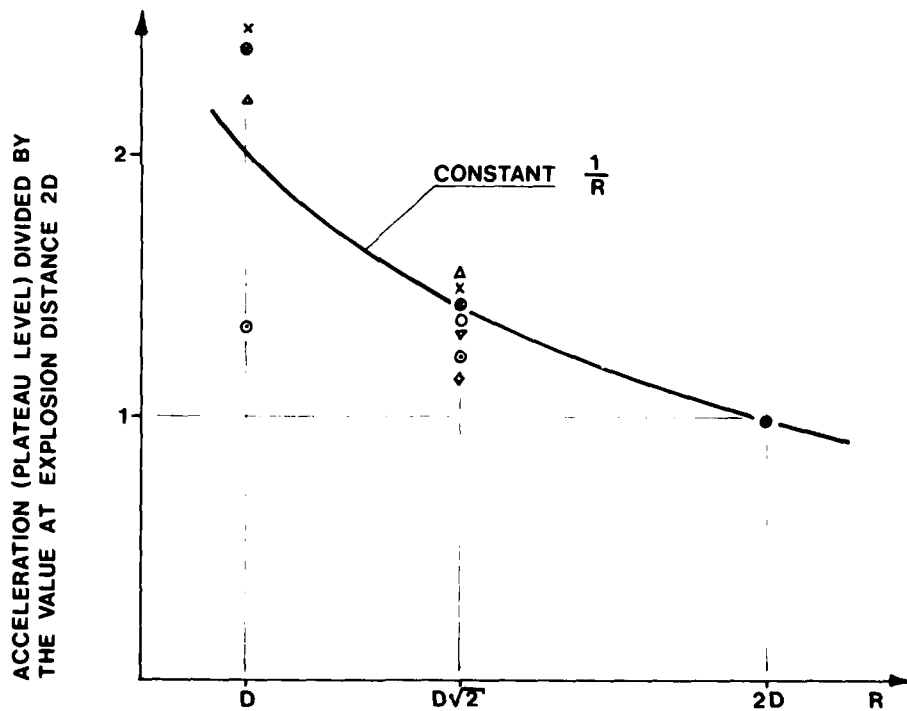


Figure 8. Shock levels as a function of explosion distance

- the results indicate that the shock excitation of a small outboard device mainly originates from the shock wave directly hitting the outboard device
- the shock level, expressed as the design shock spectrum value at a certain frequency vs explosion distance, follows reasonably well the same relationship as the peak pressure level in the water outside the hull structure vs explosion distance.

The purpose of the presentation of "STALMYGGAN" and the tests, measurements and analysis performed has been to illustrate the state-of-the-art in Sweden regarding treatment of the shock problem in submarines arising from underwater explosions. Due to the small series of products the amount of tests on components in shock testing machines and shock test platforms is small and the design of hull, parts and components must be based on limited experimental data and rather extensive theoretical analysis. The tests on "STALMYGGAN" form an important link in improving our shock specifications and design methods.

The extensive work done in the USA and published by the US Naval Research Laboratories (O'Hara et al) and other bodies has been of invaluable importance to us in our efforts to improve our technique in this field.

REFERENCES

1. International Electrotechnical Commission Publication 68-2-27
Test Ea: Shock
2. International Electrotechnical Commission Publication 68-2-27A
Appendix B Shock Spectra and Other Characteristics of Pulse Shapes
3. "Shock Spectra and Design Shock Spectra". O'Hara: G J NRL Report 5386, Naval Research Laboratory, Washington D C (November 1969).

DISCUSSION

Mr. Weinberger (Naval Ship Research and Development Center): I have several questions for Mr. Spang. What size charges did you use?

Mr. Spang: 100 Kilograms.

Mr. Weinberger: On one of your slides, you showed considerable hull deformation. Was that about what you expected?

Mr. Spang: Yes, we had expected these deformations.

Mr. Weinberger: Were the end bulkheads on this test vehicle essentially flat plates similar to the type you would have on the bulkheads of a submarine?

Mr. Spang: Yes, there were two bulkheads in each tank section connected together with shear plates.

Mr. Weinberger: So they were heavier than normal bulkheads?

Mr. Spang: No, they were the normal bulkhead construction.

Mr. Weinberger: Was there no attempt made in the bulkhead to make it heavier so that it would look like the rest of the submarine, or at least part of it?

Mr. Spang: No.

Mr. Oleson (Naval Research Laboratory): I'm curious about the shock mount that you put under your accelerometer. Our experience has been that, if we put a shock mount under an accelerometer in such a way that there is cantilever flexibility, this leads to an anomalous signal which is really a rectification phenomenon. If you get cross-axis drive, you get rectification of the cross-axis; if it rotates in a gravity field, you get some rectification essentially due to going through a neutral point. For example, with a cosine function at 0 degrees you would get some rectified gravity components. I'm not accustomed to looking at the shock spectra in an acceleration format, so I'm not exactly sure how that would show up in your spectra. However, it does show up very strongly if you integrate your accelerometer records to produce velocity records. Would you care to comment on this?

Mr. Spang: We used these shock mounts at the nearest explosion distance only in order to protect the accelerometers. We haven't investigated the problem very much, I must say.

Mr. Nilsson: Perhaps we should do as Mr. Westin suggested and divide the signals into a low frequency part and a high frequency part. The low frequency part is fairly representative in this case because, if it shows up very clearly in a velocity spectrum and not an acceleration

spectrum, it must be that it is a low frequency effect. The low frequency effect will show up in our low frequency spectrum as well as if you made a velocity spectrum out of it. So there you have the dynamics which is necessary to be able to detect it. We ought to have detected it if it were there, but we will certainly have to investigate it a little bit more in detail.

Mr. Forkois (Naval Research Laboratory): You use the term mounting frequency. Would you care to define that term?

Mr. Nilsson: When I talk about normal modes and that kind of thing, I'm talking about fixed-base frequencies. For example, in the case where I was talking about rigidly mounted components, where you use the spectrum in order to define the accelerations and the forces involved for your design, then I meant to speak about fixed-base frequency. But when I talk about mounting frequencies, I am talking about shock-mounted components.

Mr. Stathopoulos (Naval Ordnance Laboratory): I'm very much impressed with the insight you have to this very complex problem. However, my question is this; have you given any thought for future work as to how you will go about qualifying your equipment? Will it be with tests similar to this, or will you have a laboratory simulation of some type?

Mr. Nilsson: We have a slightly different position than you have on this because we make a very short series of submarines. You make a longer series and can afford to use more testing than we can. We have to do very much of this on an analytical basis. The only kind of tests we do are tests in a laboratory on a shock testing machine. We don't make any tests on a floating shock platform.

Mr. Spang: We hope that as an acceptance test on the first submarine in the coming series we can again make a full-scale test against a complete submarine to study, for instance, the beam oscillation problem.

Mr. Fritz (General Electric Company): I have a question for Mr. Spang. Can you say a few words about the damage criteria? When the designer goes through the analysis of equipment and calculates stresses, to what does he compare those stresses to find out whether he has an acceptable design?

Mr. Spang: We start from the normal static value and utilize some excessive properties due to the high strain rates.

Mr. Fritz: This implies that you are dealing with mild steels.

Mr. Spang: Yes, sir. As I said, the hull material has a yield point about 68,000 psi.

Mr. Fritz: Mild steels do show a strain rate dependency, but if you were to design with some other metals you probably would not put in a strain rate dependency.

Mr. Spång: We have performed some laboratory tests on structures of these materials and we have found a considerable strain rate effect.

Mr. Fritz: In looking at seismic design spectra, one normally sees peaks in the spectra even if a spectrum dip effect has been accommodated. These peaks tend to infer that there are some predominant environmental frequencies, so that equipments designed in that range of environmental frequencies get an extra penalty. Your shock spectra did not seem to show peaks of that kind. Would you comment on that?

Mr. Spång: Well, I'm not sure about what we should expect to have. We have made some tests before on a complete submarine using the same kind of shock spectrum analysis, and the shock spectra we have here look about the same. Actually, I didn't think that peaks of that kind would occur. The environment itself is a rather broad-band environment, with the shock wave hitting a plane section or a cylindrical section. Of course, the ship hull in itself will produce a spectrum of that kind. I suppose if you

look at the shock spectra I showed you, the shock spectra with mass-dependence and so on, there were some peaks and valleys. The real problem is to know which peaks and valleys are coming from the bending modes or ring modes of this structure and which values arise from having a component mounted at that position and pressing down the level at its fixed-base frequencies. That's a big problem and that's where the real deviation between this test body and a complete submarine occurs. In the complete submarine you will find some peaks which come from the bending modes. They will not appear here. Perhaps those are the peaks you miss here.

SHOCK ANALYSIS

SHOCK ANALYSIS ERRORS IN THE PRESENCE OF VIBRATION

Charles T. Morrow
Advanced Technology Center, Inc.
Dallas, Texas 75222

If a shock occurs during a time interval in which there is also a sustained random vibration background, the Fourier spectrum or residual shock spectrum can not be computed without some error or uncertainty. The uncertainty is proportional to the square root of the power spectral density of the random vibration and the square root of the time duration of the sample used in the computation.

INTRODUCTION

In the environmental test laboratory, it is customary to test separately to vibration and shock. Frequently when an equipment of the type tested is in use, shocks are not limited to time intervals when there is no vibration. The subject of this paper is the problem of measuring the shock in the presence of a random vibration whose power spectral density over the frequency range of interest is known. The results yield some implications also about the effect on the equipment of combining the two environments.

In shock and vibration engineering, the most common spectral description of a shock is a shock spectrum of the acceleration. In this paper, we will use the Fourier spectrum, or the Fourier transform, as it is known to mathematicians and electronic engineers. This, with its phase information preserved, is a complete description from which the wave form can be recovered exactly. It is more suitable for fundamental analyses. Once the analysis is completed, the results apply directly also to the undamped residual shock spectrum, which is identical to the magnitude of the Fourier spectrum except for a factor of 2π times the frequency, and is the most sensitive indicator of spectral energy of a shock among the various types of shock spectra in use.

One might be tempted to protest that the analysis to follow is unnecessary, for it should be sufficient to prescribe a shock test in terms of an undamped residual shock spectrum for the combined shock and random vibration. Unfortunately, the contribution of the random vibration has an uncertainty that increases monotonically with integration time. Consequently, one can not be certain solely from a single simple mea-

surement of undamped residual shock spectrum or of the magnitude of the Fourier spectrum of the total signal whether the vibration resulted in an increase or a decrease, or what would be the effect if the same shock coincided in time with a different sample of the random vibration. The analysis to follow will provide insights into this problem.

Although the undamped residual shock spectrum is, by virtue of its simple relation to the Fourier spectrum, the most fundamental spectral description of a shock and the best indicator of the spectral energy, among the various types of shock spectrum in use, many engineers prefer a damped residual shock spectrum as more representative of responses of actual hardware. The effect of random vibration on this type of spectrum is not an explicit subject of analysis here. However, selection of finite damping is equivalent to placing an upper limit on integration time. Consequently, at least qualitative inferences about the effect of random vibration on this damped spectrum can be made directly from the results of the present analysis. Furthermore, the damped residual spectrum can be calculated from the complete Fourier spectrum, if one wishes to take the time, or estimated from the undamped residual shock spectrum without phase content.

The initial shock spectrum, unfortunately often called primary, is not necessarily an indicator of spectral energy at the higher frequencies, nor is a composite spectrum made by combining initial and residual. Space will not be taken here to justify this statement. However, the effect of random vibration on these, if desired, can be obtained by extensions of the present analysis.

Before leaving this background discussion

for actual analysis, a caution should be pointed out. The response of any known linear system having many normal modes is calculable from the complete Fourier spectrum or transform and can be estimated closely, for most situations, from the undamped residual shock spectrum. Other types of shock spectra are helpful in providing additional insights into the response of a simple resonator, but do not apply directly and quantitatively to multimodal systems. It is possible to become so absorbed with the response of the simple resonator that one loses awareness of the limitations of the model as a simplification of practical structure.

THE BASIC EQUATIONS

We assume that the shock eventually to be measured will begin at time $t = 0$ and that after $t = T$ the excitation either is negligible or, for one reason or another, will be ignored. The exponential Fourier transform of the shock time function $a_s(t)$ will be

$$\begin{aligned} S_s(f) &= \int_{-\infty}^{\infty} a_s(t) e^{-j2\pi ft} dt \\ &= \int_0^T a_s(t) e^{-j2\pi ft} dt. \end{aligned} \quad (1)$$

Actually, this operation will be carried out on a combined signal $a_s(t) + a_v(t)$, where the second term is a random vibration function of power spectral density $w(f)$ over the frequency range of interest for shock data reduction:

$$\begin{aligned} S(f) &= \int_0^T [a_s(t) + a_v(t)] e^{-j2\pi ft} dt \\ &= \int_0^T a_s(t) e^{-j2\pi ft} dt + \int_0^T a_v(t) e^{-j2\pi ft} dt \\ &= S_s(f) + S_v(f). \end{aligned} \quad (2)$$

vectorially, in the complex plane, as shown in Fig. 1.

SUMMARY OF THE ANALYSIS

In Appendix I, a calculation is made of the uncertainty occurring when Fourier transform is evaluated for vibration alone. In other words, by examination of the statistics of the coefficients of the Fourier series, for successive samples of random vibration of duration T , it is determined that magnitude of the Fourier transform $S_v(f)$ has a mean value

$$|S_v| = \frac{2}{\sqrt{\pi}} [Tw(f)]^{1/2} \quad (3)$$

which increases monotonically with integration time, and a standard deviation from the mean

$$\sigma_m = [(2 - \frac{4}{\pi}) Tw(f)]^{1/2} = 1.13 [Tw(f)]^{1/2} \quad (4)$$

which also increases monotonically with integration time.

At one extreme, then, when the vibration is large with respect to the shock in the frequency range considered, all angles are equally likely, but Eq. (4) yields the uncertainty of the measurement of the magnitude. This is not very useful directly, since $S(f)$ is small by comparison with the mean value given in Eq. (3) and impractical to measure even by averaging over repeated trials. However, the uncertainty for this limiting case is at least one indication of the uncertainty for approximately equal shock and vibration, a situation very difficult to calculate directly.

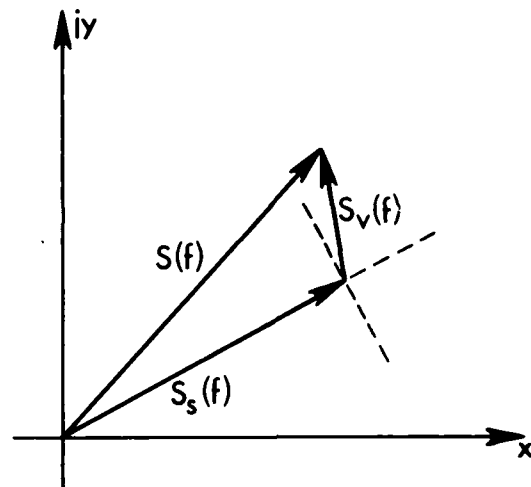


Fig. 1 - Vector Addition of $S_s(f)$ and $S_v(f)$

At the other extreme, let us consider a shock so large by comparison with the vibration that in the frequency range of interest $|S_v(f)| \ll |S(f)|$. The contribution of the vibration to the mean is negligible. In other words, for this extreme, there is no systematic effect of the vibration on the magnitude of the spectrum. The $S_v(f)$ for successive samples of vibration are vectors in the complex plane, each adding vectorially to $S(f)$ as in Fig. 1.

Since all angles of the random vibration transform are equally likely, the distribution of their projections on any straight line is the same as the distribution of their projections on either axis, is Gaussian with zero mean, and has a standard deviation

$$\sigma_p = \sigma/\sqrt{2} = [Tw(f)]^{1/2} \quad (5)$$

where σ is the root mean square value for $|S_v|$ as derived in Appendix I. In other words, the primary effect of the vibration now is a statistical uncertainty. The square root of two factor results from the fact that, by the Pythagorean theorem, the sum of the squares of the $|S_v(f)|$ is equal to the sum of the squares of the projections on any two mutually perpendicular lines and therefore equal to twice the sum of the squares of the projections on any one line, or equal to twice the variance of these projections.

If we let one set of projections lie on a line extending along $S(f)$, as in Fig. 1, Eq. (5) yields the uncertainty in the magnitude $|S(f)|$. The distribution is Gaussian. If we let another set of projections lie on a line at a right angle to $S(f)$, the standard deviation of the apparent angle may be obtained by dividing Eq. (5) by $|S(f)| = |S_s(f)|$, as follows:

$$\begin{aligned} \sigma_\phi &= \sigma_p / |S_s(f)| = \frac{[Tw(f)]^{1/2}}{|S_s(f)|} \text{ radians} \\ &= \frac{360}{2\pi} \cdot \frac{[Tw(f)]^{1/2}}{|S_s(f)|} \text{ degrees} \end{aligned} \quad (6)$$

This is of interest if one should need the phase information of the Fourier transform for accurate reconstruction of a wave shape.

CONCLUSION

The standard deviations from the mean, given by Eq. (4) for shock small compared to the vibration, and by Eq. (5) for shock large compared to the vibration, differ by less than 15 percent for the same power spectral density $w(f)$ of vibration. It seems reasonable, therefore, that the standard deviation will lie close to these formulas for intermediate relationships of shock to vibration.

To obtain expressions for the standard deviation of the undamped residual shock spectrum from the mean from Eqs. (4) and (5), multiply by $2\pi f$.

The analysis thus provides a means of estimating the standard deviation from the mean of the undamped residual shock spectrum, or of the magnitude of the Fourier spectrum, measured

in the presence of random vibration. The uncertainty of the measurement is proportional to the square root of the integration time interval T used in the computation.

The shocks that actually occur during the flight of an aerospace vehicle do not resemble the standard pulse shape of the laboratory, but tend to have an abrupt burst at the start, followed by an exponential or less regular decay. In short, there is no one definite obvious time for the end of such a shock. In the absence of vibration, accuracy increases with T . The presence of random vibration suggests decreasing T as much as possible to obtain better precision. Perhaps the best compromise is to compute the Fourier transform for several values of T , measure the power spectrum $w(f)$ for vibration occurring at nearly the same time, and for each frequency favor the largest value of T that yields an acceptable uncertainty from Eq. (5) in relation to the indicated magnitude of $S_s(f)$.

If the shock is assumed to be a reproducible phenomenon that occurs in practice in the presence of an ergodic random vibration (statistically the same from flight to flight), and an accurate measure of the magnitude of the Fourier spectrum can somehow be obtained, as by a separate experiment, then Eq. (11) becomes an indication of the uncertainty of the severity of the combined effect of shock and vibration in flight.

APPENDIX I

RANDOM VIBRATION ALONE

For the first part of the analysis, we examine $S_v(t)$, which is the Fourier transform of a sample of $a_v(t)$ of duration T . We assume $a_v(t)$ to be Gaussian and stationary or ergodic.

Suppose that such a sample is made to repeat indefinitely, as by being recorded and played back on a loop of magnetic tape, so that it becomes periodic. Then, the Fourier coefficient for the k 'th harmonic produced by this operation is given by

$$\begin{aligned} C_{ek} &= \frac{1}{T} \int_0^T a_v(t) e^{-j2\pi k f_1 t} dt \\ &= S_v(kf_1)/T. \end{aligned} \quad (7)$$

where $f_1 = 1/T$ is the fundamental frequency or the repetition rate of the sample. It will be recalled that, since C_k represents the peak rather than the root mean square value for the harmonic, and $\Delta f = f_1$ is the spacing between harmonics, $C_{ek}^2/2\Delta f$ is an elementary estimate of power spectral density. As this is not a statistically significant estimate, it is customary to perform an average for the f_k in a

sufficient bandwidth B to reduce the uncertainty to an acceptable value, thereby compromising frequency resolution if necessary. The familiar statistics of the C_{ek} lead very directly to the statistical properties of $S_v(f)$.

Now, the C_{ek} are complex numbers or vectors in the complex plane. The exponential form of the Fourier series can be converted to a sum of cosine and sine terms, with respective real coefficients C_{ck} and C_{sk} , all statistically independent of each other if evaluated for successive independent samples from a missile flight (stationarity required) or from successive flights (ergodicity required). Both the C_{ck} and the C_{sk} are in Gaussian distributions with zero means and, since all phase angles of C_{ek} are equally likely, the same variance. By definition, the sum of the squares of n such coefficients

$$\sum_{k=m}^{m+n} C_{ck}^2 \text{ or } \sum_{k=m}^{m+n} C_{sk}^2$$

over a frequency region in which $w(f)$ is constant or over successive independent samples is a chi-square distribution in n degrees of freedom.

Since

$$|C_{ek}|^2 = C_{ck}^2 + C_{sk}^2, \quad (8)$$

the summation

$$\sum_{k=m}^{m+n} |C_{ek}|^2,$$

although the $|C_{ek}|$ can never be negative, is also a chi-square distribution in n degrees of freedom. From this, the familiar result is commonly obtained that an average of $C_{ek}^2/2f_1$ for the n values of f_k in a bandwidth B, for sufficiently large n, taken as an estimate of power spectral density, has a normalized standard deviation

$$\sigma_{vn} = 1/(BT)^{1/2} = 1/\sqrt{n} \quad (9)$$

The $|C_{ek}|$, which can not be negative, occur according to the positive half of a Gaussian distribution. From the definition of the power spectral density $w(f)$ as the limit of an average of $C_{ek}^2/2f_1$ over a bandwidth or over an ensemble, the root mean square value of an infinite number of $|C_{ek}|$ is

$$\begin{aligned} \overline{|C_{ek}|^2}^{1/2} &= [2f_1 w(kf_1)]^{1/2} = [2\Delta f w(kf_1)]^{1/2} \\ &= [2w(f)/T]^{1/2} \end{aligned} \quad (10)$$

Consequently, from Eqs. (7) and (10), the root mean square value for $|S_v(f)|$ is

$$\overline{|S_v(f)|^2}^{1/2} = [2Tw(f)]^{1/2} \quad (11)$$

To proceed further, we must deduce the exact expression for the probability density of $|S_v(f)|$. The probability density for a Gaussian variable x with standard deviation σ about a zero mean is

$$p(x) = \frac{1}{\sigma\sqrt{2\pi}} e^{-x^2/2\sigma^2} \quad (12)$$

and the mean square value is given by

$$\overline{x^2} = \int_{-\infty}^{\infty} x^2 p(x) dx = \sigma^2. \quad (13)$$

If, however, the signs of all negative x are made positive, the probability density is made zero for all negative x, while that for positive x is doubled. The mean square value is now

$$\overline{x^2} = \int_0^{\infty} 2x^2 p(x) dx = \sigma^2, \quad (14)$$

as before, since p(x) is symmetrical. From Eqs. (11) and (14),

$$\sigma = [2Tw(f)]^{1/2}, \quad (15)$$

However, the distribution of $|S_v(f)|$ is shown to be twice that of an ordinary Gaussian distribution, for positive values. If the Fourier transform $S(f)$ as in Eq. (2) is evaluated when the shock, if any, happens to be negligible by comparison with random vibration, and $P(|S_v|)$ has twice the value of an ordinary

symmetrical Gaussian distribution, the mean of the possible magnitudes is given by

$$\begin{aligned}
 \overline{|S_v|} &= \int_0^{\infty} |S_v| P(|S_v|) d|S_v| \\
 &= \frac{2}{\sigma\sqrt{2\pi}} \int_0^{\infty} |S_v| e^{-|S_v|^2/2\sigma^2} d|S_v| \\
 &= \frac{2\sigma\sqrt{2}}{\sqrt{\pi}} \int_0^{\infty} \frac{|S_v|}{\sigma\sqrt{2}} e^{-|S_v|^2/2\sigma^2} d\frac{|S_v|}{\sigma\sqrt{2}} \\
 &= \frac{2\sigma\sqrt{2}}{\sqrt{\pi}} \cdot \frac{1}{2} = \frac{\sigma\sqrt{2}}{\sqrt{\pi}} = \frac{2}{\sqrt{\pi}} [Tw(f)]^{1/2} \\
 &\quad (16)
 \end{aligned}$$

which is identical to Eq. (3).

The standard deviation from the mean is given by

$$\begin{aligned}
 \sigma_m &= \left[\int_0^{\infty} (|S_v| - \overline{|S_v|})^2 P(|S_v|) d|S_v| \right]^{1/2} \\
 &= \left[\int_0^{\infty} |S_v|^2 P(|S_v|) d|S_v| \right. \\
 &\quad \left. - 2\overline{|S_v|} \int_0^{\infty} |S_v| P(|S_v|) d|S_v| \right. \\
 &\quad \left. + \overline{|S_v|}^2 \int_0^{\infty} P(|S_v|) d|S_v| \right]^{1/2} \\
 &= \left[\overline{|S_v|^2} - \overline{|S_v|}^2 \right]^{1/2} \\
 &= \left[2Tw(f) - \frac{4}{\pi} Tw(f) \right]^{1/2} \\
 &= \left[\left(2 - \frac{4}{\pi}\right) Tw(f) \right]^{1/2}
 \end{aligned}$$

from Eqs. (11) and (16). This result is identical to Eq. (4).

APPROXIMATE RESPONSE SPECTRA OF DECAYING SINUSOIDS

Arnold E. Galef
TRW Systems, Inc.
Redondo Beach, California

The response spectrum of a decaying sinusoid, as a function of frequency ratio and of the damping in the excitation and the response, is developed using an approximate technique. The results, which have been verified by comparison to digital computer results, are presented in a form convenient for engineering application.

NOMENCLATURE

- A - quasi-amplitude (initial velocity divided by damped frequency) of exciting motion
- I - impulse causing motion
- M_n - generalized mass of nth mode of structure excited
- R - response spectrum (a function of Ω , ω , ζ , ξ)
- t - time
- T - time when response amplitude reaches maximum
- X - exciting motion
- Z - equivalent damping, as fraction of critical damping
- $\delta(t)$ - relative displacement of response oscillator
- ζ - damping in response oscillator, as fraction of critical damping
- ξ - damping in excitation, as fraction of critical damping
- ϕ_{pn} - modal deflection in direction of impulse of nth mode, at point where impulse is applied
- ϕ_{qn} - modal deflection in "X" direction in nth mode, at point "q"
- Ω_n - natural frequency of nth mode

ω - natural frequency of response oscillator

INTRODUCTION

When a linear, viscously-damped structure is subjected to an impulse I at point p, the motion at point q can be represented by

$$X(q,t) = \sum_{n=1}^N \frac{I \phi_{pn} \phi_{qn}}{M_n \Omega_n \sqrt{1-\xi_n^2}} e^{-\xi_n \omega_n t} \sin \sqrt{1-\xi_n^2} \omega_n t \quad (1)$$

The frequently encountered problem of predicting the response spectrum of such motion requires, first, that the response spectrum of each of the modal components of motion be known. The modal spectra may then be combined, either by direct addition or by a less conservative root sum-square procedure.

This paper addresses the first portion of the problem--that of determining the response spectrum of a damped sinusoid as a function of response frequency and damping.

In general, finding the response spectrum of a given excitation involves finding the response motion of each of a hypothetical set of oscillators having frequency ω , damping ζ , when those oscillators are base-excited by the prescribed motion and then finding the maximum motion reached by each such oscillator. The maximum response motion, as a function of the oscillator frequency ω , is the response spectrum.

The response spectrum of either absolute or relative motion may be found. The relative motion spectrum is usually the one of greater interest, and that is the one which will be treated specifically here. However, the reader will observe that the techniques to be employed will be applicable to the absolute motion spectrum as well or, for that matter, to the response spectrum of a damped sinusoidal force.

APPROACH

The differential equation of relative motion of the hypothetical oscillators defined above is

$$\ddot{\delta} + 2\zeta\omega\dot{\delta} + \omega^2\delta = -\ddot{X} \quad (2)$$

The excitation, X , is of the form

$$X = Ae^{-\xi\Omega t} \sin \sqrt{1-\xi^2} \Omega t \quad (3)$$

When the indicated differentiation is performed and second-order terms in " ξ " are neglected in comparison to unity (small damping assumed), Equation (2) becomes

$$\ddot{\delta} + 2\zeta\omega\dot{\delta} + \omega^2\delta = A\Omega^2 e^{-\xi\Omega t} [\sin \Omega t + 2\xi \cos \Omega t] \quad (4)$$

The solution to Equation (4) may be written as the Duhamel integral (Reference 1). Neglecting second-order terms in " ξ ", the integral is

$$\delta = \frac{A\Omega^2 e^{-\xi\omega t}}{\omega} \int_0^t e^{(\zeta\omega - \xi\Omega)\tau} \sin \omega(t-\tau) [\sin \Omega \tau + 2\xi \cos \Omega \tau] d\tau \quad (5)$$

The terms within the integral may be readily manipulated into forms which are listed in widely available tables of integrals and, in principal the closed form solution to Equation (5) is obtainable. In practice, the result of this formal procedure is exceedingly cumbersome, and the subsequent determination from that result of the maximum value of δ as a function of ζ , ξ , ω , Ω , is very difficult. Consequently, solutions to this important problem have heretofore been attained only for special cases using computers rather than by continuing the above formal analysis. Most such work is unpublished, and has come into some limited distribution only through personal contacts. In Reference 2, Barton, Chobotov and Fung provide the useful service of disseminating some of the unpublished work by Curtis (Reference 3) and Rubin (Reference 4). However, the only widely available results of such calculations, by Rubin, is con-

tained in Reference 5. Rubin's results, adapted* from Reference 5, are presented as Figure 1.

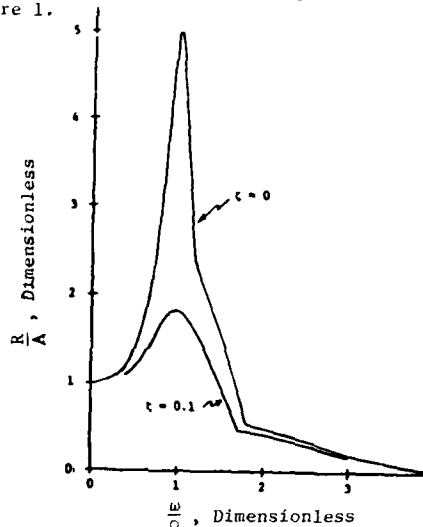


Figure 1
Response Spectra of a 10% Damped Sinusoid

It is seen that except for some minor cusps, Figure 1 is distinctly suggestive of the well-known damped response to an undamped sinusoid.

$$R\left(\frac{\omega}{\Omega}, Z\right) = \frac{A}{\sqrt{\left(1 - \frac{\omega^2}{\Omega^2}\right)^2 + 4Z^2 \frac{\omega^2}{\Omega^2}}} \quad (6)$$

(Equation (6) is plotted as Figure 2 for ready comparison to Figure 1.)

In particular, the Rubin results conform to Equation (6) in the following important respects:

1. For light to moderate damping, the peak value of the spectrum occurs at frequency ratios $\frac{\omega}{\Omega}$ near unity. The peak value is strongly dependent upon the damping (Z , or both ζ and ξ , as applicable).
2. At low frequency ratios, the response spectrum approaches unity while becoming nearly independent of the damping.

* In Reference 5, Rubin uses the highest observed value of the input motion in place of the quasi-amplitude " A " employed here. The Rubin input, \hat{A} , is related to A by

$$\hat{A} = A \exp(-\xi \cos^{-1} \xi)$$

Further, Rubin presents an equivalent static acceleration spectrum rather than the displacement spectrum considered here. The two are related by " ω^2 ", as shown in Reference 5.

3. At high frequency ratios, the response spectrum approaches zero while becoming nearly independent of the damping.

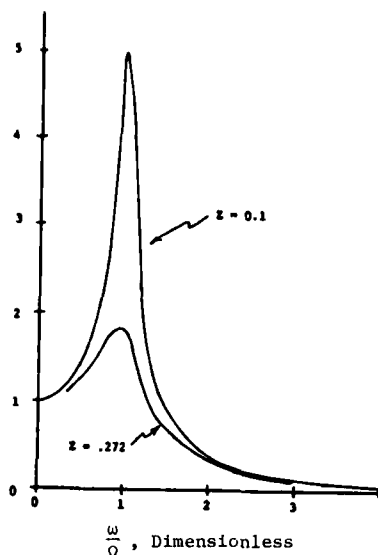


Figure 2. Response Spectra of Undamped Sinusoid

The more extensive but unpublished work of Reference 6 strongly supports the above trends. (The cusps of Figure 1 are distinctly less pronounced in Reference 6). It is assumed that these results are general and that, for engineering purposes, the cusps of Figure 1 are of no concern. Thus, after a relationship between ζ , ξ , Z , is found, the desired response spectrum of a decaying sinusoid is adequately approximated by Equation (6).

Z may be determined from the peak value of the spectrum because

$$\frac{A}{2Z} = R_{\max}. \quad (7)$$

We may estimate the peak value of the spectrum by assuming, from the cited available results, that the spectrum value occurring at the frequency ratio ω/ω_n , unity is very nearly the peak value. Thus, Equation (5) need be evaluated at, and only at that particular frequency relationship.

Equation (5) becomes

$$\hat{\delta} = \delta(\omega=\Omega) = A\zeta e^{-\zeta\Omega t} \int_0^t e^{(\zeta-\xi)\Omega\tau} \sin \Omega(t-\tau) [\sin \Omega\tau + 2\xi \cos \Omega\tau] d\tau \quad (8)$$

The simplification occurring between Equations (5) and (8) is not immediately obvious. However, when the expansions implied in Equation

(8) are performed in order to make the integration from tables of integrals, the result

$$\hat{\delta} = A\zeta e^{-\zeta\Omega t} \left\{ \sin \Omega t \int_0^t e^{(\zeta-\xi)\Omega\tau} \left[\frac{\sin 2\Omega\tau}{2} + \xi(1 + \cos 2\Omega\tau) \right] d\tau + \cos \Omega t \int_0^t e^{(\zeta-\xi)\Omega\tau} \left[\frac{\cos 2\Omega\tau - 1}{2} - \xi \sin 2\Omega\tau \right] d\tau \right\} \quad (8')$$

is enormously simpler than the equivalent expansion (not written) of the more general Equation (5).

Although laborious, the integration is straightforward. After neglecting small terms, the result is

$$\hat{\delta} = A \frac{e^{-\zeta\Omega t} - e^{-\xi\Omega t}}{2(\zeta-\xi)} \cos \Omega t \quad (9)$$

The term multiplying the cosine is the envelope of the quasi-sinusoidal result. The envelope has its maximum value when $t = T$:

$$T = \frac{\ln \xi - \ln \zeta}{\Omega(\xi - \zeta)} \quad (10)$$

For the small damping of concern the envelope does not change significantly during the time interval required for the cosine function to go through a half-cycle of oscillation. Thus, the cosine will be unity at an instant when the envelope is near its maximum; with negligible conservatism (of the same order as the nonconservatism involved in the previous neglecting of small terms), the maximum value of the relative response, or the "Response Spectrum", is determined by substituting "T" in the envelope of Equation (9). The result is

$$\hat{\delta}_{\max} = \frac{A}{2} \frac{\xi/(\zeta-\xi)}{\zeta/(\zeta-\xi)} \quad (11)$$

The forms of Equations (11) and (7) are identical, and the sought-for value of $Z(\zeta, \xi)$ is

$$Z = \frac{\zeta/(\zeta-\xi)}{\xi/(\zeta-\xi)} \quad (12)$$

Inserting the value in Equation (6) yields the engineering approximation to the damped response spectrum of a decaying sinusoid

$$R(\omega, \zeta, \xi) = \sqrt{\frac{A}{\left[\left(1 - \frac{\omega^2}{\Omega^2} \right)^2 + 4 \frac{\omega^2}{\Omega^2} \left[\frac{\zeta \xi / (\zeta - \xi)}{\xi \xi / (\zeta - \xi)} \right]^2 \right]}} \quad (13)$$

SPECIAL CASES

It will be apparent that if ζ or ξ is zero, or if $\zeta = \xi$, Equation (10) and subsequent become indeterminate.

The indeterminacies are readily evaluated using L'Hospital's rule. The results are:

$$\begin{aligned} \zeta &= 0 & Z &= \xi \\ \xi &= 0 & Z &= \zeta \\ \zeta &= \xi & Z &= 2.7183 \zeta \end{aligned}$$

NUMERICAL RESULTS

The following table presents the value of Z for a usefully wide range of ζ , ξ , which do not importantly violate the "small damping" assumption used through the development.

This work will be useful to engineers responsible for specifying shock environments in terms of response spectra.

ACKNOWLEDGEMENT

Dr. S. Rubin of Aerospace Corporation reviewed an earlier (TRW internal) version of this work and made several suggestions leading to improved clarity. His assistance was greatly appreciated.

The studies leading to this paper were performed in the course of an investigation on impact to "Minuteman", and was supported by the U.S. Air Force through the TRW Project Office, via Contract F040701-70-C-0165. Thanks are due to Mr. A. Dean, Manager of the System Design and Integration Dept., TRW, for his cooperation and support.

REFERENCES

1. Timoshenko, S. P. and Young, D. H., "Advanced Dynamics", McGraw-Hill Book Company, New York, First Edition, 1948, pp. 49-50.

Table

Equivalent Damping, Z , in Response Spectrum of Decaying Sinusoid

$\xi \backslash \zeta$	0	.01	.02	.03	.05	.075	.10	.15
0	0	.01	.02	.03	.05	.075	.10	.15
.01		.027	.04	.052	.075	.10	.13	.18
.02			.054	.067	.092	.12	.15	.20
.03				.082	.11	.14	.17	.22
.05					.14	.17	.20	.26
.075		Symmetric				.20	.24	.30
.10							.27	.34
.15								.41

SUMMARY AND CONCLUSIONS

Equation (13) or, equivalently, Equation (6) with the foregoing table, represents a convenient expression for the response spectrum with damping of a damped sinusoidal excitation.

These results are not represented to be exact, but are claimed to be sufficiently accurate for engineering purposes. The inaccuracies in these results will usually be of substantially lower magnitude than the level of uncertainties in the characteristics of the decaying sinusoid whose spectrum is sought.

2. Barton, M. V., Chobotov, V. and Fung, Y. C. "A Collection of Information on Shock Spectrum of a Linear System", Space Technology Laboratories Report EM 11-9, July, 1961.
3. Curtis, A. J., "Shock Spectra Associated with a Decaying Sinusoid", Unpublished technical correspondence, Hughes Aircraft Co., October, 1959.
4. Rubin, S., Unpublished Notes.

5. Rubin, S., "Concepts in Shock Data Analysis", Section 23, "Shock and Vibration Handbook", Volume 2, McGraw-Hill Book Company, New York, 1961, pp. 23-17 - 23-19.
6. Browne, R. A., Unpublished results of digital computer studies on response spectra using TRW program AS-161.

STEADY-STATE MOTIONS OF ORBITAL CABLE PLOWS

Martin Senator and Louis J. Scerbo
Bell Laboratories
Whippany, New Jersey

A perturbation technique is used to calculate steady-state motions of single-eccentric-roller-driven orbital actuators designed to drive vibrating cable plows. Design equations are developed, and their use in adjusting roller unbalance and in choosing mass distribution parameters to obtain desirable blade-tip orbits is illustrated.

INTRODUCTION

A vibrating-blade cable plow allows cable to be buried several feet deep in most soils with substantially reduced tractive efforts. One of the problems associated with the design and development of such a plow is discussed herein; a companion paper* considers a related problem.

Plowing, or pulling a blade through the ground, temporarily opening a narrow slit through which a cable is dropped, is often an economical way of burying telephone cable since the high cost of trenching and restoration can be avoided. Large, heavy track-laying vehicles are often required to develop the high tractive forces necessary to open a slit deep enough for safe cable burial. Consequently, current static plowing operations are often limited to off-the-road routes through rural areas. If the average tractive effort required could be substantially reduced, then smaller, lighter, roadable vehicles could be used, reducing vehicle cost. The plow could also be offset from the prime mover to simplify roadside installations, and the number of economical plowing routes would increase.

It is well known that vibration of a soil penetrator reduces average required applied bias force [1, 2, 3, 4, 5]. Recently, it has also been shown experimentally that drawbar force reductions greater than one part in twenty can be achieved with vibrating plows when the blade moves with circular translation with respect to the vehicle in a direction that produces upward penetration of virgin soil [6]. The commercial development of a low-traction, vibrating-blade

cable plow using a similar concept is being investigated at Bell Laboratories [7, 8].

Important design problems associated with the development of such a plow concern the bearing and suspension systems. The bearing must withstand the forces necessary to produce the vibration of the blade assembly; in addition, the bearing must be isolated from the shock loads produced by blade impacts against massive obstructions. The main requirements of the suspension system are that it support the blade assembly and apply the necessary bias force while isolating the vehicle proper from the vibrating blade assembly.

A prototype blade/shaker assembly (or orbital actuator), which has basic features that promise satisfactory solutions to these problems, has been designed, built, and partially tested at the BTL Chester Laboratory. The details of the design are described in Reference [9], and an isometric sketch of the orbital actuator is shown in Fig. 1. The actuator consists of a massive horizontal structural member rigidly attached to a forward-raked blade. A large cylindrical cavity at the midpoint of the horizontal member contains a heavy cylindrical roller. The roller is driven around the cavity by crank arms supported on a central shaft which, in turn, is driven by a hydraulic motor. Roller motion develops a high rotating force, virtually constant in magnitude, which is transmitted from the roller through the surface of the cavity to the actuator. Relatively high forces can be transmitted with this design without developing excessive contact stresses because the roller contacts the cavity along the

*L. J. Scerbo and M. Senator, "Transient Motions of Orbital Cable Plows."

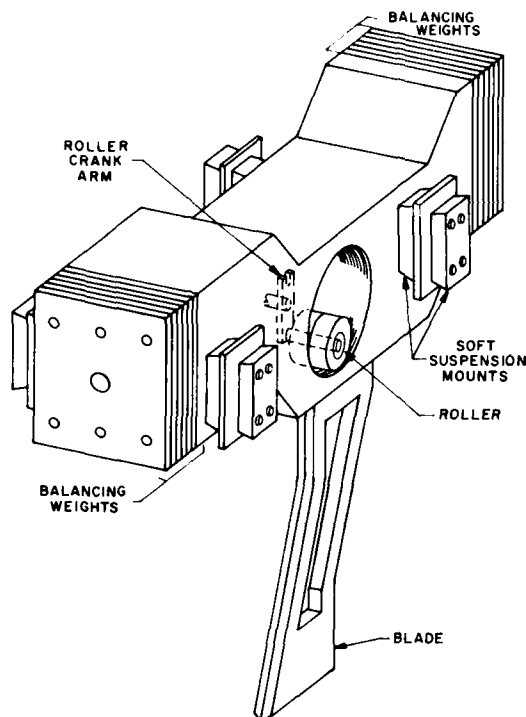


Fig. 1 - Orbital actuator

entire cavity length, because the cavity diameter is large, and because the roller and cavity have centers of curvature on the same side of their common boundary. This design also allows balancing weights to be added to either end of the horizontal member to adjust the location of the actuator mass center. If the mass center is brought near the center of the cavity, nominally circular translational blade motion results; by shifting the balancing masses, various desirable combinations of translational and rotational blade motion can be obtained. The actuator is suspended by rubber shear sandwich mounts located near the ends of the horizontal member. These mounts can transmit the required support and bias forces to the actuator while providing vibration isolation between the actuator and the vehicle frame.

An important feature of this design is its simplicity. The desired orbital motions of points on the blade are developed naturally by the interaction of the rotating force (which is simply generated by the single-eccentric-roller shaker) with the mass of the blade/shaker assembly. Motion-constraining linkages and bias or auxiliary support force-applying mechanisms

are unnecessary. The motion of the actuator is limited mainly by its inertia, and the shaking forces transmitted to the vehicle frame are minimal.

Another important feature of this design is the use of a single-eccentric-roller shaker. The roller transmits the load directly to the cavity. Roller and cavity are in contact along their common length. This provides a large area for transmitting the shaking force, thereby allowing large roller unbalance and high shaking force, which develop large blade-tip amplitude and high penetration rate. By way of contrast, conventional counterrotating-eccentric-weight shakers need rolling contact bearings, which then must transmit the full shaking load and which compete for space with the eccentrics.

STEADY-STATE MOTIONS

In this paper, blade/shaker assembly equations of motion for steady-state conditions are developed and solved and some uses of this solution are discussed and illustrated. The assumptions underlying the analysis are explained and tentatively justified. Notation for the idealized actuator system is introduced and the equations of motion derived. A perturbation technique is used to solve for periodic steady-state motions of this system. Next, these solutions are used to find design equations expressing the motions of important points on the blade/shaker assembly as functions of time and system parameters. Finally, some illustrative examples for the prototype orbital actuator are presented. The results suggest further problems that should be considered.

ASSUMPTIONS

One of the basic assumptions underlying the analysis is that useful information about the motions of points on the actuator can be obtained by studying the zero-soil-force, zero-bias-force, steady-state inertially forced motions (the "free" motions) of the system. This assumption is justified both by knowledge of general vibrating systems and by previous experience with vibrating plows. Note first that harmonic force amplitude exceeds maximum design soil strength and maximum available bias force. For example, in the design of the orbital actuator, the values chosen for these quantities were 300,000 lbs, 50,000 lbs, and 5000 lbs respectively. Force ratios like these imply that the system is inertially limited (as opposed to spring or friction limited); and inertially limited, forced vibrating systems have vibration amplitudes that are virtually independent of damping.* Also, previous experience with the

*For example, a critically damped single-degree-of-freedom linear system that is forced at five times its undamped natural frequency has an amplitude that is 92.3 percent of the amplitude of a similarly forced undamped system.

design and testing of smaller vibrating plows has shown that useful characteristics of the motions, such as vibration amplitudes and bearing loads, can generally be satisfactorily estimated by neglecting soil and bias forces and considering only the steady-state, inertially forced motions.

This approach should not suggest that the effects of relatively small quantities (such as advance per cycle) can always be ignored. But, even when relatively small quantities are of interest, the free motions studied here provide a convenient and usually adequate basis for their estimation.

Another assumption is that the shaker/blade assembly acts like a rigid body. Calculations show that the lowest natural frequency of the shaker/blade assembly is about 330 Hz. Since the maximum crank speed of the actuator is only about 80 Hz, the maximum ratio of forcing to natural frequency is about 0.24. This low ratio justifies the rigid body assumption.

It can also be assumed that elastic and dissipative suspension forces can be neglected. The natural frequencies of in-plane vibration of the (rigid) shaker/blade assembly and its support structure (through the mounts) are all less than 10 Hz, while the lowest steady-state running speed is 40 Hz. Thus, the steady-state inertia forces greatly exceed the elastic and dissipative suspension forces, and the suspension forces can be neglected.

The eccentric roller is assumed to roll on the bearing race without slipping. This assumption is reasonable since the high normal contact force and the absence of any restraint on roller rotation insure that the available friction force always exceeds the tangential reaction necessary to prevent slipping.

The design analysis also neglects gravity forces. This is justified by the usually low ratio (about 0.0004 for the prototype actuator) of roller weight to steady-state centrifugal force.

Finally, the angular velocity of the crank with respect to the shaker/blade assembly is assumed to be constant. Previous experience with eccentric-weight shakers and study of an analytical model [15] suggest that the assumption is reasonable. The justification for the present case follows directly from measurements and from numerical solutions of the start-up equations presented in the companion paper.

NOTATION

Fig. 2 shows the idealized system with the coordinates and symbols used. Point O is the center of the bearing, point P is the tip of the blade, point G is the combined mass center of the shaker/blade assembly and the balanced portion of the rotating mass, point C is the center of the roller, and point E is the mass center

of the entire orbital actuator. In the equilibrium position, P is a distance d below and h in front of O, while G is ϵ_V below and ϵ_H behind O. The distance between O and G is denoted by ϵ . Roller eccentricity OC is denoted by e , and the radius of the solid roller by βe . Fixed orthogonal X and Y axes are taken with positive directions forward and upward respectively. The angle of rotation of the actuator is denoted by θ and is taken as positive in the forward into upward sense. The relative rotation angle of the crank is called Ψ , and is measured in the positive θ direction from a downward line through O. It equals ωt because constant relative angular velocity is assumed, where ω is the angular velocity and t is time. The mass of the roller is αm , while the combined mass of the shaker/blade assembly and the balanced rotating mass is m . The radius of gyration of mass m about G is b , while that of the solid roller about its center, C, is $\beta e/\sqrt{2}$.

We denote the X and Y displacements of point O by x and y respectively, and use x and y with appropriate subscripts to denote the displacements of other points. Then, in terms of x , y , θ , and Ψ , the mass centers C and G have displacements

$$x_C = x + e \sin(\Psi + \theta) \quad (1a)$$

$$y_C = y + e[1 - \cos(\Psi + \theta)] \quad (1b)$$

and

$$x_G = x - \epsilon \cos(\theta + \gamma) + \epsilon \cos \gamma \quad (1c)$$

$$y_G = y - \epsilon \sin(\theta + \gamma) + \epsilon \sin \gamma \quad (1d)$$

where γ is the polar coordinate angle of G, measured from a rearward line through O.

DERIVATION

D'Alembert's technique is used to develop the equations of motion because it simplifies the algebra by eliminating internal forces and allowing a choice of moment center that uncouples the rotational equation from the two translational ones. Fig. 3 shows the appropriate free-body diagram. The accelerations have been computed by differentiating Eqs. (1a-1d), by noting that γ is constant, and by using the assumption of rolling without slipping. (Note that separate inertia forces and torques are not shown for the balanced rotating mass. Since this mass is only a small fraction of m , and the relative crank speed in the steady state is virtually constant, this procedure is sufficiently accurate.)

Since there are no externally applied forces or torques acting on the idealized system, the dynamic equilibrium equations contain only the appropriate inertia force terms. The two translational equations are force sums in the X and Y

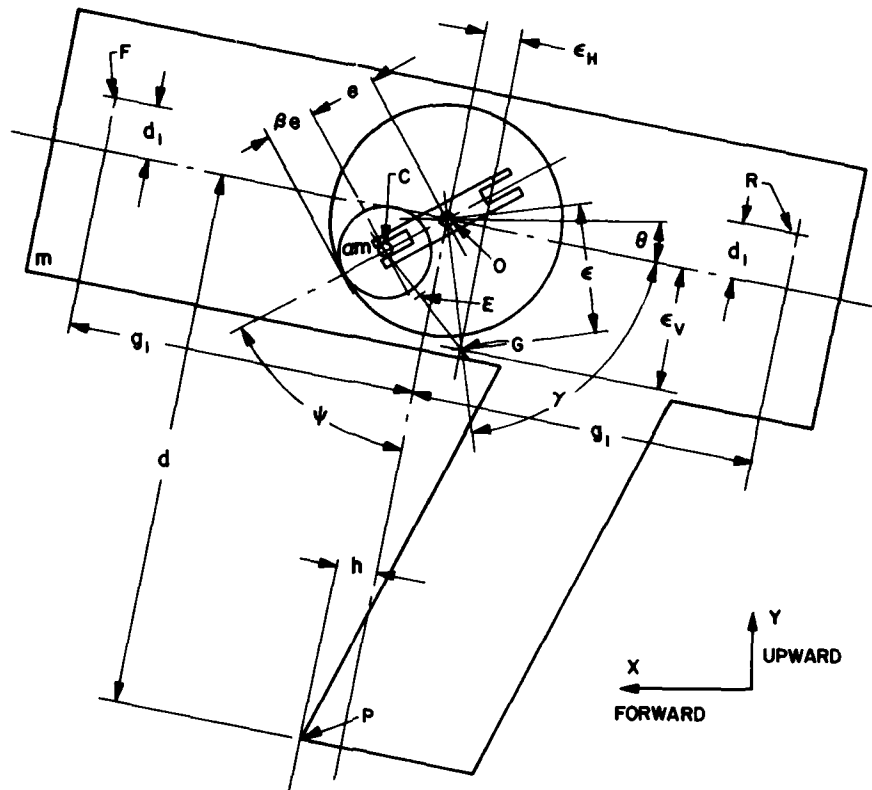


Fig. 2 - Idealized orbital actuator

directions, while the rotational equation is a moment sum about point E, the instantaneous mass center of the system. Since the moments about E of the \ddot{x} and \ddot{y} inertia forces at C and G are equal and opposite, the rotational equation is not coupled to the other two. After cancelling an m, the three equations of motion become

$$\begin{aligned} (1 + \alpha)\ddot{x} - \alpha e(\dot{\Psi} + \dot{\theta})^2 \sin(\Psi + \theta) \\ + \alpha e(\ddot{\Psi} + \ddot{\theta}) \cos(\Psi + \theta) + \epsilon(\dot{\theta})^2 \cos(\theta + \gamma) \\ + \epsilon\ddot{\theta} \sin(\theta + \gamma) = 0, \end{aligned} \quad (2)$$

$$\begin{aligned} (1 + \alpha)\ddot{y} + \alpha e(\dot{\Psi} + \dot{\theta})^2 \cos(\Psi + \theta) \\ + \alpha e(\ddot{\Psi} + \ddot{\theta}) \sin(\Psi + \theta) + \epsilon(\dot{\theta})^2 \sin(\theta + \gamma) \\ - \epsilon\ddot{\theta} \cos(\theta + \gamma) = 0, \end{aligned} \quad (3)$$

and

$$\begin{aligned} b^2\ddot{\theta} + \alpha \frac{(\beta e)^2}{2} \left(\ddot{\theta} - \frac{\ddot{\Psi}}{\beta} \right) \\ + \left[\alpha e(\dot{\Psi} + \dot{\theta})^2 \right] \left[\frac{1}{1 + \alpha} \epsilon \cos(\gamma - \Psi) \right] \\ + \left[\alpha e(\ddot{\theta} + \ddot{\Psi}) \right] \left[\frac{1}{1 + \alpha} \{ e - \epsilon \sin(\gamma - \Psi) \} \right] \\ - \left[\epsilon(\dot{\theta})^2 \right] \left[\frac{\alpha}{1 + \alpha} e \cos(\gamma - \Psi) \right] \\ + \left[\epsilon\ddot{\theta} \right] \left[\frac{\alpha}{1 + \alpha} \{ \epsilon - e \sin(\gamma - \Psi) \} \right] = 0. \end{aligned} \quad (4a)$$

By gathering terms, Eq. (4a) can be written in the form

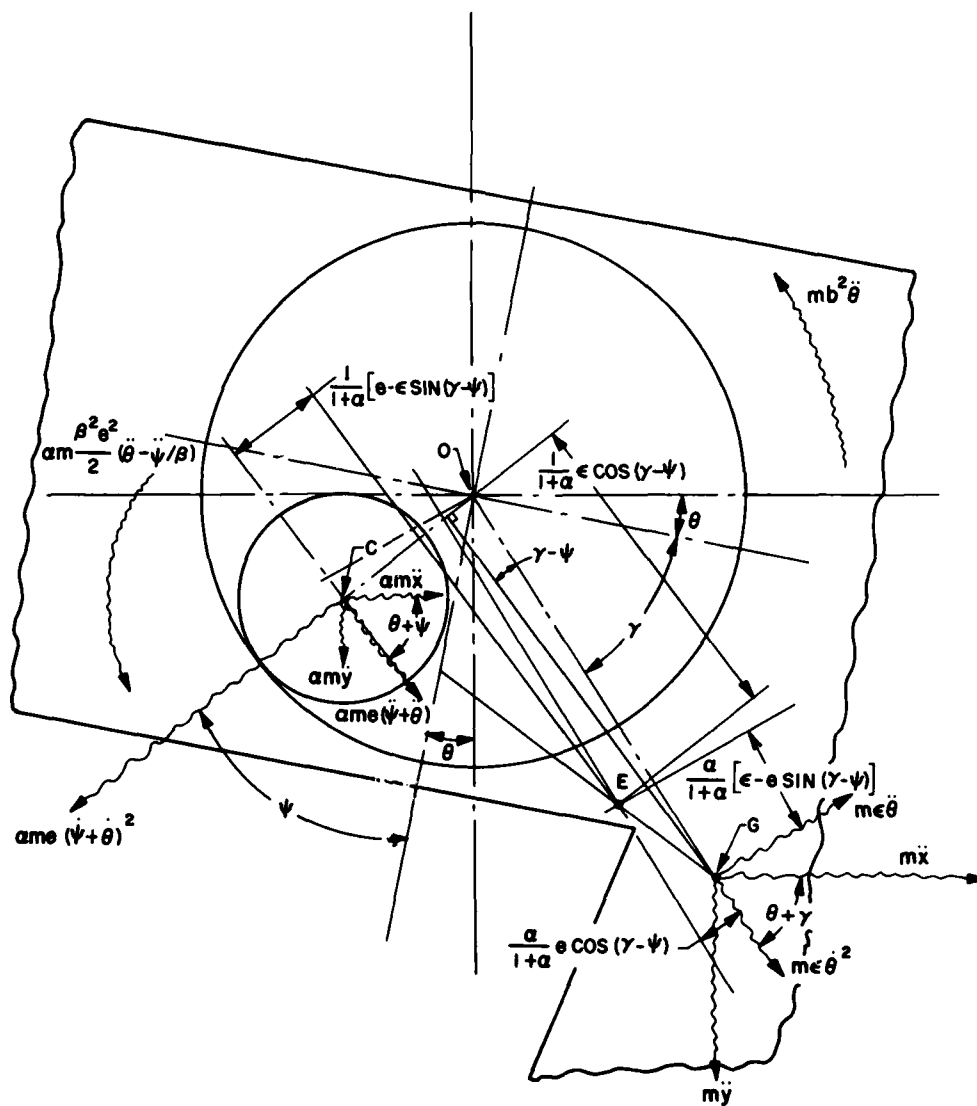


Fig. 3 - Reversed inertia forces

$$f^2(\ddot{\theta}) + \left(\frac{ae^2}{1+\alpha} - \frac{a\beta e^2}{2} \right) \ddot{\Psi} - 2\ddot{\theta} \frac{ae\epsilon}{1+\alpha} \sin(\gamma - \Psi) + \frac{ae\epsilon}{1+\alpha} (\dot{\Psi} + \dot{\theta})^2 \cos(\gamma - \Psi) - \ddot{\Psi} \frac{ae\epsilon}{1+\alpha} \sin(\gamma - \Psi) - \frac{ae\epsilon}{1+\alpha} (\dot{\theta})^2 \cos(\gamma - \Psi) = 0, \quad (4b)$$

where the positive quantity, f (called augmented radius of gyration), defined by

$$f^2 = b^2 + \alpha \frac{\beta^2 e^2}{2} + \frac{ae^2}{1+\alpha} + \frac{ae^2}{1+\alpha} \quad (4c)$$

exceeds the radius of gyration, b . Finally, the assumption of constant relative angular velocity is used to simplify these equations, giving

$$\begin{aligned} \ddot{x} &= \frac{ae}{1+\alpha} (\omega + \dot{\theta})^2 \sin(\omega t + \theta) \\ &- \frac{ae}{1+\alpha} (\ddot{\theta}) \cos(\omega t + \theta) \\ &- \frac{\epsilon}{1+\alpha} (\dot{\theta})^2 \cos(\theta + \gamma) \\ &- \frac{\epsilon}{1+\alpha} \theta \sin(\theta + \gamma), \end{aligned} \quad (5)$$

$$\begin{aligned} \ddot{y} &= -\frac{ae}{1+\alpha} (\omega + \dot{\theta})^2 \cos(\omega t + \theta) \\ &- \frac{ae}{1+\alpha} \ddot{\theta} \sin(\omega t + \theta) \\ &- \frac{\epsilon}{1+\alpha} \dot{\theta}^2 \sin(\theta + \gamma) \\ &+ \frac{\epsilon}{1+\alpha} \ddot{\theta} \cos(\theta + \gamma), \end{aligned} \quad (6)$$

and

$$\begin{aligned} \ddot{\theta} &= -\frac{ae\epsilon}{f^2(1+\alpha)} \left[(\omega^2 + 2\omega\dot{\theta}) \cos(\omega t - \gamma) \right. \\ &\left. + 2\ddot{\theta} \sin(\omega t - \gamma) \right]. \end{aligned} \quad (7)$$

SOLUTION

Equation (7) suggests that if the dimensionless quantity

$$a \equiv \frac{ae\epsilon}{f^2(1+\alpha)} \quad (8)$$

is small, then the forced periodic part of angular displacement, θ , will also be small. This is in accord with physical intuition since it is expected that rocking amplitude will become smaller if any of the factors in the numerator of "a" decrease or if the factor f^2 , in the denominator, increases. Thus, rocking amplitude is small if: eccentric mass fraction, $\alpha/(1+\alpha)$, is small; roller eccentricity, e , is small; offset, ϵ , between the center of applied rotating force and the center of driven mass is small; or if radius of gyration, b , of m about G , or augmented radius of gyration, f , is large.

The quantity "a" is small for the prototype actuator, and we expect it to be small for any foreseeable cable plow design. In the perturbation solution that follows, "a" is assumed to be small although the factors making it small are not specified. Whenever products of "a" and any of its factors appear, the order of the term is considered to be the power of "a." This procedure guards against dropping terms that may be significant for some configurations at the price of making the solution somewhat more complicated.

Thus, the steady-state solutions are:

$$x(t) = x_0(t) + ax_1(t) + a^2x_2(t) + \dots \quad (9a)$$

$$y(t) = y_0(t) + ay_1(t) + a^2y_2(t) + \dots \quad (9b)$$

$$\theta(t) = a\theta_1(t) + a^2\theta_2(t) + \dots \quad (9c)$$

where the x_i , y_i , and θ_i are periodic functions of t , with least period equal to $2\pi/\omega$, the time for one crank revolution. Substituting Eqs. (9a)-(9c) into Eqs. (5)-(7), expanding the trigonometric terms in θ in power series, and grouping terms of the same order together gives

$$\begin{aligned} &\ddot{x}_0 + a\ddot{x}_1 + a^2\ddot{x}_2 \\ &= \left[\frac{ae}{1+\alpha} \omega^2 \sin \omega t \right] + a \left[\frac{ae}{1+\alpha} \left\{ \omega^2 \theta_1 \cos \omega t \right. \right. \\ &\quad \left. \left. + 2\omega \dot{\theta}_1 \sin \omega t - \ddot{\theta}_1 \cos \omega t \right\} - \frac{\epsilon}{1+\alpha} \ddot{\theta}_1 \sin \gamma \right] \\ &\quad + a^2 \left[\frac{ae}{1+\alpha} \left\{ 2\omega \dot{\theta}_2 \sin \omega t + \ddot{\theta}_1^2 \sin \omega t \right. \right. \\ &\quad \left. \left. + 2\omega \dot{\theta}_1 \theta_1 \cos \omega t - \omega^2 \frac{\theta_1^2}{2} \sin \omega t \right. \right. \\ &\quad \left. \left. + \omega^2 \theta_2 \cos \omega t - \ddot{\theta}_2 \cos \omega t + \ddot{\theta}_1 \theta_1 \sin \omega t \right\} \right. \\ &\quad \left. - \frac{\epsilon}{1+\alpha} \left\{ \ddot{\theta}_1^2 \cos \gamma + \ddot{\theta}_2 \sin \gamma + \ddot{\theta}_1 \theta_1 \cos \gamma \right\} \right], \end{aligned} \quad (10)$$

$$\begin{aligned}
& \ddot{y}_0 + a\ddot{y}_1 + a^2\ddot{y}_2 \\
& = -\left[\frac{ae}{1+\alpha}\omega^2 \cos \omega t\right] + a\left[\frac{ae}{1+\alpha}\omega^2 \theta_1 \sin \omega t\right. \\
& \quad \left.- 2\omega\dot{\theta}_1 \cos \omega t - \ddot{\theta}_1 \sin \omega t\right] + \frac{\epsilon}{1+\alpha}\ddot{\theta}_1 \cos \gamma \\
& \quad + a^2\left[\frac{ae}{1+\alpha}\omega^2 \cos \omega t - \ddot{\theta}_1^2 \cos \omega t\right. \\
& \quad \left.+ 2\omega\dot{\theta}_1 \theta_1 \sin \omega t + \omega^2 \frac{\theta_1^2}{2} \cos \omega t\right. \\
& \quad \left.+ \omega^2 \theta_2 \sin \omega t - \ddot{\theta}_2 \sin \omega t - \ddot{\theta}_1 \theta_1 \cos \omega t\right] \\
& \quad + \frac{\epsilon}{1+\alpha}\left[-\ddot{\theta}_1^2 \sin \gamma + \ddot{\theta}_2 \cos \gamma - \ddot{\theta}_1 \theta_1 \sin \gamma\right], \quad (11)
\end{aligned}$$

$$\begin{aligned}
& a \\
& a\ddot{\theta}_1 + a^2\ddot{\theta}_2 + a^3\ddot{\theta}_3 \\
& = -a\left[\omega^2 \cos (\omega t - \gamma)\right] \\
& \quad - a^2\left[2\omega\dot{\theta}_1 \cos (\omega t - \gamma) + 2\ddot{\theta}_1 \sin (\omega t - \gamma)\right] \\
& \quad - a^3\left[2\omega\dot{\theta}_2 \cos (\omega t - \gamma) + 2\ddot{\theta}_2 \sin (\omega t - \gamma)\right]. \quad (12)
\end{aligned}$$

Equation (12) can be solved sequentially for θ_1 , θ_2 , ... independently of x and y . Equations (10) and (11) can then be solved sequentially for x_0 , y_0 ; x_1 , y_1 ; ... after the corresponding order solutions for θ have been found.

Carrying these solutions out gives the periodic steady-state motions:

$$x_0(t) = -\frac{ae}{1+\alpha} \sin \omega t, \quad (13a)$$

$$y_0(t) = \frac{ae}{1+\alpha} \cos \omega t; \quad (13b)$$

$$a\theta_1(t) = a \cos (\omega t - \gamma), \quad (14a)$$

$$\begin{aligned}
ax_1(t) = & -a\left[\frac{1}{2}\frac{ae}{1+\alpha} \cos (2\omega t - \gamma)\right. \\
& \left.+ \frac{\epsilon}{1+\alpha} \sin \gamma \cos (\omega t - \gamma)\right], \quad (14b)
\end{aligned}$$

$$\begin{aligned}
ay_1(t) = & a\left[-\frac{1}{2}\frac{ae}{1+\alpha} \sin (2\omega t - \gamma)\right. \\
& \left.+ \frac{\epsilon}{1+\alpha} \cos \gamma \cos (\omega t - \gamma)\right]; \quad (14c)
\end{aligned}$$

$$a^2\theta_2(t) = -a^2\left[\frac{1}{2} \sin (2\omega t - 2\gamma)\right], \quad (15a)$$

$$\begin{aligned}
a^2x_2(t) = & a^2\left[\frac{ae}{1+\alpha}\frac{1}{4} \sin \omega t + \frac{1}{8} \sin (\omega t - 2\gamma)\right. \\
& \left.+ \frac{3}{8} \sin (3\omega t - 2\gamma)\right] \\
& + \frac{\epsilon}{1+\alpha}\left[-\frac{3}{8} \cos (2\omega t - \gamma)\right. \\
& \left.+ \frac{1}{8} \cos (2\omega t - 3\gamma)\right], \quad (15b)
\end{aligned}$$

$$\begin{aligned}
a^2y_2(t) = & a^2\left[\frac{ae}{1+\alpha}\frac{1}{4} \cos \omega t\right. \\
& \left.+ \frac{1}{8} \cos (\omega t - 2\gamma) - \frac{3}{8} \cos (3\omega t - 2\gamma)\right] \\
& + \frac{\epsilon}{1+\alpha}\left[-\frac{3}{8} \sin (2\omega t - \gamma)\right. \\
& \left.- \frac{1}{8} \sin (2\omega t - 3\gamma)\right]; \quad (15c)
\end{aligned}$$

$$a^3\theta_3 = a^3\left[\cos (\omega t - \gamma) - \frac{1}{3} \cos (3\omega t - 3\gamma)\right]. \quad (16)$$

Once the displacement components of O and the rotation angle θ are known for the steady-state, zero-suspension force, zero-bias force, zero-soil force case, the corresponding motions of the blade-tip (point P) and of the centers of the front and rear supports (points F and R) can be found from Fig. 2 by using the rigid-body assumption:

$$x_P = x + d \sin \theta - h(1 - \cos \theta) \quad (17a)$$

$$y_P = y + d(1 - \cos \theta) + h \sin \theta \quad (17b)$$

and

$$x_{F,R} = x \mp g_1(1 - \cos \theta) - d_1 \sin \theta \quad (18a)$$

$$y_{F,R} = y \pm g_1 \sin \theta - d_1(1 - \cos \theta) \quad (18b)$$

where d_1 is the common height of F and R above O, g_1 is the horizontal projection of the equal distances between F or R and O, and the upper signs are associated with point F and the lower signs with point R.

DESIGN EQUATIONS

For many design purposes, Eqs. (9) and (13)-(18), which express the periodic, steady-state, free motions of four important points on the actuator, can be further simplified by neglecting the higher order displacement terms. Terms that are the products of small rotation angles and large arms must be retained, however, since they contribute appreciable displacement components.

To carry out these simplifications, note that, for the prototype actuator and for foreseeable cable plow designs, the quantities $\alpha e/f$, d_1/f , and h/f are small compared to 1, the quantities d/f and g_1/f are of ordinary magnitude, and the quantity ϵ/f may either be small or of ordinary magnitude, depending upon the size and arrangement of the balance weights. Thus, neglecting $\alpha e/f$, d_1/f , h/f , and "a" in comparison to 1, the components of ϵ in Eqs. (9) and (13)-(18) can be used to obtain the following design parametric equations for the elliptical trajectories of points O, P, F, and R. These design quantities are indicated by the additional subscript, d.

$$x_{O_d}(t) = -\frac{\alpha e}{1+\alpha} \left[\left(1 + \frac{\epsilon_V^2}{f^2(1+\alpha)} \right) \sin \omega t + \frac{\epsilon_V \epsilon_H}{f^2(1+\alpha)} \cos \omega t \right], \quad (19a)$$

$$y_{O_d}(t) = \frac{\alpha e}{1+\alpha} \left[\left(1 + \frac{\epsilon_H^2}{f^2(1+\alpha)} \right) \cos \omega t + \frac{\epsilon_V \epsilon_H}{f^2(1+\alpha)} \sin \omega t \right]; \quad (19b)$$

$$x_{P_d}(t) = -\frac{\alpha e}{1+\alpha} \left[\left(1 - \frac{d\epsilon_V}{f^2} + \frac{\epsilon_V^2 \epsilon_H}{f^2(1+\alpha)} \right) \sin \omega t - \left(\frac{d\epsilon_H}{f^2} - \frac{\epsilon_V \epsilon_H}{f^2(1+\alpha)} \right) \cos \omega t \right], \quad (20a)$$

$$y_{P_d}(t) = y_{O_d}(t); \quad (20b)$$

and

$$x_{F_d, R_d}(t) = x_{O_d}(t), \quad (21a)$$

$$y_{F_d, R_d}(t) = \frac{\alpha e}{1+\alpha} \left[\left(1 + \frac{g_1 \epsilon_H}{f^2} + \frac{\epsilon_H^2}{f^2(1+\alpha)} \right) \cos \omega t + \left(\frac{\epsilon_V \epsilon_H}{f^2(1+\alpha)} + \frac{g_1 \epsilon_V}{f^2} \right) \sin \omega t \right]. \quad (21b)$$

To the same order of accuracy, the normal reaction at the bearing surface is constant and given by

$$R_{N_d} = \frac{\alpha m e \omega^2}{1+\alpha}. \quad (22)$$

Two other quantities of interest in design are the horizontal amplitude at the blade-tip, X_{O_d} , and the amplitude/frequency product, ωX_{O_d} . Design values can be derived for these quantities by using Eqs. (19a) and (22):

$$X_{O_d} = \frac{\alpha e}{1+\alpha} A, \quad (23a)$$

$$(\omega X_{O_d})_d = \sqrt{\alpha m e} \sqrt{R_{N_d}} \frac{1}{m \sqrt{1+\alpha}} A, \quad (23b)$$

or

$$(\omega X_{O_d})_d = X_{O_d} \frac{\sqrt{R_{N_d}}}{\sqrt{m}} \sqrt{A}, \quad (23c)$$

or

$$(\omega X_{O_d})_d = \frac{1}{\omega} \frac{R_{N_d}}{m} A \quad (23d)$$

where A is defined by

$$A = \sqrt{\left[1 - \frac{d\epsilon_V}{f^2} + \frac{\epsilon_V^2}{f^2(1+\alpha)} \right]^2 + \left[\frac{d\epsilon_H}{f^2} - \frac{\epsilon_V \epsilon_H}{f^2(1+\alpha)} \right]^2} \quad (23e)$$

ILLUSTRATIVE EXAMPLES

The use of these design equations can be illustrated by applying them to the prototype actuator in two steps. First, it will be shown how roller unbalance, $\alpha m e$, can be chosen. During this step, total actuator mass and actuator mass distribution are held constant so that the parameters m , f , ϵ_V , ϵ_H , and $1+\alpha$ remain essentially

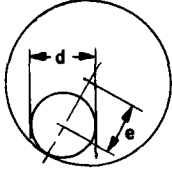
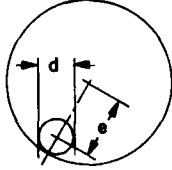
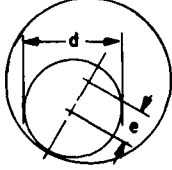
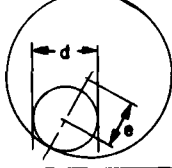
constant. Then, the effects of changes in total mass and mass distribution are shown by keeping roller unbalance constant and examining four limiting mass distributions.

Roller Unbalance

Examination of Eq. (23b) shows that the amplitude/frequency product, ωX_0 , increases as the square root of roller unbalance, $\omega m e$, when design bearing load, R_{N_d} , and system mass and mass distribution parameters are fixed. Furthermore, a large blade-tip amplitude/frequency product is desirable since plow penetration rate is approximately a linearly increasing function of the amplitude/frequency product (as implied in References [4]-[6] and [10]-[14]).

Table I compares four roller designs. In all cases, roller length is 16.25 in. and the inside diameter of the cavity is 13.75 in. These dimensions correspond to those used on the prototype actuator. Case 1 shows the roller actually used in the prototype. It is steel and has the largest possible diameter that will still leave room for a central shaft to carry the roller drive arms. Case 2 considers a steel roller half the diameter of the one actually used. Case 3 is a steel roller with a diameter two-thirds that of the cavity, a value that maximizes roller unbalance but requires a more complicated drive arrangement, since it prevents the use of a central drive shaft. Case 4 is a roller of the same diameter as the one actually used but made of a (considerably more expensive) high density material that doubles roller mass. For each parameter, the entries are ratios of the values to those of Case 1.

TABLE I
Four Cases of Roller Unbalance

Case No., Roller Dia. Eccentricity	Sketch	Roller Mass Ratio	Eccentricity Ratio	Roller Unbalance and Amplitude Ratios	Crank Speed Ratio for Same Design Bearing Load	Amplitude/ Frequency Product Ratio
1 $d = 6.00$ in. $e = 3.875$ in.		1.00	1.000	1.000	1.000	1.000
2 $d = 3.000$ in. $e = 5.375$ in.		0.250	1.388	0.347	1.695	0.590
3 $d = 9.167$ in. $e = 2.286$ in.		2.33	0.591	1.375	0.854	1.175
4 $d = 6.00$ in. $e = 3.875$ in.		2.00	1.000	2.00	0.707	1.414

For example, Table I shows that if roller diameter is reduced by a factor of 2 (Case 2), roller mass decreases by a factor of 4, eccentricity increases 39 percent, roller unbalance and blade-tip amplitude decrease 65 percent, design crank speed for a constant bearing load increases 70 percent, and the amplitude frequency product decreases 41 percent. The 70-percent increase in crank speed would reduce the allowable design bearing load from that of Case 1 and cause an additional decrease in the amplitude frequency product that is not reflected in Table I. Case 3 (roller diameter $2/3$ of cavity diameter), which leads to the maximum possible amplitude frequency product with a steel roller, is seen to have a much heavier roller but a smaller eccentricity than Case 1, so that the amplitude frequency product increases by only 18 percent. Here the increase is underestimated slightly, since the 15-percent decrease in design crank speed would allow a small increase in design bearing load. Case 4 (double-density roller) is the most dramatic

because it shows a 41-percent increase in the amplitude/frequency product. Again, the increase is underestimated because allowance for the 29-percent reduction in design crank speed has not been made.

Thus, when shaker-bearing capacity limits the design, the greatest practical roller unbalance should be chosen since it gives the greatest amplitude frequency product, the greatest design blade-tip amplitude, and the lowest design crank speed.

Mass Distribution

Next, effects of changing total mass and mass distribution are illustrated by examining four mass distributions attainable with the prototype actuator. Fig. 4 shows the idealized dimensions and mass distribution used in the calculations, and Table II lists the parameters for the four cases. Case 1, the stripped actuator, consists

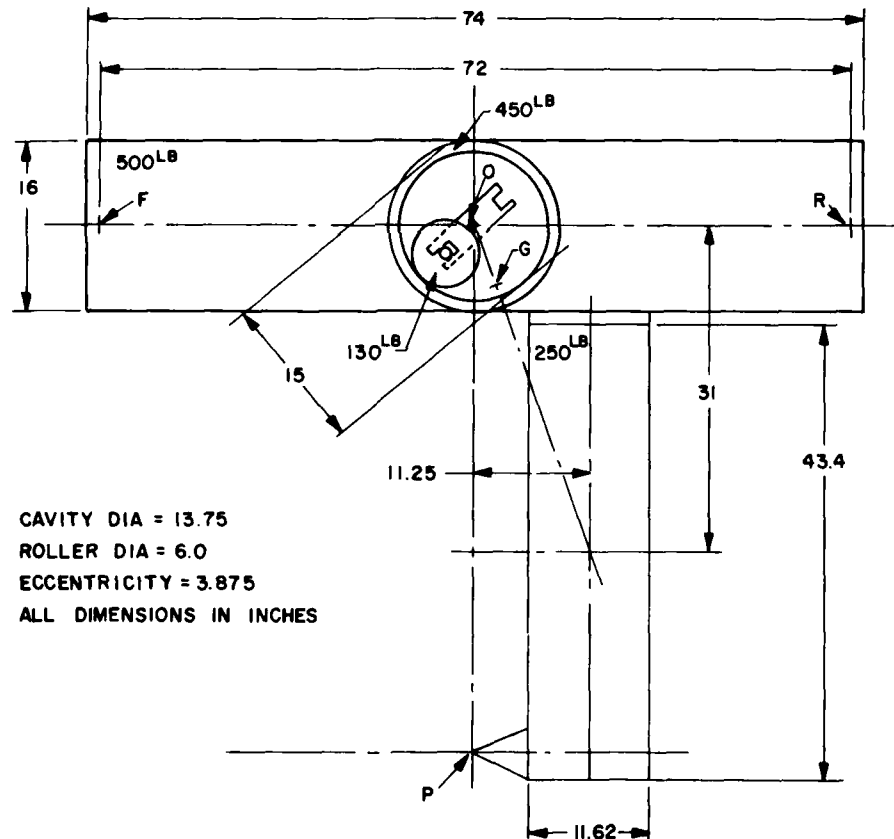
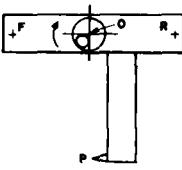
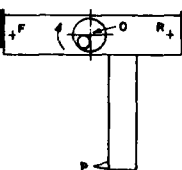
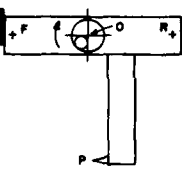
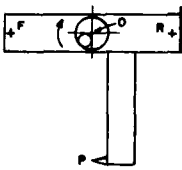


Fig. 4 - Idealized dimensions and mass distribution for prototype actuator with balance weights removed

TABLE II
Four Mass Distribution Cases

Case No.	Sketch	Parameters	X_O , ω , and ωX_O for $RN_d = 300,000$ lbs	Support Center Orbits
1	Stripped 	$\epsilon_H = 2.34$ in. $\epsilon_V = 6.46$ in. $\epsilon = 6.87$ in. $\gamma = 70.05^\circ$ $b^2 = 433$ in. ² $f^2 = 440$ in. ² $a = 0.00591$ $ae/(1+a) = 0.379$ in.	$X_O = 0.1603$ in. $\omega = 505$ rad/sec $\omega X_O = 81.0$ in./sec	Major Axis 0.562 in. Minor Axis 0.333 in. Area 0.588 in. ² Perimeter 2.86 in. Controlling* Front
2	Balanced 	$\epsilon_H = 0$ in. $\epsilon_V = 1.475$ in. $\epsilon = 1.475$ in. $\gamma = 90^\circ$ $b^2 = 894$ in. ² $f^2 = 895$ in. ² $a = 0.000390$ $ae/(1+a) = 0.2365$ in.	$X_O = 0.218$ in. $\omega = 494$ rad/sec $\omega X_O = 107.8$ in./sec	Major Axis 0.244 in. Minor Axis 0.230 in. Area 0.176 in. ² Perimeter 1.49 in. Controlling* Front
3	Front Mass 	$\epsilon_H = -13.79$ in. $\epsilon_V = 1.475$ in. $\epsilon = 13.87$ in. $\gamma = 173.9^\circ$ $b^2 = 699$ in. ² $f^2 = 712$ in. ² $a = 0.00461$ $ae/(1+a) = 0.2365$ in.	$X_O = 0.307$ in. $\omega = 499$ rad/sec $\omega X_O = 153$ in./sec	Major Axis 0.462 in. Minor Axis 0.238 in. Area 0.346 in. ² Perimeter 2.26 in. Controlling* Rear
4	Rear Mass 	$\epsilon_H = 16.61$ in. $\epsilon_V = 1.475$ in. $\epsilon = 16.67$ in. $\gamma = 5.08^\circ$ $b^2 = 613$ in. ² $f^2 = 631$ in. ² $a = 0.00624$ $ae/(1+a) = 0.2365$ in.	$X_O = 0.369$ in. $\omega = 494$ rad/sec $\omega X_O = 182.3$ in./sec	Major Axis 0.559 in. Minor Axis 0.238 in. Area 0.419 in. ² Perimeter 2.61 in. Controlling* Front

*The support-point trajectory parameters are listed for the point with maximum excursion.

of only the 1200 lbs of blade, bearing housing, and support structure. Case 2, the balanced actuator, has an additional 800 lbs of balance weight split between the front and rear locations so as to position the mass center, G, close to and directly below the rotation center, O. Cases 3 and 4 are unbalanced: in Case 3, the 800 lbs of added

weight are at the front; in Case 4, the 800 lbs are at the rear.

The steady-state absolute trajectories traced by the blade-tip, P, the bearing center, O, the front support center, F, and the rear support center, R, are shown for each of the four cases in Figs. (5a)-(5d). The same vertical

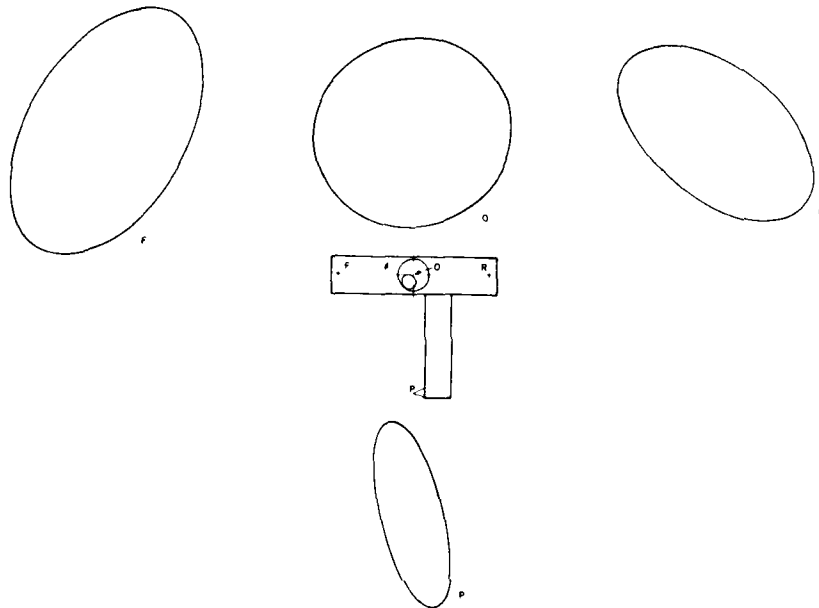


Fig. 5a - Orbits for stripped plow

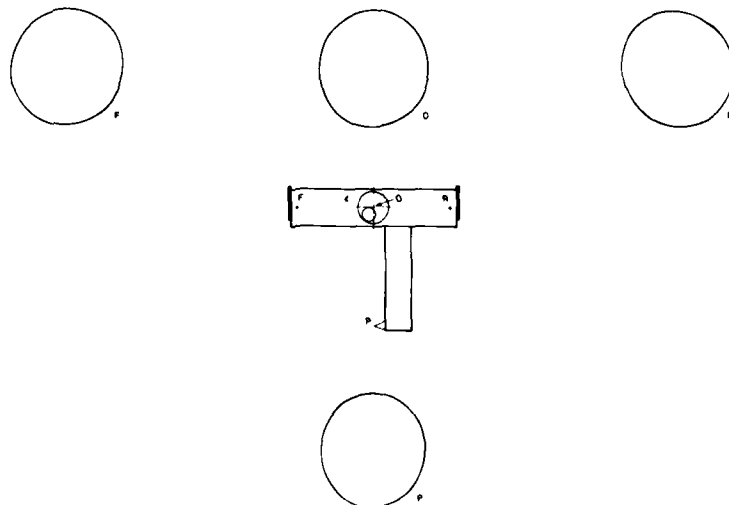


Fig. 5b - Orbits for balanced plow

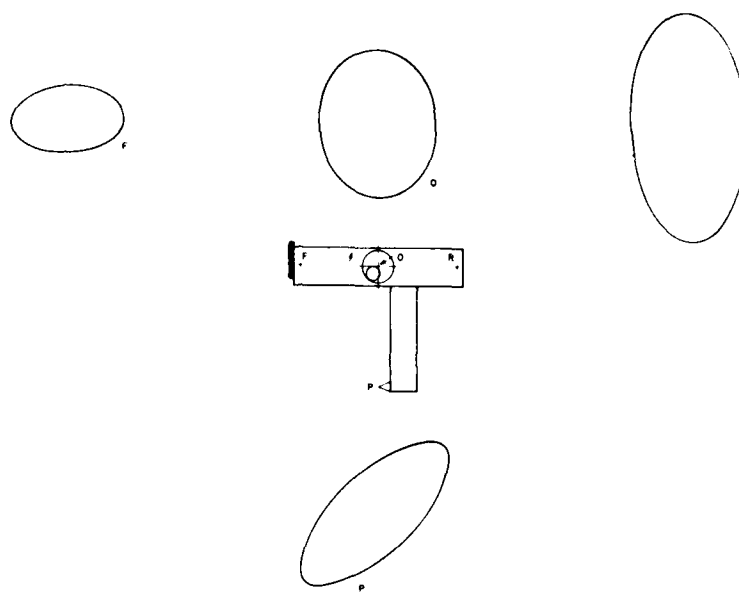


Fig. 5c - Orbits for front mass plow

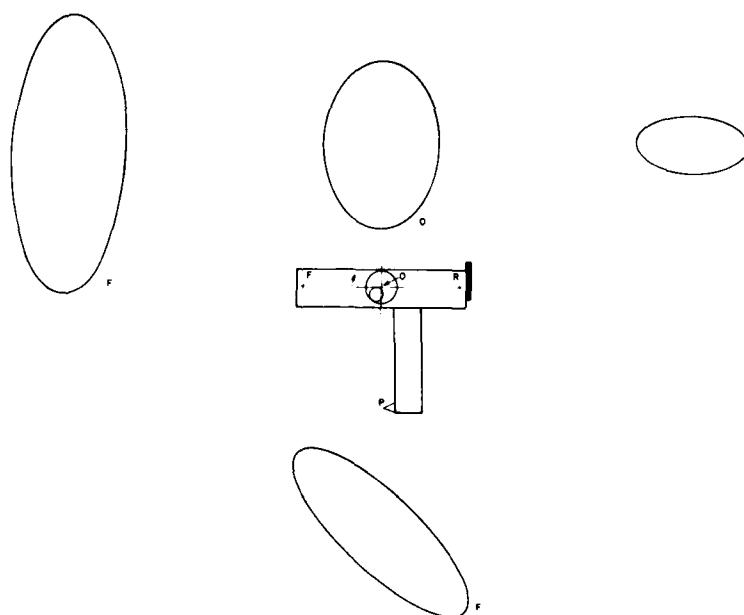


Fig. 5d - Orbits for rear mass plow

and horizontal scales are employed throughout to show true geometric properties and to permit easy comparisons.

Before comparing the four configurations, consider the reasons that led to investigating the effects of adding balancing masses. First, the blade-tip motion is the superposition of the motion of the mass center and rigid-body rotation about the mass center. Also, the actuator is an inertially limited system. Thus, the motion of the mass center is out of phase with that of the roller; for example, the mass center is at its rearmost position when the roller is at its forwardmost position.

The motion at the blade tip produced by rotation about the mass center depends on the relative locations of points O, G, and P, the force center, the rotation center of the actuator body, and the point whose motion is to be found. For the stripped prototype actuator, and for practical shaker/blade configurations without added mass, these points essentially lie along a vertical line with G between O and P. The reason for this orientation is that the massive blade must be mounted underneath the shaker. For this orientation, the peak forward component of rotational motion of P occurs when the roller is at its forwardmost position because, at this instant, the torque on the inertially limited system is peaking in the direction that would produce rearward displacement. Thus, the horizontal component of rotational displacement is out of phase with the horizontal component of mass-center displacement, and an effect of rotation is to reduce horizontal blade-tip amplitude.*

By adding balancing masses, the location of the actuator mass center can be shifted, and both the phase and amplitude of the motion of P can be modified. Thus, by investigating the effects of balancing masses, an arrangement may be found that either eliminates the destructive interference between mass center motion and rotational motion or perhaps even produces constructive interference.

*An instructive heuristic derivation of the equation predicting the reduction in horizontal displacement amplitude caused by rotation is suggested by this discussion. The torque producing the rocking has an amplitude equal to the product of centrifugal force, R_{Nd} , and the arm, ϵ_V . The rotation amplitude equals the torque divided by the product of central moment of inertia, mb^2 , and square of circular frequency, ω^2 . Finally, the reduction in displacement amplitude is the product of rotation amplitude and the arm, $d - \epsilon_V$. This gives

$$-\Delta X_0 = \frac{(R_{Nd} \epsilon_V)(d - \epsilon_V)}{mb^2 \omega^2} = \frac{(ae)(\epsilon_V)(d - \epsilon_V)}{(1 + a)b^2}$$

which, for $b \approx f$ and $\epsilon_H \approx 0$, agrees well with the value obtained from Eqs. (23a) and (23e).

†The addition of balancing masses may also increase ability to dislodge buried obstacles. If the actuator is rigid enough, the momentum transferred to the obstacle during impact would be greater since both actuator mass and central moment of inertia increase with the addition of the balancing weights. See Reference [9] for a discussion of this effect.

Now consider the balanced actuator (Case 2, Table II). Addition of the 800 lbs of balancing mass has three immediate effects: it brings mass center, G, appreciably closer to rotation center, O, thereby reducing the moment arm of the rotating force and causing a decrease in rocking torque amplitude; it increases the central moment of inertia, mb^2 ; and it increases total system mass, causing a decrease in eccentric mass fraction, $a/(1 + a)$. The first two effects tend to reduce the horizontal component of rocking motion at P. The third effect, however, tends to decrease the amplitude of mass center motion, thereby reducing the horizontal blade-tip amplitude. For the balanced actuator, the mass addition decreases mass center amplitude from $ae/(1 + a) = 0.379$ in. to 0.237 in., but net horizontal blade-tip amplitude increases from $X_0 = 0.160$ in. to 0.218 in. With a design bearing load, R_{Nd} , of 300,000 lbs, and with allowance for the small change in the quantity $1 + a$, the addition of the balancing masses increases the amplitude/frequency product from 81 in./sec to 108 in./sec, an increase of 33 percent.†

A further increase in the amplitude/frequency product can be obtained by using unsymmetric configurations of the balancing weights. When all the added mass is at the front (Case 3 in Table II), point G lies approximately along the horizontal line between O and F. Because of this horizontal offset, the rocking motion contributes an additional vertical displacement component to the motion of P. The result is to cause P to trace a downwardly tilted ellipse in inertial space as shown in Fig. 5c. For the rear mass case (4), G lies approximately along the line between O and R, and the inertial path of P is an upwardly tilted ellipse, as shown in Fig. 5d.

Table II shows that the rear-mass configuration produces the largest amplitude/frequency product of the four mass distribution cases considered. This product is 2.25 times that of

the stripped configuration and 1.69 times that of the balanced configuration. Furthermore, the shape of the blade-tip trajectory is more desirable in the rear mass case than in the other three cases. One reason is that it provides reasonably steep upward cutting for all practical ratios of advance-per-cycle to horizontal amplitude. By way of contrast, the narrow, downward-tilted elliptical orbit of Case 3 produces upward cutting for only small values of this ratio. Another advantage of the Case 4 P-orbit is that the ratio of perimeter to horizontal projection is relatively small. This suggests that losses due to skin friction will be comparatively low. Thus, from a penetration rate point of view, it may be concluded that the rear-mass configuration offers significant advantages.

Fig. 5 also shows the inertial paths of the centers of the mounts. These trajectories indicate the relative displacements expected across the mounts, and therefore the magnitude of the design problems associated with the mounts. The properties of the controlling mount-center trajectory for each case are summarized in Table II, which lists major and minor diameters, areas, and perimeters. In going from the stripped to the balanced mass case, peak displacement at the mounts is reduced by a factor of about 2. For the front and rear mass cases, the displacements at the mount near the mass center are reduced still further, while those of the more distant mount are increased. However, the controlling orbits in these cases are approximately the same size as those for the stripped configuration. Initial tests on the prototype actuator indicate that satisfactory mount life under steady-state conditions can be attained for any of these orbits. Therefore, mount endurance need not be the controlling factor in the design choice of a suitable mass arrangement.

SUMMARY AND RECOMMENDATIONS

Equations were found which describe the zero-soil-force, zero-bias-force, periodic steady-state, inertial motions of points on an orbital actuator as functions of system mass distribution and geometric parameters.

Two applications of these equations in plow design were illustrated. First, four cases of roller unbalance were compared. It was shown that the largest practical value of roller unbalance should be chosen because the blade-tip amplitude/frequency product (a measure of penetration rate) increases as the square root of roller unbalance when actuator mass, mass

distribution, geometry, and design bearing load remain constant.

The steady-state solutions were also used to study effects of changing total actuator mass and mass distribution. It was shown that the addition of balancing masses to the stripped configuration changes the blade-tip orbit from a narrow ellipse with a nearly vertical major axis to a nearly circular ellipse, wider by 36 percent; the mass addition also reduces the absolute displacement amplitudes at the mounts by a factor of about 2. Since this mass addition increases the amplitude frequency product by 33 percent, the analysis shows that the balanced configuration is more desirable than the stripped configuration.

Two unbalanced configurations were also considered, one with all additional mass at the front and the other with all additional mass at the rear. The rear-mass configuration was shown to have a very desirable blade-tip orbit. The horizontal projection of this orbit is 69 percent greater than that of the balanced configuration and its narrow, upwardly tilted, elliptical shape produces upward cutting for all practical ratios of advance-per-cycle to horizontal amplitude. Relative skin-friction energy dissipation is also less for this orbit than for the other cases studied.

One disadvantage of the rear-mass configuration is the relatively large displacement amplitude at the front support. In future designs, however, it may be possible to relocate the front support to reduce the displacement amplitude across it. This aspect of the rear-mass configuration should not present a severe problem.

In view of these results, both the rear-mass and the balanced configurations deserve serious consideration in ongoing development efforts.

A problem with a rear-mass configuration plow is anticipated during start-up. As crank speed increases, it passes through a range corresponding to the natural frequencies of the actuator/mounts/support structure system. If driving motor torque is low, it is possible for the roller to "lock in" at these resonant frequencies and to run in this speed range long enough to cause unacceptably large displacements. This tendency has been observed in the balanced prototype plow, and it is expected to be more severe with the plow in the rear-mass configuration. This problem requires further analytical study before experiments are undertaken with a rear-mass configuration plow.

REFERENCES

1. I. I. Blekhman, "An Investigation of the Process of Vibrational Driving of Piles and Sheet Piles," *Inzh. Sb., Inst. Mekh. Akad. Navk SSSR*, Vol 19, pp 55-64, 1954. Translated by Associated Technical Services, Inc., No. RJ-4524.
2. O. A. Savinov and A. Ya. Luskin, "Current Status and Outlook of the Vibrational Method for Pile Driving," *Mekhanizatsiya Stroitel'stva*, Vol 9 (5), pp 26-29, 1952.
3. D. N. Koppes, "Field Tests of Commercial Vibrating Cable Plows," Bell Laboratories unpublished work.
4. J. C. Maclay, D. F. Milsark, and D. B. Sherman, "Effects of Vibration of a Rigid Lawn Plow Assembly on Drawbar Pull (1964 Chester Tests)," Bell Laboratories unpublished work.
5. R. J. Boyd and C. L. Nalezny, "A Model of Vibratory Soil Cutting," SAE Paper 670750, presented at the Farm, Construction, and Industrial Machinery Meeting, Milwaukee, Wisconsin, Sept. 1967.
6. W. F. Bilotta, R. J. Boyd, R. E. Warren, and C. L. Nalezny, "Upward Cutting Vibratory Plowing," SAE Paper 710729, presented at the National Farm, Construction, and Industrial Machinery Meeting, Milwaukee, Wisconsin, Sept. 1971.
7. A. G. Vedejs, "Putting Telephone Lines Below Ground," Bell Laboratories Record, pp 13-21, Jan. 1971.
8. L. J. Scerbo, "Orbital Cable Plow - Prospectus for Project," Bell Laboratories unpublished work.
9. L. J. Scerbo, "Orbital Cable Plow - Design and Test Program for Orbital Actuator," Bell Laboratories unpublished work.
10. M. Senator and R. E. Warren, "Penetration Rates of Fore-Aft Vibrating Plows," *Transactions ASAE*, Vol 14, No. 2, pp 242-247, 1971.
11. M. Senator, "Penetration Rates and Stability of Motions of a Harmonically Forced Fore-Aft Vibrating Plow," Bell Laboratories unpublished work.
12. M. Senator and R. E. Warren, "Predicting Penetration Rates of Plows with Combined Vertical and Fore-Aft Vibration and Flexible Blades," SAE Paper 700040, presented at Automotive Engineering Congress, Detroit, Michigan, Jan. 1970.
13. C. F. Aquino, "Orbital Cable Plow - Estimation of Performance and Power Requirements," Bell Laboratories unpublished work.
14. C. L. Nalezny, "Analysis of Upward Soil Cutting with a Vibratory Plow," SAE Paper No. 710728, Sept. 1971.
15. M. Senator, "Limit Cycles and Stability of a Nonlinear Two-Degree-of-Freedom Autonomous Vibratory System," *Journal of Eng. for Ind., Trans. ASME*, Vol 91, Series B, No. 4, pp 959-966, Nov. 1969.

TRANSIENT MOTIONS OF ORBITAL CABLE PLOWS

Louis J. Scerbo and Martin Senator

Bell Laboratories
Whippany, New Jersey

The following paper investigates the transient start-up motions of a single-eccentric-roller-driven orbital actuator designed to drive vibrating cable plows. Three special mass distributions, which have desirable blade-tip orbits in the steady state, are studied in detail.

The differential equations of motion are developed and solved, and the numerical results are used to predict inertial and relative displacements at various points in the system. These displacements are used to evaluate the capability of the suspension system.

It was found that, for certain combinations of applied torque and mass distribution, resonance at the highest natural frequency produces constant, repetitive motions. This "lock-in" is characterized by large displacements which are unacceptable to the simple suspension system. It was also found that lock-in is controlled by the magnitude of the applied torque and can be avoided by applying a torque which exceeds a specific critical value.

INTRODUCTION

The plowing of a temporary opening in the earth is often an economical and ecologically attractive alternative to customary burying technology (trenching, backhoeing, etc.) in the installation of utility cable and gas pipe. A vibrating cable plow currently being designed for this purpose uses an orbital actuator driven by a single-eccentric roller.

Investigators have shown that vibration reduces the average applied bias force needed to penetrate the earth. The work of Senator and Warren [1], Nalezny [2], and Scerbo and Pope [3] has shown experimentally and analytically that some combination of a vibrating plow share's horizontal and vertical motion promises significant drawbar reductions. In order to implement this motion for full-scale in-situ testing, an orbital actuator has been designed, built, and tested in-air at Bell Laboratories Chester location. The details of the design are given in Ref. [4], and an isometric sketch of the actuator is shown in Fig. 1. The actuator consists of a horizontal member rigidly attached to a forward-raked blade. A cavity in the horizontal structure contains a roller whose motion produces the high rotating force imparted to the actuator.

A companion paper [5] investigating the steady-state motions of an orbital actuator shows that a rearrangement of the actuator's mass distribution increases the amplitude/frequency product and thus enhances the potential penetration rate. By adding or moving balancing weights, the mass distribution can be changed from the usual low mass-center configuration either to a balanced configuration (with the actuator's mass center near the center of excitation) or to a rear- or front-mass configuration. Although adjustment of the mass center increases the amplitude/frequency product and produces desirable changes in the blade-tip motions, it also emphasizes problems associated with the actuator's transient response during start-up. Under certain conditions, the roller can "lock in" at the actuator's natural frequencies, producing unacceptably large displacements.

In the following paper, the orbital cable plow's differential equations of motion are developed and solved for the transient start-up condition, and a numerical integration technique is used to find the transient and steady-state motions. The problem of lock-in (and the resultant displacements at the blade tip and across the mounts) is investigated in detail for the

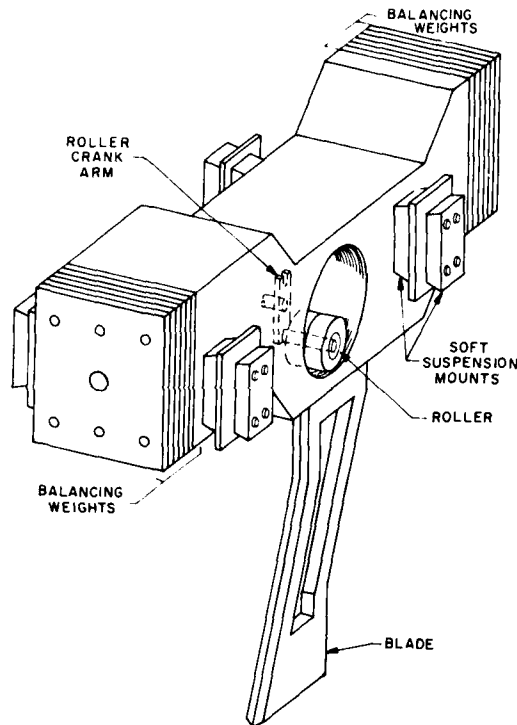


Fig. 1 — Orbital actuator

desirable unbalanced configurations. The displacements predicted by the equations are then compared to the capability of the suspension system.

DESCRIPTION OF THE MODEL

In simulating the nonlinear, in-plane, transient problem, the mathematical model used was that of an orbital actuator supported by a grounded frame. As shown in Fig. 2, the model consists of four main components. The first two make up the orbital actuator itself: a rigid T-shaped actuator frame of mass M_1 with center of gravity at G_1 and radius of gyration b_1 ; and an eccentric roller excitor of mass αM_1 , rolling at an eccentric radius, e , about the center, O , of the cavity in the actuator frame. A set of massless nonlinear springs and dashpots acting at points F and R models the suspension system. The fourth component of the model is a rigid frame of mass M_2 with center of gravity at G_2 and radius of gyration b_2 . The outer frame is coupled to ground by a set of very soft springs and dashpots, which are included primarily for

computational convenience. This model is used to simulate the orbital actuator running in the in-air test facility at the Chester location.

In the balanced configuration, G_1 , the mass center of the actuator, is directly above G_2 , the mass center of the frame. However, when weight is shifted to the front or rear, G_1 and G_2 are offset horizontally from each other so that, with a fixed roller, the vibrating system has six degrees of freedom. Three of these vibrational degrees of freedom are at very low frequencies (dependent upon grounding spring elasticity and configuration) and can be ignored. The remaining three frequencies and their corresponding mode shapes are determined by the stiffness and configuration of the springs connecting the two masses, M_1 and M_2 , and by the distribution of mass. These frequencies and the mode shapes of their relative motions directly affect suspension system life. Although the idealized system with a fixed roller can be linearized by assuming small angular rotations, the varying angular speed of the roller and its continuously changing position introduce an essential nonlinearity.

The basic simplifying assumptions of the analysis are that the bodies are rigid and that the angular rotations of the actuator frame (θ) and supporting structure (ϕ) remain small. The rigid-body assumption is justified because the lowest natural frequency which could cause dynamic deformations of the structures is four to five times higher than the highest anticipated operating frequency. The small-angle assumption is justified by the low ratio of applied torque to the polar moments of inertia of the actuator and the supporting structure.

ENERGY DISSIPATION MODEL-ROLLING FRICTION

The term R_{RF} in the differential equations of motion accounts for energy dissipation due to rolling friction. Inclusion of such a term is justified by in-air experiments which have shown that an additional 10 hp (not accounted for by mechanical, suspension, or windage losses) must be supplied to drive the shaker in the steady state. If the rolling-friction force is modeled as the product of a coefficient of rolling friction times the nonoscillatory value of the normal contact force, R_N , a 10-hp loss at 2500 rpm can be accounted for by using a coefficient of friction of 5.4×10^{-4} . This coefficient of rolling friction for hardened steel rolling on hardened steel compares favorably with those given in Refs. [6] and [7]. Therefore, the mechanism for rolling-energy dissipation is modeled as a frictional force (R_{RF}) acting tangent to the bearing race, with a magnitude of 5.4×10^{-4} times the instantaneous value of the normal contact force.

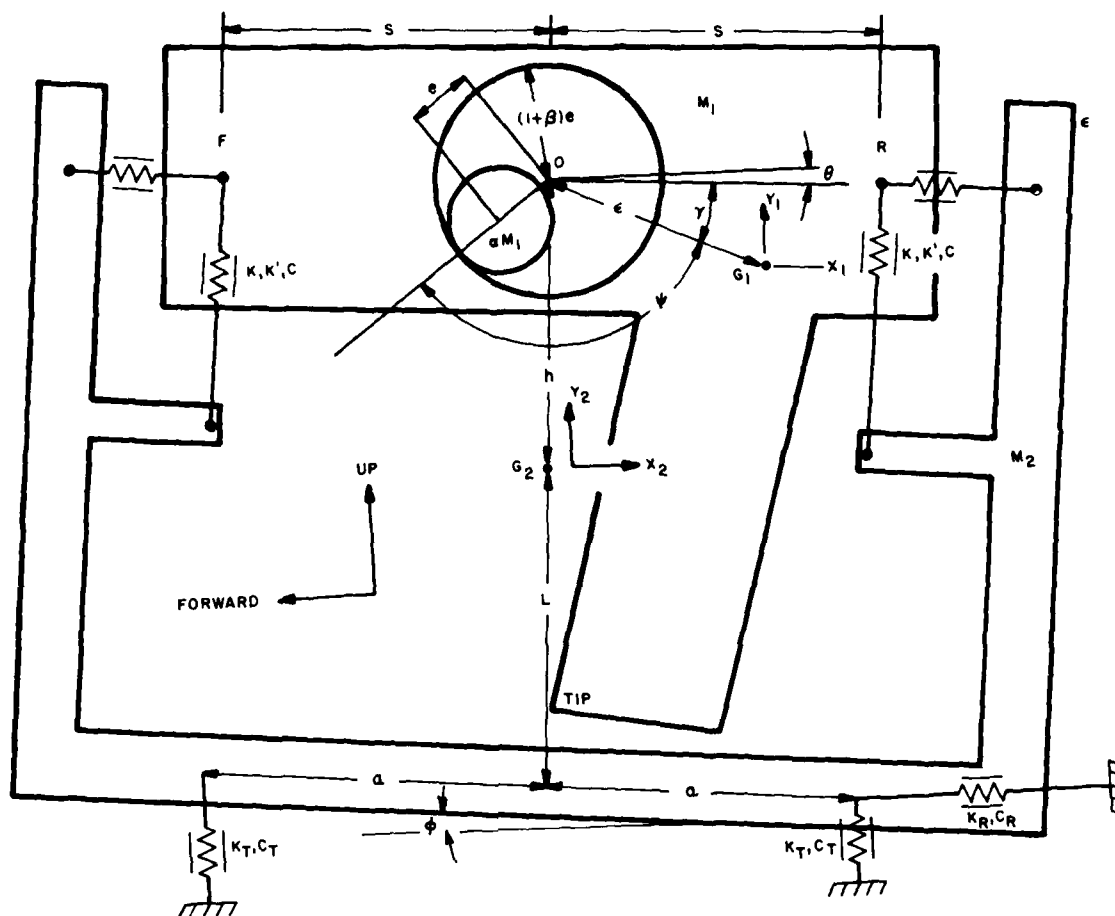


Fig. 2 — Model of orbital actuator's in-air test facility

DERIVATION OF THE DIFFERENTIAL EQUATIONS OF MOTION

The differential equations of motion for the seven-degree-of-freedom, in-plane vibrating system can now be derived. The free-body diagrams for the actuator frame and eccentric roller mechanism are given in Fig. 3. Some of the equations contain expressions in terms of $\epsilon \angle \gamma$, which locates the center of gravity, G_1 , with respect to the center of excitation, O . The angles Θ and ϕ are the angular rotations of the actuator frame and the supporting structure respectively. ψ is the angular position of the rotating eccentric and instantaneous normal force vector, R_N . The tangential, bearing, contact, and rolling-friction forces are denoted by R_T , R_B , R_C , and R_{RF} respectively.

By application of D'Alembert's principle to the main masses (the actuator and supporting structure), and by summing both the horizontal and vertical forces and the moments about the displaced centers of gravity, six equations can be written. These equations are in terms of the seven system variables (x , y , Θ , x_2 , y_2 , ϕ , ψ) and four unknown internal reactions (R_N , R_T , R_B , R_C). The internal reactions are related to the system parameters through the five non-trivial differential equations of motion of the crank-arm mechanism and eccentric roller. The crank-arm mechanism's equation of motion in the radial direction is trivially satisfied.

After linearizing the displacement terms at the support points in accord with the small-angle assumption, introducing the following notation:

$$\eta = \sin[\pi - (\gamma + \theta + \psi)], \quad \Delta = \sin(\gamma + \theta),$$

$$\mu = \cos[\pi - (\gamma + \theta + \psi)], \quad \delta = \cos(\gamma + \theta),$$

and eliminating internal reactions, the seven independent system equations are:

$$(1 + \alpha)\ddot{x}_1 - (\epsilon\Delta + \alpha\epsilon\eta)\ddot{\theta} - (\alpha\epsilon\eta)\ddot{\psi}$$

$$= \epsilon\dot{\theta}^2\delta - \alpha\epsilon(\dot{\theta} + \dot{\psi})^2\mu + \frac{K}{M_1}(x_2 + h\phi - x_1)$$

$$+ \frac{K'}{M_1}(x_2 + h\phi - x_1)^3 + \frac{C}{M_1}(\dot{x}_2 + h\dot{\phi} - \dot{x}_1),$$
(1)

$$(1 + \alpha)\ddot{y}_1 - (\epsilon\delta - \alpha\epsilon\mu)\ddot{\theta} + (\alpha\epsilon\mu)\ddot{\psi}$$

$$= -\epsilon\dot{\theta}^2\Delta - \alpha\epsilon(\dot{\theta} + \dot{\psi})^2\eta + \frac{K}{M_1}(y_2 - y_1)$$

$$+ \frac{K'}{M_1}(y_2 - y_1)^3 + \frac{C}{M_1}(\dot{y}_2 - \dot{y}_1),$$
(2)

$$\epsilon\Delta\ddot{x}_1 + \epsilon\delta\ddot{y}_1 - \left[(b_1^2 + \epsilon^2) + \frac{\alpha\beta\epsilon^2}{2}(1 + \beta) \right] \ddot{\theta}$$

$$+ \left[\frac{\alpha\epsilon^2}{2}(1 + \beta) \right] \ddot{\psi}$$

$$= \frac{T}{M_1} + g\epsilon(\cos \gamma - \delta)$$

$$- \left[0.54 \frac{\alpha\epsilon^2}{1 + \alpha}(1 + \beta)\dot{\psi}^2 \times 10^{-3} \right] \text{sign } \dot{\psi}$$

$$- \frac{K}{M_1}S^2(\phi - \theta) - \frac{K'}{M_1}S^4(\phi - \theta)^3 - \frac{C}{M_1}S^2(\dot{\phi} - \dot{\theta}),$$
(3)

$$-\alpha\epsilon\eta\ddot{x}_1 + \alpha\epsilon\mu\ddot{y}_1 + \left[\alpha\epsilon^2 \left(1 - \frac{\beta}{2} \right) \right] \ddot{\theta} + \frac{3\alpha\epsilon^2}{2} \ddot{\psi}$$

$$= \frac{T}{M_1} - \alpha g\epsilon\mu - \left[0.54 \frac{\alpha\epsilon^2}{1 + \alpha}(1 + \beta)\dot{\psi}^2 \times 10^{-3} \right]$$

$$\text{sign } \dot{\psi},$$
(4)

$$M_2\ddot{x}_2 = -K(x_2 + h\phi - x_1) - K'(x_2 + h\phi - x_1)^3$$

$$- C(\dot{x}_2 + h\dot{\phi} - \dot{x}_1)$$

$$- K_R(x_2 - L\phi) - C_R(\dot{x}_2 - L\dot{\phi}),$$
(5)

$$M_2\ddot{y}_2 = -K(y_2 - y_1) - K'(y_2 - y_1)^3$$

$$- C(\dot{y}_2 - \dot{y}_1) - K_T(y_2) - C_T(\dot{y}_2),$$
(6)

$$M_2b_2^2\ddot{\phi} = -KS^2(\phi - \theta) - K'S^4(\phi - \theta)^3$$

$$- CS^2(\dot{\phi} - \dot{\theta}) - K(x_2 + h\phi - x_1)h$$

$$- K'(x_2 + h\phi - x_1)^3h - C(\dot{x}_2 + h\dot{\phi} - \dot{x}_1)h$$

$$- 2K_Ta^2\phi - 2C_Ta^2\dot{\phi}$$

$$+ K_R(x_1 - L\phi)L + C_R(\dot{x}_1 - L\dot{\phi})L.$$
(7)

These equations are nonlinear, even for small displacements, because the driving force (R_N) on the system is a gradually increasing function of a system-dependent variable (ψ). Thus, the most practical analytical investigation of the system's transient behavior is a numerical integration of the differential equations.

MINIMUM CONSTANT STARTING TORQUE

The differential equations of motion for the eccentric roller are based on the assumption that the roller does not slip on the inside diameter of the bearing race and always remains in contact with it. This implies that the normal contact force, R_N , between the roller and race is always positive. A positive R_N can be satisfied only if the roller's centripetal acceleration builds up rapidly enough to overcome the separating component of the gravitational force. If the eccentric roller leaves the race, damage to the hardware might result from impact, chatter, and sliding contact problems when the roller recontacts the race. Preliminary estimates of the magnitude of constant applied torque needed to insure a positive contact force can be obtained by introducing the simplifying assumption of a step function torque input.

The first revolution of the crank arm is critical. During this time, the normal contact force, R_N , is small compared to the translational inertia force terms, $M_1\ddot{x}_1$ and $M_1\ddot{y}_1$, and the torque magnitude, T , is very small compared to the rotational moment of inertia $M_1b_1^2\ddot{\theta}$. Furthermore, with the exception of crank-arm angular velocity, displacements and velocities obtained during the first revolution are small. Therefore, a first order of smallness model will include \ddot{x}_1 , \ddot{y}_1 , $\ddot{\psi}$ and $\ddot{\psi}$ terms; terms containing $\dot{\theta}$, $\dot{\phi}$, \dot{x}_1 , \dot{x}_1 , \dot{y}_1 , \dot{y}_1 will be set equal to zero. The free-body diagrams for

this portion of the analysis are identical to those given previously. After simplifying this reduced set of equations, a single second order differential equation in terms of ψ is obtained:

$$\ddot{\psi} = -\Omega \sin \psi + \tau; \quad (t > 0^+), \quad (8)$$

where

$$\Omega = \frac{2g}{(3 + \alpha/1 + \alpha)e}, \quad \tau = \frac{2T}{(3 + \alpha/1 + \alpha)M_1 e^2}.$$

Eq. (8) is the equation of motion of a frictionless compound pendulum driven by a step function of torque. By a standard technique, the angular velocity can be expressed as a function of torque amplitude and crank angle ψ :

$$\frac{\dot{\psi}^2}{2} = \Omega (\cos \psi - 1) + \tau \psi. \quad (9)$$

The torque necessary to insure a positive contact force during the first revolution is obtained by substituting the expression for $\dot{\psi}^2$ given in Eq. (9) into the equation for R_N . This equation is obtained by summing forces in the radial direction for the free-body diagram (Fig. 3B).

$$R_N \approx \alpha M_1 (e \dot{\psi}^2 + g \cos \psi). \quad (10)$$

Combining Eqs. (9) and (10) and rewriting the result for the limiting case $R_N \geq 0$ in dimensional terms gives a single transcendental equation in terms of ψ ,

$$4 \left(\frac{T \psi}{\alpha M_1 g e} - 1 \right) \geq - \left(7 + \frac{\alpha}{1 + \alpha} \right) \cos \psi.$$

The minimum value of T , denoted by T^* , which satisfies the equation for all ψ , occurs when the two sides of the equation are equal. Its value can be obtained graphically by plotting each side of the equation as a function of ψ and then adjusting the slope of the left-hand term to satisfy the equation. This procedure, illustrated in Fig. 4, yields:

$$T^* \approx \frac{3}{\pi} \alpha M_1 g e \quad (R_N = 0)$$

This result is very accurate. Several numerical solutions of the exact equations showed that no substantial difference was introduced when the second order terms were included. Fig. 5 shows that when the condition $T = T^*$ was applied to the numerical model, R_N became

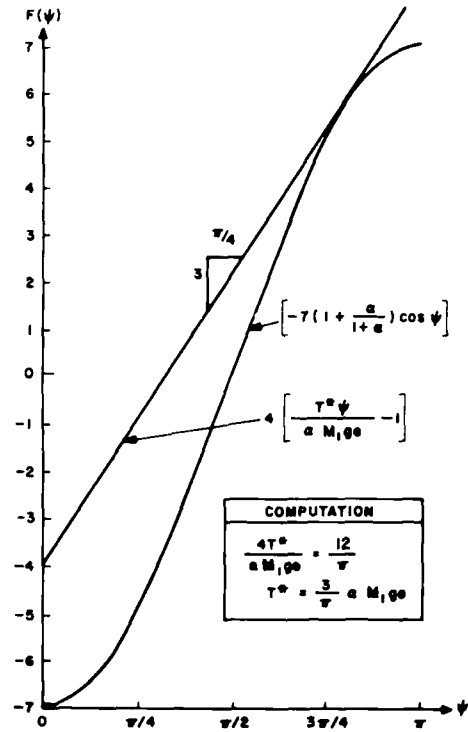


Fig. 4 — Graphic determination of minimum torque

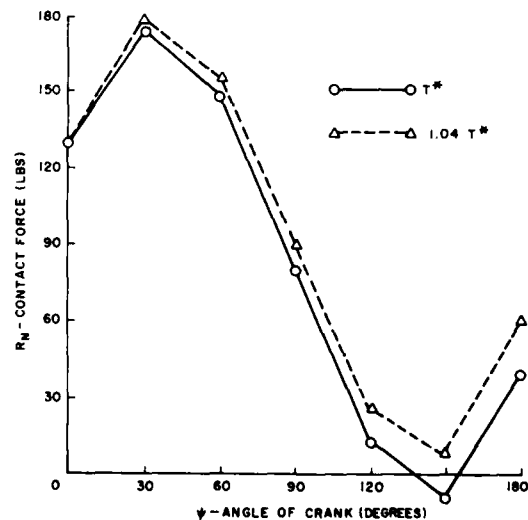


Fig. 5 — Numerical predictions of contact force for various torque values

negative at approximately 135 degrees; for $T = 1.04T^*$, R_N remained positive. This is substantially what is shown in the approximation.

NUMERICAL SOLUTIONS

The integration routine for the numerical solutions was a sixth order Adams-Bashforth predictor, Adams-Moulton corrector routine with fourth order Runge-Kutta starting and provisions for halving and doubling of the integration step size. A standard high efficiency matrix inversion package was used to solve for the individual derivative at each step.

Initial conditions for all numerical solutions correspond to the system at rest in its equilibrium position with the roller at the bottom of the actuator cavity.

The balanced, rear-mass, and front-mass configurations, which had shown desirable blade-tip orbits in the steady-state analysis, were investigated numerically to determine their transient start-up characteristics. Four types of torque vs time (or angular speed) characteristics were considered as variable parameters for each of the three cases. A step function, a linear ramp terminating at a constant torque, a double step, and an exponential approach to a step function were chosen to model torque-speed characteristics which could be obtained when starting hydraulic motor systems. The rate of torque buildup was adjusted in each case to insure a positive contact force (R_N) during the first crank revolution.

The results are shown graphically in two ways: as a plot of crank-arm angular velocity ($\dot{\psi}$) vs time; and as the computer-generated paths, similar to stroboscopic illuminations, traced by points of interest on the actuator, either on the support structure or on a fixed plane in inertial space.

Fig. 6 shows two types of crank-arm angular velocity response: plot A shows a true transient response terminating in steady state at the desired operating frequency; plot B shows the transient conditions resulting in a constant average crank speed much lower than the operating frequency. During the transient for each type of plot, the crank-arm angular velocity levels off at three distinct angular speeds, which were found to be in the neighborhood of the three undamped natural frequencies of in-plane relative vibration. Plot B shows that leveling off at the highest natural frequency (slower speed) is permanent. This condition is known as "lock-in."

As shown in Figs. 6A and 7, the traced paths for plot type 6A spiral out elliptically from the starting point and reach their greatest excursion when rotational speed approaches the highest natural frequency of in-plane vibration. The points then spiral in to approach the steady-state, almost elliptical paths corresponding to roller rotation at operating frequency.

However, other types of motion are also possible. When a low torque is applied to the kind of mass distribution that gives rise to curves like plot 6B, the angular speed of the crank locks in at a low resonant speed. This results in high displacement-amplitude motions characteristic of forcing near resonance (see Figs. 6B and 8). These motions are denoted as "transient" because they occur at an angular speed which should exist only in the transient response, yet they are "constant" since, for repeated cycles, all points of the actuator trace identical paths. In these cases, input energy is completely dissipated by the combination of damping across the mounts and rotational friction, leaving insufficient driving torque to increase roller angular speed to its proper operating value.

DISCUSSION OF THE RESULTS

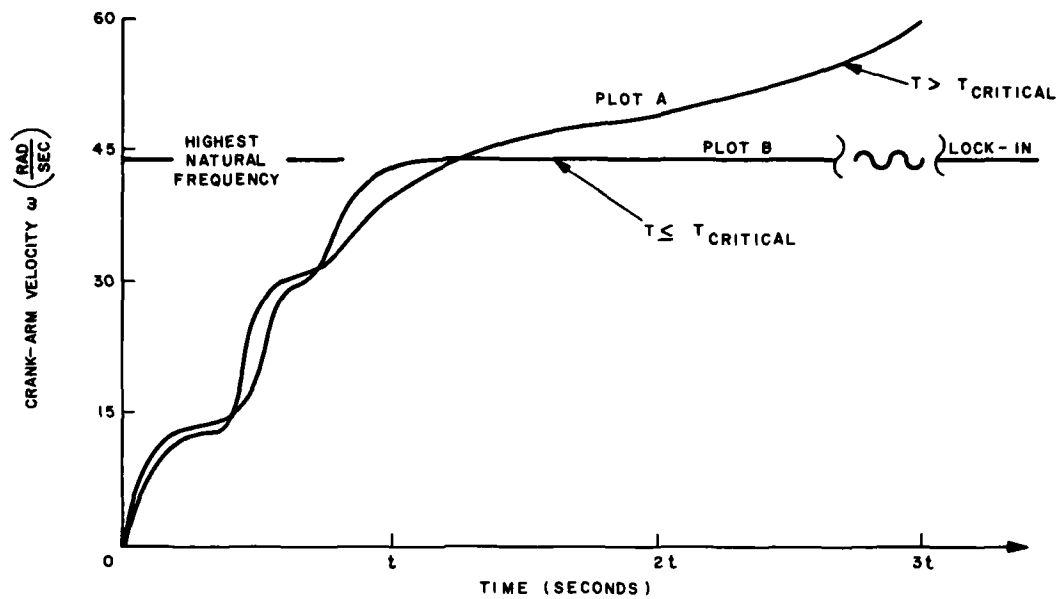
These general results can be applied to the three specific mass-distribution cases. The response of the balanced configuration to step torque inputs of practical magnitude is similar to that given in Figs. 6A and 7 (terminating in steady state). The system has a transient resonant response at each of its natural frequencies and nearly circular steady-state motions at the blade tip and suspension points.

The transient response for the rear-mass case is that shown in Figs. 6, 7, and 8. The rear-mass actuator exhibits either breakthrough or lock-in, depending upon the applied torque amplitude. For torques below a critical value, the system locks in at resonance (Figs. 6B and 8); for higher values, it breaks through and runs at design speed (Figs. 6A and 7). Although the final shape of the blade-tip orbit is the same in both cases (an ellipse with its major axis tilted upward in the direction of penetration), the lock-in orbit is considerably larger than that obtained in the steady state.

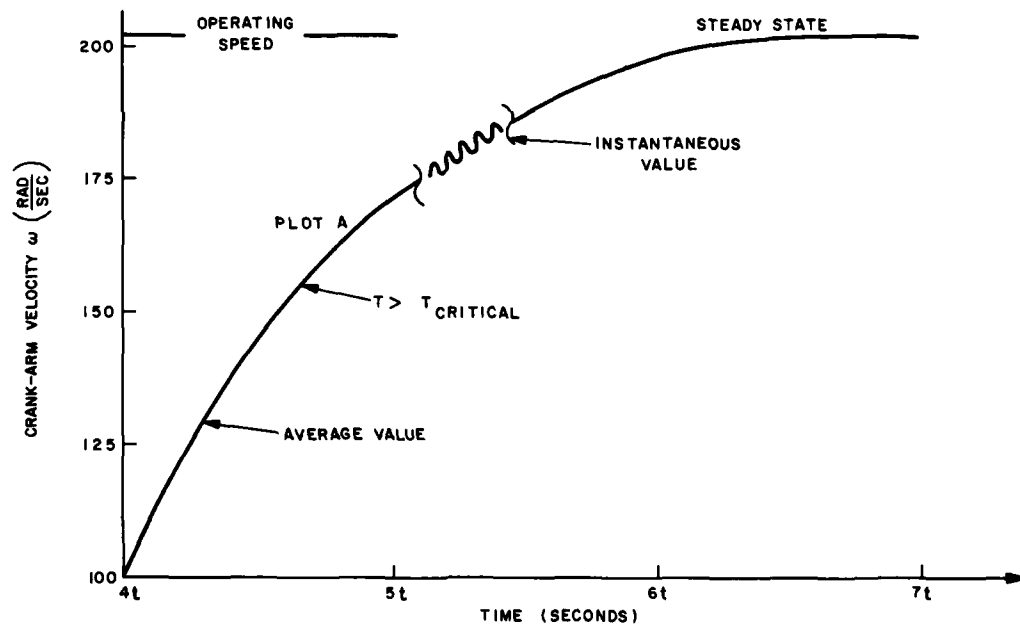
The front-mass case is similar to the rear mass except that it has a lower critical torque. Also, its characteristic ellipse is tilted downward in the direction of penetration, and its lock-in frequency is lower. The difference in lock-in frequency is linked to the fact that the system's highest natural frequency increases with increasing ϵ (displacement of the center of gravity with respect to the center of excitation).

The maximum relative displacements across the suspension mounts occur during temporary or permanent lock-in. An estimate of the displacement magnitudes was obtained by running the three mass distributions with appropriate constant applied torque to simulate both temporary and permanent conditions. Steady-state solutions were also obtained for purposes of comparison.

The results, shown in Table 1, indicate that the maximum amplitudes of the transient motions during start-up are 1.5 to 2.5 times larger than



Initial response



(BOTH TIME SCALE t AND TYPE OF PLOT DETERMINED BY APPLIED TORQUE)

Response after breakthrough ending in steady state

Figure 6. General history of crank-arm velocity as a function of applied torque

TABLE 1
Maximum Amplitudes At Supports

Case	Parameters	Steady State	Lock-In	True Transient	Controlling Support*
Balanced Mass	$\epsilon = 1.48 \text{ in.}$ $\gamma = 90^\circ$ $b^2 = 894 \text{ in.}^2$ $T_{\text{crit}} = 3/\pi \alpha M_1 g \epsilon$	0.237 in.	Not Observed	0.552 in.	Front
Front Mass	$\epsilon = 13.87 \text{ in.}$ $\gamma = 173.9^\circ$ $b^2 = 699 \text{ in.}^2$ $T_{\text{crit}} = \alpha M_1 g \epsilon$	0.462 in.	0.675 in.	0.670 in.	Rear
Rear Mass	$\epsilon = 16.67 \text{ in.}$ $\gamma = 5.08^\circ$ $b^2 = 631 \text{ in.}^2$ $T_{\text{crit}} = 9/5 \alpha M_1 g \epsilon$	0.559 in.	1.198 in.	1.191 in.	Front

*Controlling support is support location with maximum excursions

those observed in the steady state. The rubber shear sandwich suspension system could tolerate these motions only if they occur briefly during start-up. However, these large motions persist indefinitely when the actuator locks in at resonance. This mode of vibration is unacceptable for the simple suspension system and should be avoided. Table 1 shows that by supplying a constant torque which exceeds T_{critical} , the actuator will not lock in at resonance and the objectionable amplitudes will indeed be transient.

The shaping of the torque input curves was shown to have very little qualitative or quantitative effect on the results. In general, the system's transient response was similar to its response to the constant step torque inputs, though more extended in time. The maximum amplitudes associated with the transients for shaped inputs were within ± 5 percent of the results given in Table 1, indicating that lock-in is substantially controlled by the final magnitude of the applied torque and is relatively insensitive to the detailed nature of the buildup. However, the buildup must be rapid enough to insure a positive contact force during the first crank revolution.

CONCLUSIONS

The differential equations of motion of an orbital cable plow were developed and solved for the transient start-up condition. Numerical solutions were obtained for the transient and steady-state motions at the support points and at the blade tip for the three mass distributions

which had exhibited desirable blade-tip orbits in steady state. Maximum amplitudes at the support points during the actuator's transient response were found to be 1.5 to 2.5 times larger than the maximum excursions given by the steady-state solutions (see Table 1).

Constant motions, other than those predicted by steady-state solutions at the operating frequency, were found to exist for particular combinations of applied torque and mass distribution. Analytic determinations of the system's undamped natural frequencies and corresponding mode shapes showed that the combined vertical and torsional resonance of the system near or during lock-in is directly associated with the system's highest natural frequency. A method by which lock-in can be studied and avoided was developed.

The prototype actuator's suspension system was found capable of withstanding all the steady-state and transient motions except those resulting from the constant "transient" lock-in response in the front- and rear-mass configurations. It was found that lock-in was governed by one system parameter, the applied torque. The final magnitude of the applied torque substantially determined the mode of vibration near resonance. By adjusting the value of the applied torque, the lock-in mode could be eliminated. The study thus indicates that the desirable steady-state blade-tip amplitude, frequency product offered by unbalanced configurations is obtained at the price of a relatively high torque required to assure breakthrough and operation at design speed.

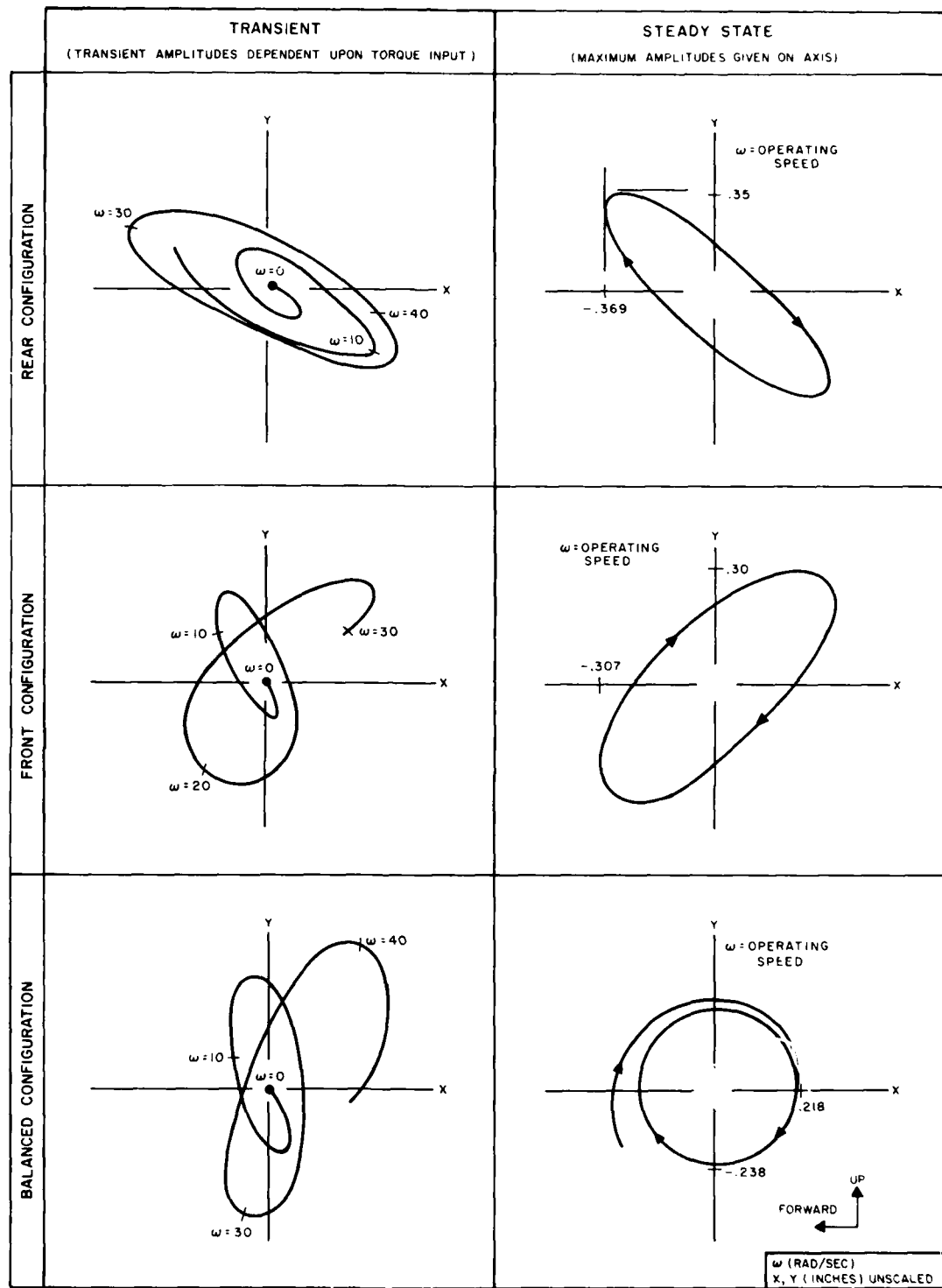


Figure 7. Motions at tip of blade in inertial space ($T > T_{\text{critical}}$)

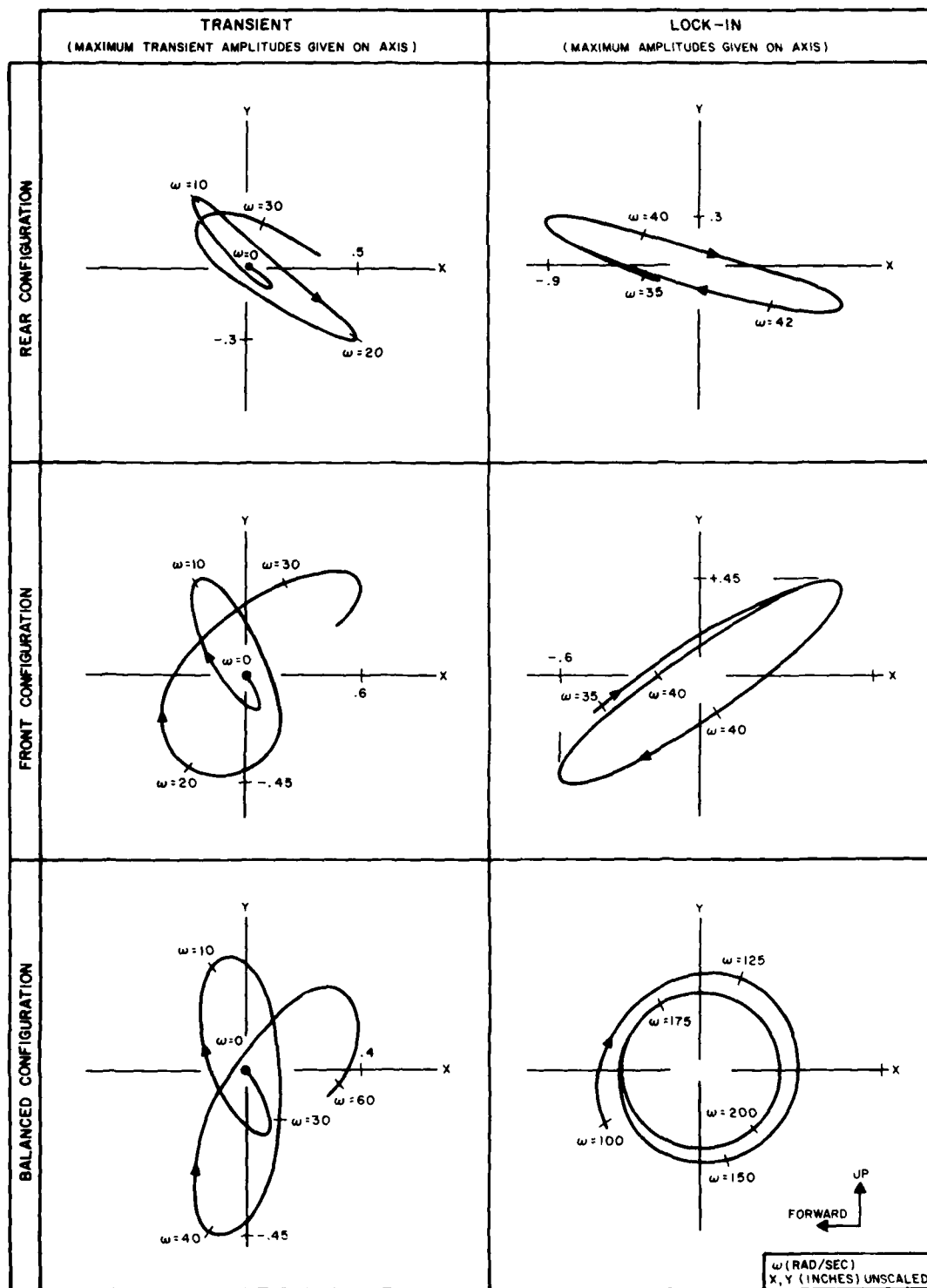


Figure 8. Motions at tip of blade in inertial space ($T \approx T_{critical}$)

REFERENCES

1. M. Senator and R. E. Warren, "Predicting Penetration Rates of Plows with Combined Vertical and Fore-Aft Vibration and Flexible Blades," S.A.E. Paper 7000040, presented at Automotive Engineering Congress, Detroit, Michigan, Jan. 1970.
2. C. L. Nalezny, "Analysis of Upward Soil Cutting with a Vibrating Plow," Bell Laboratories unpublished work, Dec. 15, 1969.
3. L. J. Scerbo and D. L. Pope, "The Effect of Upward Cutting on Drawbar Reduction - An Approximate Solution," Bell Laboratories unpublished work, Aug. 13, 1972.
4. L. J. Scerbo, "Orbital Cable Plow - Design and Test Program for Orbital Actuator," Bell Laboratories unpublished work, May 13, 1970.
5. M. Senator and L. J. Scerbo, "Steady-State Motions of Orbital Cable Plows," The Shock and Vibration Bulletin 43, 1973.
6. J. B. Bidwell, "Rolling Contact Phenomena," proceedings of a symposium at General Motors Research Laboratory, Warren, Michigan, Oct. 1960, Elsevier, 1962.
7. T. Baumeister and L. S. Marks, Standard Handbook for Mechanical Engineers, Seventh Edition, pp. 3-40, McGraw Hill, New York, 1967.

SHOCK WAVE INDUCED TRANSIENT PRESSURE ENVIRONMENT ABOUT THE SPRINT II MISSILE CAUSED BY LAUNCH CELL EJECTION

Anthony J. Culotta
Martin Marietta Aerospace
Orlando, Florida

A subscale test program was conducted to ascertain the shock wave-induced pressure loads imposed on the SPRINT II missile as it is ejected from a pressurized launch cell. Cell pressurization was accomplished by means of a solid propellant gas generator. High response pressure data was obtained on the sides and base of the model with and without the effect of partially opened cell doors. Pressure data was also obtained within the launch cell and eject performance is compared with theoretical predictions. High speed photographs of the cell exhaust flow as the missile is ejected, with and without the influence of cell doors, are also presented.

INTRODUCTION

When a missile leaves a pressurized launch tube, a shock wave (termed a porting shock wave) will be generated as the missile uncovers the mouth of the tube. This shock wave, driven by expanding launch tube gas, will propagate into the ambient atmosphere along the missile surface. Although passage of this shock wave is extremely rapid, the highly transient pressure loads caused by the shock wave have become an area of concern with respect to the structural dynamic response of the missile. Not only primary missile structure response to these shock imposed loads is of interest, secondary structure and internal missile components are also of concern.

Porting shock wave generation is independent of the means by which the launch tube is pressurized. Pressurization can be accomplished by missile motor ignition or by a gas generation source. For the latter, the gas dynamic phenomena associated with the firing of projectiles or the gun launch of missiles falls within the area of intermediate ballistics. Prior investigation in this area has been associated with gun tubes and the far field effects such as noise and primary muzzle flash. With increasing interest in the gun launch of relatively fragile, fin-stabilized guided projectiles, the near field environmental effects on projectile performance and structural integrity must also be investigated. For the definition of the porting shock wave, we are concerned with the near field effects. These effects are essentially over by the time the emerging gas has traveled a distance on the order of several missile or projectile diameters.

If the projectile or missile has a simple geometric shape and the area in the vicinity of the launch tube mouth is clean (no flow obstructions), then analytical techniques are available (References 1 and 2) which yield quantitative results on the time dependent pressure field about the missile. However, for SPRINT II, the area in the vicinity of the tube mouth may not be clean. For nuclear hardening, environmental, and security considerations, cell doors cover the launch tube mouth. Con-

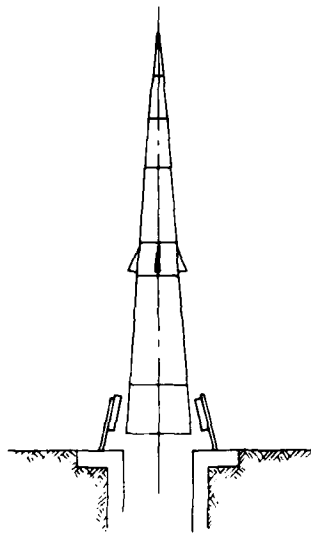


Figure 1. Missile-Tube Door Configuration at Eject

sidering the variational limits imposed on the door actuation system (with the inclusion of external effects), the base of the missile will clear the door edge by 6 inches minimum as shown in Figure 1. Because of the proximity of the doors to the missile during ejection, the porting shock wave can reflect off these doors and back onto the missile structure with appreciable pressure amplification. The existence of partially opened cell doors precludes accurate theoretical prediction of the pressure field about the missile because of the multi-dimensional aspects of the problem. For this reason, a subscale test program was performed to measure missile surface pressure-time history subsequent to missile porting with the influence of cell doors.

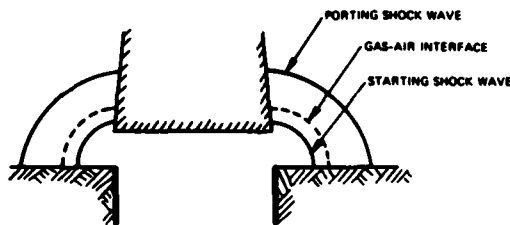
In addition to this surface pressure history, it was desirable to obtain base pressure history. Subsequent to missile ejection, there is considerable launch tube flow which is axially di-

rected for a short period of time. This axial flow will cause base pressure on the missile to take some finite time to decay to ambient pressure. The interest in determining this decay time is generated by the desire to delay missile motor ignition until the base pressure decays to ambient pressure.

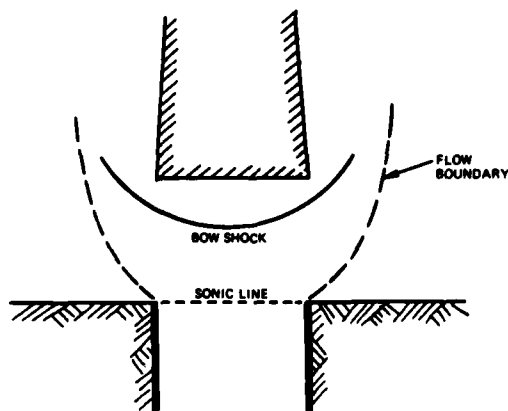
DISCUSSION

A. GAS DYNAMICS

Certain gas dynamic phenomena are known to occur when the base of the missile uncovers the launch tube. With the expansion of launch tube gas, the porting shock wave will be initially cylindrical, becoming near spherical at large distances from the shock wave origin. As the emerging tube gases expand, there is evidence (References 3 and 4) that another shock wave (termed a starting shock wave) will be formed in the expanding gas. The existence of this starting shock wave is caused by flow overexpansion and has no analogy in steady flow expansions. However, when this shock wave forms, the velocity of propagation of the porting shock wave is greatly effected. The probable shock wave and gas-air interface configuration during the initial phase of gas expansion is shown below.



A very short time after missile ejection, sonic flow will be established at the open annular area between the missile base and tube mouth. The flow will remain sonic at this opened area until the area becomes larger than the tube mouth area. When this occurs, sonic flow will be established across the tube mouth and gas flow momentum will be largely directed in the axial rather than the radial direction as shown in the following sketch.



Flow will remain sonic at the tube mouth at least for that period of time it takes a rarefaction wave to traverse the length of the tube, reflect from the bottom and again traverse the tube to the mouth.

To obtain insight as to the shock wave configuration subsequent to porting with the effect of doors, a water table flow analogy was used. With this analogy, a two-dimensional model of the tube-missile-door configuration at the time of eject was placed on a light table covered with shallow water. Generating waves through the opened area between the missile model base and tube mouth qualitatively illustrated that shock wave reflection from the doors does occur. Photographic data of the shock wave patterns were not obtained. However, Figure 2 shows an illustration of the formation that was observed. Only the major waves are represented; smaller wavelets have been deleted for clarity. The initial water wave or simulated porting shock wave is shown at t_1 . The arrows indicate the direction in which the shock wave is traveling. At t_2 , a portion of the porting shock wave has reflected from the door. Total porting shock wave reflection has occurred at t_3 , with imminent reflected shock impingement on the missile surface. Multiple shock wave reflection between the door and missile surface occurs before the shock wave system leaves the door vicinity as shown at t_4 .

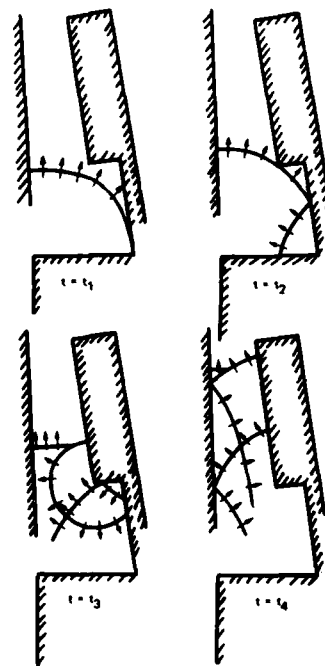


Figure 2. Water Table Wave Patterns

Some estimate may be made, at least until shock wave reflection from the missile surface (t_3 of Figure 2), as to the pressure history on the missile surface subsequent to porting. To accomplish this, blast wave theory was used. Graphical results of Sedov (Reference 5). To use blast wave theory, an assumption must be made as to the amount of released energy transmitting the porting shock wave. Since a large percentage of the emerging gas momentum is directed against the missile base when flow becomes choked at the tube mouth, it was assumed that no additional energy was supplied to the shock wave after tube mouth sonic flow was established. With this assumption, an estimate was made as to the total energy of the emerging gas. Although this energy is released over a finite period of time (the time from porting to sonic flow across the tube mouth).

for purposes of applying blast wave theory to predict shock wave decay, the energy was assumed to be released instantaneously. This corresponds to the shock tube situation where non-instantaneous diaphragm removal can be simulated by instantaneous diaphragm removal. The starting condition for the application of blast wave theory is the initial strength of the porting shock wave determined from one-dimensional considerations as in a shock tube. Expanding the emerging gas flow cylindrically, the pressure within the shock processed flow as a function of distance along the missile surface at various times was determined and presented in Figure 3. This analysis was used to provide some qualitative knowledge as to anticipated model pressure loads.

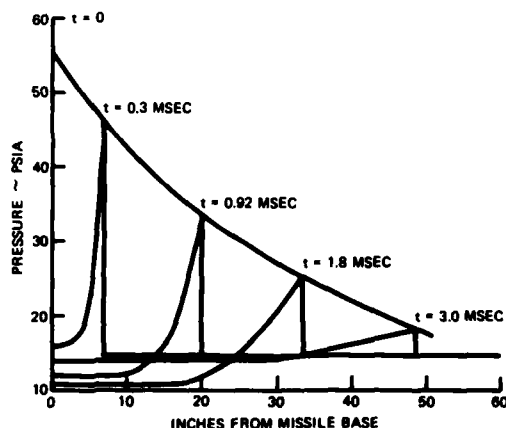


Figure 3. Full Scale Skirt Pressure Time History (Blast Wave Theory)

B. SUBSCALE DYNAMIC SIMULATION

In any subscale simulation, the parameters to be investigated determine the conditions which must be duplicated between the full scale and subscale systems. This investigation was concerned with the magnitude and time duration of pressure. Since pressure is one of the state variables of a gas, the gas dynamic equations of motion must exhibit similarity between the subscale and full scale systems. Denoting t' as non-dimensional time such that $t' = t/\tau$, l' as non-dimensional length such that $l' = l/L$, and the dependent variables of velocity and sound speed non-dimensionalized with respect to some reference velocity, then the gas dynamic equations of motion will exhibit gas dynamic similarity between the full scale and subscale systems if the ratio of L/τ remains constant. The reference velocity chosen was the stagnation sound speed of the gas.

Since a shock wave is also involved in the flow, similarity must be established with respect to the Rankine-Hugoniot relations. It can be shown that the transmission of a shock wave is similar in two systems if the ratio of specific heats, pressure ratio, and sound speed ratio are identical across the shock wave.

Therefore, at time of eject, if the stagnation sound speed of the emerging gas, the ratio of specific heats, the cell pressure to ambient pressure ratio, the eject velocity, and ambient conditions are identical, then complete similarity is established for constant L/τ . This implies that if the reference length is reduced by some scale factor, the time for an event to occur over

the reference length will also be reduced by the same scale factor.

With the scaling parameters established, several methods were investigated to satisfy the desired conditions. These methods involved the use of a hot or cold gas for tube pressurization. If a cold gas were used, the porting shock wave speed cannot be reproduced since no cold gas or gas mixture exists which has a low ratio of specific heats on the order of 1.2 and molecular weight of approximately 4. Use of a cold gas for determining unsteady flow characteristics and extrapolating these data to predict hot gas effects was determined to be too uncertain in terms of test objectives. Two hot gas sources were investigated for the subscale simulation. These sources were a combustible gas mixture and a solid propellant. For the combustible gas, a mixture of hydrogen and air was assumed to be burned in a constant volume process. This gas was isentropically expanded to produce work on accelerating the SPRINT skirt model. However, because of the required high initial charge pressures, and the potential for detonation rather than desired deflagration, gas mixtures were judged inferior to the use of solid propellant.

PROCEDURE

A. TEST FACILITY

With the scaling parameters established for the test program, model size was investigated. As previously stated, pressure time history on the missile surface is the desired parameter to be investigated. In accomplishing this goal, primary concern was placed on the response of the instrumentation system. As shown in the dynamic scaling discussion, to properly simulate missile ejection, event times vary directly with the model scale.

From the standpoint of the dynamic response of the full scale missile structure, it was desirable that pressure pulse widths on the order of 10 microseconds be defined. The selected scale factor and overall instrumentation system response are functions of this requirement. Considering the response capability of existing components of the instrumentation system, pressure transducer size, and cost, it was determined that the model should be no smaller than approximately $\frac{1}{4}$ scale. For a $\frac{1}{4}$ scale model, the overall instrumentation system should be capable of discerning pressure pulse widths on the order of $2\frac{1}{2}$ microseconds.

Since a model launch tube must be constructed, commercially available steel pipe (Schedule 140) was used with a machined I.D. of 12 Inches. This established the exact scale of 22.75 percent.

1. Gas Generator

SPRINT II is ejected from its cell by means of a gas generator; the cell becomes the missile launch tube during the ejection process. With the requirements specified by the dynamic simulation, the following conditions at model ejection must be satisfied as near as possible.

- 1) Model Velocity = 285 ft/s
- 2) Tube Pressure at Ejection = 92 psia
- 3) Tube Gas Temperature at Porting = 4380°R
- 4) Tube Gas Specific Heat Ratio = 1.2.

To accomplish these objectives, Hercules Inc. FAE-7 composite modified double base propellant was selected for use in the sub-scale gas generator. Variation in gas generator design parameters produced the following specifications which most nearly matched the desired eject conditions.

Propellant -- FAE-7 (Hercules Inc.)
 Weight -- 0.22 pound
 Burn Time -- 0.030 second
 Chamber Pressure (maximum) -- 4200 psia
 Throat Area -- 0.361 square inch
 $T_C = 6420^\circ R$
 $C^* = 5180 \text{ ft/s}$
 $R_p = 52.7 \text{ feet lb/}^\circ R$
 $\rho_p = 0.062 \text{ lb/cu in}$
 $\gamma = 1.19$

With these gas generator specifications, theoretical predictions of the eject conditions vs model weight were made and are presented in Figure 4. As shown, full scale eject conditions could not be matched exactly.

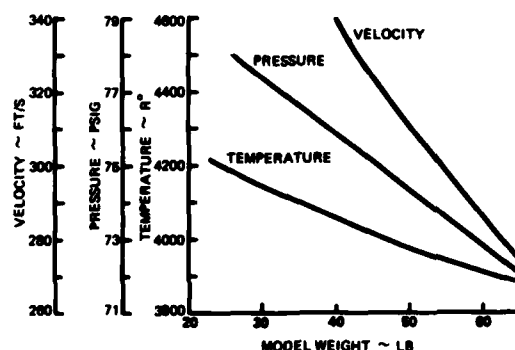


Figure 4. Launch Tube Performance vs Model Weight

The gas generator designed for the test program is shown in Figure 5. The generator contained propellant in an internal/end burning configuration. The internal ballistics of the generator indicated that all the propellant would be burned 0.030 second after diaphragm rupture. The igniter consisted of 20 grams of pelletized $BKNO_3$ which was initiated by a single commercial rib. To record the pressure-time history during gas generator operation, a Norwood Model III Pressure transducer was flush-mounted within the combustion chamber.

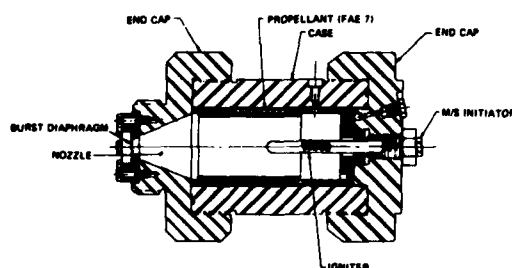


Figure 5. Gas Generator Porting Shock Test Program

2. Model

The model represented the aft skirt section of the SPRINT II missile since this was the area in which data was desired. A scaled base seal and rub strip were also used. The model was constructed of aluminum and designed to withstand a maximum longitudinal acceleration of 500g. A center guide cable was used to prevent lateral motion after ejection and to guide the model during model deceleration. Two smaller guide cables were also used to provide support for the model instrumentation cable.

The fully instrumented model weighed 38 pounds with provision for ballasting to 54 pounds. This provision was necessary to provide adjustment to eject performance to account for the uncertainties in the theoretical analysis. The model with pressure transducers installed is shown in Figure 6. Model instrumentation will be discussed in a following section.



Figure 6. SPRINT II Skirt Model

3. Model Deceleration System

Since the ejected model must be stopped in some non-destructive fashion in a short distance, an energy absorbing system of crushable honeycomb was selected. The design criteria for the honeycomb column was to limit model deceleration to 500g. The column was constructed of nine individual precrushed discs laminated to aluminum sheet with a steel bushing. Lateral support for the honeycomb column was obtained by tensioning the model center guide cable to 10,000 pounds.

4. Launch Tube Doors

Three sets of model doors were constructed for use during the test program; each with a different fixed opening angle. Those angles selected are shown in Figure 7. Each set of doors was fixed in opening angle since door motion during ejection was relatively small compared to missile and porting shock

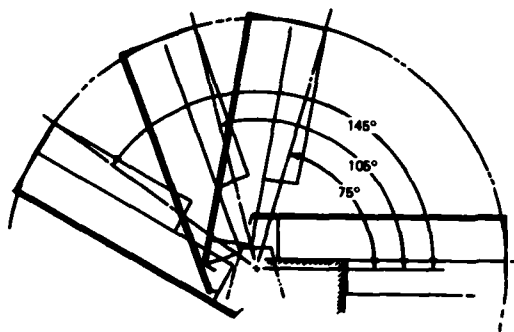


Figure 7. Model Door Opening Angles

wave motion. Figure 8 represents the launch tube with worst case doors installed.

The assembled test fixture without doors is shown in Figure 9. A labeled test apparatus schematic is shown below:

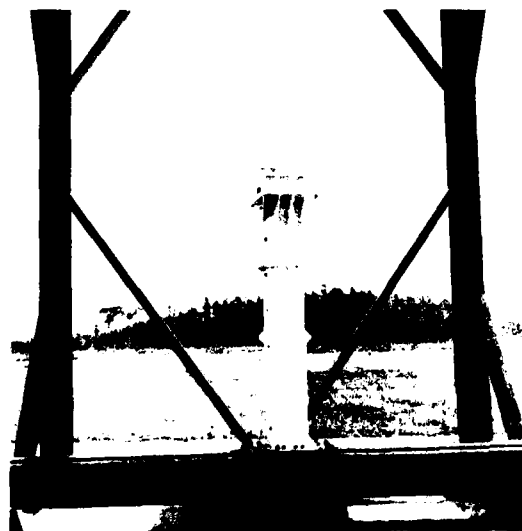
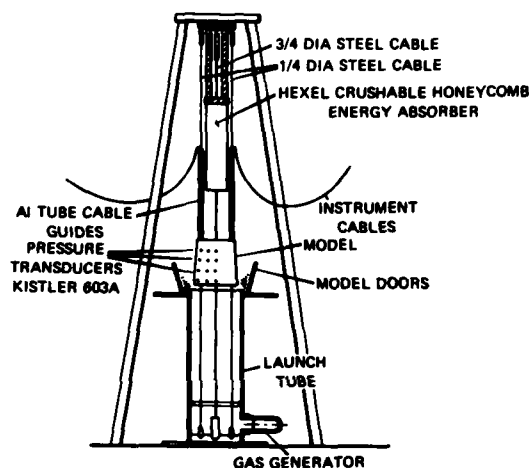


Figure 8. Launch Tube With Doors

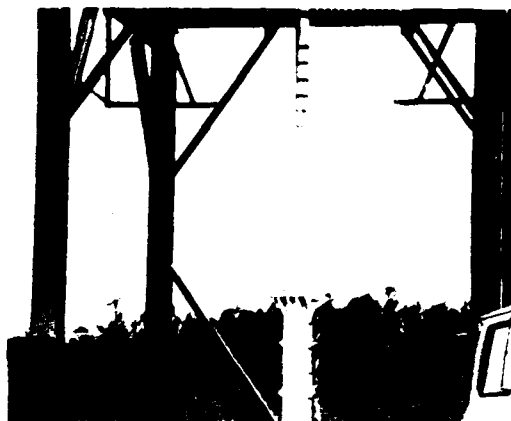


Figure 9. Porting Shock Test Facility Without Doors

B. INSTRUMENTATION

1. Launch Tube Instrumentation

The launch tube was instrumented with six Statham Model PA 839-400 pressure transducers at specific locations along the tube length. These pressure transducers were used to compare launch eject performance with theoretical predictions and provide a means for determining model velocity. The overall instrumentation system response using these transducers was 1 KHz. Although this response is low, it was sufficient for recording launch tube pressure during the ejection cycle.

2. Model Instrumentation

The launch eject model consisted of a 22.75 percent aft skirt section with a scaled rub strip and base seal. The model was constructed of aluminum with a removable panel to provide access to the pressure transducers. The pressure transducers (Kistler Model 603A) were located on three meridional rays; 0, 45, and 90 degrees. The 0 degree ray was in line with the door centerline. A base pressure transducer was also installed. In addition to these active transducers, a blind transducer was installed within the model for the purpose of recording noise generated during the ejection process. The location of the pressure transducers on the model aft skirt section is shown in Figure 10.

C. AUXILIARY TESTING

To ascertain the effects on overall system response in an environment similar to that expected during the test program, several areas of concern were investigated. These areas were:

- 1) Electrical noise which could be produced by the whipping action of the coaxial cable land lines during model ejection thus degrading the transducer signal.
- 2) The charge amplifiers may not have sufficient capability to drive long land lines to the recorder.
- 3) The pressure pulse may be distorted by the effective pressure sensitive face of the transducer.

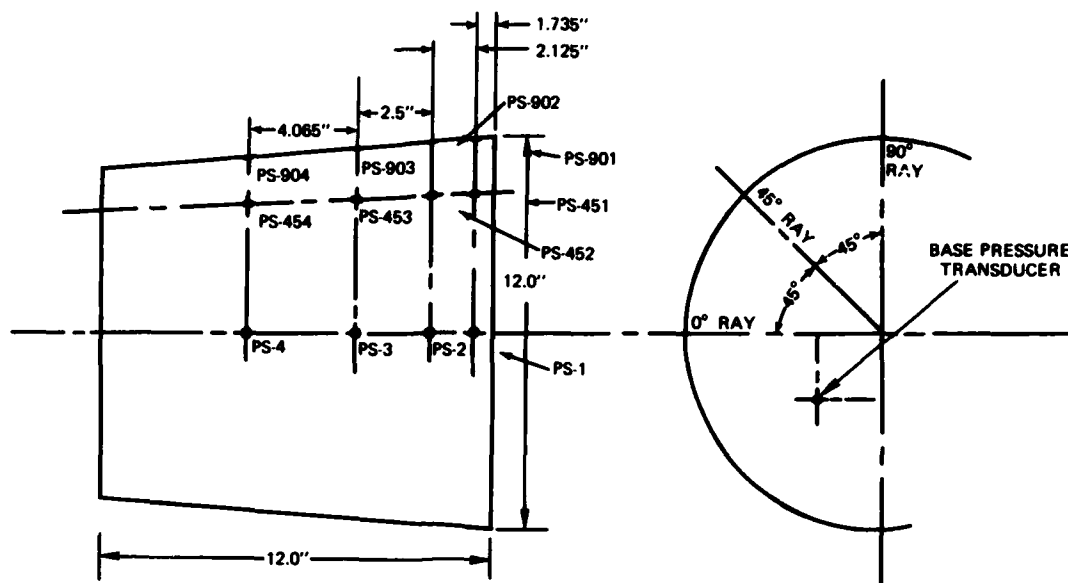


Figure 10. Pressure Transducer Locations

- 4) Thermal effects caused by hot exhaust flow from the tube could distort the data.
- 5) The high "g" environment during launch could effect the transducer output signal.

To investigate the severity of these problem areas several auxiliary tests were conducted to isolate conditions which would prevent satisfactory data acquisition. The tests were accomplished in a simulated eject environment for various components of the data acquisition system. These components were:

- 1) The microdot cable
- 2) The pressure transducer
- 3) The charge amplifiers and tape recorders.

1. Microdot Cable

The microdot cable used in the test program was Endevco type 3060A-300. One end of a length of cable was accelerated to a velocity of 300 ft/s in the Martin Marietta air gun while cable noise was monitored at the stationary end. The test indicated that noise generated by cable motion in a simulated environment was acceptable.

2. Pressure Transducer

The pressure transducer used for the high response data acquisition was the Kistler Model 603A. This transducer was mounted on a shaker table and accelerated to 500g in both lateral and longitudinal directions. Transducer signal was monitored during the test. This test indicated that the transducer signal degradation was within manufacturer's specification and acceptable for the test program.

It was also desirable to investigate transducer response to various mounting configurations and to thermal pulse protection. To accomplish this, the transducers were mounted in

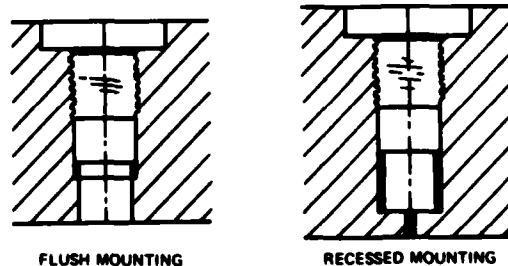
the flush and recessed mount configurations (per manufacturer's recommendation) in the Martin Marietta 6 foot x 6 foot shock tube and subjected to a known pressure pulse (See sketch below). It was determined from these tests that the recessed mount configuration was not satisfactory. This mounting arrangement produced excessive ringing over a wide range of pressure port opening diameters. The flush mounted transducer performed in a satisfactory manner to the applied pressure pulse.

For thermal protection, a thin layer of General Electric RTV 102 coating was applied to the face of the transducers. This coating degraded the transducer rise time to 2.5 microseconds which was within acceptable limits.

3. Charge Amplifiers and Tape Recorder

The charge amplifiers used in the test program were Endevco Model 2713B. These charge amplifiers were used in conjunction with a Sangamo Model 3568, 14 track, Group I magnetic tape recorder. Input signals through the charge amplifiers over anticipated line lengths at the test site were monitored with the recorder. These tests indicated that frequency response and noise level were within acceptable limits.

As a result of the auxiliary tests that were performed with the instrumentation system, overall system response time



was determined to be approximately 3 microseconds with acceptable signal degradation due to dynamic effects. This response satisfies the approximate $2\frac{1}{2}$ microsecond response time requirement established in a preceding section. The results of the tests also indicate that the greatest source of error in the instrumentation system will be caused by the finite time required for the shock wave to pass over the pressure sensitive face of the transducer.

RESULTS

A. WITHOUT DOORS

The first test performed with the assembled subscale launch eject components was concerned with system performance. For this test, gas generator operation, launch tube performance, instrument cable survivability, model deceleration, instrumentation system noise, and pressure transducer thermal effects were the investigated areas. To obtain better flow visualization of the emerging gases, model doors were not installed for the first firing. The model was only partially instrumented, having one column of pressure transducers along the 0 degree meridian ray. Camera coverage consisted of two Fastax cameras with film speeds of 4000 to 5000 frames/second. A typical high speed photographic sequence of a launch event is shown in Figures 11, 12, and 13.

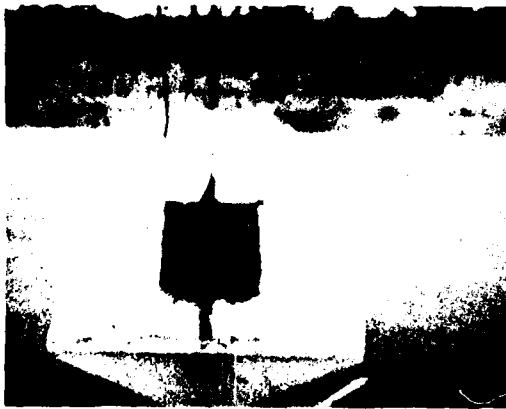


Figure 11. Launch Eject Sequence



Figure 12. Launch Eject Sequence



Figure 13. Launch Eject Sequence

The results of the first firing indicated the necessity of providing an additional burst diaphragm in the gas generator. Also, launch tube performance was such that eject velocity of the missile was higher than desired. To compensate for this, the model was ballasted to full capability (54 pounds) in subsequent tests. The instrument cables survived through launch and data acquisition. However, the cables parted during model deceleration. The crushable honeycomb column buckled after the first several discs had collapsed during model deceleration. Even with buckling, sufficient energy was absorbed as not to damage the model or the transducers. Pressure data obtained from the test indicated that a thermal protection coating would be necessary for subsequent tests inasmuch as moderate data distortion occurred during the later part of the data acquisition phase. This data had the characteristic signature of transducer face heating effects.

The most significant test result was that the anticipated pressure levels were not achieved anywhere on the model surface. Since the test was performed without doors, a direct comparison with blast wave theory can be made as to magnitude of pressure. Blast wave theory as used in this investigation overpredicts the magnitude of pressure on the skirt by a factor of 2. To this extent, detailed measurements of the emerging gas flow were made from the photographic data in an attempt to better understand the gas expansion process.

Figure 14 shows the trajectory of the emerging gas-air interface in the radial direction for an approximate model eject velocity of 320 ft/s, a launch tube pressure at eject of 90 psia, cell gas temperature of 4200°R and $\gamma = 1.22$. Also shown is the theoretical one-dimensional prediction of the initial slope of the gas-air interface in the t, r plane. As shown, agreement is excellent. With the initial slope of the gas-air interface, the initial slope of the porting shock wave can be computed. The speed of this shock wave was determined to correspond to $M = 1.86$. It is important to note that the velocity of the gas-air interface does not immediately decrease upon expansion to the outside environment. This is indicative of energy being supplied to the driven gases at a finite rate. It also indicates (Reference 6) that the porting shock wave strength in the radial direction is constant for some period of time. From simple wave theory, this time may be estimated by constructing a right running characteristic from the interface at a point where velocity appears to

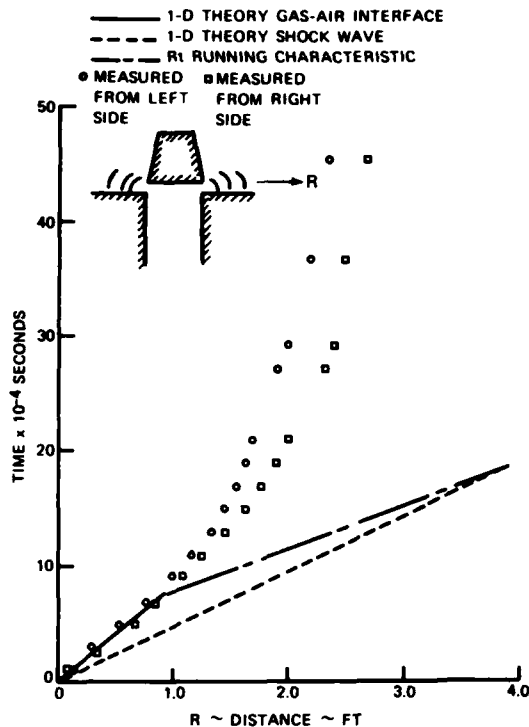


Figure 14. Exhaust Flow Trajectory After Porting: Radial Direction

change. The intersection of this characteristic with the shock wave will give the time duration for approximately constant shock wave speed. This is shown in Figure 14 to be equal to 1.9 milliseconds. The pressure immediately after passage of the porting shock wave was calculated to be 57 psia.

Theory indicates that for a constant speed cylindrical or spherical expansion, there exists an isentropic compression of air between the shock wave and gas-air interface. The pressure at the gas-air interface will be only slightly higher at any given time since an isentropic compression cannot tolerate severe gradients. With a pressure in the immediate vicinity of approximately 60 psia, flow emerging from the annular area will be at least near sonic. Pressure for sonic flow was computed to be 50 psia for a cell pressure of 90 psia at ejection. Therefore, the velocity of the emerging gas should be near 2600 ft/s. However, the largest velocity measured was 1200 ft/s. This difference strongly suggests the existence of the imbedded starting shock wave mentioned previously. The existence of the starting shock wave accounts for a large decrease in the energy of the expanding launch tube gas flow. From the data, it appears to have formed in less than 0.05 millisecond.

In the longitudinal direction, the direction of most interest here, the trajectory of the expanding gas-air interface is shown in Figure 15. As shown, the gas first decelerates and then accelerates. This occurs approximately 1.5 milliseconds after ejection. As stated in the discussion, it was expected that in large the direction of gas momentum would change from radial to axial direction when sonic flow becomes established across the

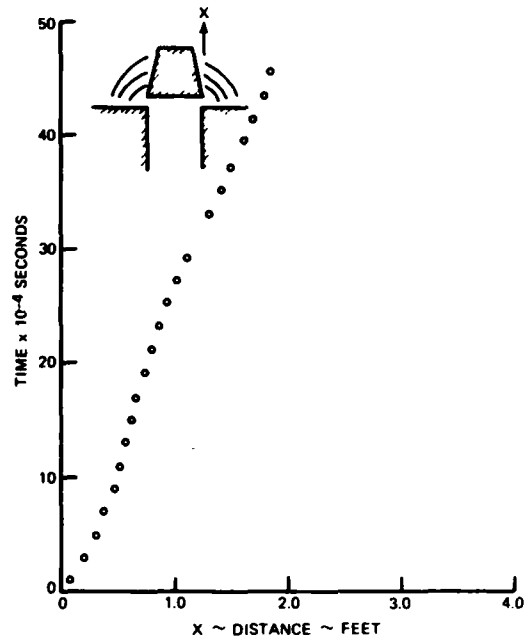


Figure 15. Exhaust Flow Trajectory After Porting: Axial Direction

mouth of the launch tube. The time for this occurrence was calculated to be at least 1 millisecond and probably not later than 2 milliseconds after ejection considering discharge losses and formation of a bow shock in front of the missile base. It was encouraging to see the data indicate this momentum transfer. Figure 16 shows the trajectory data replotted in proximity to the launch tube mouth. Initial velocity of the gas-air interface was measured to be approximately 850 ft/s relative to a fixed

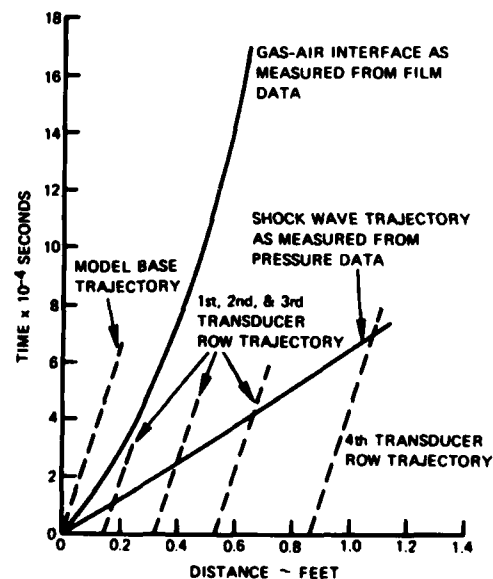


Figure 16. Exhaust Flow Trajectory After Porting: Axial Direction

coordinate system. With an eject velocity of 320 ft/s, the gas-air interface has an initial velocity of 530 ft/s relative to the model. It was observed from the photographic data that the model was surrounded by air moving at approximately the same speed at the time of ejection. With this observation, the initial shock wave Mach No. must be computed using interface velocity relative to the model rather than to fixed coordinates. This results in an initial shock wave Mach No. of 1.32 in the axial direction, a velocity of 1505 ft/s relative to the model and 1825 ft/s relative to fixed coordinates. The pressure behind this $M = 1.32$ shock wave was computed to be 27.4 psia. From the test data, the pressure on the first row of transducers nearest the base lip indicated a pressure of approximately 27 psia \pm 2 psia. Again, agreement is excellent.

At this point, it becomes possible to apply a one-dimensional approach to predict the initial strength of the shock wave in the axial direction. If a one-dimensional unsteady expansion is accomplished in the axial direction with the already accomplished unsteady radial expansion, using as the reference conditions those corresponding to sonic flow at the annular opened area, the shock wave speed and gas-air interface speed can be determined. The pressure corresponding to this wave speed was calculated to be 35 psia which is in much better agreement with the measured 27 psia than the 55 psia of blast wave theory.

B. WITH DOORS

Subsequent to the first firing test without doors, two separate, identical tests using the worst case door configuration were conducted with a fully instrumented, fully ballasted model. The data may be separated into two areas: One pertaining to launch cell performance and the other pertaining to pressure history on the missile surface subsequent to ejection. The former will be presented first.

For the two tests, the gas generator pressure histories are shown in Figure 17. The data indicates the excellent reproducibility obtained with the short burn time gas generator. Although theoretical predictions indicated much shorter burn times than measured, the discrepancy can be attributed to the fact that the propellant grain thickness was on the order of the propellant staple length and to the transient blow down characteristics of the gas generator. The fact that the gas generator was adding gas to the system at time of eject did not negate the data. The measurement program for surface pressure was over 1 millisecond after ejection. The mass added to the system during this event was less than 1/2 percent. Launch tube per-

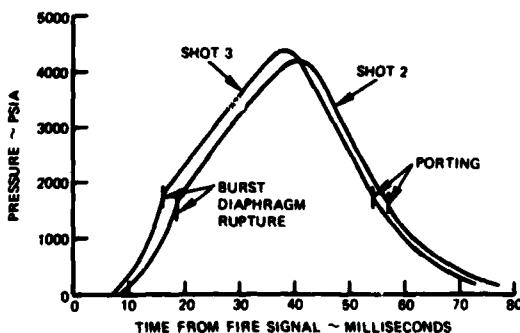


Figure 17. Gas Generator Pressure - Time History

formance measurements for the two tests show identical displacement vs time. Eject velocity was measured from film data and determined to be 300 ± 10 ft/s for both tests. Pressure-time history in the launch tube was also measured to be identical. These data are presented in Figure 18 for the two tests. Theoretical performance predictions are also shown using the measured gas generator pressure time histories. The discrepancy between measured and theoretical predictions can be attributed to the tube heat transfer. The theoretical model underestimates energy loss due to heat transfer for small diameter launch tubes.

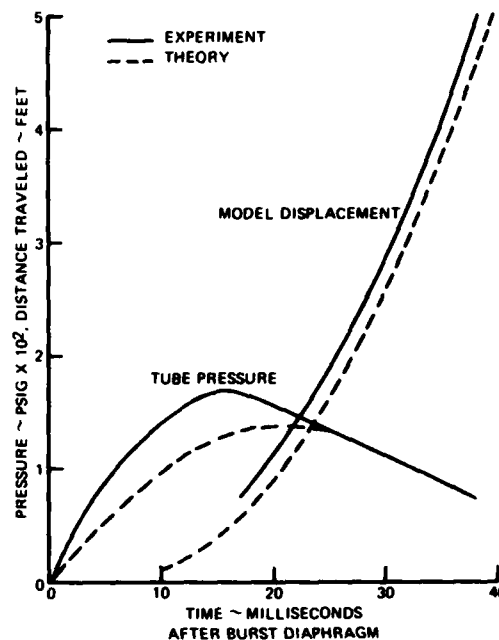


Figure 18. Launch Tube Performance - Shots 2 and 3

Launch tube gas temperature at time of eject could not be measured directly during this test program. To determine gas temperature, two methods were employed. The first method was to use the equation of state, since the pressure, weight of gas, volume, and gas constant can be easily determined at time of eject. The second method used the pressure data obtained along the launch tube subsequent to eject. This data indicated the arrival time of the leading expansion wave at each pressure transducer. With arrival times, the lead wave speed may be determined. Since this wave travels at sonic velocity, the temperature may be determined from the sound speed equation. From the data, launch tube sound speed at ejection was calculated to be approximately 3000 ft/s for all tests. Correspondingly, gas temperature at eject was calculated to be 4350°R . From the perfect gas law, gas temperature was calculated to be 4200°R .

In summary, launch tube performance was near enough full scale performance to render the pressure data valid. This is reviewed as follows:

	22.75% Model	Full Scale
Velocity at Eject	300 ft/s \pm 10 ft/s	285 ft/s
Pressure at Eject	90 psia \pm 5 psia	92 psia

Temperature at Eject (Computed)	$4275^{\circ}\text{R} \pm 75^{\circ}\text{R}$	4380°R
Gas Ratio of Specific Heats (Computed)	1.22	1.2

The pressure data on the model surface during the data acquisition phase for both tests is shown in Figures 19, 20, and 21. Some of the data was not interpretable at various locations on the model and is so indicated. Study of the data from just one test indicates that only meager results can be obtained. However, when the data from the two tests is overlayed, a remarkable degree of correlation is evident. The predominant waveforms were selected from this correlation and were used for further data reduction.

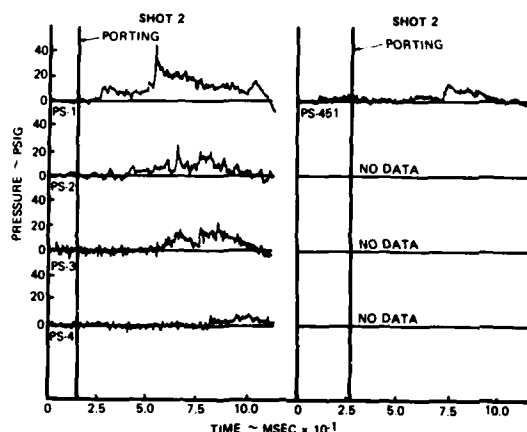


Figure 19. Model Skirt Pressure Data: Shot 2

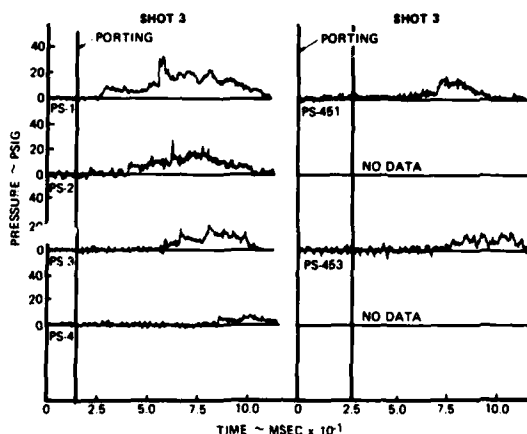


Figure 20. Model Skirt Pressure Data: Shot 3

As the data indicates, the zero meridian ray produces the highest pressure. The 45 degree meridian ray indicates that the first transducer to feel a pressure pulse does so prior to ejection. This is valid data since there is a small amount of gas leakage prior to ejection in this meridional plane because of the sealed

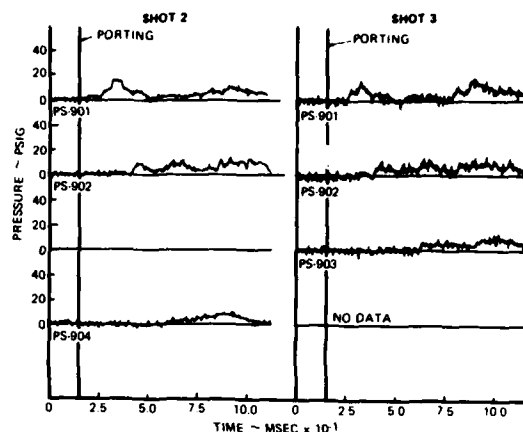


Figure 21. Model Skirt Pressure Data: Shots 2 and 3

antenna notches that were modeled in the launch tube as shown in Figure 22. The 90 degree meridian ray shows little door effect.

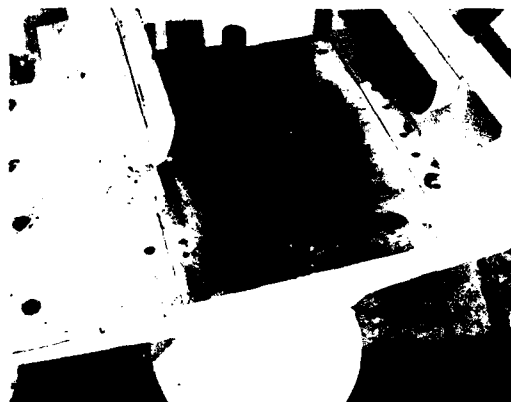
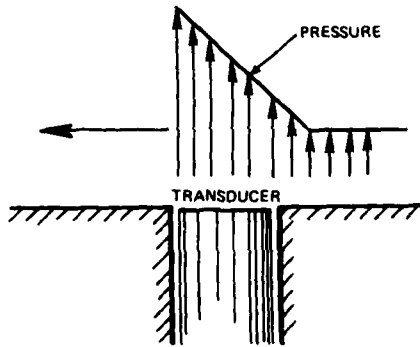


Figure 22. Launch Tube Mouth

C. PRESSURE DATA REDUCTION

Since the phenomena investigated in this test program are shock wave induced, the change in pressure across the shock wave is discontinuous. For all practical purposes, this discontinuous change is instantaneous. Because of the response associated with the various components of the experimental data acquisition system, it is impossible to record instantaneous changes in pressure without distortion. There will always exist a finite rise time for the entire system for instantaneous input. Since rise time can be measured from the test data (with the reasonable assumption that the functional input to the system changes instantaneously), then a correction may be applied to the data to negate rise time effects. The data indicates that a representative shock wave speed over the face of the transducers was 1500 ft/s. Since the effective pressure sensitive face of the transducer is 0.165 inch, the shock wave will take approximately 9 microseconds to traverse the face of the transducer. For a sawtooth pressure profile of the form obtained from the test program, the pressure transducer will see a maximum pressure when the

pressure pulse-transducer orientation is as shown below (disregarding transducer response time which is small). This indicates that rise time on the order of 9 microseconds should be obtainable from the test data results. Rise time was measured from the test data and was determined to be on the order of 10 microseconds. Using the measured 10 microsecond rise time, the data may be corrected to obtain the maximum pressure of the sawtooth waveform. This was accomplished by first visually smoothing the data and then determining what magnitude of the pressure spike and decay rate represents the average pressure sensitive face of the transducer.



Figures 23 and 24 show the results of rise time data correction for two identical tests using the worst case door configuration. The corrected data shows a maximum pressure of 56 psig for test 2 and 54 psig for test 3 for the first transducer nearest the door above the base of the model.

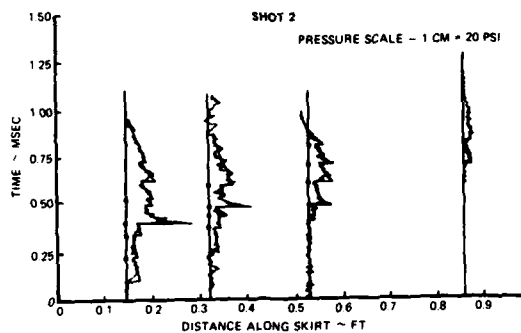


Figure 23. Model Skirt Pressure Data: Shot 2

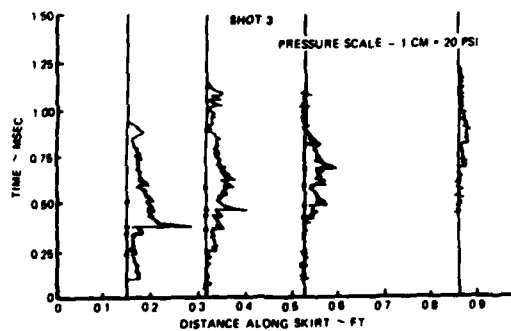


Figure 24. Model Skirt Pressure Data: Shot 3

To complete the pressure history over the entire skirt, the data must be extrapolated to the skirt-base junction since the data indicates the maximum pressure is higher at the junction. Without knowledge of the shape and direction of the shock wave causing the maximum pressure spike, data extrapolation would be difficult to justify. For this reason, the water table was again used in an attempt to correlate the prominent waves with experimentally observed pressure pulses. The first of these prominent waves precedes all other waves and corresponds to the non-interacted porting shock wave in the axial direction. Until this wave passes the third row of transducers, the strength of this wave appears unmodified by the presence of doors. This wave is denoted as Wave A in Figures 25 and 26. The approximate position of Wave A is shown at the stated times as obtained from the pressure data. After the third transducer is passed by the porting shock wave, reflected shock waves catch up with the porting shock wave and modify its strength. Using the results of Figure 14, at $t = 0.135$ millisecond, the porting shock wave just reaches the lower inside of the door. In the axial direction, from Figure 16, the porting shock wave has traveled 0.225 foot referenced to fixed coordinates and 0.184 foot along the model skirt. Figure 25a shows the approximate shock wave configuration at $t = 0.135$ millisecond. The first transducer (PS-1) recorded the passage of the shock wave at $t = 0.1$ millisecond. At $t = 0.25$ millisecond, the second transducer (PS-2)

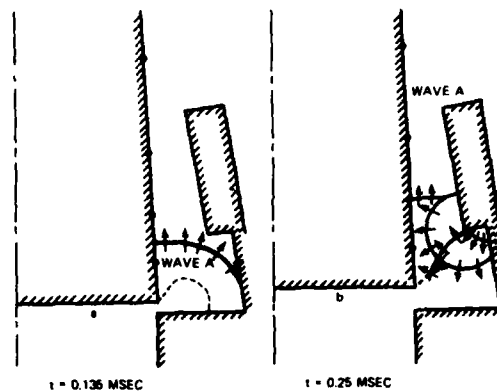


Figure 25. Water Table Flow Field Representation

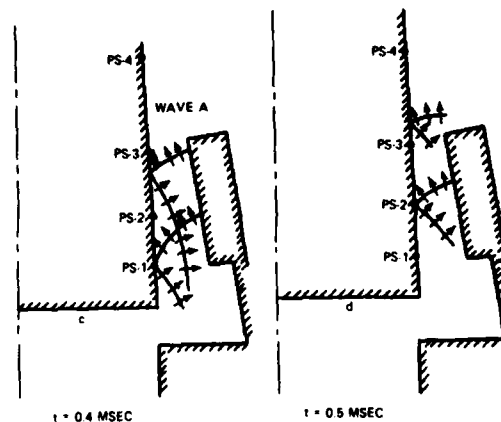


Figure 26. Water Table Flow Field Representation

records the passage of the porting shock wave in the axial direction. In the radial direction, porting shock wave reflection from the door has occurred. As shown (Figure 25b), the reflection consists of several interacting shock waves. At approximately $t = 0.4$ millisecond, the first transducer (PS-1) feels the maximum pressure pulse. The interpreted shock wave configuration is shown in Figure 26c. The second transducer (PS-2) feels the maximum pressure pulse approximately 0.1 millisecond later. The interpreted shock wave configuration at this time is shown in Figure 26d.

From this interpretation, it was observed that the most probable cause for the maximum pressure pulse was the reflection of that shock wave shown to coincide with the first transducer at $t = 0.4$ millisecond (Figure 26c). The origin of this shock wave was the inside corner of the door ground plane junction.

Some characteristics of this wave and its reflection from the missile surface may be inferred from the data to predict the maximum pressure at the base lip. From Figures 25 and 26, the ratio of maximum pressure after shock wave reflection to the pressure just before shock wave passage (thus the reflected shock wave strength) for the first three transducers along the 0 degree meridional ray was measured and plotted as a function of distance along the model skirt. If it is assumed that the shock wave configuration at the base lip is identical to the configuration at maximum pressure as interpreted from this simulation for the first three transducers, then the strength of the reflection may be smoothly extrapolated to the base lip. This was accomplished and is shown in Figure 27. Since the maximum porting shock wave pressure at the lip has already been established to be approximately 27 psia, applying the maximum extrapolated reflected shock wave strength of Figure 27 to this pressure results in a maximum skirt pressure of approximately 110 psia at the base lip.

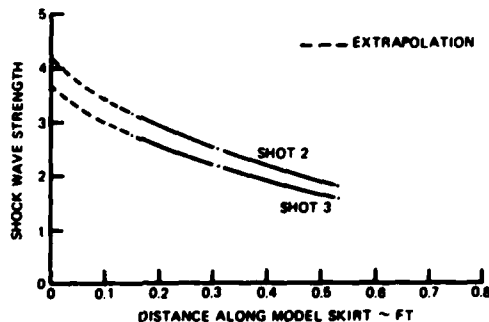


Figure 27. Reflected Shock Wave Strength vs Distance Along Model Skirt

One test was conducted, under identical conditions to the previously discussed tests, with that set of doors corresponding to the intermediate door opening angle. The results of this test (Figures 28 and 29) indicated that the pressure pulse associated with shock wave reflection was not as severe as the worst case door configuration. For this reason, the remaining set of doors was not tested.

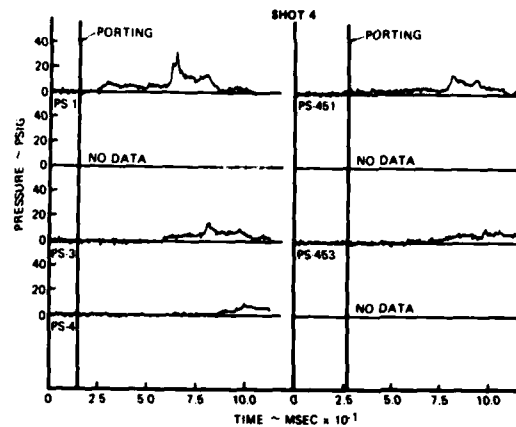


Figure 28. Model Skirt Pressure Data: Shot 4

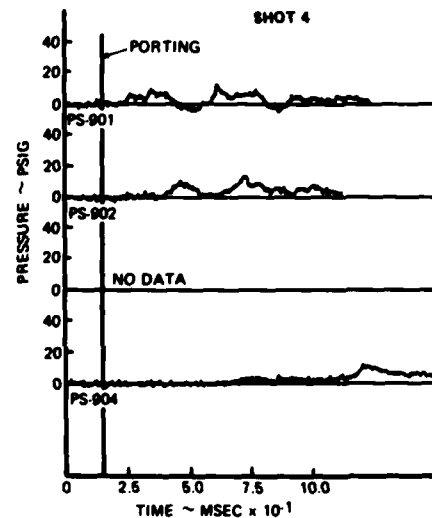


Figure 29. Model Skirt Pressure Data: Shot 4

D. BASE PRESSURE DECAY TIME

Base pressure decay time will depend on the length of time it takes the launch tube to blow down after ejection. The ejection event can only be propagated (by means of expansion waves) into the launch tube at the local sound speed of the gas within the tube. At ejection, the sound speed is approximately 3000 ft/s. It will take approximately 10 milliseconds for the ejection event to influence the gas at the bottom of the launch tube for the full scale configuration. Reflected expansion waves from the tube bottom will require slightly less time to propagate to the tube mouth. In all, outflow should not be diminished for the first 15 milliseconds after ejection.

The launch tube gas flow subsequent to ejection is identical to closed pipe flow with a diaphragm opening into the atmosphere. It is known that flow will first be expelled from the tube resulting in an overexpansion within the launch tube. The

flow will then be drawn back into the tube resulting in an overcompression within the launch tube. This overexpansion and overcompression is cyclic and will occur several times before viscous effects damp it out. This cyclic flow was observed to occur in the film data from all the tests. Consistently, three out-flow cycles were observed. However, the launch tube pressure transducers were not sensitive enough to record the pressure variation.

Base pressure decay after ejection was measured during the subscale tests and typical results are shown in Figure 30. For the subscale tests, base pressure decays to ambient approximately 4 milliseconds after ejection. This relates to 18 milliseconds for the full scale configuration.

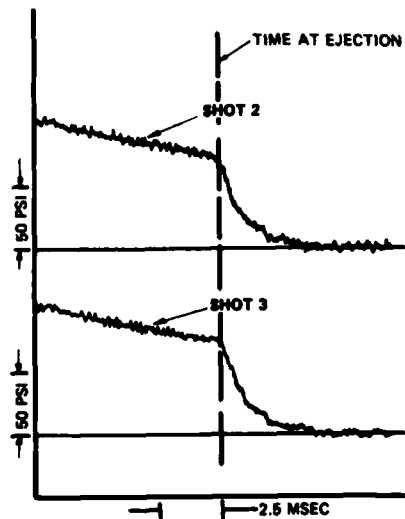


Figure 30. Base Pressure History After Ejection

CONCLUSIONS

The results of the test program indicate all test objectives were met. Experimental data of sufficient quality and quantity have been obtained for use in dynamic structural analysis. The following conclusions are made:

- 1) With the worst case door opening angle, maximum skirt pressure was determined to be 110 psia. All greater door opening angles will result in lower maximum pressure.
- 2) The entire transient pressure environment is essentially complete within a time span of 4 milliseconds after ejection for the full scale configuration.
- 3) It takes approximately 18 milliseconds for the base pressure to decay to ambient pressure after full scale ejection.
- 4) One-dimensional analyses can be used to predict initial speed of the emerging gas-air interface and porting shock wave. The application of blast wave theory in the axial direction does not produce accurate results.
- 5) The data indicate formation of an imbedded starting shock wave in the emerging launch tube flow which decreases strength of the porting shock wave.

REFERENCES

- 1 Taylor, T. D., "Calculation of Muzzle Blast Flow Fields", Picatinny Arsenal TR 4155, 1970
- 2 Noh, W. F., "A Time Dependent, Two-Space-Dimensional Coupled Eulerian - Lagrange Code", Methods in Computational Physics, Academic Press, 1964
- 3 Culotta, A. J., "A Computer Program for the Solution of Unsteady I-D Flow Fields", 6th Aerospace Sciences Meeting, AIAA, New York, N. Y., 1966
- 4 Smith, C. E., "An Analytical Study of the Starting Process", SUDAER 135, 1962
- 5 Sedov, L. I., "Similarity and Dimensional Methods in Mechanics", Inforsearch LTD, 1969
- 6 Courant-Friedrichs, "Supersonic Flow and Shock Waves", Interscience Publishers, Inc., 1956

SHOCK TESTING

DIGITAL CONTROL TECHNIQUE FOR SEISMIC SIMULATION

G. C. Kao, K. Y. Chang, W. W. Holbrook
Wyle Laboratories, Scientific Services and Systems Group
Eastern Operations, Huntsville, Alabama 35807

A digital iteration technique for controlling large electro-hydraulic test systems to simulate ground motions is presented in this paper. The technique is based on the closed-loop control concept with input control waveforms generated by an on-line digital computer. Generally, a typical test sequence consists of three intermediate-level and one full-level tests with actual specimens installed on the test fixture. During calibration, the response and its corresponding input waveform obtained from each intermediate-level test are used to compute the input waveform for the next higher level test. The total test time required for each test sequence is approximately four minutes, exclusive of plotting. The digital iteration control (DIC) technique was verified on a 30,000 force-pound seismic simulator and a 150,000 force-pound shock machine. Excellent test results were observed.

INTRODUCTION

Control equipment used in commercial nuclear reactor power plants and antiballistic missile (ABM) systems are required to remain functional during earthquakes and other ground motions due to nuclear weapon effects. It is essential that such equipment be tested to the specified shock environments to verify design reliabilities.

In recent years, much effort has been expended in developing new transient test control techniques to simulate seismic motions. Most ground shock environments are defined in terms of their "shock spectrum". Each spectrum may represent the motion of a particular location or event. A spectrum may also represent the enveloped maxima of all spectra in typical localities. To meet ground motion requirements, as defined by a shock spectrum, simulation control equipment must be capable of generating an input control waveform to drive the test machine to the desired motion.

The shock spectrum testing as described above is normally accomplished by the close-loop analog control techniques [1]. The typical approach of analog control techniques may be depicted by the block diagram as shown in Figure 1. The basic control equipment consist of a complex waveform synthesizer and a shock spectrum analyzer. The synthesizer is composed

of a series of electronic filters (resonators) which generate either damped sinusoidal or sinebeat waves. The outputs from each filter are modulated by three parameters which control: amplitude, phase and rate of decay (damping). By properly adjusting all the control parameters of the synthesizer, a complex waveform can be generated to drive a non-linear test system. The subsequent response at the output control point is analyzed by a shock spectrum analyzer and the measured shock spectrum is compared with the required to determine the accuracy of the test result. The deviations in the synthesized spectra are corrected through iterative adjustment of the synthesizer filters.

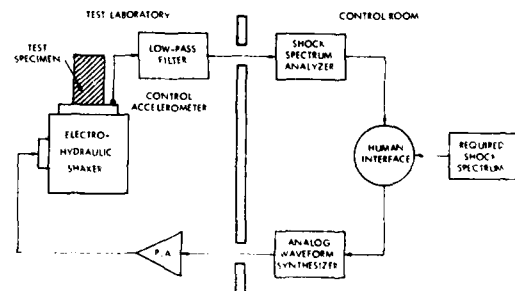


Figure 1. Block Diagram of Analog Control Approach

In order to avoid damaging specimens during testing, analog shock testing is carried out in two stages. In the first stage a dummy mass with a weight identical to the specimen is used to calibrate the synthesizer for different levels of inputs. In the second stage the dummy weight is replaced with the actual specimen, and the tests are conducted at successive increasing levels employing calibrated inputs obtained in the first stage. Further modifications of the synthesizer outputs are often needed to compensate for dynamic couplings between the specimen and the test system. Since electro-hydraulic test systems are quite non-linear, a large number of calibration pulses are often required, and fatigue damage to test specimens might result. Furthermore, the accuracy of the analog control approach is restricted by the total number of filters available for adjustments.

A digital iteration control (DIC) technique has been developed to improve the quality and the speed of shock testing electro-hydraulic test systems. This technique eliminates the need for dummy-weight calibration, and at the same time, refined adjustments of input controls can be achieved by means of a digital computer. In addition, more accurate testing can be achieved with a minimum number of trial runs. This paper describes the operating principles of the DIC technique for one-dimensional testing, and the results of preliminary test data obtained from a 30,000 force-pound and a 150,000 force-pound test system.

DIGITAL ITERATION CONTROL (DIC)

Recent work in the area of digital controls on linear systems has been reported in References 2, 3 and 4. The DIC approach in shock testing centers on the generation of an equivalent transfer function for the non-linear test system for the full-level test. The concept of transfer function of a typical test system may be described schematically by Figure 2. The portion of the system contained between the control feedback function and the output response control point constitutes a mechanical "blackbox" which is represented by Figure 3. The ratio of the output response and the input voltage defines the transfer function of the test system. Mathematically speaking, the transfer function is expressed by Equation (1):

$$H(f) = \frac{A(f)}{E(f)} \quad (1)$$

where: $E(f)$ = Input control voltage

$A(f)$ = Output response

f = Frequency, Hz

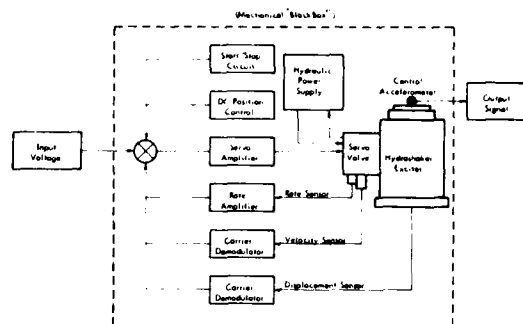


Figure 2. Block Diagram of Electro-Hydraulic Test System

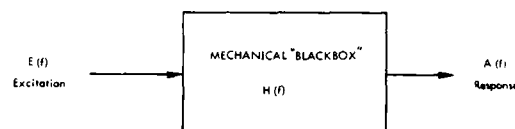


Figure 3. Block Diagram of Response-Excitation Transfer Function

Based on Equation (1), the required output responses and the input waveforms are to be specified in the frequency domain. This requirement does not present a problem for output responses specified in the forms of time-history; but for output criteria specified in terms of shock spectra, an equivalent time-history must be generated for each spectrum in order to meet DIC formats. Several methods [5, 6, 7] are available for performing the shock spectrum-to-time-history transformation.

Since the system is non-linear, the transfer function as defined in Equation (1) is dependent on the characteristics of the input waveform. The development of the DIC technique was based on the assumption that the transfer functions between two successive tests at two slightly different input levels would not deviate significantly from each other. Therefore, if the transfer function obtained from a lower level test is used to generate input waveforms for the next higher level test, the resultant errors in the output response would be insignificant.

In the DIC test, the first low-level input waveform is generated by dividing the required output by a trial transfer function. The trial function could be generated by either of the three excitation techniques; namely: the sinesweep, the random and the transient techniques. Sometimes it is also admissible to use the transfer function generated from a previous test. The

input and output of the first trial run is used to compute the improved transfer function of the test system and the input waveform for the next higher level test. The same procedure is repeated until the full-level testing is achieved. However, it must be realized that the total number of trial runs must be kept to a minimum, so that no damage will be introduced to test specimens. Recent test results have shown that a total of three trial runs is adequate to provide a good transfer function for the final full-level test. The control sequence as described above is depicted by the block diagram as shown in Figure 4, and a more detailed description regarding the control technique can be found in Reference 8.

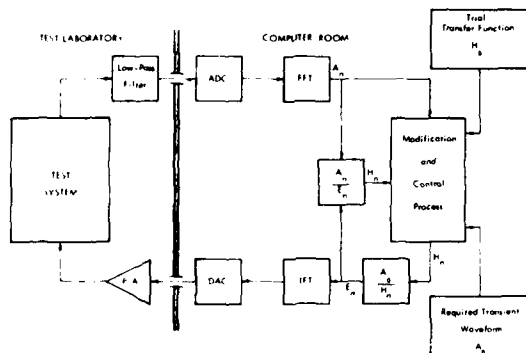


Figure 4. Logic Diagram for Digital Iteration Control (DIC) Procedures

The software employed in the DIC system consists of a main program and three subprograms. The main program is used to compute the transfer function and the input control voltage. In addition, it examines the incoming response data which is then compared with the required response waveform in terms of individual Fourier Spectra. The results of the error analysis are printed out on the line printer. The three subprograms consist of: The Fast Fourier Transform (FFT) Program, the Inverse Fourier Transform (IFT) Program, and the Data Conversion (DACADC) Program. The FFT Program is employed to transform the output response signal from the time domain for computing the transfer function. The IFT Program is used to transform the computed input waveform from the frequency domain into the time domain. The DACADC Program was written in assembly language and is used to convert the analog output response signal into digital forms and the digital input waveform into analog forms.

The hardware systems employed in DIC tests consist of a Sigma 5 computer with 16K word memory core, two high-speed tape drives, one MD-51 Analog-to-Digital Converter (ADC), one Digital-to-Analog (DAC) Converter and a CALCOMP Plotter. The ADC can operate at a maximum sampling rate of 100,000 samples per second. The sample word sizes are 15 bits plus sign and 10 bits plus sign for the ADC and DAC, respectively.

The present DIC system employs a total of 2048 data points to represent a transient waveform. Several possible operating ranges of the system are presented in Table 1.

TABLE 1
OPERATING RANGE OF PRESENT DIC SYSTEM

Sampling Rate (Samples/Second)	Duration of Waveform (Seconds)	Upper Frequency (Hz)	Lower Frequency (Hz)
20,000	0.10	10,000	10.0
2,000	1.0	1,000	1.0
1,500	2.0	500	0.5
200	10.0	100	0.10
100	20.0	50	0.05
60	34.0	30	0.03

The extension of the frequency range can be achieved by increasing the total number of data points used in defining required waveforms.

To safeguard test equipment against damage due to erroneous signals, each intermediate input-time history was plotted for visual inspection prior to testing. The actual time required for a four-test sequence would be less than four minutes, exclusive of plotting time.

DESCRIPTION OF TEST SYSTEMS

The DIC concept was verified with a 30,000 force-pound and a 150,000 force-pound test system, as shown in Figures 5 and 6, respectively.



Figure 5. The 30,000 Force-Pound Seismic Simulator

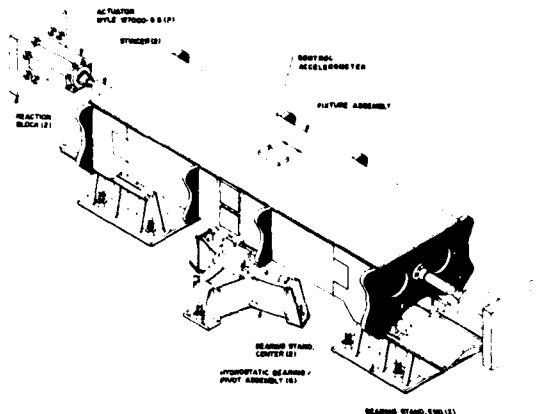


Figure 6. The 150,000 Force-Pound Shock Machine in the Push-Pull Mode

The 30,000 force-pound system has been used extensively to simulate seismic environments using analog control techniques. It basically consists of a 6 ft x 14 ft test platform which was constructed using 24 in. I-beams and weighs approximately 9,000 pounds. The test platform in its present configuration, is driven by three vertical actuators and one larger horizontal actuator. The actuators have a vertical and horizontal force rating of 30,000 force-pound and are controlled by conventional electro-hydraulic servo valves and servo amplifiers. The weight of the fixture is supported by four air springs located at the corners of the fixture. The operating frequency range of this system is from 1 Hz to 100 Hz. For the verification test, a dummy cabinet with dummy weights installed was mounted on the platform. The control accelerometer was located at the actuator/platform interface as shown in Figure 7. The force was applied in the direction of the lateral actuator. The hydraulic power supply of this system consists of a positive displacement pump supplying a total of 200 gpm at 3000 psi. Peak flow requirements were provided through a precharged accumulator.

The second system is shown in Figure 6. This machine was designed originally to simulate motions due to nuclear blasts and has an operating frequency range between 1 Hz to 500 Hz. The test table is 5 ft wide and 17 ft long. The structure is made entirely of aluminum and weighs approximately 11,000 pounds. The source of excitation was provided by two 75,000 force-pound hydraulic actuators in a push-pull mode. The hydraulic power supply serving this system consisted of four 120 gpm positive displacement pumps supplying a total of 480 gpm at 3000 psi. Peak flow capability was provided by precharged accumulator banks with 525 gpm at 3000 psi. The test table was supported by six hydrostatic bearings. The bearing stands and the reaction of blocks of the actuators were tied to the reaction mass which weighs approximately 1.5 million pounds. Conventional electro-hydraulic



Figure 7. Close-up of the Electro-Hydraulic Shaker

servo valves and servo amplifiers were used to provide input waveforms to the actuators. The control accelerometer was located at the center of the table. No additional test specimen other than the table itself was employed in performing the verification tests.

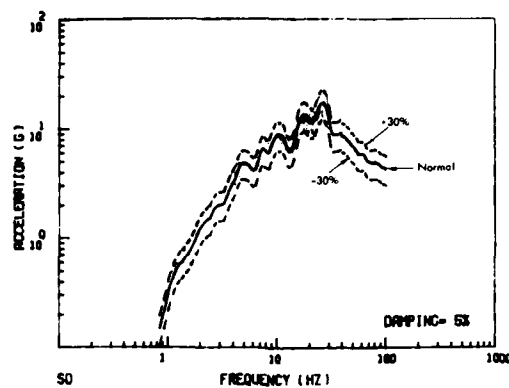
TEST RESULTS

For the 30,000 force-pound test system, the required output shock spectrum and its corresponding time history are shown in Figures 8(a) and 9(a), respectively. The test frequency of the control spectrum was set between 1 Hz and 100 Hz. The tolerance limits for this test were specified as $\pm 30\%$.

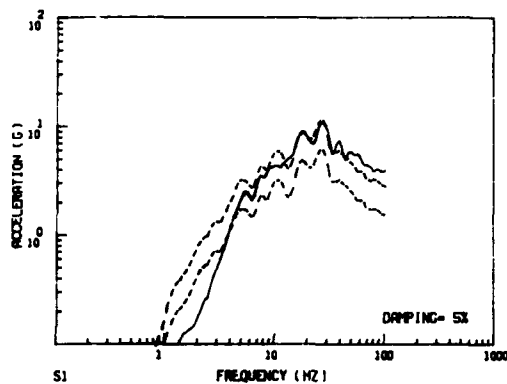
The verification tests were conducted at three levels:

- Two tests at one-half level
- One test at three-quarter level, and
- One test at full level.

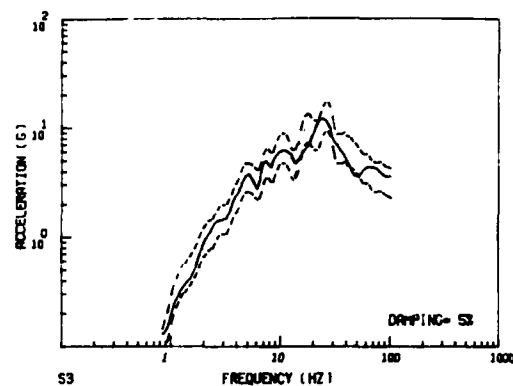
The results of the above tests are presented in the shock-spectrum form as shown in Figure 8, and in the time-history form as shown in Figure 9. The transfer function used in the first 1/2-level test was obtained through a low-level sinesweep excitation in the frequency range of 5 Hz to 30 Hz (limitation of analog sinesweep monitor). The test result was extrapolated to 1 Hz at the low frequency end, and to 100 Hz at the high frequency end. Obviously, the sinesweep transfer function, as shown in Figure 10, did not provide the proper input waveform to excite the test system. Hence, the output shock spectrum, as shown



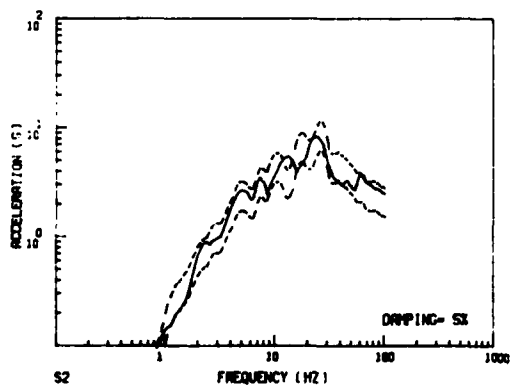
(a) Shock Spectrum of Required Transient Waveform



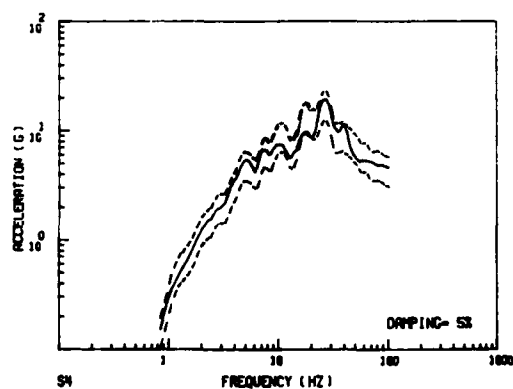
(b) Shock Spectrum of First 1/2-Level Test



(d) Shock Spectrum of 3/4-Level Test



(c) Shock Spectrum of Second 1/2-Level Test



(e) Shock Spectrum of Full-Level Shock Test

Figure 8. Results of Shock Testing Employing 30,000 Force-Pound Simulator

in Figure 8(b), is low for frequencies below 5 Hz and high for frequencies above 30 Hz. The results of the second 1/2-level test have shown significant improvements over the first test. The improvements made in the system transfer functions through iterative correction at higher test levels have lead to a successful test at the full level, as shown in Figure 8(e).

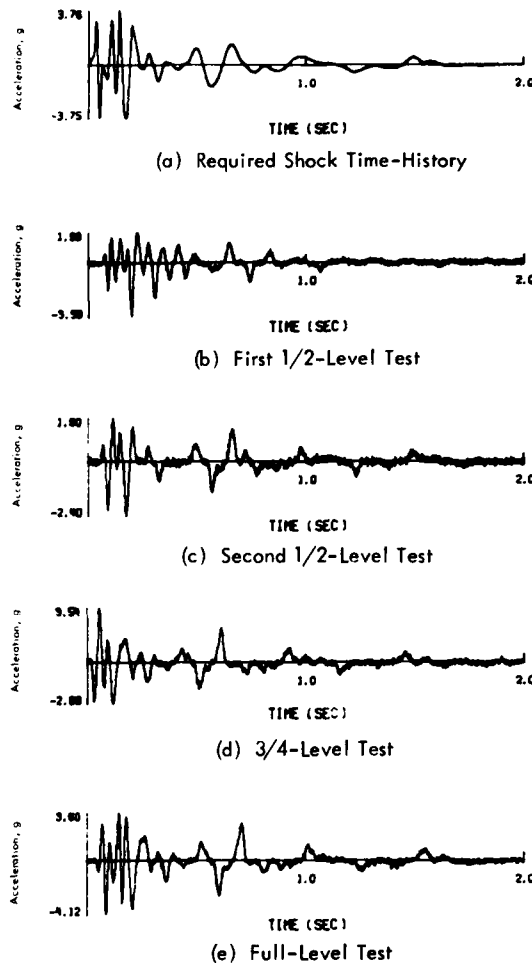


Figure 9. Shock Time-Histories of the Control Accelerometer of Seismic Simulator

The measured transfer function of the test system at full input level is shown in Figure 11. The major resonant frequencies are shown as 16, 35, 46, 57, 79 and 90 Hz.

The tests performed on the 150,000 force-pound system were based on the shock spectrum, as shown in Figure 12(a), and its corresponding time-history, as shown in Figure 13(a). The tolerance limits for the tests were set as follows:

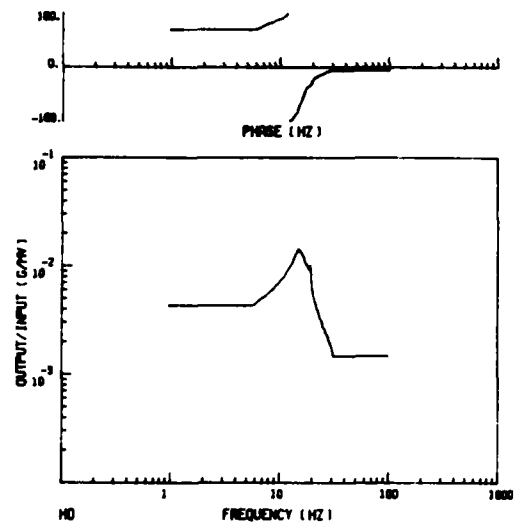


Figure 10. Low-Level Sinesweep (Linear) Transfer Function of Test System

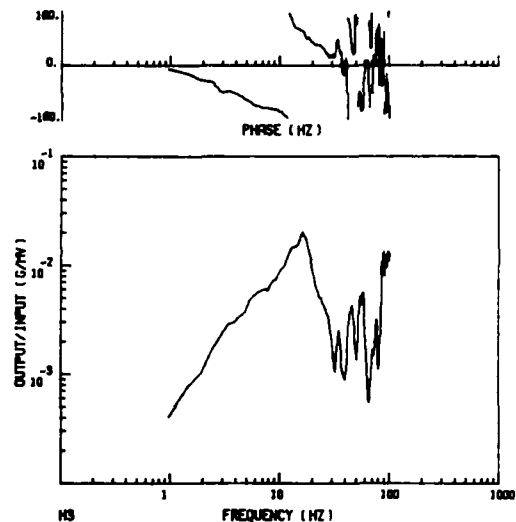
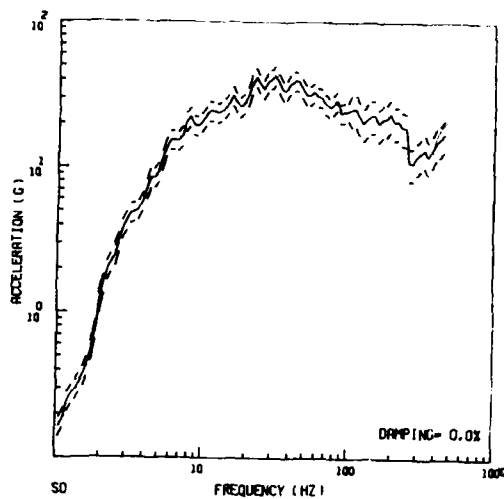


Figure 11. Equivalent Transfer Function of Test System at Full Level

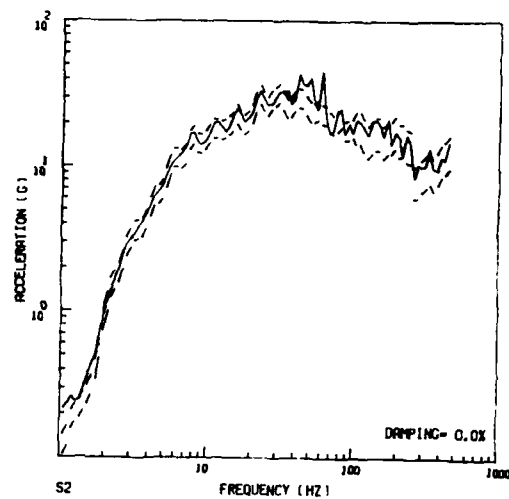
Frequency Range	Tolerance Limits
1 - 100	$\pm 15\%$
100 - 500	$\pm 25\%$

A total of three tests were performed at the following levels:

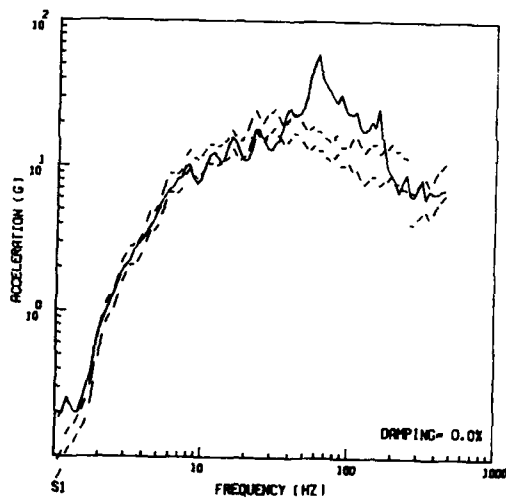
- One 1/2-Level Test
- One 3/4-Level Test
- One Full Level Test



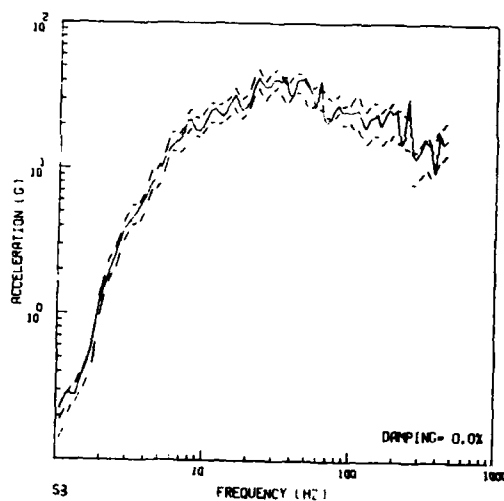
(a) Required Shock Spectrum



(c) Shock Spectrum of 3/4-Level Test



(b) Shock Spectrum of 1/2-Level Test



(d) Shock Spectrum of Full-Level Test

Figure 12. Results of Shock Testing Employing 150,000 Force-Pound Shock Machine

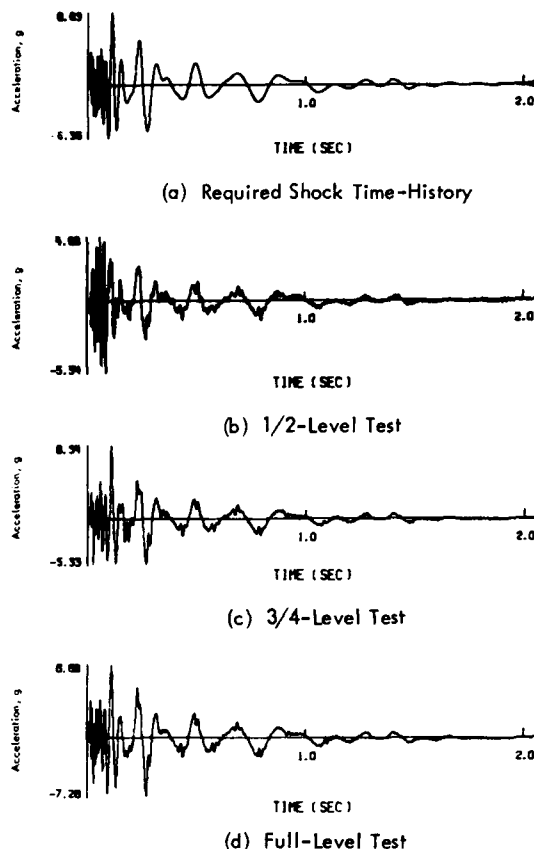


Figure 13. Shock Time-Histories of the Control Accelerometer of 150,000 Force-Pound Shock Simulator

The input waveform for the first 1/2-level test was generated by a transfer function obtained from a previous test. The initial transfer function is shown in Figure 14. Consequently, the shock spectrum of the first test does not possess the proper shape, as shown in Figure 12(b). The results of the second test at 3/4-level, however, has shown significant improvement over the first, as shown in Figure 12(c). The majority of the measured shock spectrum is within the tolerance limits. The results of the final test at full-level are shown in Figure 12(d). The required tolerance limits are violated only in the vicinities of 65 Hz and 260 Hz, respectively. These two frequencies are identified as the primary resonance frequencies of the test system. Since the deviations are so small, it is considered as acceptable for normal shock testing. The time-history of the full level test has shown excellent agreement with the required one.

In addition, the measured system transfer function of the full-level test is presented in Figure 15. The major resonant frequencies of the test system in the operational range were measured as 30, 65, 260, 300, 350 and

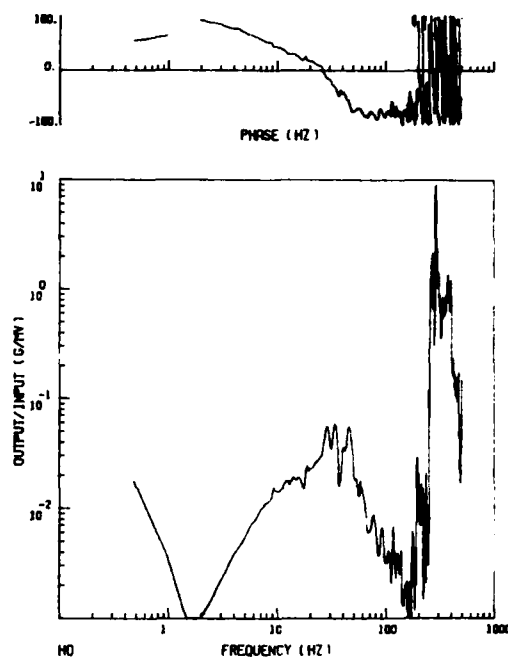


Figure 14. Initial Transfer Function of the 150,000 Force-Pound Test System

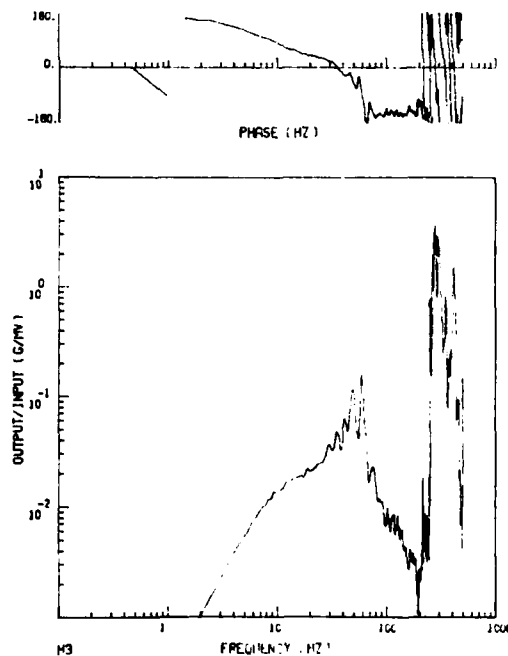


Figure 15. Equivalent Transfer Function of the 150,000 Force-Pound Shock Test System

400 Hz, respectively. A shift of the primary resonant frequencies was observed in the system transfer function.

CONCLUSIONS

The results of the test program as described in the previous sections have demonstrated the feasibility and the practicality of the DIC technique in performing day-to-day shock testing. The clear advantages of the DIC technique are:

- Reduction of test time to reach full test level;
- Elimination of dummy weight calibration;
- Reduction of possible fatigue damage to test specimens; and
- Improvement of test system control through variable bandwidth adjustments.

The major obstacle in the performance of DIC tests is in the area of controlling the required spectrum in resonant frequency ranges. There are two kinds of resonances that must be dealt with in any electro-hydraulic test systems; namely: the structural resonance and the test system resonance. The majority of structural resonance could be resolved by designing structural members to be rigid enough so that resonances are kept outside of the test frequency range. The test system resonance is attributed to the resonance of oil columns. Such resonances are caused by the compliance of the oil column and the combined mass of the table and the fixture. These resonances always lie within the test frequency range and must be coped with through iteration controls so that more accurate system transfer functions at various stages can be obtained to generate control signals. In addition, greater control accuracies can be achieved through the DIC technique by keeping the incremental level small. However, it must be recognized that the resonances of electro-hydraulic test systems are inherent problems that must be dealt with through control schemes, and cannot be totally avoided through mechanical or hydraulic designs. Attempts are being made to improve the controllability of the present DIC technique in the system resonant ranges. The results of such studies will be made public when information becomes available.

ACKNOWLEDGEMENTS

This paper represents the results of a Wyle in-house research effort. The authors are indebted to W. T. Brooks, Vice President and General Manager, Scientific Services and Systems Group, Wyle Laboratories, for his support in developing the DIC Program and to numerous personnel of Wyle/Huntsville Facility for providing the necessary analytical and experimental assistance throughout the duration of this study.

REFERENCES

1. Shipway, G., "A New Technique for Seismic Shock Simulation," Wyle Laboratories Test Report, Norco, California Facility.
2. Favour, J.D., LeBrun, J.M. and Young, J.P., "Transient Waveform Control of Electromagnetic Test Equipment," The Shock and Vibration Bulletin, Bulletin 40, Part 2, pp. 157-171, December 1969.
3. Otts, J.V. and Hunter, N.F., "Shock Testing on Vibration Machines by Digital Techniques," Sandia Laboratories Technical Memorandum, SC-TM-72-0304, June 1972.
4. Fisher, D. K., "Theoretical and Practical Aspects of Multiple-Actuator Shaker Control, Control," Paper presented at the 43rd Shock and Vibration Symposium, December 1972.
5. Yang, R. C., "Development of a Waveform Synthesis Technique," The Ralph M. Parsons Co., Document No. SAF-64, August 1970.
6. Smallwood, D. O. and Witte, A. F., "The Use of Shaker Optimized Periodic Transients in Matching Field Shock Spectra," Sandia Laboratories, Development Report SC-DR-71-0091, May 1972.
7. Tsai, N.C., "Spectrum-Compatible Actions for Design Purposes," J. Engineering Mechanics Division, Proceedings of American Society of Civil Engineers, EM 2, April 1972.
8. Kao, G and Chang, K., "Control of Electro-Hydraulic Shaker by Digital Iteration Techniques," Society of Automotive Engineers Paper No. 720823.

DISCUSSION

Mr. Favour (Boeing Company): In your modification of control circuitry do you just make a direct linear comparison, or do you do anything to insure that you do not exhibit an unstable situation such that you overcorrect in your modification of the transfer function?

Mr. Kao: The technique which we used was to average the one before or the one after.

Mr. Favour: So you are ensembling?

Mr. Kao: Yes. You also can use some other statistical approach to insure it will be within the expected nonlinear range.

Mr. Linton (Naval Weapons Station, Seal Beach): How quickly can you make those successive hits, within an order of magnitude?

Mr. Kao: Based on our own records, including printing and plotting, it would last no more than three minutes per hit. For example, if you have three or four hits you could probably finish in a matter of five or ten minutes, depending on how successfully the signal is coming through.

Mr. Powers (McDonnell Douglas): You made a comparison of the required Fourier spectra and the actual Fourier spectra, in other words the test spectra and the one that was required. If your specification was in fact given in terms of a shock spectrum, how did you determine what was the required spectrum? Many different inputs will produce a given shock spectrum.

Mr. Kao: It is true that the time history with respect to a given shock spectrum is not unique. We use a certain computer program by which we prescribe the required amplitudes and corresponding frequency points. This program will then generate a time history which will satisfy a shock spectrum. We use that shock spectrum and go through a Fourier analysis to come up with the Fourier spectrum for the required wave form and then use that as a basis for comparison.

Mr. Favour (Boeing Company): In the parameters you were using, a thousand samples per second for two seconds, you should have been controlling to 500 Hz, yet your plots were terminated at 100 Hz. What is your performance from 100 to 500?

Mr. Kao: We still control from 1 to 500 Hz without any problems by adjusting the controlling bandwidth using averaging techniques.

Mr. Gaberson (Naval Civil Engineering Laboratory): When you are going through these different hits and gradually increasing the level, what is happening to the specimen that is on the table? If you don't have a specimen on there, but have a dummy mass, doesn't this feed back into your system and change the wave form?

Mr. Kao: Yes. The objective of the iteration procedure is to try to account for the dynamic feedback of the test system. That is, if you use a dummy mass for your calibration testing, you have to have a very heavy shake table in order to compensate for the dynamic response of the specimen. Using digital techniques you could place the actual test specimen on the fixture and, using a low level excitation and bringing the thing along one step at a time, you can achieve the objective of shock testing more efficiently than by using a dummy mass. Did I answer your question?

Mr. Gaberson: Could it not be damped as you go up?

Mr. Kao: It might, but using digital control you would probably hit the specimen fewer times than if you were to use analog.

PYROTECHNIC SHOCK SIMULATION
USING THE RESPONSE PLATE APPROACH

CHARLES L. THOMAS
HONEYWELL INC.
ST. PETERSBURG, FLORIDA

The capabilities to produce a shock response spectrum by using a series of isolated plates excited by an explosive ordnance are shown. A test program to show the effect that each physical parameter has on the shock response spectrum was performed. The test data and a discussion of test results are presented.

INTRODUCTION

The shock transients produced by pyrotechnic devices on spacecraft may be simulated in the laboratory by several techniques, such as the electrodynamic exciter synthesizer, drop shock, barrel tester, actual firing of flight hardware, and the response plate. This presentation is devoted to developing a shock response spectrum using the response plate approach. The response plate technique uses two plates referred to as the base plate and the response plate as shown in Figures 1 and 2. The test hardware is secured to the response plate which is mounted to the base plate on standoffs and isolators. The ordnance is placed under the base plate. The system is supported off the floor by ropes. The detonation of the explosive produces the shock transient. The acceleration time history of a typical pulse is shown in Figures 3 and 4. Figure 5 shows the repeatability of four shock response spectrums produced by this technique. The horizontal response is shown in Figure 6. If this technique is selected to simulate a given shock response spectrum, the design and development of the fixture should take into account that the shock spectrum may be influenced by the amount, placement and shape of the explosive, size and material of the response plate, size and material of the base plate, weight of the hardware, height of the base plate from the floor, isolation material and isolator preload. This paper presents data to show the effect each of these parameters has on the shock response spectrum.

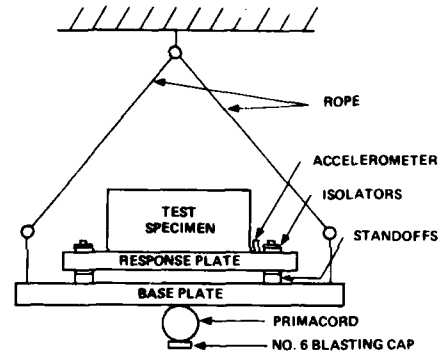


Figure 1. TEST CONFIGURATION

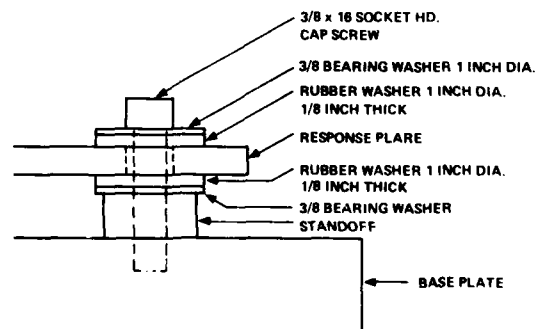


Figure 2. ISOLATION JOINT CONFIGURATION

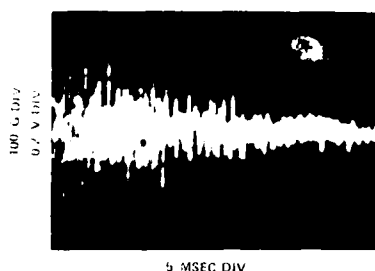


Figure 3. PULSE DURATION

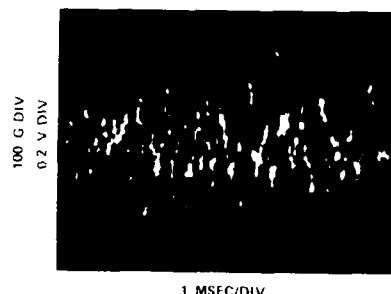


Figure 4. PULSE FREQUENCY

Table 1. TEST CONFIGURATIONS

Test No.	Base Plate Material	Base Plate Thickness (inches)	Response Plate Material	Response Plate Thickness (inches)	Isolation of Isolator Material	Compression of Isolator (inches)	Base Height Above Floor (inches)	Amount of Primacord (inches)	Distance of Explosive From Base	Shape of Charge	Specimen Weight
1	Phenolic	1	Alum.	1/8	ZZR765	0.004	16	10	Tangent	0	14
2	Alum.	2	Alum.	1/8	ZZR765	0.004	16	10	Tangent	0	14
3	Alum.	1/2	Alum.	1/8	ZZR765	0.004	16	10	Tangent	0	14
4	Alum.	1	Alum.	1/8	ZZR765	0.004	16	10	Tangent	0	14
5	Alum.	1	Mag.	1/4	ZZR765	0.004	16	10	Tangent	0	14
6	Alum.	1	Steel	1/4	ZZR765	0.004	16	10	Tangent	0	14
7	Alum.	1	Masonite	1/4	ZZR765	0.004	16	10	Tangent	0	14
8	Alum.	1	Phenolic	1/4	ZZR765	0.004	16	10	Tangent	0	14
9	Alum.	1	Alum.	1/4	ZZR765	0.004	16	10	Tangent	0	14
10	Alum.	1	Alum.	3/8	ZZR765	0.004	16	10	Tangent	0	14
11	Alum.	1	Alum.	1/2	ZZR765	0.004	16	10	Tangent	0	14
12	Alum.	1	Alum.	1/4	MIL-46089	0.004	16	10	Tangent	0	14
13	Alum.	1	Alum.	1/4	MIL-R-3065	0.004	16	10	Tangent	0	14
14	Alum.	1	Alum.	1/4	None	NA	16	10	Tangent	0	14
15	Alum.	1	Alum.	1/4	ZZR765	0.1250	16	10	Tangent	0	14
16	Alum.	1	Alum.	1/4	ZZR765	0.0625	16	10	Tangent	0	14
17	Alum.	1	Alum.	1/4	ZZR765	0.004	8	10	Tangent	0	14
18	Alum.	1	Alum.	1/4	ZZR765	0.004	16	20	Tangent	0	14
19	Alum.	1	Alum.	1/4	ZZR765	0.004	16	40	Tangent	0	14
20	Alum.	1	Alum.	1/4	ZZR765	0.004	16	0	Tangent	0	14
21	Alum.	1	Alum.	1/4	ZZR765	0.004	16	10	0 Inches	0	14
22	Alum.	1	Alum.	1/4	ZZR765	0.004	16	10	8 Inches	0	14
23	Alum.	1	Alum.	1/4	ZZR765	0.004	16	10	16 Inches	0	14
24	Alum.	1	Alum.	1/4	ZZR765	0.004	16	20	Tangent	0	14
25	Alum.	1	Alum.	1/4	ZZR765	0.004	16	20	Tangent	Sphere	14
26	Alum.	1	Alum.	1/4	ZZR765	0.004	16	10	Tangent	0	7
27	Alum.	1	Alum.	1/4	ZZR765	0.004	16	10	Tangent	0	28
28	Alum.	1	Alum.	1/4	ZZR765	0.004	16	10	Tangent	0	42
29	Alum.	1	Alum.	1/4	ZZR765	0.004	16	10	Tangent	0	70

TEST PROGRAM

A test program was performed using the fixture configurations shown in Table I. All base plates were 24 inches square. All response plates were 19 inches square. Specimen weights were 12 inches square aluminum plates.

REPEATABILITY

To demonstrate the repeatability of this type testing, test number 9 was repeated four times. The test fixture was dismantled and reassembled between each test.

HORIZONTAL RESPONSE

Horizontal response data was taken for test number 22 to compare the cross axis shock response spectrums to the vertical shock response spectrum.

BASE PLATE MATERIAL

To determine the effect of the base plate material on the shock response spectrum, a phenolic and an aluminum plate were tested. Test numbers 1 and 2 (all test configurations are shown in Table I) represent the configuration during these tests.

BASE PLATE SIZE

The thickness of the base plate was varied from 2 to 1/2 inches to demonstrate the influence of this factor on the shock response spectrum. Test configurations were as shown in test numbers 2, 3, and 4.

RESPONSE PLATE MATERIAL

The effect of the response plate material was investigated by test numbers 5, 6, 7, 8, and 9. The materials studied were masonite, magnesium, aluminum steel and phenolic.

RESPONSE PLATE SIZE

Aluminum plates 1/8, 1/4, 3/8 and 1/2 inch thick were used to study the influence that the size of the response plate had on the shock spectrum. Test numbers 4, 9, 10 and 11 represent the test setups used.

ISOLATION MATERIAL

Three types of isolation rubber were tested to determine the effect each had on the shock response spectrum. These were ZZR-765 Silicone rubber, MIL-R-46089 sponge rubber, and MIL-R-30650 rubber. The isolation joint is shown in Figure 2. Compression of the rubber was approximately 0.004 inch in each test. Tests number 9, 12 and 13 are representative of the configurations involved.

ISOLATOR COMPRESSION

To determine the effect of isolator compression on the shock response spectrum, the preload on ZZR-765 Silicone rubber isolators was increased from 0.004 to 0.125 inch. The rubber was then removed entirely to show the hardmounted condition. The setups shown in tests number 9, 14, 15 and 16 were used to study this parameter.

BASE HEIGHT FROM FLOOR

The normal height was 16 inches. The plate was lowered to 8 inches to determine what effect this parameter had on the spectrum. Refer to tests 9 and 17.

AMOUNT OF EXPLOSIVE

The influence of the amount of explosive was determined by detonating various amounts of charge under the plate. The test was performed using a No. 6 blasting cap to detonate a length of 50 grain per foot PETN Primacord. The charges used were the cap only, cap and 10 inches of cord, cap and 20 inches of cord, and cap with 40 inches of cord. Refer to tests number 9, 18, 19 and 20.

LOCATION OF EXPLOSIVE

The location of the charge was changed from directly against the plate to 8 inches below the plate to 16 inches below the plate (secured to the floor). Configurations were as shown in tests number 21, 22 and 23.

SHAPE OF EXPLOSIVE

This factor was studied by testing various charge configurations. In each case, the ordnance was a No. 6 electric blasting cap and 20 inches of 50 grain/ft Primacord. The cord was shaped in a sphere, a circle and a V. Refer to tests number 18, 24 and 25.

SPECIMEN WEIGHT

The weight of the specimen was varied from 7 to 70 pounds by adding aluminum plates to the specimen mass. The specimen was 12 inches by 12 inches aluminum plates. The 7 pound specimen was a 1/2 inch plate. The 70 pound specimen was 5 inches thick. The other parameters were represented by configurations shown in tests number 26, 27, 28 and 29.

DISCUSSION OF RESULTS

REPEATABILITY

The repeatability of this technique is shown in Figure 5. This area represents the upper and lower bounds from four shocks. The maximum differential was 7 db. This may be reduced by a better designed isolation system. The isolation system used during this testing had no provision to center the bolt in the response plate clearance hole. Consequently, the bolts were able to interfere with the response plate causing an increase in energy to the response plate. It is also recommended that a bottoming type isolator be used to assure repeatable compression.

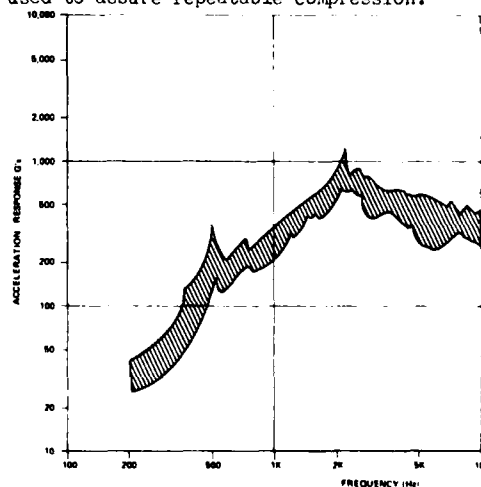


Figure 5 REPEATABILITY

HORIZONTAL RESPONSE

The horizontal response of a typical shock is shown in Figure 6. The horizontal axis response differed up to 11 db from the vertical, but averaged about 6 db lower.

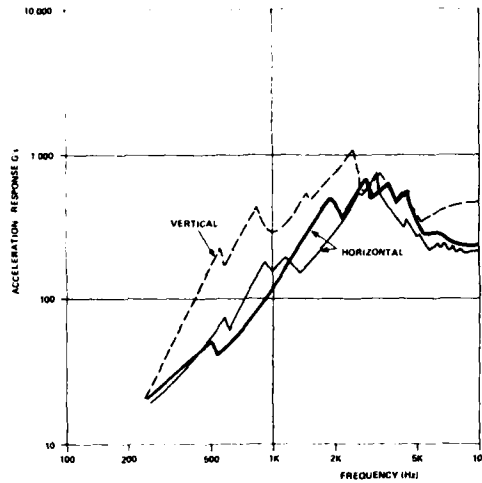


Figure 6. HORIZONTAL RESPONSE

EFFECT OF BASE PLATE MATERIAL

The shock response spectra obtained during the tests on the 1 inch phenolic base plate (test number 1) and the 1 inch aluminum base plate (test 2) are shown in Figure 7. These show that the base plate material had little effect on the resulting shock response spectrum. An aluminum plate is recommended because it resisted the explosion better than the phenolic.

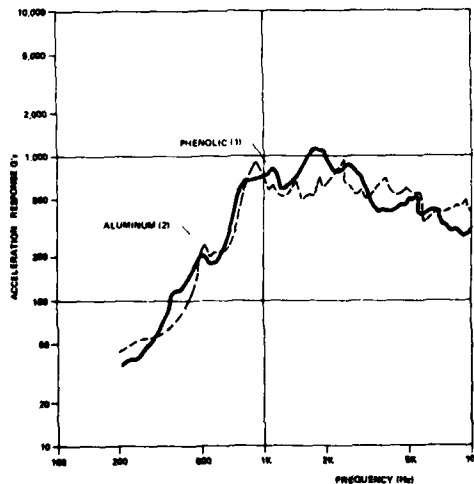


Figure 7. BASE PLATE MATERIAL

EFFECT OF BASE PLATE THICKNESS

Base plate thickness of 2, 1, and 1/2 inches were tested and had little effect on the shock response spectrum. The plots of these spectra are shown in Figure 8. A plate thickness greater than 1 inch is recommended since the bottom of the plate does get severely galled after repeated shocks.

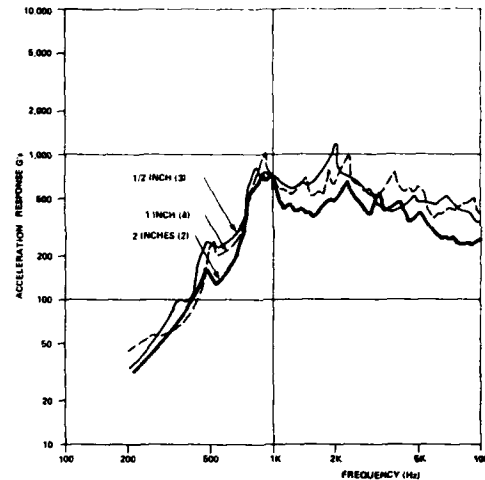


Figure 8. BASE PLATE THICKNESS

EFFECT OF RESPONSE PLATE MATERIAL

Figure 9 shows the spectra obtained from the different response plate materials. This parameter had the greatest influence in the 400 to 2K frequency range. Phenolic and masonite had peaks in the spectrum at a lower frequency than aluminum and steel. This should enable shaping the spectrum in this frequency area.

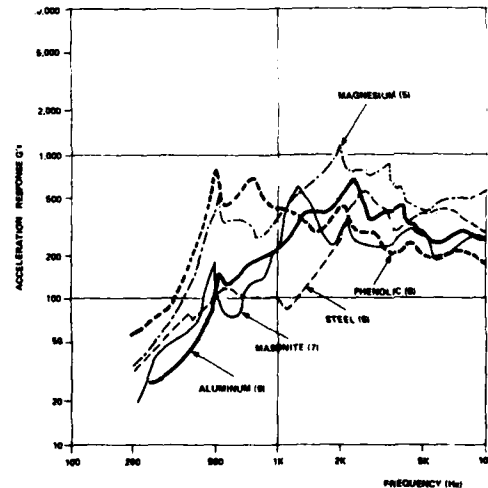


Figure 9. RESPONSE PLATE MATERIAL

EFFECT OF RESPONSE PLATE THICKNESS

The spectra from the testing on response plate thickness of 1/8, 1/4, 3/8 and 1/2 inch are shown in Figure 10. As the thickness increased the spectrum response g's decreased.

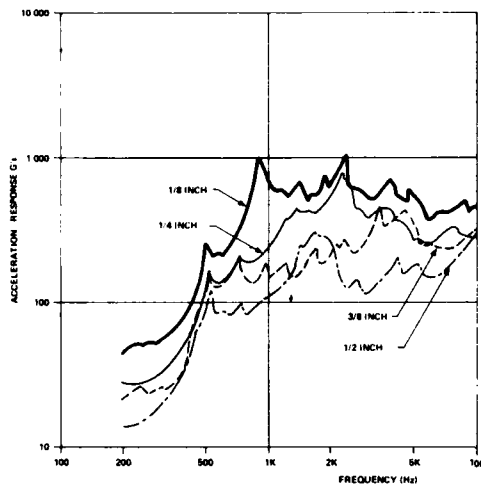


Figure 10. RESPONSE PLATE THICKNESS

EFFECT OF ISOLATOR MATERIAL

The spectra that results from using different types of rubber are shown in Figure 11. As shown, the trend indicates that as the stiffness of the isolation joint increases, the response g's above 1.5K increases. Below 1.5K, the spectra are not influenced. This gave some control over the shaping of the spectrum in the high frequency area. The 1.5K rolloff was only applicable to this test configuration. A different response plate material might change this rolloff point.

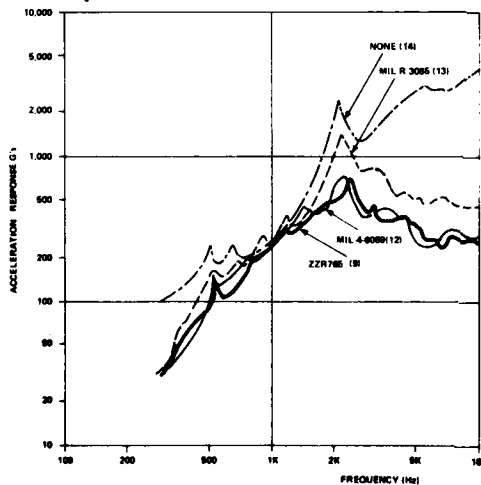


Figure 11. ISOLATOR MATERIAL

EFFECT OF ISOLATOR COMPRESSION

Figure 12 shows the effect that tightening the isolation joint had on the shock spectrum. The tests were performed by first tightening the bolts snug (0.001 inch of compression), one turn (0.0625 inch compression), and two turns (0.1250 inch compression). The rubber washers were ZZR-765 1/8 inch thick and 1 inch in diameter with a 3/8 clearance hole for the bolt. The spectra increased with increased preload with a more pronounced effect in the higher frequencies. This appears somewhat different from that observed by varying isolator material.

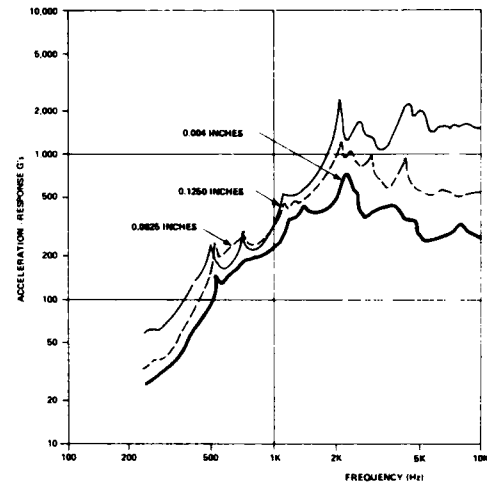


Figure 12. COMPRESSION OF ISOLATOR

EFFECT OF BASE PLATE HEIGHT

The effect of the base plate height above the floor was studied by lowering the plate from 16 inches to 8 inches above the floor. The spectra showed little difference as shown in Figure 13.

EFFECT OF AMOUNT OF EXPLOSIVE

Figure 14 represents the relationship between the amount of charge and the shock response spectrum. As the charge was increased the shock response spectrum increased. This was observed over the entire frequency range, however, the upper frequencies tended to increase more than the lower frequencies.

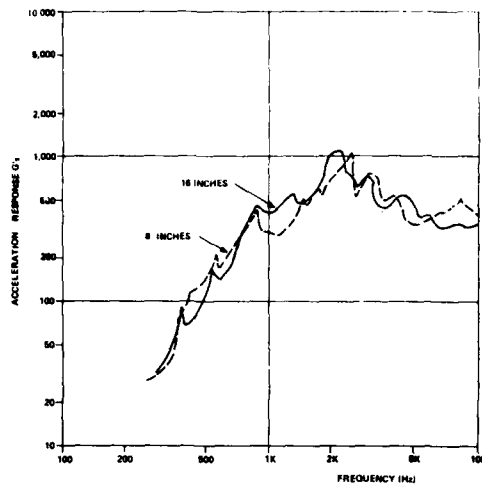


Figure 13. BASE PLATE HEIGHT

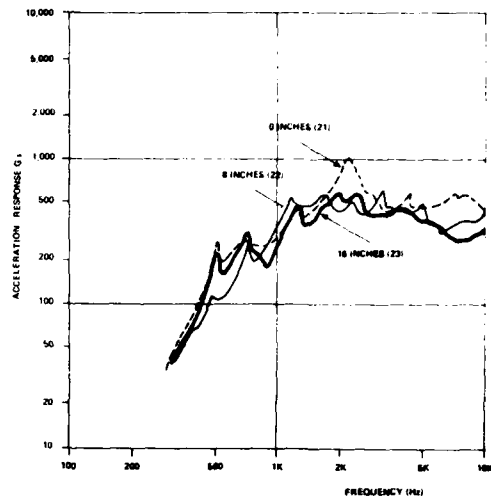


Figure 15. PLACEMENT OF EXPLOSIVE

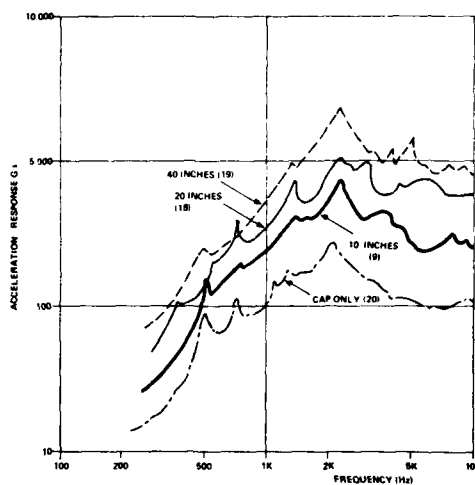


Figure 14. AMOUNT OF EXPLOSIVE

EFFECT OF PLACEMENT OF EXPLOSIVE

The location of the explosive under the plate was varied from directly against the plate to 16 inches below the plate. The influence of this parameter was negligible as can be seen in Figure 15.

EFFECT OF THE SHAPE OF EXPLOSIVE

The shape of the explosive was changed from a tangential 20-inch circumference circle, to two 10-inch concentric circles formed 90 degrees to each other to resemble a sphere, to a V-shaped charge. In all cases the total explosive was 20 inches of Primacord and a detonation cap. The spectrum (Figure 16) showed little variance, however, the V charge did display a greater response above 5K Hz than the other two.

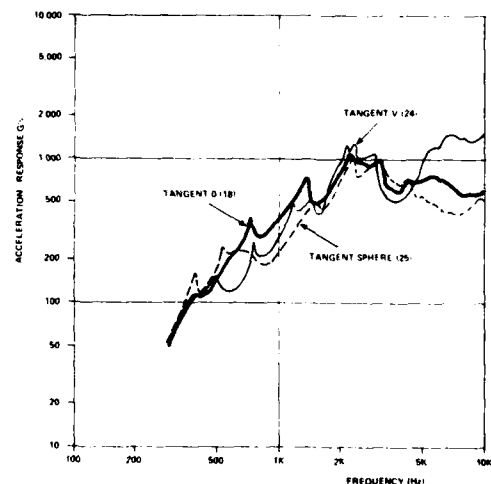


Figure 16. SHAPE OF EXPLOSIVE

EFFECT OF SPECIMEN WEIGHT

The specimen weight was increased from 7 to 70 pounds. However, the spectrums showed no dependence on this variable. Refer to Figure 17.

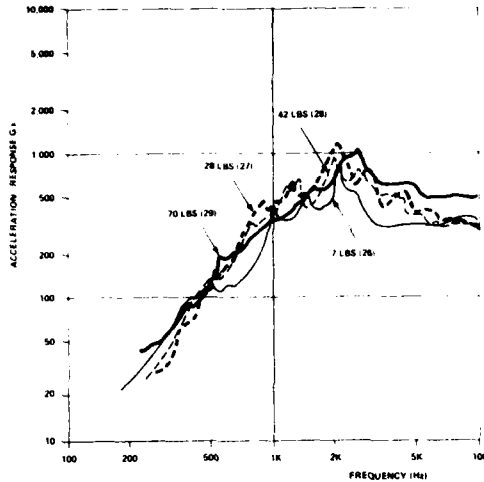


Figure 17. SPECIMEN WEIGHT

SUMMARY

The response plate technique provides an inexpensive, controllable simulated pyrotechnic environment. If this approach is selected, the following relationships will be helpful in the design and modification of a test fixture: the amount of the explosive increased the entire shock response spectrum; increasing the isolation joint stiffness increased the shock response spectrum above 1500 Hz but had little effect on the spectrum below 1500 Hz; the material of the response plate altered the entire shape of the shock response spectrum; and as the thickness of the response plate increased, the shock response spectrum decreased. These parameters offer some control for shaping the shock response spectrum to a given specification. The base plate material, base plate thickness, specimen weight, height of the fixture, shape of the explosive and placement of the explosive had no appreciable effect on the shock response spectrum for the test configurations used during this study.

DISCUSSION

Mr. Galef (TRW Systems): I am sure you must have spent some time thinking about the reasons why we had so little effect from, for example, the explosive being right in contact as opposed to being sixteen inches away. Why there was so little effect from the weight of the specimen? I would very much like to have the benefit of your thoughts.

Mr. Thomas: The system is excited by a pressure wave generated by the explosive and the closer to the explosive the greater is the pressure, but the area is less. So, given the area the input should be the same. The overall effect on the displacement of the base plate would be the same in all instances.

Mr. Galef: Do you think the difference in coupling through the air and through solids is trivial in comparison to that? It is a little bit hard to accept.

Mr. Thomas: When we put the explosive directly against the base plate, we did see higher response in the high frequency area of the shock spectrum. We did see an increase, but it was slight.

Mr. Koen (Bell Telephone): What kind of sampling rate did you use in the response spectra? Were they undamped?

Mr. Thomas: We used an analog shock spectrum analyzer.

Mr. Koen: I might suggest then that in the undamped spectra I've seen I would expect that your system would have a very low sampling rate. I believe you need to get up in the 10 KHz region, something like a sampling rate of 80 KHz. I've seen spectra from similar kinds of tests, and they were extremely jagged on an undamped basis in the high frequency end.

Mr. Thomas: We analyzed at a Q of 10.

Mr. Certel (Kinetic Systems): I am a little curious about the use of an explosive as opposed to striking the base plate with a ballistic impact. Is there any particular advantage to using an explosive over just a plain bang on the bottom of the anvil?

Mr. Thomas: During preliminary calibration of the fixture, we used this technique to test the isolator compression. We dropped the ball on it and monitored the shock response on the response plate when the ball was dropped on the base plate. You may put more into one corner than the other. The explosive was there and we were using this technique on one of the projects in-house, so we just employed this for one of the other contracts.

Mr. Certel: Did you try computing shock spectra for the simple mechanical impact by any chance?

Mr. Thomas: No. I did a little work on this when I first started out, but I went over to the explosive.

Mr. Powers (McDonnell-Douglas): What type of transducers did you use?

Mr. Thomas: I used an Endevco 2225 and an Endevco 2730 charge amplifier.

TEST METHOD TO QUALIFY
ELECTRONIC COMPONENTS IN
SHOCK AND SUSTAINED ACCELERATIONS

R. K. Melzer
Sperry Univac DSD
St. Paul, Minnesota

A unique method has been developed in holding electronic components properly in a test fixture for shock and centrifuge qualification testing. The components are frozen into a fixture block. This method gives the highest degree of undisturbed energy transmission into each test specimen without discrimination of physical tolerances of the components, location in the fixture, or fixture elasticity. A special shock machine was developed for these tests to provide the necessary undercooled test equipment, which is also explained. Centrifuges are operating undercooled to control the bearings and are just ideal for this application.

INTRODUCTION

The environmental qualification of electronic components is one of the first steps in the way of designing, manufacturing, and testing electronic equipment from the component and the raw material level to a reliable operating unit. The end product will show better cost savings and fewer rejects in the course of development and manufacturing if the testing was carefully performed on the electronic components.

The stress levels and test procedures for DIODES, TRANSISTORS, RESISTORS, and INTEGRATED CIRCUITS are contained in the following military specifications:

MIL-S-19500	GENERAL SPECIFICATION FOR SEMICONDUCTOR DEVICES
MIL-STD-750	TEST METHODS FOR SEMICONDUCTOR DEVICES
MIL-STD-883	TEST METHODS AND PROCEDURES FOR MICROELECTRONICS

One significant problem in qualifying these components in the mechanical environments of shock and sustained acceleration is the transmissibility of the acceleration and stress levels from the test machine to the specimens. The outputs of the shock machine can be monitored by accelerometers, but the component itself is too small to allow the monitoring of its response by accelerometers without changing its dynamic parameters. Here we depend on the perfect solid mounting of the components to the test fixture and we assume that the component gets what the machine gives, or in other words, a 100% transmissibility.

It is well known that the oldest method of clamping the components to a fixture plate is imperfect as soon as more than three components are used. For economical and time schedule reasons and the great number of components to be tested, it is, however, desirable to test more than three items during one test run. The clamping method results in a statically indeterminate system. Uniform clamping to give each component the same transmissibility cannot be accomplished because of variation in the physical dimensions (tolerances) of the components. The use of elastic clamping adapters has been applied to cover these dimensional differences. These adapters had to have low stiffness properties (rubber) to avoid damage of the components, and created additional resonance problems.

Paraffin, wax, and epoxy have been used to mold the components into fixtures. Paraffin and wax are very soft and do not adequately transmit shock pulses, but the molding and recovery of the parts is simple. Epoxy molding is better than paraffin or wax in view of the pulse transmissibility (see Figure 1); however, the curing and recovery of the parts into and out of the fixture is a time consuming operation.

UNIVAC DSD recommended, investigated, and uses ice for the embedding medium of the components, and has proven its feasibility.

THE PULSE TRANSMISSIBILITY OF ICE

A number of studies and tests have been performed to obtain knowledge of the transmissibility of pulse forces through ice. A qualitative mean (not the chemistry interpretation) for the dynamic properties of elastic solid materials in propagating induced shock waves is the velocity of sound. The velocity of

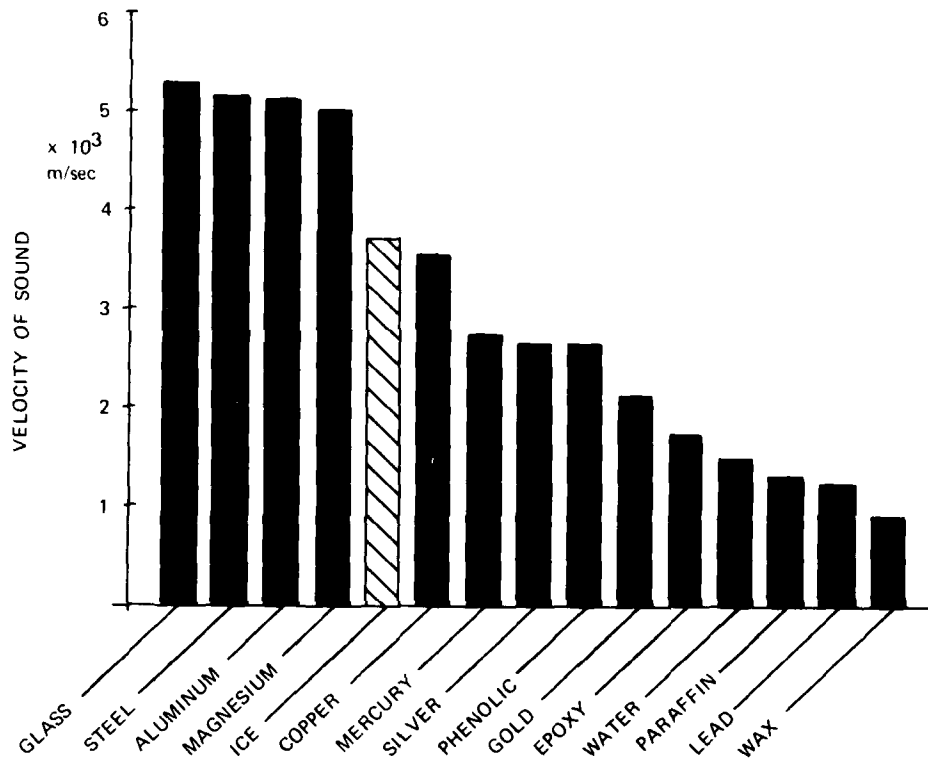


Figure 1. Spectrum of Velocity of Sound For Different Materials

sound for these materials can be determined from the expression

$$c = \sqrt{E/\rho} \quad \text{m/sec}$$

where E is the modulus of elasticity and ρ is the specific mass of the material. Figure 1 shows a comparison of these values for the most relevant materials as given in Ref. [1]. The data for ice was found in Ref. [2]. It can be seen that ice has a wave propagation in value just below that of metals and is far above that of epoxy, wax, or paraffin.

Further knowledge of the shock transmissibility of ice was gained by shock tests with accelerometers, one attached to an aluminum block, the other attached to the ice, frozen into a cavity of the same block. The tests were run on a JAN-S-44 shock machine at different drop heights. Two ENDEVCO 2213 accelerometers with identical calibration data, two amplifiers, and two filters of the same make and the same cut-off settings were used. The pulse responses were recorded on a dual trace memoscope. A diagram of the test setup is given in Figure 2.

Three typical pulse records from these tests are given in Figure 3. They represent the response of three different

shock levels for a 1.0 M.S. pulse duration. The filter cut-off was set at 2,500 Hz for a ratio of 5:1 to the pulse frequency. The ice in the aluminum block was changed between the record of 3b and 3c to check the effect of two different freezing setups. The similarity of the two response curves, that of aluminum and that of ice in the records, is remarkable. The ice has the tendency of higher damping property than aluminum. The transmissibility of ice from these and other tests can be derived to be 96% of that of aluminum. The ice column did not shatter or granulate under the inertial forces of the transducer mass, which were considerably higher and attached to a smaller contact area than that of an imbedded component.

HOW TO FREEZE COMPONENTS INTO A FIXTURE

An aluminum fixture-block of 2 inches cube for quick change of test axes was prepared with holes to fit the size of the components. Several of these components were placed into these holes, then filled with tap water and placed in a refrigerator for freezing (Figures 4, 5, and 6). Notable in Figure 6 are the ice domes on top of the cavities that indicate the expansion of ice during the crystallization. These domes are shaved flush to the surface of the aluminum block to provide a flat surface of any side when installed in the shock machine (Figure 13). Figure 7 shows the insertion of a big dual in-line flatpack into the shock block in the bigger holes. The

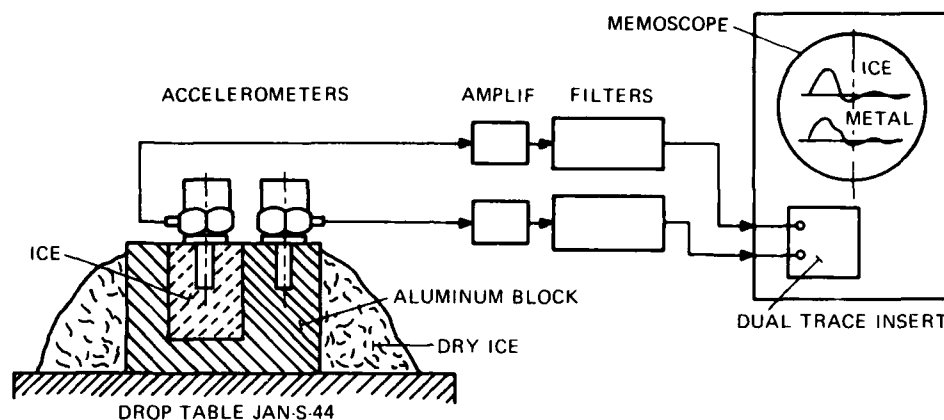


Figure 2. Test Setup to Measure the Shock Transmissibility of Ice

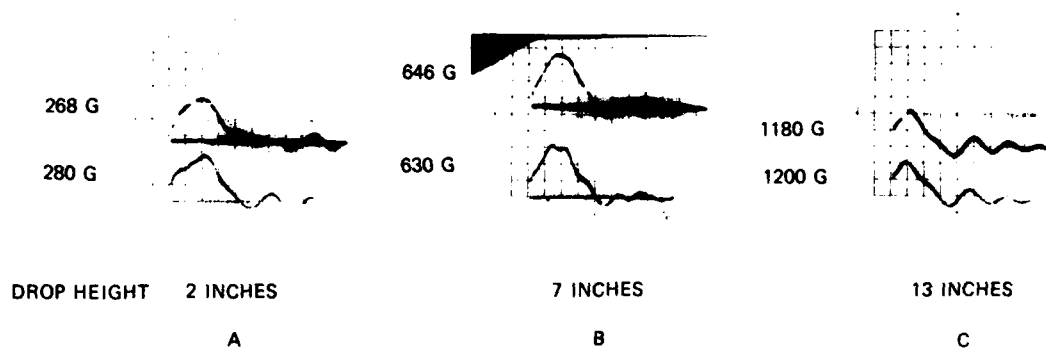


Figure 3. Pulse Records

complicated multiple prong-type shape of the flatpack reveals particularly the simplicity of this holding method by simply inserting the component in water and using the natural transform of water to ice to give a hundred percent clamping condition. This freezing program was first performed at low temperatures of -40 to -60°C in an unspecified manner, with regard to the freezing temperature. The emphasis was directed to a short freezing time for economical reasons. Compact components like resistors did not show any damage to the body, but components with membrane-type covers like transistors and flatpacks often suffered dented covers, see Figure 8. The dents in the covers were so deep that the components suffered electrical shorts. The freezing process of water produces a pressure buildup when changing from the fluid to the solid medium. To make the process of mounting components by freezing successful, it was necessary to obtain additional information in regard to the extent and the cause of the damaging pressure buildup. A study of this phenomenon was conducted to explore the functions of freezing temperature and the freezing on the components.

The following stepwise studies were initiated to investigate the problem:

1. Perform a literature study,
2. Freeze a large number of transistors randomly located in the hole of the block to get statistical data,
3. Freeze several transistors fitted with a strain gauge on the flat top of the cover to get comparable pressure data,
4. Freeze a specially developed and calibrated pressure transducer to get data of the ice pressure in three mutually perpendicular axes.

The literature study revealed that an enormous amount of work has been performed over the years on the properties of ice. Practically all physical and technical characteristics above and far below the freezing point are available. Relevant



Figure 4. Insertion of Components in the Shock Block



Figure 6. The Shock Block After Freezing



Figure 5. Filling the Shock Block With Tap Water

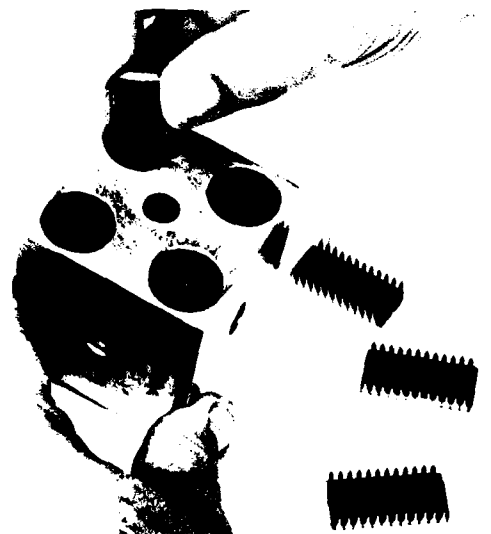


Figure 7. Insertion of Big Dual In-Line Flatpacks

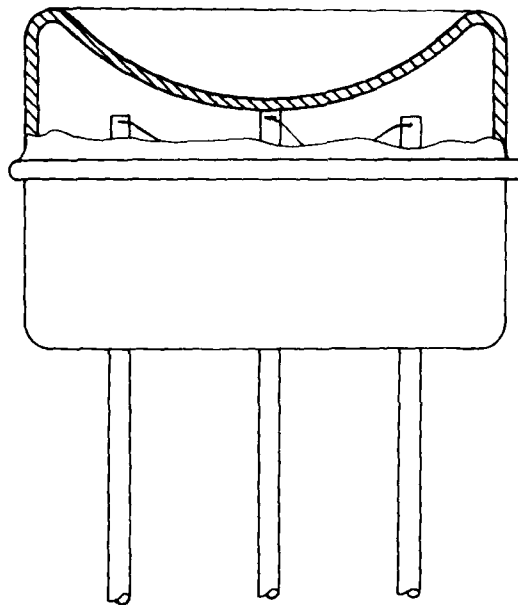
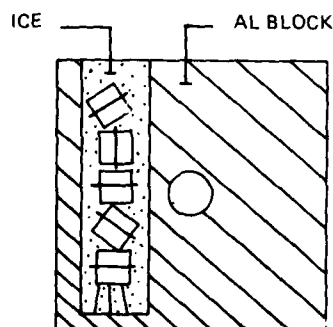


Figure 8. Damaged Transistor

information of the pressure buildup at 0°C and close to it is missing. This information, however, appeared important because it is not desirable to work in the medium or low temperatures with all their possible damage potentials while holding the components in ice. Only the volume increase of 9% at the transition from water to ice at 0°C is given in Ref. [3].

The first experimental study was done with a large number of rejected TO-5 transistors, frozen in the test blocks. Two different ambient temperatures were used. The test setup and results are given in Figure 9. The conclusion from this investigation was that the lower ambient freezing temperature caused the greater internal pressure.

During the second experimental study we placed a strain gauge on the top of a TO-5 transistor and a thermocouple on the strain gauge wires. The strain gauge was not calibrated in terms of pressure during these tests. The strain results are therefore proportional to pressure, and evaluated to compare the pressure on a percent basis between the different freezing rates. The top limit of 100% for the ordinate pressure scale in Figure 10 was selected for the maximum strain, measured during this test series at -42°C ambient freezing temperature. When the transistor was frozen into the block which is used for shock tests, the response of the strain gauge and the thermocouple were recorded. Tests were run using four different ambient temperatures, -9°C , -25°C , -33°C , and -42°C , which gave four different freezing rates. The ambient temper-



AMBIENT TEMPERATURE	-25°C	-90°C
EXPOSURE TIME	2 HOURS	2 HOURS
NUMBER OF TRANSISTORS	373	204
NUMBER OF FAILURES	0	24
PERCENT FAILURE	0%	11.8%

Figure 9. Freezing Test of TO-5 Transistors With Random Location

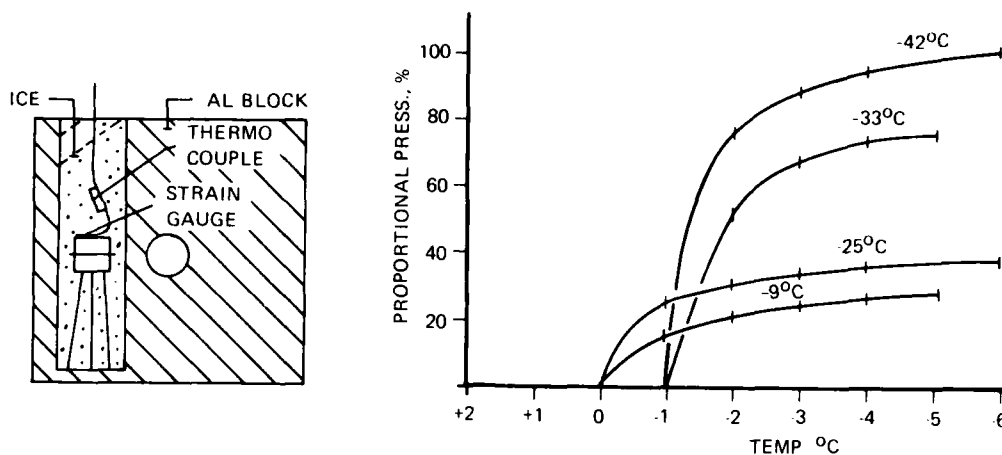


Figure 10. Freezing Test of TO-5 Transistor With Strain Gauge and Thermocouple

atures in the freezer were held within $\pm 3^\circ\text{C}$ and the freezing time ranged from 72 minutes at -9°C to 20 minutes at -42°C . Figure 10 shows a sketch of the test setup and a summary of the test results. It is apparent from the curves that there is a sudden and relatively large increase in pressure when the ice is forming in the range from 0°C to -4°C where ice approaches its biggest density. The severity of this increase is determined by the freezing rate, which depends on the ambient temperature. The tests with the higher freezing rate, -33°C and -42°C , started to build up pressure at -1°C . This occurrence was not further investigated, but can have two explanations. First, the higher freezing rate can be unstable at the freezing temperature. Second, the buildup of ice crystals is initiated by impurities in the water. Chemically clean water was undercooled in a test to a temperature of -72°C before ice crystals were formed, Ref. [4]. Since the same tap water was used for all these tests, it also can be a combination of both explanations.

The conclusion that can be drawn from these tests is that the least internal pressure occurs with the slowest freezing rate and the highest practical ambient freezing temperature.

We arrived at a point in the study of the ice potting where the knowledge of the actual pressure expressed in psi was desirable. From a theoretical analysis the TO-5 transistor cap would plastically deform around 75 psi. The actual pressure must be held reasonably below that level. Since the freezing cavities are of a side ratio greater than 1.0, determined by the length over the diameter, the pressure data in these two directions was necessary to know. A pressure transducer was designed, made of an aluminum block, 0.5 inches cube, with diaphragms on three mutually perpendicular sides of the block. The elastic deformations of the diaphragms under external pressure were monitored with strain-gauges attached to the center of the diaphragms on the inside of the hollow block. This transducer was calibrated in a device designed for calibrating of hydraulic gauges so that the strain data received during the freezing process could be converted into pressure data. The test setup is demonstrated in Figure 11. The size of the block was made as small as seemed to be practical. Its size

and the dimensions of the hole for freezing were made proportional to that of the TO-5 transistor conditions.

The first series of tests, starting with a short freezing time, was performed, of which the results are given in Figure 11. These tests were not further explored because actual freezing and testing of components with a low freezing rate at less than 10°C ambient temperatures and 60 to 120 minutes freezing time did not produce any failures. The results of Figure 11, however, indicate a noticeable difference of the pressure buildup in the transverse and axial direction. This information was used for the orientation of components with pressure sensitive planes.

Ice has a positive coefficient of thermal expansion which indicates that the ice tends to contract with a decrease in temperature. Therefore, storing of test blocks with frozen components at a lower ambient temperature than that used to freeze the components in the block will cause an increase of the internal pressure. This effect is further promoted by the aluminum block which contracts at a rate almost 10 times that of ice. Therefore, storage of frozen blocks, until the time of testing, must be kept at the same ambient temperature as the freezing temperature.

RESULTS OF THE FREEZING STUDIES

The results of the freezing studies to embed electronic components in ice for shock and sustained acceleration tests revealed that this method is better than potting methods of other embedding materials. It surpasses any clamping fixture and showed better pulse transmissibilities, is simpler in handling, and permits faster test procedures. An internal UNIVAC freezing procedure was accomplished that concentrates to hold the ambient freezing temperature between -4°C and -10°C and to hold the freezing time between 60 and 120 minutes, depending upon the size of the cavity. A comparison of available data of this method with the epoxy potting is given in Figure 12.

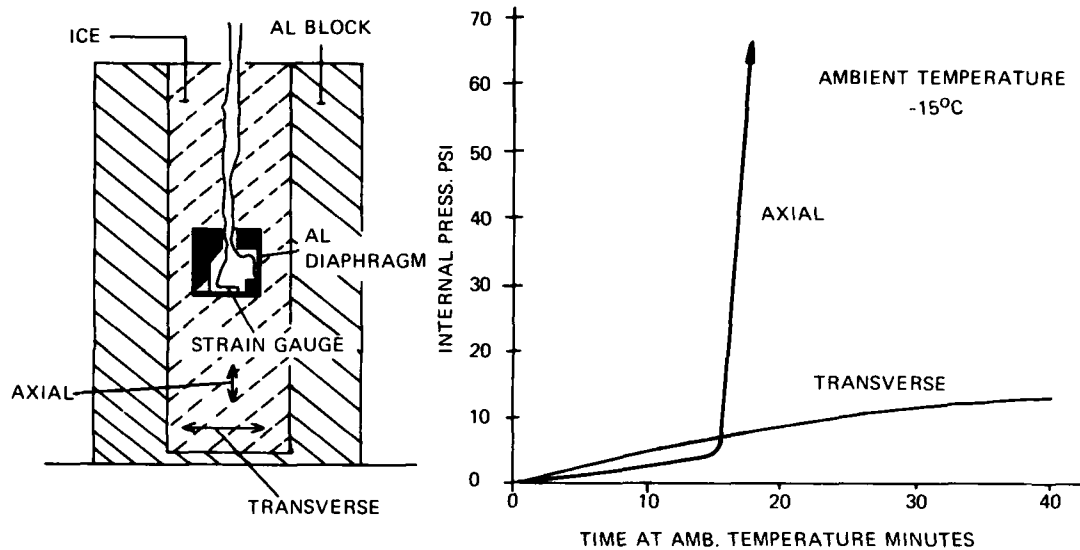


Figure 11. Freezing Test of a Pressure Transducer

<u>ICE TEST</u>		<u>EPOXY TEST</u>	
FREEZING	60 MIN.	CURING	360 MIN.
TESTING 3 AXES	5 MIN.	TESTING 3 AXES	5 MIN.
THAWING	5 MIN.	DISSOLVING	2160 MIN.
TOTAL TIME	70 MIN.		2525 MIN.
TIME RATIO	1		~ 36
SHOCK TRANSMISSIBILITY	96 TO 100%		
FREEZING TEMPERATURE	-4°C TO -10°C		
FREEZING TIME	≅ 60 TO 120 MIN.		
STORAGE TEMPERATURE OF FROZEN BLOCKS	-4°C TO -10°C		

Figure 12. Processing Data of Two Potting Methods

Hermetic seal tests with different types of components have been performed before and after the shock and centrifuge tests for which the components were frozen into the fixture blocks within the limits of the established processing specification. No seal break or lower degradation of the checked components could be determined.

THE SHOCK TEST MACHINE

Shock testing to be done with the undercooled component and fixture-block on the conventional type of shock machines was impractical. The machine had to be undercooled from the room ambient temperature to at least the temperature level of the components to avoid melting of the ice and loosening of the components in the fixture. A temperature chamber for the whole machine would be uneconomical and a chamber for the test anvil only would have to be shock proof with all the design complications.

A very compact shock machine was designed (Figures 13, 14, and 15). The free fall of the anvil table was reduced to a 2-inch height and the necessary potential energy to provide the required end or contact velocity was stored in a prestressed coil spring. This principle is not new and has been applied in different forms of potential energy storing by commercially available shock machines on the market. The anvil table is carrying the 2-inch cube aluminum block into which the components are frozen (Figure 14). The cube shape of the fixture-block was selected for quick change of the specified three mutually perpendicular test axes. The contact material for the anvil table on the base is a 0.25-inch thick and 3.0-inch diameter pad of die-rubber of 67 to 68

durometer hardness. The basic design provides a spring for a 1,500 G acceleration level. The rubber pad was experimentally determined to give a 0.0005 second time duration. The same spring compressed to a higher prestress level by changing a compression block on top of the machine (Figure 13) provides a 3,000 G acceleration level. The time duration of this pulse was measured at 0.0002 seconds by using the same rubber pad. Pulses that have been measured with this machine are given in Figure 16. These graphs represent (A) the basic pulse, (B) a check of the acceleration of the anvil when the spring is released, and (C) the repeatability of the pulse. The filter cut-off frequency was set at 7,500 Hz at a ratio of 7.5 to 1.0 to the pulse frequency. Of particular interest was to prove the anvil acceleration effect when released from the cams. The records are running from right to left. No acceleration can really be detected. A theoretical figure is in the magnitude of 50 G or 3.3% of the maximum pulse acceleration.

The motion of the anvil is controlled by two cams which are driven by an electric motor and a reduction gear. The running speed of the system is adjusted to one shock per second and can be set for a selected number of blows, depending on the specification of the component to be tested (Figure 13).

The shock tester itself is held at an operational temperature of -15°C . This is achieved with a refrigeration unit of 0.33 HP capacity. The layout of the cooling unit and the insulation container housing the shock machine are given in Figures 13 and 15.

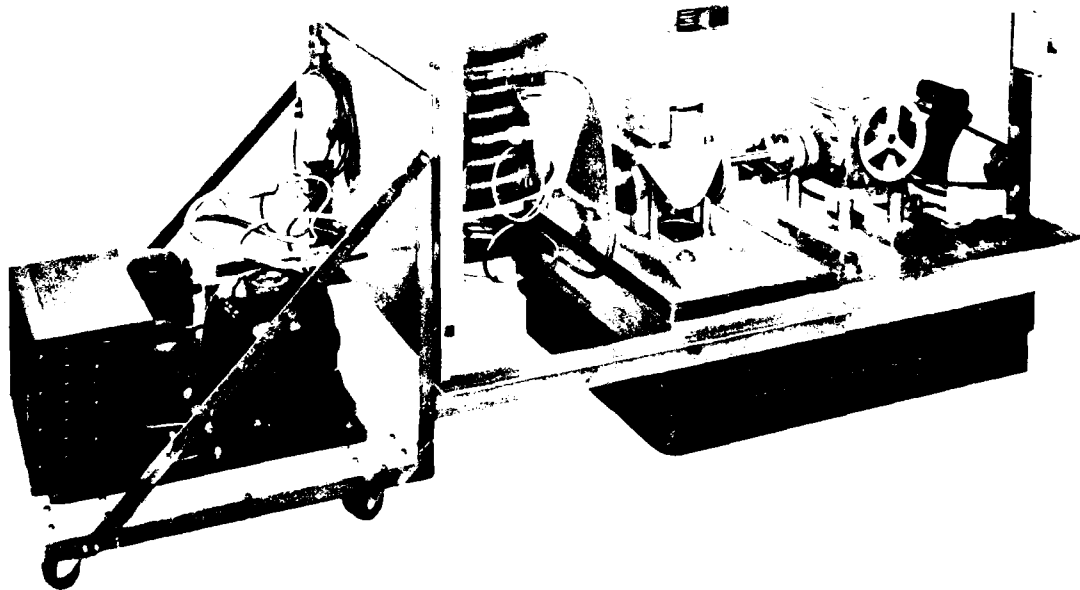


Figure 13. Shock Machine Assembly

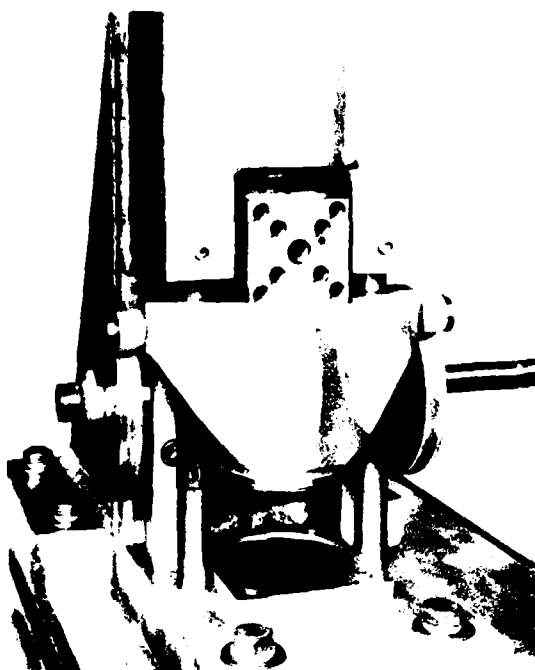


Figure 14. Shock Machine Detail

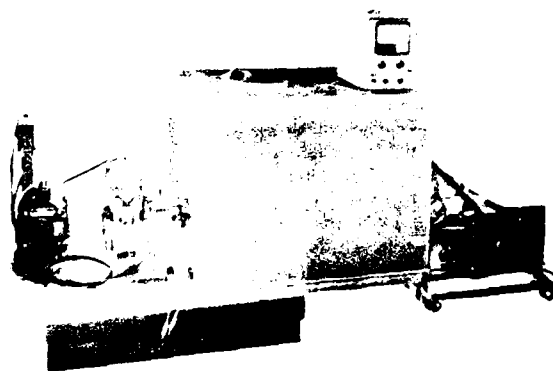


Figure 15. Shock Machine With Thermal Insulation Cover

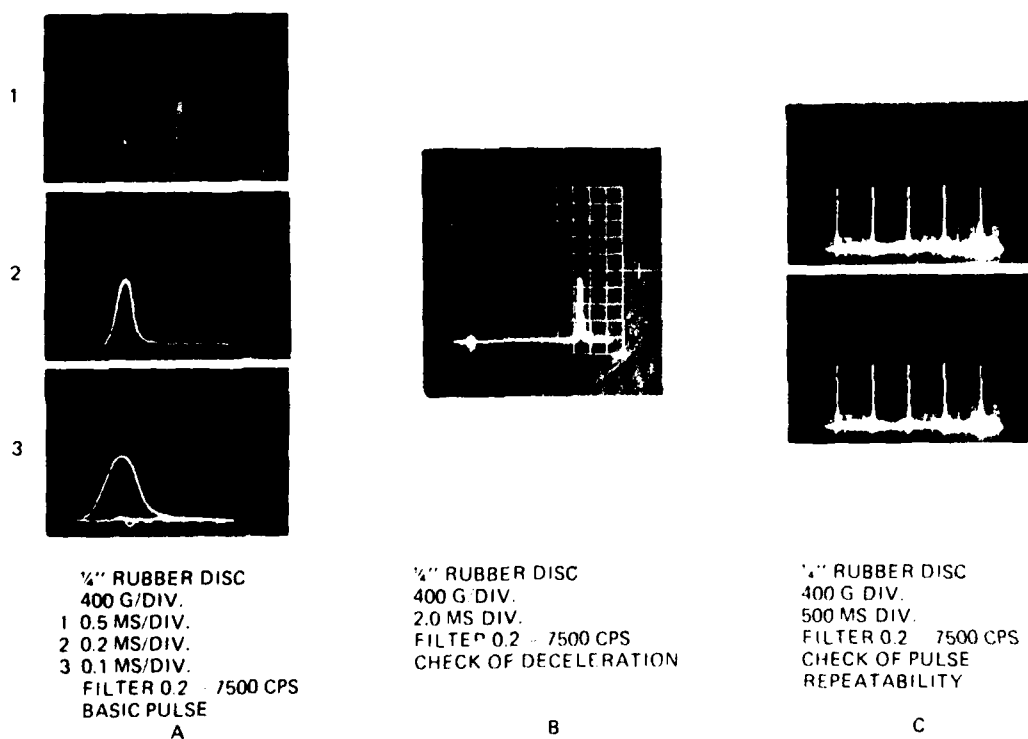


Figure 16. Pulse Records of the Shock Machine

THE SUSTAINED ACCELERATION TESTING

The use of the ice potting method for testing electronic components requires a test machine to be operated in an undercooled temperature field. Centrifuges that are used to load parts up to 50,000 G are running with shaft and bearing velocities of 25,000 RPM. This requires special care of cooling the bearings which is achieved with a refrigeration system that holds the shaft bearings and wheel at -15°C . These properties of the centrifuge were just predestined to use the ice potting method for sustained acceleration testing.

Univac uses a centrifuge for these tests made by the International Equipment Company (Figure 17). Test heads were designed in cooperation with the manufacturer that permit the components to be frozen in. The heads carry ring-type inserts with cutouts at the periphery which house aluminum blocks $1.0 \times 1.0 \times 1.75$ inches with a cavity 0.75 inches in diameter to hold the components. Two-way oriented cutouts are applied to permit testing of the components in all specified directions (Figure 18). The fixture-blocks in Figure 18 are oriented in different directions to demonstrate the

variety. During actual test they have a uniform orientation to test in one particular direction. The insertion of a flatpack is demonstrated in Figure 19. Care is taken to place the components in the center of the cavity to hold a uniform radius and a constant G-level during the test. The parts are frozen in the block by the same procedure as the parts are frozen in the shock blocks. A low as possible freezing rate is applied with an ambient temperature between -4°C to -10°C over a period of 60 to 120 minutes. No failures or crushed parts have been encountered.

Sustained acceleration tests with electronic components have been performed at 20,000 G, 30,000 G, and 40,000 G with no problems or deteriorating effects on the ice. When the 50,000 G level is exceeded the ice begins to granulate and the component begins to loosen. This phenomenon of ice under extremely high sustained acceleration has not been investigated to understand this behavior in nature or to give explanatory data. The mechanical limit of using ice to hold electronic components for this type of test can be set at 40,000 G.

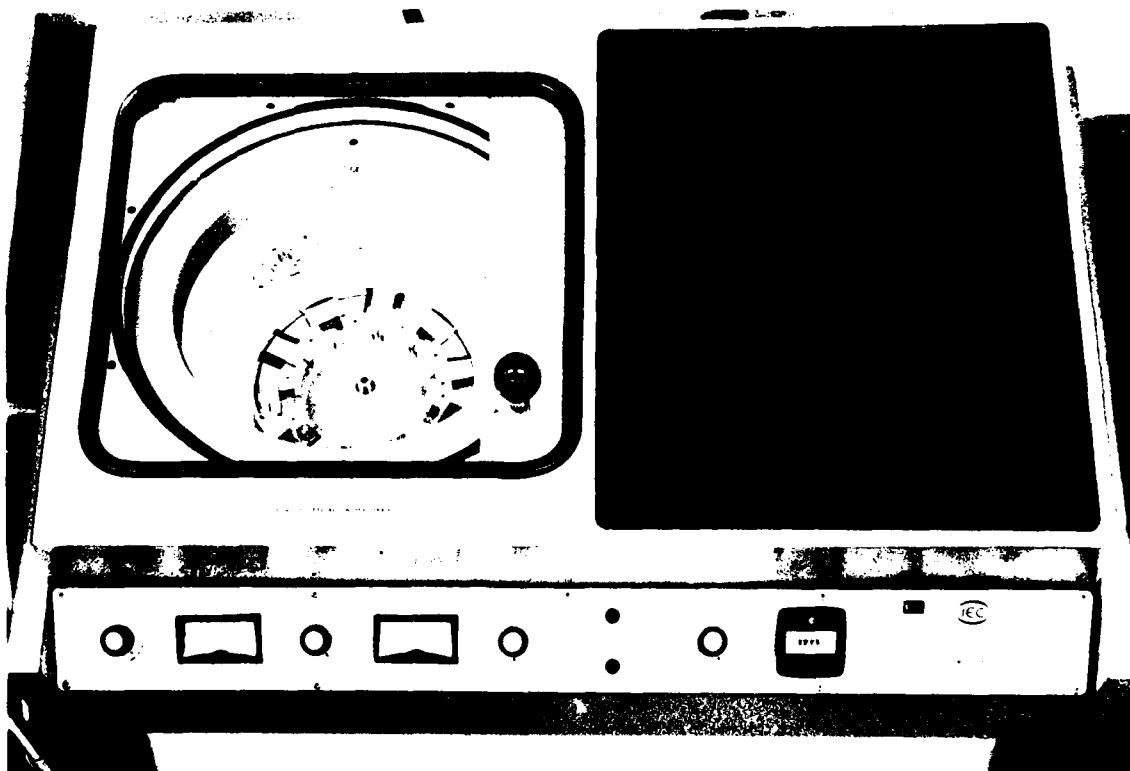


Figure 17. Centrifuge



Figure 18. Centrifuge Head With Insert Ring and Component Housing Blocks



Figure 19. Insertion of Flatpacks Into the Centrifuge Block

CONCLUSION

This paper describes the development of a method to freeze electronic components into a fixture-block for shock and sustained acceleration testing, and leads to draw the following conclusions:

1. The transmissibility of shock pulses through ice is 96% that of structural metals.
2. The freezing process must be controlled and the freezing rate kept as low as possible to avoid critical pressure buildup. This can be achieved with an ambient freezing temperature between -4°C and -10°C .
3. The method is simpler, more reliable, and more economical than those of clamping fixtures or other potting materials.
4. The method is restricted to environmental tests for which the test equipment can be undercooled during the tests within reasonable costs.

REFERENCES

1. Charles D. Hodgman, M.S., Robert C. Weast, Ph.D.,

Samual M. Selby, Ph.D., Handbook of Chemistry and Physics, pp. 2317-2318. Chemical Rubber Publishing Co., Cleveland, Ohio, 1956.

2. N. E. Dorsey, Properties of Ordinary Water Substance, pp. 460-461. Reinhold Publication Corp., New York 1940.
3. K. F. Voitkowski, "The Mechanical Properties of Ice," A.D. Rept. 284777, 1960, Translated from Russian by the American Meteorological Society, Boston, Mass.
4. W. Rau, "Molecular Structure of Deeply Super-Cooled Water," Nature, Weekly Journal of Science, Vol. 157, No. 3983, pp. 267, March 1946.

ACKNOWLEDGEMENTS

The author wishes to acknowledge the funding of this work by the engineering management of Univac DSD and the cooperation of R. R. RUEGEMER, A. M. NESS who performed most of the development work, and D. D. JOHNSON who is using this method successfully for Univac Products. The support and encouragement by the Univac patent department, which obtained a patent for this method (No. 3,194,052), is appreciated.

THE USE OF SILAKER-OPTIMIZED PERIODIC TRANSIENTS IN MATCHING FIELD SHOCK SPECTRA*

D. O. Smallwood
Sandia Laboratories
Albuquerque, New Mexico 87115

and

A. F. Witte
Kaman Sciences Corporation
Colorado Springs, Colorado 80907

Present methods of matching field shock spectra in the laboratory are often inadequate. Classical pulses produced on conventional shock machines often result in poor synthesis of field shock spectra at either the high-frequency or low-frequency end of the spectrum or both. The match of shock spectra is usually very limited in frequency range.

A technique has been developed and is described in this report which utilizes decaying periodics produced on vibration exciters to match shock spectra over a very wide frequency range. These periodics, consisting of decaying cosines superimposed on a cosine bell, are well suited to reproduction on both electrodynamic and electrohydraulic exciters. The acceleration, velocity, and displacement characteristics of these transients meet limitations imposed by the physical capabilities of vibration exciters.

The method of synthesizing shock spectra consists of adding several cosine transients having frequencies, decay rates, and amplitudes necessary to produce a composite shock spectrum closely matching the field shock spectrum. The mechanics of determining frequencies, decay rates, and amplitudes is simple since the spectra for individual decaying cosine components add in the frequency domain.

Digital techniques can be used to synthesize the transients and to provide properly conditioned input signals for accurate real time control and reproduction of these transients on vibration exciters.

NOMENCLATURE

$\ddot{x}(t)$ acceleration at any time

A peak value of acceleration in the time domain

$\dot{x}(t)$ velocity at any time

$x(t)$ displacement at any time

τ duration of a shock pulse or transient (sec)

ζ decay rate

ω circular frequency (rad/sec)

ω_n circular natural frequency (rad/sec)

t time

i $\sqrt{-1}$ or an integer subscript

B a constant

*This work was supported by the U. S. Atomic Energy Commission.

INTRODUCTION

The work described in this paper was initiated primarily for the purpose of developing a technique for producing transient vibrations on low-frequency electrohydraulic exciters. However, the resulting technique is one which is suitable for use on both electrohydraulic and electrodynamic exciters. The technique utilizes summed decaying periodics which have been optimized for exciter operation to match shock spectra over wide frequency ranges, and is philosophically similar to the technique developed by Yang and Saffell [1].

The normal procedure for matching (enveloping) shock spectra of field transients or an ensemble of field transients is to use shock spectra of "classical" pulses (half-sine, terminal peak sawtooth, haversine, etc.). These classical pulses are then produced on conventional shock machines. This generally results in a good match of field shock spectra over a very limited frequency range and severe overtests and/or undertests over the rest of the frequency range of interest.

A specific physical example will illustrate this point. The example is that of a boxcar rail hump. The time history of a typical event is shown in Fig. 1. The shock spectrum* of this event is shown as Curve c on Fig. 2. The average and maximum composite shock spectra for many similar events are shown as Curves a and b, Fig. 2. Two half-sine pulses are included as Curves d and e. As can be seen, a low-level, long-duration half-sine (Curve e) closely matches the composite spectrum below 50 Hz but is a serious undertest at the higher frequencies. The higher level, short duration half-sine (Curve d) will cover the higher frequencies but overtest the low frequencies. Clearly, the ratio of high-frequency energy to low frequency energy is larger for the field data than a half-sine.

This is only one example of many field records which indicate oscillatory transient vibrations which are poorly simulated by classical waveforms. Examination of flight shock data also results in the indication of poor simulation.

Vibration exciters (electrodynamic and electrohydraulic) provide a versatile means of producing transient vibrations or shock pulses

*All shock spectra reported in this report are for a 3 percent damped single degree of freedom system unless stated otherwise.

as long as the acceleration, velocity, and displacement requirements meet the physical limitations of the exciters. Because of these limitations, vibration exciters are poorly suited to reproduction of classical pulses as will be explained in the next section. However, they are well suited for the reproduction of oscillatory type transients.

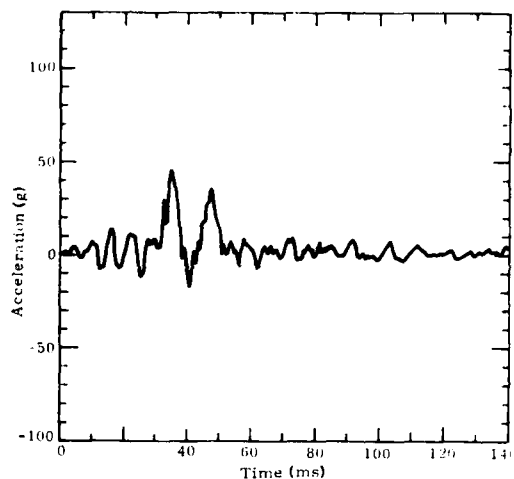


Fig. 1 - Standard boxcar rail hump time history

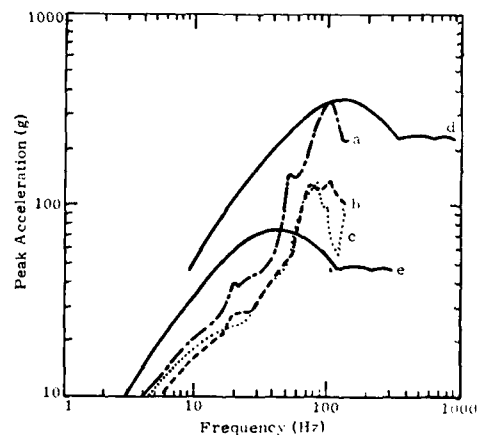


Fig. 2 - Standard boxcar rail hump shock spectra
a - maximum standard boxcar composite;
b - average standard boxcar composite;
c - a single standard boxcar event time history
d - 200-g, -6-msec half-sine
e - 43-g, 20-msec half-sine

VIBRATION EXCITER LIMITATIONS

The types of transient vibration or shock pulses which can be accurately reproduced on both electrodynamic and electrohydraulic exciters are very much dependent on the physical limitations of the exciters. These limitations are listed in Table 1 and are briefly discussed here.

TABLE 1
Exciter Limitations

Limitation No.	Initial	Final	Maximum
1	$\ddot{x}(0) = 0$	$\ddot{x}(\tau) = 0$	Limited
2	$\dot{x}(0) = 0$	$\dot{x}(\tau) = 0$	Limited
3	$x(0) = 0$	$x(\tau) = 0$ (Electrodynamic)	Limited

The initial and final acceleration and velocity of a transient must be zero for both electrodynamic and electrohydraulic exciters. As with any type of testing machine, maximum attainable values of acceleration and velocity are limited. Acceleration is actually limited by the force capabilities of the exciter.

Flexures in electrodynamic exciters generate restoring forces which return the exciter table to its originating position (defined as zero), and limitation 3 holds. This is not a requirement for electrohydraulic systems; however, by imposing this limitation one can take advantage of both the forward and return portion of the stroke to generate the required transient. This effectively results in doubling the displacement capacity of the exciter for generating transients. Thus for the purposes of this discussion limitation 3 will also be considered a limitation for an electrohydraulic exciter.

REPRODUCTION OF CLASSICAL PULSES

Consider the half-sine shock pulse shown in Fig. 3 where acceleration, velocity, and displacement are defined by the following relationships:

$$\ddot{x}(t) = A \sin \pi t / \tau \quad (1)$$

$$\dot{x}(t) = \frac{A\tau}{\pi} (1 - \cos \pi t / \tau) \quad (2)$$

$$x(t) = A\tau^2 / \pi^2 (\pi t / \tau - \sin \pi t / \tau) \quad (3)$$

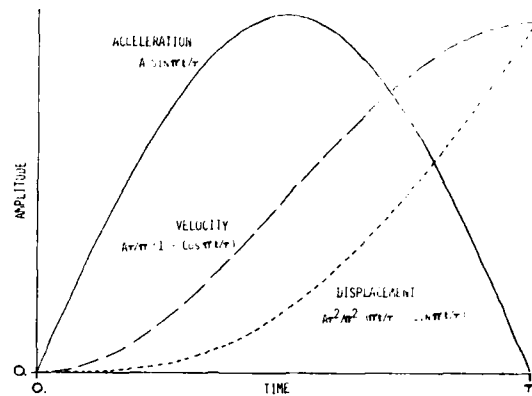


Fig. 3 - Half-sine acceleration, velocity, and displacement characteristics

One can see that the limitations of zero final velocity and zero final displacement have not been met. Classical pulses (haversine, parabolic cusp, triangle, square wave, etc.) all result in residual velocities and displacements and therefore cannot be accurately reproduced on vibration exciters without modifying the pulses.

DECAYING SINUSOIDS TO MATCH SHOCK SPECTRA

The first attempt to develop a method for matching shock spectra over wide frequency ranges was to use decaying sinusoids. This provides an excellent means of matching shock spectra but results in velocities and displacements which do not meet the limitations of electrodynamic and electrohydraulic exciters. However, a brief discussion of the use of decaying sinusoids is included at this point since the technique provided a considerable contribution in the evolution of developing a more suitable transient for reproduction on vibration exciters.

Consider, therefore, a single frequency transient whose acceleration, velocity, and displacement characteristics are described in the time domain by the following relationships:

$$\ddot{x}(t) = A e^{-\zeta \omega t} \sin \omega t \quad (4)$$

$$\begin{aligned} \dot{x}(t) = & \frac{-A e^{-\zeta \omega t}}{\omega (\zeta^2 + 1)} (\zeta \sin \omega t + \cos \omega t) \\ & + \frac{A}{\omega (\zeta^2 + 1)} \end{aligned} \quad (5)$$

and

$$x(t) = \frac{A e^{-\zeta \omega t}}{\omega^2 (\zeta^2 + 1)^2} (\zeta^2 \sin \omega t + 2\zeta \cos \omega t - \sin \omega t) + \frac{At}{\omega (\zeta^2 + 1)} - \frac{2\zeta A}{\omega^2 (\zeta^2 + 1)^2} \quad (6)$$

These relationships are graphically illustrated in Fig. 4. The reader can immediately observe that the final velocity and displacement are nonzero and do not meet the shaker limitations previously described. Disregarding these disadvantages at this point, consider the normalized shock spectra of a single frequency decaying sinusoid shown in Fig. 5 for varying decay rates. Several things are interesting to note:

- 1) Shock spectra levels of greater than two can be obtained. (Classical pulses result in maximum values of shock spectra of two or less.)
- 2) Maximum shock spectra levels decrease with increasing decay rates.
- 3) Shock spectra for high decay rates ($\zeta = 0.5$) approach the shape of that obtained when using a half-sine.

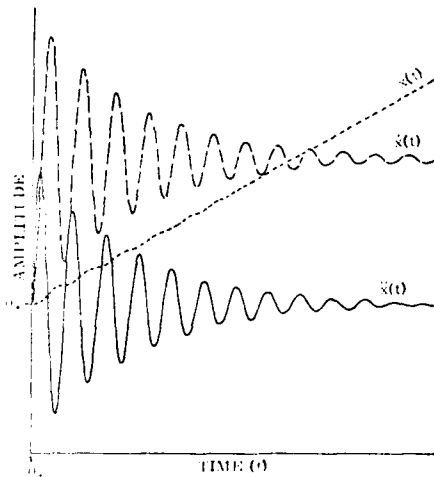


Fig. 4 - Decaying sinusoid acceleration, velocity, and displacement characteristics

By adding several decaying sinusoids of various frequencies, amplitudes, and decay rates one can obtain a shock spectrum which is the composite of the shock spectra of the

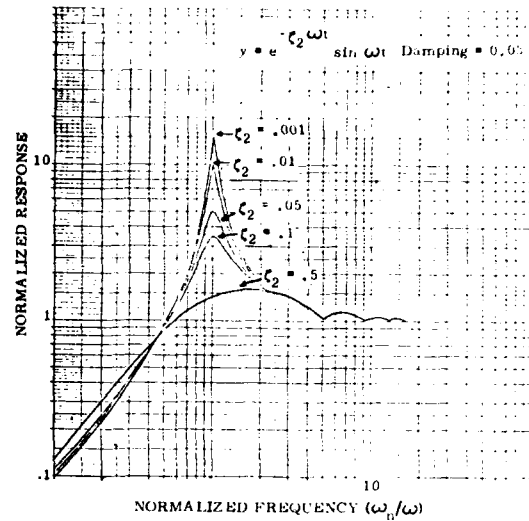


Fig. 5 - Normalized shock spectra for a single frequency decaying sinusoid

individual single frequency decaying sinusoids. Thus by judiciously choosing frequencies, amplitudes, and decay rates of the individual decayed sinusoids one can obtain an accurate match of a field shock spectrum. The resulting transient is described by the following relationship,

$$\ddot{x}(t) = \sum_{i=1}^n A_i e^{-\zeta_i \omega_i t} \sin \omega_i t \quad (7)$$

Figure 6 illustrates an example of matching a field shock spectra using decayed sinusoids. The curve represented by the solid line is the envelope of shock spectra of an ensemble of field pulses obtained from switching/humping ATMS rail cars at 11-mph switching speeds [2]. The dashed line represents a match obtained using five decaying sinusoids. A match to 1.0 Hz resulted in a pulse duration (τ) of 359 msec. The residual velocity and displacement were 185 inches/second and 62 inches, respectively. Shortening the pulse duration (i.e., truncation of the pulse) to 150 msec resulted in a match of the shock spectra to 2.2 Hz (degradation indicated by the dotted curve), with the residual velocity and displacement of 210 inches/second and 22 inches, respectively. Decreasing the duration of the pulse to 75 msec resulted in considerable degradation of the shock spectra and a match to approximately 5.5 Hz. The residual velocity and displacement were approximately 170 inches/second and 8 inches, respectively. The acceleration, velocity, and displacement

relationships for matching shock spectra to 2.2 Hz are shown in Fig. 7. Decaying sinusoids provide a means of matching shock spectra over wide frequency ranges but residual velocities and displacement are nonzero.

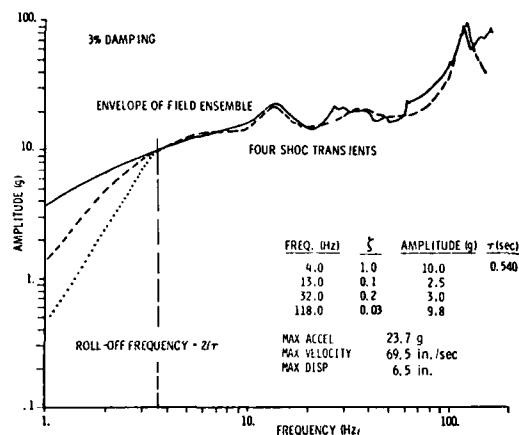


Fig. 6 - Matched shock spectra using summed decayed sinusoids

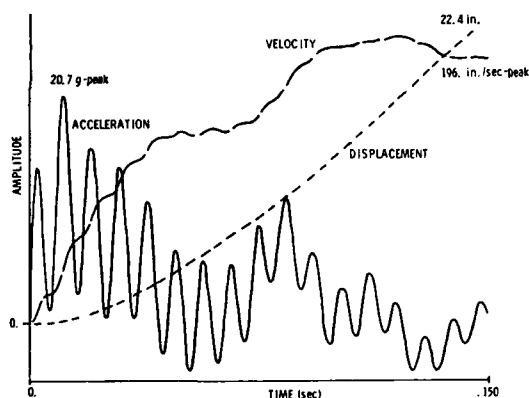


Fig. 7 - Acceleration, velocity, and displacement relationships for ATMX car shock spectra match using decaying sinusoids

SHAKER OPTIMIZED TRANSIENT THEORY

One can see from previous examples that decaying periodics offer an excellent means of matching shock spectra over wide frequency ranges. The problem is to develop a periodic transient such that residual velocities and displacements are zero.

Consider the periodic function shown in Fig. 8a which is defined by

$$\ddot{y}(t) = A e^{\zeta \omega t} \cos \omega t \quad (-\tau/2 \leq t \leq 0) \quad (8)$$

$$\ddot{y}(t) = A e^{-\zeta \omega t} \cos \omega t \quad (0 \leq t \leq \tau/2)$$

where τ is of such length that acceleration, \ddot{y} , has sufficiently decayed to zero at $-\tau/2$ and $\tau/2$. Integrating the function from $t = -\tau/2$ to $t = \tau/2$ using $\dot{y}(-\tau/2) = 0$ results in a positive nonzero velocity at $\tau/2$.

For acceleration inputs, one way to assure that the velocity boundary conditions are met is to calculate the area under the acceleration input function (this is the residual velocity; it is also the zero frequency term of the Fourier spectrum), and superimpose a pulse with a residual velocity equal and opposite to the calculated value. Ideally, the superimposed pulse should change the input pulse as little as possible while reducing the zero frequency term of the Fourier spectrum of the input to zero. A good pulse for this purpose is the cosine bell described in Eq. (9).

$$s(t) = \begin{cases} B \cos^2 \pi t / \tau & (-\tau/2 < t < \tau/2) \\ 0 & (\text{elsewhere}) \end{cases} \quad (9)$$

Thus two independent variables (B , τ) are available for reducing the residual velocity to zero. One of the variables can be used to control the residual displacement. If the reciprocal of the pulse duration, $1/\tau$, is small compared to the lowest resonant frequency of the system, the effect on the response of the structure will be small.

If the cosine bell is superimposed on the previous function, the result is shown in Fig. 8c and is defined by

$$\ddot{x}(t) = A e^{-\zeta \omega t} \cos \omega t - B \cos^2 \pi t / \tau \quad (0 \leq t \leq \tau/2) \quad (10)$$

$$\ddot{x}(-t) = \ddot{x}(t)$$

By integrating this function and evaluating the necessary constants, the value of B can be obtained such that the zero velocity boundary conditions are satisfied. The required B is given by,

$$B = \frac{4A\tau}{\tau\omega(\zeta^2 + 1)} \quad (11)$$

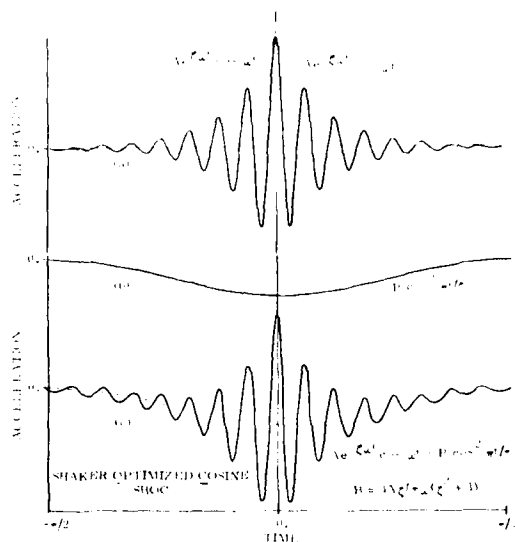


Fig. 8 - A SHOC pulse

Substituting into the previous equation

$$\ddot{x}(t) = A e^{-\zeta \omega t} \cos(\omega t) - \frac{4A\zeta}{\tau \omega (\zeta^2 + 1)} \cos^2(\pi t / \tau), \quad (12)$$

$$\dot{x}(t) = \frac{A e^{-\zeta \omega t}}{\omega (\zeta^2 + 1)} [-\zeta \cos(\omega t) + \sin(\omega t)] \quad (13)$$

$$+ \frac{2A\zeta}{\omega (\zeta^2 + 1)} \left[\frac{1}{2} - \frac{t}{\tau} - \frac{1}{2\pi} \sin\left(\frac{2\pi t}{\tau}\right) \right],$$

and

$$x(t) = \frac{-A\zeta}{\omega(1+\zeta^2)} \left[\frac{1}{4\tau} (2t - \tau)^2 - \frac{\tau}{2} \cos^2(\pi t / \tau) \right] \quad (14)$$

$$+ \frac{A e^{-\zeta \omega t}}{\omega^2 (1+\zeta^2)^2} \left[(\zeta^2 - 1) \cos(\omega t) - 2\zeta \sin(\omega t) \right]$$

$$0 \leq t \leq \tau/2.$$

Figure 8c shows a typical resulting time history. The magnitude of the cosine bell has been exaggerated to illustrate the concept. The normalized shock spectra of a single-frequency SHOC (Shaker Optimized Cosine) for several decay rates is shown in Fig. 9. Note that the

general character (and hence the advantages) of the spectrum of the decaying sinusoids is preserved. If the pulse duration (τ) is decreased, the required displacement will decrease and because the low-frequency energy has been reduced the shock spectrum will start to roll off at a frequency approximately equal to $2/\tau$. Thus a compromise is frequently required between the lowest frequency at which the shock spectrum can be matched and the displacement available. It has also been found that because of the symmetry about $t = 0$, the pulses will add in the frequency domain (i.e., shock spectrum) as well as in the time domain. This simplifies the construction of complex spectrum spectra when the pulses are summed.

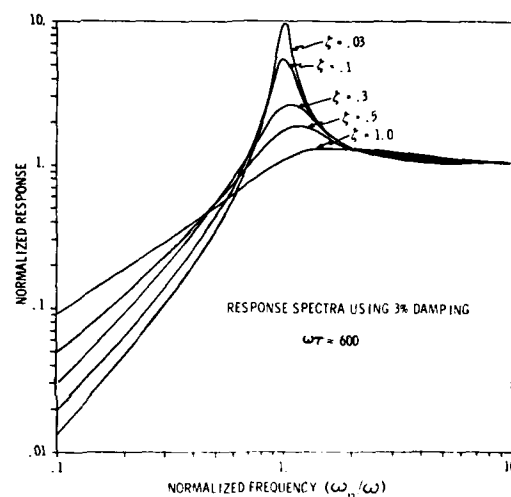


Fig. 9 - Normalized shock spectra for SHOC pulses

An example of a typical acceleration, velocity, and displacement time history is shown in Fig. 10. The time has been shifted by a factor of $\tau/2$ for convenience. Note that the desired boundary conditions have been met (i.e., the initial and final acceleration, velocity, and displacement are all zero).

EXAMPLES OF MATCHING SHOCK SPECTRA USING THE SHOC PULSE

The first example will be for an ATMX rail hump. The shock spectrum was matched using four frequencies. The resulting shock spectrum is shown in Fig. 11. As can be seen the spectra match well above 3.5 Hz. The low frequency roll-off is a function of τ . If τ is increased, the spectra can be matched at a

lower frequency; however, the required displacements will increase. The pulse duration (τ) picked was to limit the displacement at less than 8 inches (a physical limit of Sandia's low-frequency system). The acceleration, velocity, and displacement time histories are shown in Fig. 12.

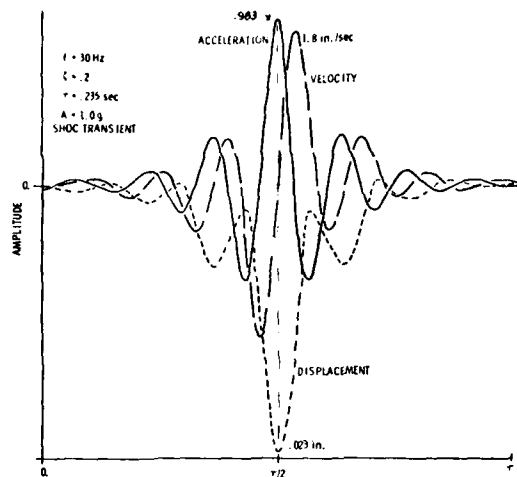


Fig. 10 - Acceleration, velocity, and displacement of a SHOC pulse

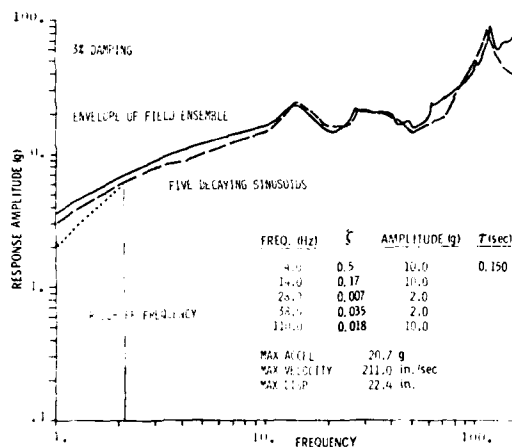


Fig. 11 - Using the SHOC pulse to match the ATMX rail hump shock spectrum

The second example is included to illustrate that relatively smooth spectra can also be enveloped using the SHOC technique. The envelope was developed to represent a portion of a flight environment of a missile system. As can be seen from Fig. 13, three superimposed SHOC pulses envelope the required spectrum. The acceleration, velocity, and displacement

limits are well within the capabilities of an electrodynamic system.

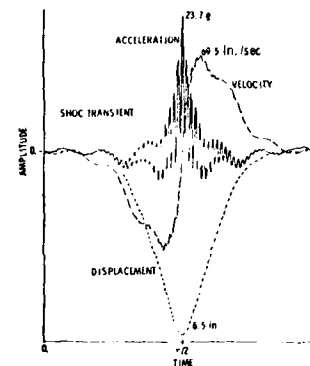


Fig. 12 - Time history of the SHOC pulse used to match the ATMX rail hump shock spectrum

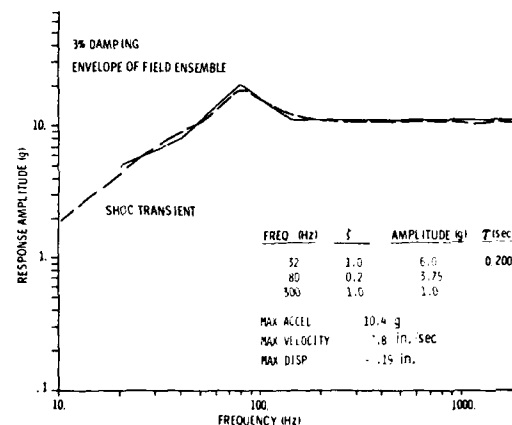


Fig. 13 - The use of a SHOC pulse to match a smooth shock spectrum

The third example illustrates a case where the pulse was duplicated in the laboratory. The simulation was of a transient launch vibration of a missile structure. The test set-up is shown in Fig. 14. The testing was performed on a slip table driven by an MB C-220 electrodynamic shaker. The pulse was reproduced using the LeBlun, Favour technique [3]. A Xerox Sigma V computer was used to perform the required calculations and to generate the input pulse. The shock spectrum envelope of the field event is shown in Fig. 15 as the desired curve. Plus and minus 30 percent lines are included as an acceptable error band. The predicted shock spectrum, shown on Fig. 15, is the spectrum of an ideal SHOC pulse with six components (the components

are listed on Fig. 15). The time history of the ideal SHOC pulse and the actual pulse measured at the input accelerometer are shown in Figs. 16 and 17, respectively. The shock spectrum of the actual pulse is also included in Fig. 15. As can be seen, the differences between the predicted and desired spectra are small. In other tests, cases have been found where the reproduced time history differed significantly from the desired pulse due to noise, system nonlinearities, etc. However, the shock spectra usually differed by less than 30 percent. This is not unreasonable as the shock spectrum is a tolerant measurement of the characteristics of a time history.

The acceleration peaks of a SHOC pulse are predominantly positive. For some transient testing a pulse may be desired which has approximately equal numbers of positive and negative peaks of comparable amplitude. This can be accomplished by alternating the signs of the components of the SHOC pulse. However, the procedures become slightly more tedious if the signs are allowed to change. In some cases a spectrum can be matched with a smaller required displacement by alternating the signs of the frequency components.

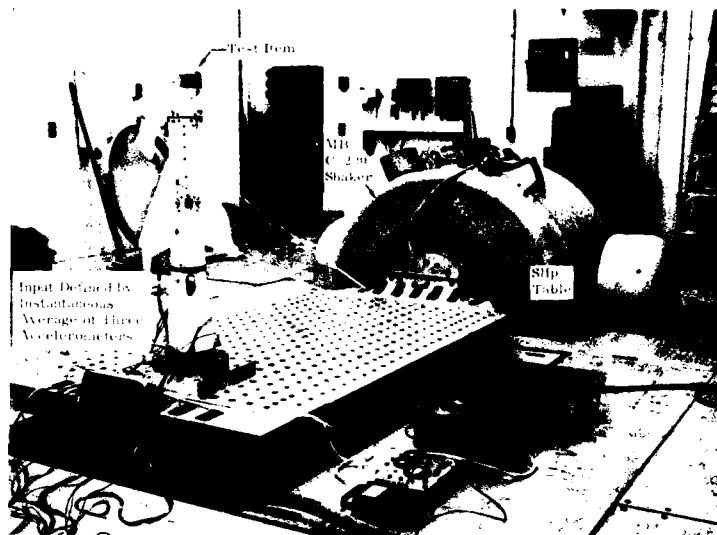


Fig. 14 - Test setup for SHOC test

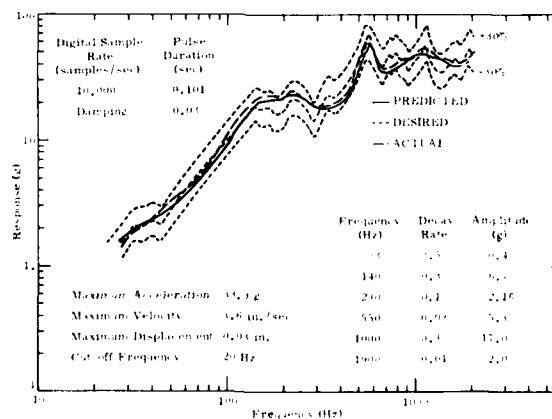


Fig. 15 - Shock spectra of a launch event and simulation

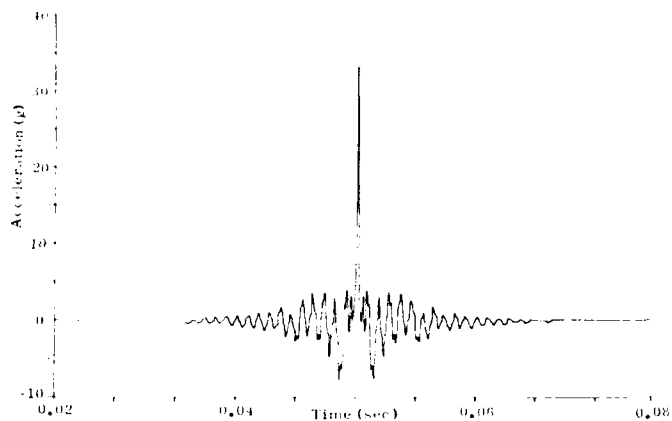


Fig. 16 - Desired time history of the SHOC pulse used to simulate a launch event

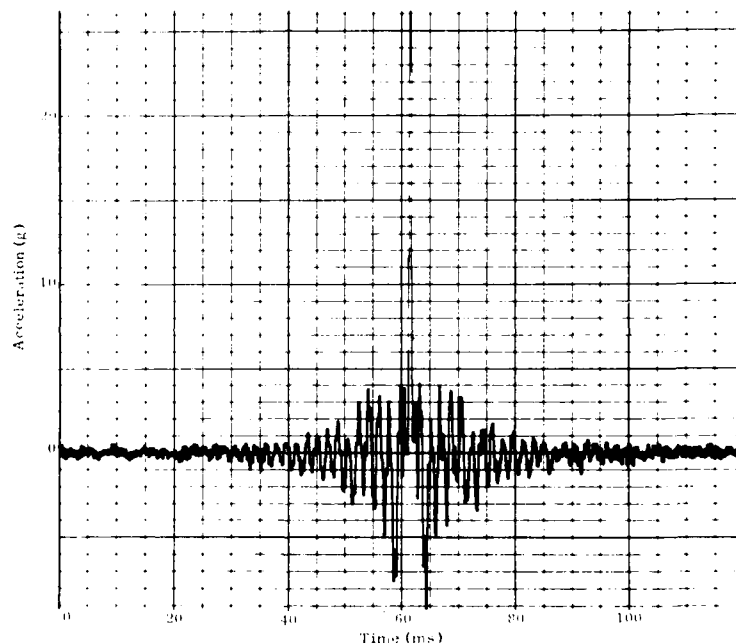


Fig. 17 - Actual time history of a SHOC pulse used to simulate a launch event

PROCEDURES FOR MATCHING A SHOCK SPECTRUM WITH A SHOC PULSE [4]

As was mentioned earlier in the text, the shock spectra of the components of the SHOC pulse can be added to produce the spectrum of the composite. The procedure for matching a complex spectrum is therefore a relatively simple procedure. Three items make this

possible. First, the spectrum at frequencies much lower than the frequency of a SHOC component will be small. This implies that the high-frequency components will have little effect on the spectrum at the lower frequencies. Second, the principal effect on the spectrum of a SHOC component will be near the frequency of the component. The shock spectrum at this point can be many times the

peak amplitude of the component. And third, at frequencies much higher than the frequency of a SHOC component the spectrum will be equal to the peak amplitude of the component. Since the peak amplitudes of all the components occur at the same time ($t = 0$), the peak amplitude of the composite will be equal to the sum of the peak amplitudes of the components. And the shock spectrum of the composite of high frequencies will be equal to this peak amplitude.

CONCLUSIONS

It has been shown that the proposed SHOC pulse can be used to match a great variety of shock spectra. The pulse has characteristics lending itself toward reproduction on existing shaker systems. The technique has been used successfully on electrodynamic shaker systems.

REFERENCES

1. Robert C. Yang and Herbert R. Saffell, "Development of a Waveform Synthesis Technique - A Supplement to Response Spectrum as a Definition of Shock Environment," Shock and Vibration Bulletin, No. 42, Part 2, Naval Research Laboratories, Washington, D.C., January 1972.
2. J. T. Foley, summary of rail switching/humping shock environment criteria, Data Bank Code No. EDB A1202, Sandia Laboratories, Albuquerque, New Mexico, July 1969.
3. Jay M. LeBrun and John Favour, "Feasibility and Conceptual Design Study - Vibration Generator Transient Waveform Control System," Final Report prepared for NASA June 1969, Contract NAS5-15171, Goddard Space Flight Center, Greenbelt, Maryland, by Aerospace Group, The Boeing Company, Kent, Washington. This report also released as Boeing Document D2-114438-1.
4. D. O. Smallwood and A. F. Witte, "The Use of Shaker Optimized Periodic Transients in Matching Field Shock Spectra," SC-DR-71 0911, Sandia Laboratories, Albuquerque, New Mexico, May 1972.

DISCUSSION

Mr. Koen (Bell Laboratories): We have used the summation of damped sinusoids in our tests. We fed in a damped sinusoid and a damped co-sinusoid and calculated the response spectrum from the test. We found that the shaker produces a response spectrum for neither a damped sinusoid nor a damped co-sinusoid. The thing that is produced is an amplification in the neighborhood of the predominant frequency of the sinusoid. I suggest that the analytical results you showed for the bell sinusoid would be significantly different in the neighborhood away from the predominant frequency on an experimental basis. Secondly, in the synthesized wave form test, we fix the damping which the person is allowed to use. Through a method of what we call single damped sinusoid calibration tests, we come up with a set of predistorted inputs so that we maintain, for example, a 5% damped sinusoid. I might add that, if we had not done that, while we can match the shock spectrum, we might get away with a very un-severe test by choosing very low damping factors in the damped sinusoid test.

Mr. Witte: Was that a question?

Mr. Koen: It was just an observation on changing the damping and the amplification to what ever value you pick. For example, if you change the damping, you can come up with a very mild test but still match the criteria.

Mr. Witte: We have the option of either changing damping, amplitude or frequency.

Mr. Koen: We specify the damping you're permitted to have and you're not allowed to change that when you match the criteria.

Mr. Witte: Now wait a minute. This is the decay rate of the cosine. It is not the damping of the shock spectra.

Mr. Koen: No, I meant the decay rate of your bell sine.

Mr. Witte: Why are you fixed on decay rate? Why can't you vary this?

Mr. Koen: We want to get a specific type of a wave form that has a specific shock severity. As you probably know, you can match the response spectrum in many different ways.

Mr. Witte: That's correct.

Mr. Koen: We also used both damped and undamped response spectra in our criteria. We found that unless you use the proper damping you only meet one spectra and not the others.

Mr. Witte: What is this criteria? I guess I don't understand. What is the severity criteria?

Mr. Koen: I'll try to pose it another way. If we allow the damping to vary, we find that equipment can pass and still meet the response spectrum. Once we fix the damping, the same equipment would not pass with the same response spectrum.

Mr. Witte: I would think that that would be a problem with shock spectra technique itself.

Mr. Koen: Yes

Mr. Witte: This wasn't the argument. I was arguing the point that we can match shock spectra very effectively.

Mr. Smallwood: What the gentleman said is true. There is a philosophical argument here. He chose to try to reproduce decayed cosines recognizing that the shaker won't reproduce them really. We chose to choose a wave form which we could reproduce on the shaker with the view to doing a better job of predicting before the test what we're really going to get from the shaker.

Mr. Favour (Boeing Company): I think you're saying that here is an industry that's wrestling with the problem of tests being specified primarily with the shock spectrum, but recognizing that this is not the entire answer. So, now the customer also wants people to test to a time history.

Mr. Witte: Right. One thing that we should consider when we're trying to match shock spectra, if shock spectra is the criteria, is that the wave form of the transient that we use should look something like the wave form that we actually see in the field environment. I think this is very very important. A half-sine or a haversine is a very poor simulation of the oscillatory type transient that we see in the field.

Dr. Morrow (LTV): In connection with the observation that the shock spectrum by itself may not completely define shock severity so one is inclined to specify a time history requirement as well, I would like to make a point. If one uses what has been unfortunately called the primary spectrum, this has very little correlation with shock severity. One can easily show that at high frequencies it merely yields the peak value of whatever time function is used. One should deemphasize primary (initial) and composite spectra and place more emphasis on residual shock spectra or on Fourier spectra.

Mr. Schell (Shock and Vibration Information Center): In the matching of the test data to the predicted or calculated data that you showed on your slide, was this a rigid mass load on the table or was it a reactive type load?

Mr. Witte: It was a missile structure and it was a reactive type load.

Mr. Fandrich (Radiation Inc.): Let's get back to the discussion of shock spectrum and time histories. In 1971 I published a paper in the Institute of Environmental Sciences Proceedings that described a piece of analog equipment that generates exactly the same thing you did, a summation of decaying sinusoids. The intent of the paper was to describe a piece of equipment that generates a time history similar to those seen in the field rather than a shock spectrum. I think this method can be used either for shock spectrum or time history. In that paper I show an actual recorded shock from the field, something I stole out of another paper photographically, and a very good reproduction of that of a complicated time history. So I think using this kind of summation of decaying sinusoids can be satisfactory both in shock spectrum and time history.

A TRANSIENT VIBRATION TEST TECHNIQUE USING LEAST FAVORABLE RESPONSES

D. O. Smallwood
Sandia Laboratories
Albuquerque, New Mexico 87115

A technique is described wherein the response of a linear structure to a transient vibration is maximized to produce the largest possible response for any input whose Fourier spectrum magnitude is equal to or less than a given envelope. It is shown how this technique can be used as a practical test criterion. Examples are given to illustrate the technique and to show typical results. In two examples the method is compared with the shock spectrum approach. The method will usually produce responses which are 1.1 to 2.5 greater than the structural response to a classical (for example, a half sine) pulse or to a typical field pulse. Thus the method provides a conservative, but not an overly conservative, test environment.

NOMENCLATURE

In general lower case letters denote functions of time. The corresponding upper case letter is the Fourier transform of the time function and is a function of frequency.

x - an input function
 y - an output function
 $h(t)$ - the system impulse response function
 $H(\omega)$ - the system frequency response function
 ω - circular frequency
 Ω - circular frequency
 i - $\sqrt{-1}$
 t - time
 $|H|$ - the magnitude or absolute value of the complex quantity H

H^* - the conjugate of the complex quantity H

l - a constant

K - a constant

$|y(t)|_{\max}$ - the maximum value for the absolute value of y at any time

X_e - an envelope of the Fourier spectrum of $X(\omega)$

$E[]$ - the expected value

M, N - constants (see Eqs. 12, 13)

ϕ - a phase angle

p - a probability density function

A, B - random variables, also used to designate two field events

A, B - also a constant

A^*, B^* - used to designate the modified field events A and B

NOMENCLATURE (cont)

- σ - the standard deviation
- τ - a pulse duration
- p - a circular frequency
- ζ - damping coefficient, the fraction of critical damping
- $\delta(t)$ - the Dirac delta function, a unit impulse

INTRODUCTION

Transient vibration reproduction on shakers has advanced rapidly in recent years [1,2]. It is now possible to reproduce any waveform on a shaker which is within the frequency, force, displacement, and velocity limits of the vibration system being used. The use of digital computers and digital to analog converters makes it possible to reproduce any pulse which can be expressed analytically or as a series of time samples. Now that the capability has been developed, the question arises as to which pulse to reproduce. The first impulse is to reproduce a field pulse. This has many advantages. It certainly represents a realizable field environment. The difficulty is that even though this field environment was realized in the past, there is no guarantee that it will happen again in a future event. Further, if a test specimen survives the past environment it does not guarantee survival in the future since one is not sure that this particular measurement represents the most severe case possible. Another difficulty arises when several field environment samples are available and all different. Which record do you use to perform qualification tests? It is also sometimes desirable to combine several environments into one test. Again this becomes difficult when the field environment is used to represent the environment in a test laboratory. One way out of this dilemma is to select the "worst" field environment, if this can be defined.

One method of picking the worst environment is to compute the shock spectrum (sometimes called the response spectrum) of the field records. It is then assumed that any transient vibration with a shock spectrum equal to or greater than the composite shock spectrum of all field records will be a conservative test. The difficulty with this technique is that a single degree of freedom system is assumed even though the assumption is not true for many real systems. Thus, both overtests and undertests can result. Another technique for defining the

worst environment has been suggested [3-7] and will be discussed in this report.

BASIC THEORY OF LEAST FAVORABLE RESPONSES

Assume that the system can be represented by a linear system as shown in Fig. 1, where $H(\omega)$ is the system frequency response function, and $x(t)$ and $y(t)$ are the system input and response, respectively. Note that it is not required that $x(t)$ and $y(t)$ have the same physical units. For example, $x(t)$ could be an acceleration and $y(t)$ the relative strain between two points. Let $X(\omega)$ and $Y(\omega)$ be the Fourier spectra of $x(t)$ and $y(t)$.

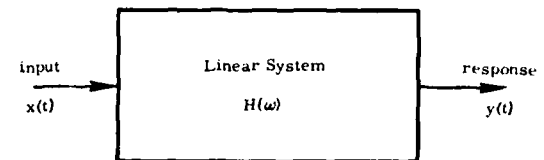


Fig. 1 - Single Input/Single Output linear system

Then

$$X(\omega) = \int_{-\infty}^{\infty} x(t) e^{-i\omega t} dt, \quad (1)$$

$$x(t) = \frac{1}{2\pi} \int_{-\infty}^{\infty} X(\omega) e^{i\omega t} d\omega, \quad (2)$$

$$Y(\omega) = \int_{-\infty}^{\infty} y(t) e^{-i\omega t} dt, \quad (3)$$

and

$$y(t) = \frac{1}{2\pi} \int_{-\infty}^{\infty} Y(\omega) e^{i\omega t} d\omega. \quad (4)$$

With the aid of the frequency response function

$$y(t) = \frac{1}{2\pi} \int_{-\infty}^{\infty} H(\omega) X(\omega) e^{i\omega t} d\omega, \quad (5)$$

*In this memorandum, the words "worst-case" and "least favorable" are used interchangeably.

Shinozuka [3,4] showed that $x(t)$ having a Fourier spectrum given by

$$X(\omega) = \frac{X_e(\omega) H^*(\omega)}{|H(\omega)|} \quad (6)$$

will result in the maximum absolute response $|y(t)|_{\max}$ for all possible inputs $x(t)$ having a Fourier spectrum whose magnitude is equal to or less than $X_e(\omega)$. This can be seen as follows:

$$\begin{aligned} |y(t)| &= \left| \frac{1}{2\pi} \int_{-\infty}^{\infty} X(\omega) H(\omega) e^{i\omega t} d\omega \right| \\ &\leq \frac{1}{2\pi} \int_{-\infty}^{\infty} |X(\omega)| |H(\omega)| d\omega \\ &\leq \frac{1}{2\pi} \int_{-\infty}^{\infty} X_e(\omega) |H(\omega)| d\omega = 1 \end{aligned} \quad (7)$$

If an input $X(\omega)$ can be found which will give a response $|y(t)| = 1$ for some time t it will be a least favorable input. That is, the input will result in the maximum value for the absolute value of $y(t)$. If the value for $X(\omega)$ given in Eq. (6) is chosen,

$$\begin{aligned} y(t) &= \frac{1}{2\pi} \int_{-\infty}^{\infty} \frac{X_e(\omega) H^*(\omega)}{|H(\omega)|} H(\omega) e^{i\omega t} d\omega \\ &= \frac{1}{2\pi} \int_{-\infty}^{\infty} X_e(\omega) |H(\omega)| e^{i\omega t} d\omega \end{aligned} \quad (8)$$

and at $t = 0$

$$y(0) = \frac{1}{2\pi} \int_{-\infty}^{\infty} X_e(\omega) |H(\omega)| d\omega = 1 \quad (9)$$

Thus it is seen that the input given in Eq. (6) will result in the maximum possible response. In addition it is seen that this maximum response will occur at $t = 0$. The physical significance of Eq. (6) can be more readily seen by writing $H(\omega)$ in polar form.

$$H(\omega) = |H(\omega)| e^{i\phi(\omega)},$$

where

$$\phi = \tan^{-1} \frac{\text{Im}[H(\omega)]}{\text{Re}[H(\omega)]} \quad (10)$$

Equation (6) becomes

$$X(\omega) = X_e(\omega) e^{-i\phi(\omega)},$$

and the product

$$H(\omega) X(\omega) = X_e(\omega) |H(\omega)| e^0 \quad (11)$$

Thus at the output, for the worst-case input, the phase angle is zero at all frequencies at $t = 0$. That is, all the frequency components will constructively add at $t = 0$.

One objection to the resulting input is that it is not causal, i.e., $x(t)$ for $t < 0$ is not zero. However, it will be noticed later that the input decays rapidly for both positive and negative time. If a time duration τ is defined such that $x(t)$ is arbitrarily small for $t < -\tau$ or $t > \tau$ then the time history can be truncated at $\pm\tau$ without seriously changing the input or response. Strictly speaking the truncated input will not produce the least favorable response; however, the response can be arbitrarily close to the least favorable response. A new input can then be defined by shifting the time τ such that

$$\begin{aligned} z(t) &= x(t - \tau) \quad \text{for } 0 < t < 2\tau \\ &= 0 \text{ elsewhere} \end{aligned}$$

thus removing the causal objection. The maximum response will now occur near $t = \tau$, and the Fourier spectrum will be given approximately by

$$Y(\omega) = X_e(\omega) |H(\omega)| e^{-i\omega\tau}$$

Drenich [3] showed that for all envelopes X_e , such that

$$\frac{1}{2\pi} \int_{-\infty}^{\infty} |X_e(\omega)|^2 d\omega \leq M^2 \quad (12)$$

where M is a finite constant, a least favorable envelope is

$$X_e = \frac{M}{N} |H(\omega)|$$

where

$$N^2 = \int_{-\infty}^{\infty} h^2(t) dt = \frac{1}{2\pi} \int_{-\infty}^{\infty} |H(\omega)|^2 d\omega \quad (13)$$

and $h(t)$ is the impulse response function.

Using Eqs. (11), (12), and (13) the least favorable input becomes

$$X(\omega) = \frac{M}{N} |H(\omega)| e^{-i\omega\tau}$$

or

$$x(t) = \frac{M}{2\pi N} \int_{-\infty}^{\infty} H^*(\omega) e^{i\omega t} d\omega = \frac{M}{N} h(-t) \quad (14)$$

Except for a scale factor, M/N , the least favorable input is the time-reversed impulse response.

If in addition to restrictions on the Fourier modulus, additional restrictions can be placed on the phase or delay of the Fourier spectrum, the least favorable response can be reduced to values less than those given by Shinozuka's formulation. In the limit it is shown that the problem is reduced to the deterministic case where the complete Fourier spectrum (both magnitude and phase) are specified. This case is discussed in detail in another report [7] and will not be repeated here for the sake of simplicity.

PRACTICAL CONSIDERATIONS

Errors -- In a real case, the exact point on a structure where damage is likely to occur is seldom known. Also, measurement errors will occur when measuring the system transfer functions and the input spectrum envelope. Additional errors will occur when the least favorable input is generated. To examine the effect of these errors consider the following. The least favorable response is given by Eq. (9).

$$y(0) = \frac{1}{2\pi} \int_{-\infty}^{\infty} X_e(\omega) |H(\omega)| d\omega = 1$$

If however an error in the phase angle is included (this error can be an error in $\phi(\omega)$ or in our ability to generate $X(\omega)$), $y(0)$ can be expressed as

$$\begin{aligned} y(0) &= \frac{1}{2\pi} \int_{-\infty}^{\infty} X_e(\omega) e^{-i\tau(\omega)} |H(\omega)| e^{i\tau(\omega)} e^{iA} d\omega \\ &= \frac{1}{2\pi} \int_{-\infty}^{\infty} X_e(\omega) |H(\omega)| e^{iA} d\omega \end{aligned} \quad (15)$$

In general A will be a random variable $A(\alpha, \omega)$. The expected value of $y(0)$ is given by

$$\begin{aligned} E[y(0)] &= E \left[\frac{1}{2\pi} \int_{-\infty}^{\infty} X_e(\omega) |H(\omega)| e^{iA} d\omega \right] \\ &= \frac{1}{2\pi} \int_{-\infty}^{\infty} X_e(\omega) |H(\omega)| E[e^{iA}] d\omega \end{aligned} \quad (16)$$

The expected value of e^{iA} is given by

$$E[e^{iA(\alpha, \omega)}] = \int_{-\infty}^{\infty} e^{i\alpha} p_A(\alpha) d\alpha$$

where $p_A(\alpha)$ is the probability density function of the random variable A .

If it is assumed that A is relatively small such that $y(0)$ will be near the maximum value of $|y(t)|$ and further assume that A is normally distributed with a zero mean and variance σ^2 , where σ can be a function of ω , then

$$p_A(\alpha) = \frac{1}{\sigma\sqrt{2\pi}} e^{-1/2(\alpha/\sigma)^2} \quad (17)$$

and

$$E[e^{iA}] = e^{-\sigma^2/2}$$

Therefore

$$E[y(0)] = \frac{1}{2\pi} \int_{-\infty}^{\infty} X_e(\omega) |H(\omega)| e^{-\frac{\sigma(\omega)^2}{2}} d\omega \quad (18)$$

If σ is independent of ω ,

$$E[y(0)] = I e^{-\sigma^2/2} \quad (19)$$

The result is a biased estimate, i.e., the expected value of $y(0)$ will always be less than 1. However, σ can be quite large and not affect the results significantly (see Fig. 2). For example, an error with a standard deviation of 10 degrees will result in an 8 percent error.

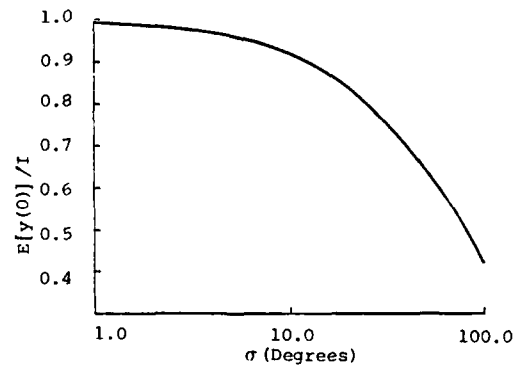


Fig.2 - Normalized error as a function of the phase error

Consider now an error in the amplitude. Again the error could be an error in $|H(\omega)|$ and/or an error in $X_e(\omega)$. Rewriting Eq. (8) to include the error term gives

$$\begin{aligned} y(t) &= \frac{1}{2\pi} \int_{-\infty}^{\infty} X_e(\omega) |H(\omega)| \left(1 + B(\beta, \omega)\right) e^{i\omega t} d\omega \\ &= \frac{1}{2\pi} \int_{-\infty}^{\infty} X_e(\omega) |H(\omega)| e^{i\omega t} d\omega \\ &\quad + \frac{1}{2\pi} \int_{-\infty}^{\infty} X_e(\omega) |H(\omega)| B(\beta, \omega) e^{i\omega t} d\omega, \end{aligned} \quad (20)$$

where B is a random variable denoting the error in the product $X_e(\omega) |H(\omega)|$. Then

$$y(0) = 1 + \frac{1}{2\pi} \int_{-\infty}^{\infty} X_e(\omega) |H(\omega)| B(\beta, \omega) d\omega$$

and the expected value of $y(0)$ is given by

$$\begin{aligned} E[y(0)] &= E \left[1 + \frac{1}{2\pi} \int_{-\infty}^{\infty} X_e(\omega) |H(\omega)| B(\beta, \omega) d\omega \right] \\ &= 1 + \frac{1}{2\pi} \int_{-\infty}^{\infty} X_e(\omega) |H(\omega)| E[B(\beta, \omega)] d\omega. \end{aligned} \quad (21)$$

If the expected value of B is zero, i.e., a zero mean, then $E[y(0)] = 1$. However, as long as

$$\frac{1}{2\pi} \int_{-\infty}^{\infty} X_e(\omega) |H(\omega)| E[B(\beta, \omega)] d\omega \geq 0, \quad (22)$$

$$E[y(0)] \geq 1.$$

Equation (22) implies that errors in measuring $H(\omega)$ will have little effect as long as the errors are not biased.

Drawing Envelopes -- For the case where $H(\omega)$ is a nondimension motion transfer function (for example, acceleration/acceleration), the mechanical impedance of the structure will be high where $|H(\omega)|$ is large. This will result in a notch in the Fourier spectrum of the input unless the driving impedance is much larger. Thus for the case where the structural impedance is comparable to the source impedance the product $X_e(\omega) |H(\omega)|$ will tend to be smoother than either X_e or H .

Therefore frequently the envelope $X_e(\omega)$ need not cover all the peaks in the field environment Fourier spectrum as long as Eq. (22) is valid. For many cases an envelope as sketched in Fig. 3 might be suitable.

If evidence exists to indicate that the Fourier spectrum of the field environment is strongly influenced by system dynamics (i.e., dips will occur in the Fourier spectrum near the fixed-base natural frequencies of the system), Eq. (22) indicates that even a lower envelope would be in order.

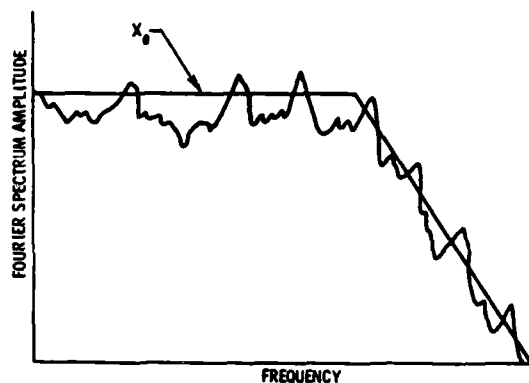


Fig. 3 - An envelope of a Fourier spectrum

If little is known about $H(\omega)$, X_e should be heavily biased toward the peaks of the field spectra. As more is learned about $H(\omega)$, $X_e(\omega)$ can be modified to lower the levels. Of course, uncertainty in the field environment must be accounted for.

ANALYTIC EXAMPLES

Single Degree of Freedom System -- In order to gain a little insight, an example using a single degree of freedom system will be given of the least favorable input of a pulse having the same frequency content as a square wave. The transfer function of the single degree of freedom system will be of the form,

$$H(\omega) = \frac{\omega_n^2}{\omega_n^2 - \omega^2 + 2i\zeta\omega\omega_n},$$

where

ω_n = the natural frequency of the system

$$= 2\pi(100)(\text{rad/sec})$$

ζ = the fraction of critical damping

$$= 0.05$$

The results are shown in Fig. 4. (The time on Fig. 4 parts (c) and (d), has been shifted by $\tau/2$ for convenience.) The input pulse is shown first followed by the response of the single degree of freedom system to the input pulse. Shown next is the least favorable (or worst-case) input pulse having the same Fourier envelope as the preceding input pulse. And last is the response of the single degree of freedom system to the least favorable input. A tendency to concentrate the high-frequency portion of the pulse near $t = 0$ is evident.

One further example will illustrate the point. Let

$$H(\omega) = 1 \quad (\text{a rigid body})$$

$$X_e(\omega) = K/\Omega \quad \text{for } -\Omega < \omega < \Omega$$

$$= 0 \quad \text{elsewhere}$$

$$y(t) = \frac{K}{2\Omega\pi} \int_{-\Omega}^{\Omega} e^{i\omega t} d\omega$$

$$y(t) = \frac{K}{\pi\Omega t} \sin(\Omega t)$$

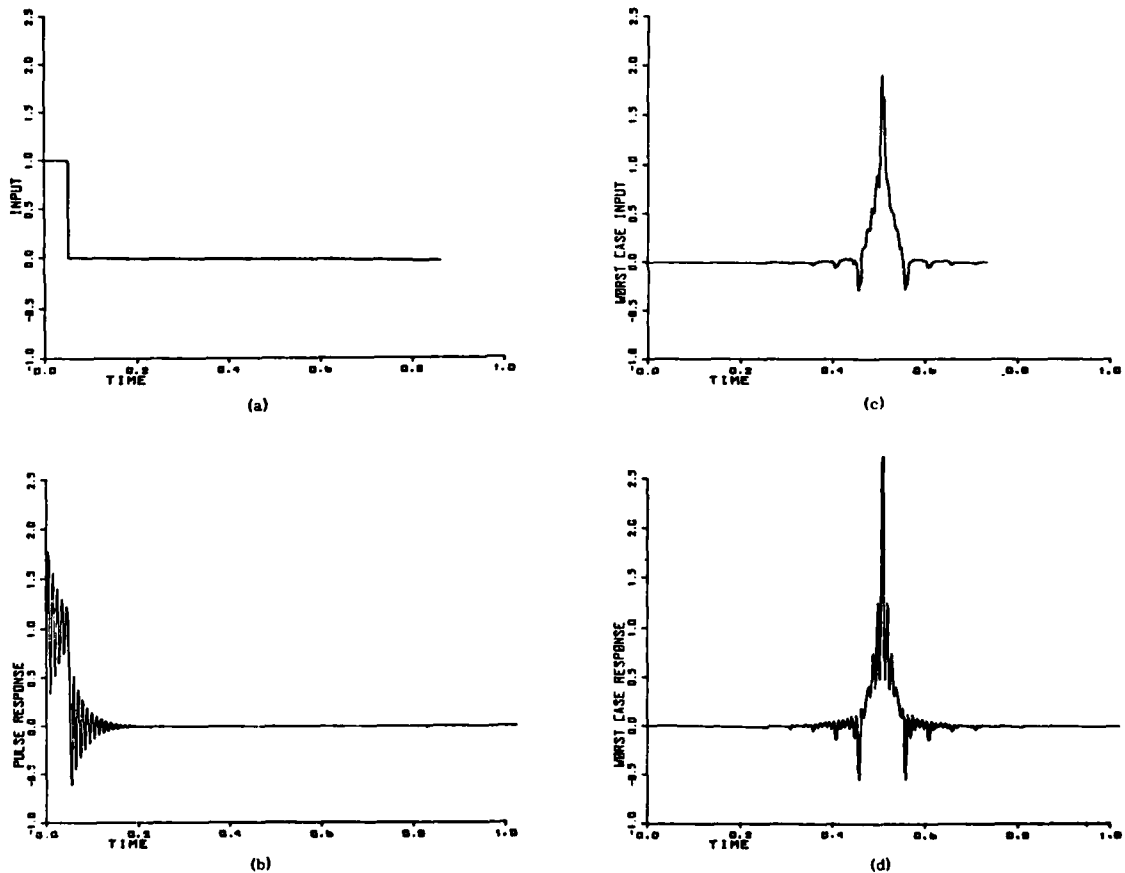


Fig. 4 - A 0.05-second square wave

Thus the least favorable input is the familiar $\sin x/x$ function. And the limit as Ω approaches infinity is

$$\lim_{\Omega \rightarrow \infty} Y(t) = K\delta(t)$$

where $\delta(t)$ is the Dirac delta function.

Five-Mass System -- To further illustrate the technique, the response of a five-mass system will be studied. A five-mass system was chosen as a system sufficiently complex to represent motions different from a one degree of freedom system, yet simple enough for the motion to be understood. The system used is shown in Fig. 5. The input will always be at mass 1.

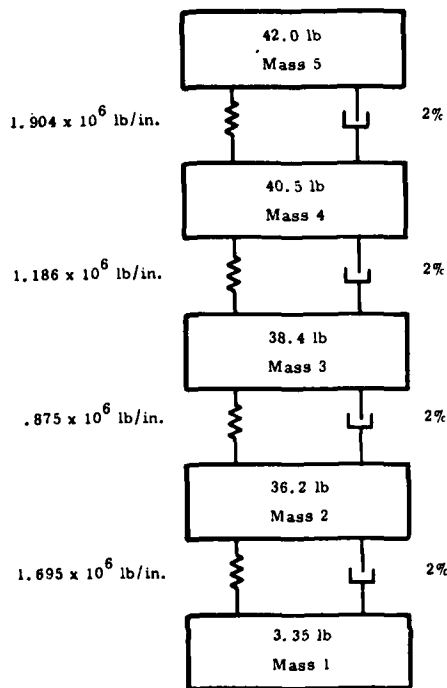


Fig. 5 - Five-mass system

The magnitudes of the required transfer functions H_{ij} are shown in Fig. 6 where i is the input mass and j is the response mass.

For an input to the system two field records are used (the field records are the separation shocks called events A and B generated on two flights during stage separation of a

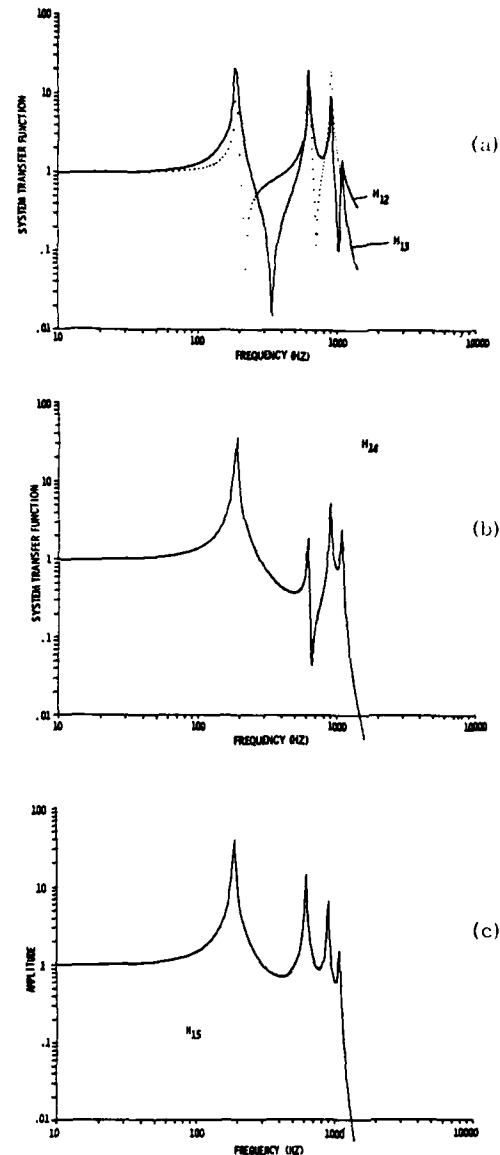


Fig. 6 - Frequency transfer functions for the five-mass system

missile system). The time histories of these events are shown in Fig. 7. The Fourier spectrum and the shock spectrum of the events are shown in Figs. 8 and 9. The shock spectrum of a terminal peak sawtooth is included for later use. The Fourier spectra were enveloped with two envelopes. The first is the exact envelope of the events A and B. The second will be referred to as envelope C and is shown on Fig. 8. If a more conservative

envelope is desired the responses can be predicted, as the response is proportional to the magnitude of the envelope as long as the shape of the envelope is not changed. To illustrate the type of responses expected the responses of mass 5 to the events A and B (the field records) are shown in Fig. 10.

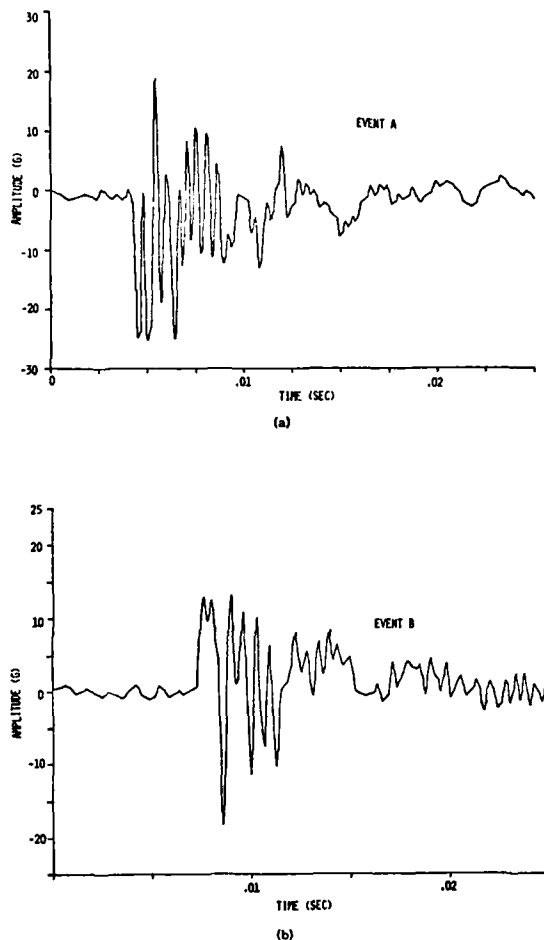


Fig. 7 Time history of events A and B

The worst-case response of mass 5 to an input of envelope C is shown as Fig. 11. The results are summarized as Fig. 12. The peak response for each mass is plotted for the various inputs described on the figure. The response to the sawtooth is included as a comparison with the shock spectrum approach. Curve G is an oscillatory type pulse which matches the shock spectrum envelope of events

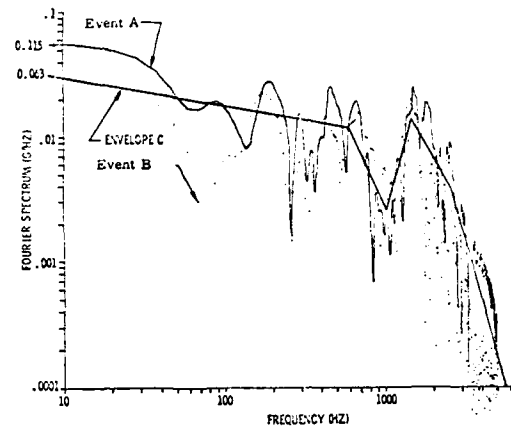


Fig. 8 - Fourier spectra of events A and B

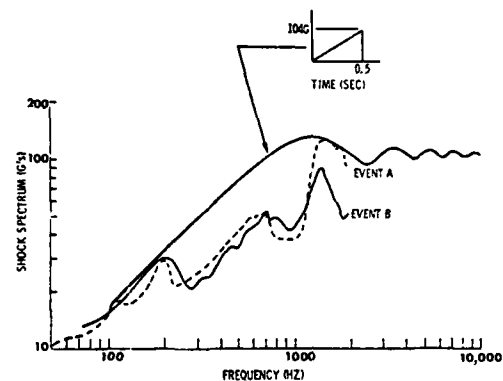


Fig. 9 - Shock spectra of events A and B

A and B [8]. The usual procedure for shock spectrum testing is to envelope the shock spectrum with the spectrum of a test pulse. The test pulse is then used to test the system. From Fig. 10 it can be seen that the spectrum of the sawtooth does a credible job enveloping the spectra of the events A and B at the high and low ends of the spectrum. The sawtooth overtests the mid-frequencies. Figures 13 and 14 shows that the SHOC pulse matches the spectrum quite well. It is recognized that for multiple degree of freedom systems the shock spectrum technique should be applied with caution. As can be seen the worst-case responses are about a factor of two above the field responses. The responses of the various masses to the least favorable input for mass 5 generally lie between the least favorable response and the field responses. This is encouraging as it shows system insensitivity to the location of the worst-case reference points for establishing the transfer function $H(\omega)$.

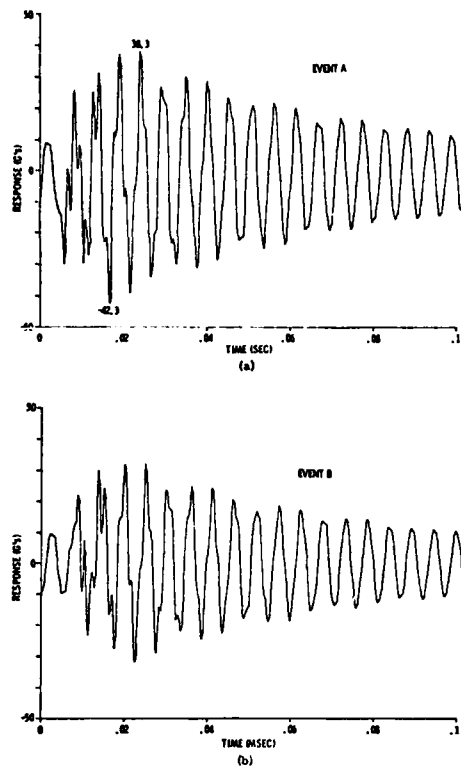


Fig. 10 - Mass-five response to events A and B

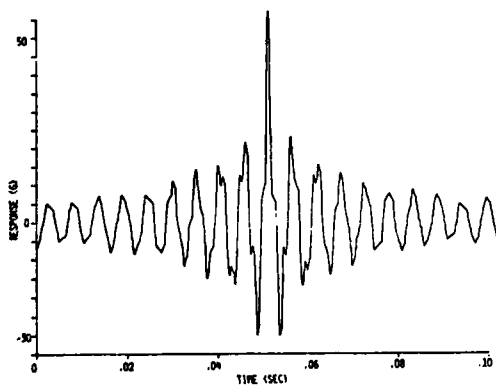


Fig. 11 - Mass-five worst-case response to envelope C

FIELD RESPONSES
 A - RESPONSE TO FIELD PULSE A
 B - RESPONSE TO FIELD PULSE B
WORST CASE RESPONSES
 C - W.C.R. TO ENVELOPE OF A & B
 D - RESPONSE TO THE W.C. INPUT FOR MASS 5 (ENVELOPE OF A & B)
 E - RESPONSE TO THE W.C. INPUT FOR MASS 5 (ENVELOPE C)
SHOCK SPECTRUM SIMULATION
 F - RESPONSE TO A 10G 0.5 MSEC TERMINAL PEAK SAWTOOTH
 G - "SHOC" PULSE

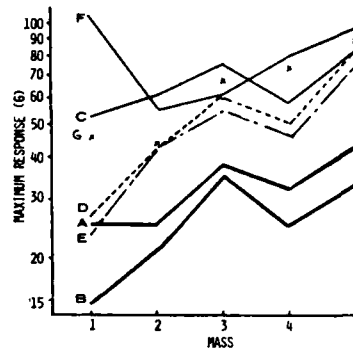


Fig. 12 - Summary of five-mass system response to events A, B, and related pulses

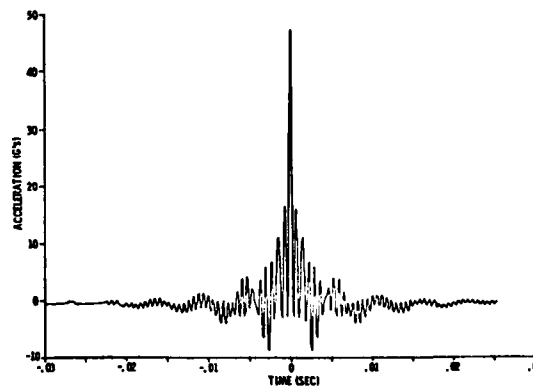


Fig. 13 - SHOC pulse time history

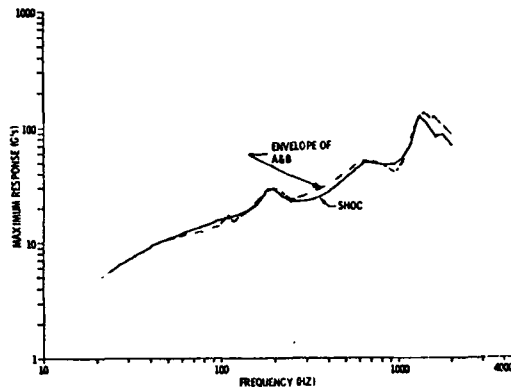


Fig. 14 - SHOC pulse shock spectrum

As Fig. 12 illustrates, even when the least favorable input is based on the response of mass 5 the response of the remaining masses tends to be higher than the typical field data. In any event the least favorable response can be predicted and the responses of masses can be compared with the least favorable result to establish the need for further testing. The figure also shows that the least favorable input is not an unreasonable test as the responses are only a factor of two above the field responses. In fact on the basis of many examples the ratio of the least favorable response to field response will usually be in the range from 1.1 to 2.5 with ratios over 2 relatively rare. The relatively minor differences between curves D and E illustrate that the technique is not sensitive to minor changes in the envelope. It also indicates that good results can be obtained even if some of the peaks of the Fourier spectrum are not enveloped. This topic was discussed earlier.

The shock spectrum approach is seen to produce an overtest on mass 1 while testing to acceptable levels on masses 3, 4, and 5.

For a second example the same field events are used except that the frequency content is lowered by an order of magnitude. That is, the event time history is the same except the time axis has been changed from 0 to 0.025 second to 0 to 0.25 second. An equivalent example would be to keep the field records the same and raise the natural frequencies of the spring mass model an order of magnitude. These events will be referred to as A* and B*. The results are summarized as Fig. 15. Again it is seen that the least favorable responses have roughly the same shape as the field responses. The differences between the least favorable responses and the

responses to the least favorable input for mass 5 are even less than before. This is because the transfer functions (H_{ij}) vary less than before in the frequency range where most of the pulse energy is located. Again the ratio of the least favorable response to the maximum field responses is generally less than 2.

- A - RESPONSE TO PULSE A*
- B - RESPONSE TO PULSE B*
- C - WORST CASE RESPONSE (ENVELOPE A* & B*)
- D - RESPONSE TO THE WORST CASE INPUT TO MASS 5
- E - RESPONSE TO A 105g 5 msec TERMINAL PEAK SAWTOOTH
- F - 'SHOC' PULSE

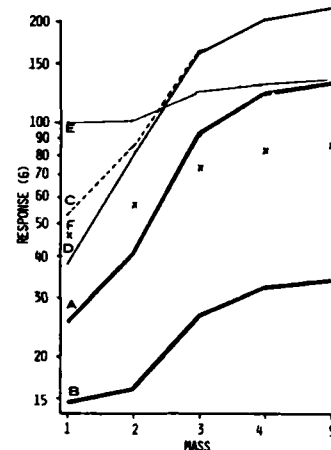


Fig. 15 - Summary of five-mass system response to events A*, B*, and related pulses

It is seen that the shock spectrum technique using the SHOC pulse produces an overtest on mass 1 and an undertest on masses 3, 4, and 5. The sawtooth produces an acceptable test due to the excess energy in the mid-frequencies. Figure 15 also illustrates the danger in reproducing a field event as a test. Events A* and B* have very similar time histories, Fourier spectra, and shock spectra. However, if event B* were used as a test event the system would be seriously undertested.

IMPLEMENTATION OF THE LEAST FAVORABLE TEST TECHNIQUE

A proposed method for implementation of the formulation by Shinozuka will be briefly discussed. The other techniques of Drenich and Smallwood [3, 7], discussed in the Basic Theory section, could be implemented in a similar fashion.

The proposed implementation technique is a modification of a transient waveform reproduction technique discussed in Ref. 2. A block diagram of the technique is shown in Fig. 16. Briefly, the test item would be mounted on an input device (here assumed to be an electrodynamic or electrohydraulic shaker). A low level calibration pulse would then be applied to the system. The calibration pulse could be any transient with energy at all the frequencies of interest. Shown in Fig. 16 is a fast sine sweep (typically a log sweep from 5 to 2000 Hz in 100 msec). Another suggested calibration pulse would be a burst of pseudo-random noise (the sum of many sinusoids with equal amplitude and random phase).

The Fourier transform of the calibration pulse, the observed mechanical input, and the structural response would then be computed.

From this information the required frequency transfer functions could be computed. The frequency transfer functions combined with the stored function $X_e(\omega)$ could be used to compute the electrical input which will produce the desired least favorable response. This input would then be used for the test while observing the actual test mechanical input and structural response.

The technique was tested using a cantilever beam to simulate a test specimen. The transfer function $|H_{IR}|$ of the system is shown in Fig. 17. The predicted least favorable response and the actual response for $X_e(\omega)$ envelope C (Fig. 8) are shown in Figs. 18 and 19.

CONCLUSIONS

It has been shown that the least favorable response approach to transient vibration testing is a practical technique. No important advances in the state of the art need to be made to implement the technique. The technique offers many advantages including:

1. A single degree of freedom system is not assumed. The actual dynamic behavior of the test item is considered.
2. The technique will produce a conservative test. However, the results are not usually overly conservative.
3. The response can be predicted for comparison with the test results for judgments concerning the acceptability of a particular test.

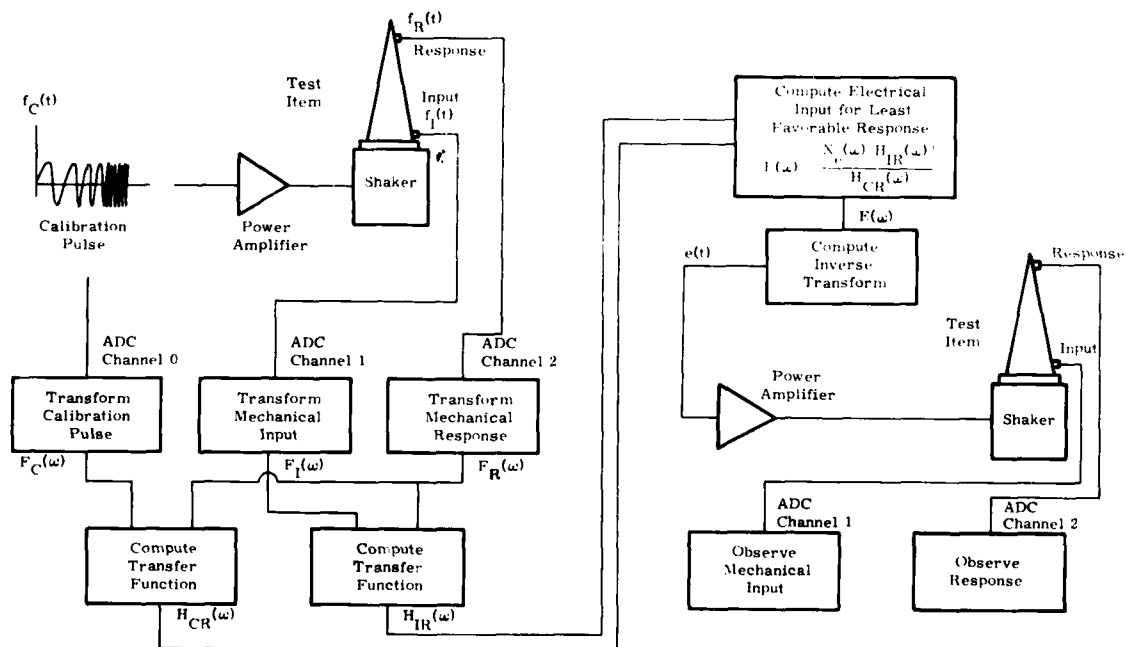


Fig. 16 - Implementation of the least favorable response test technique

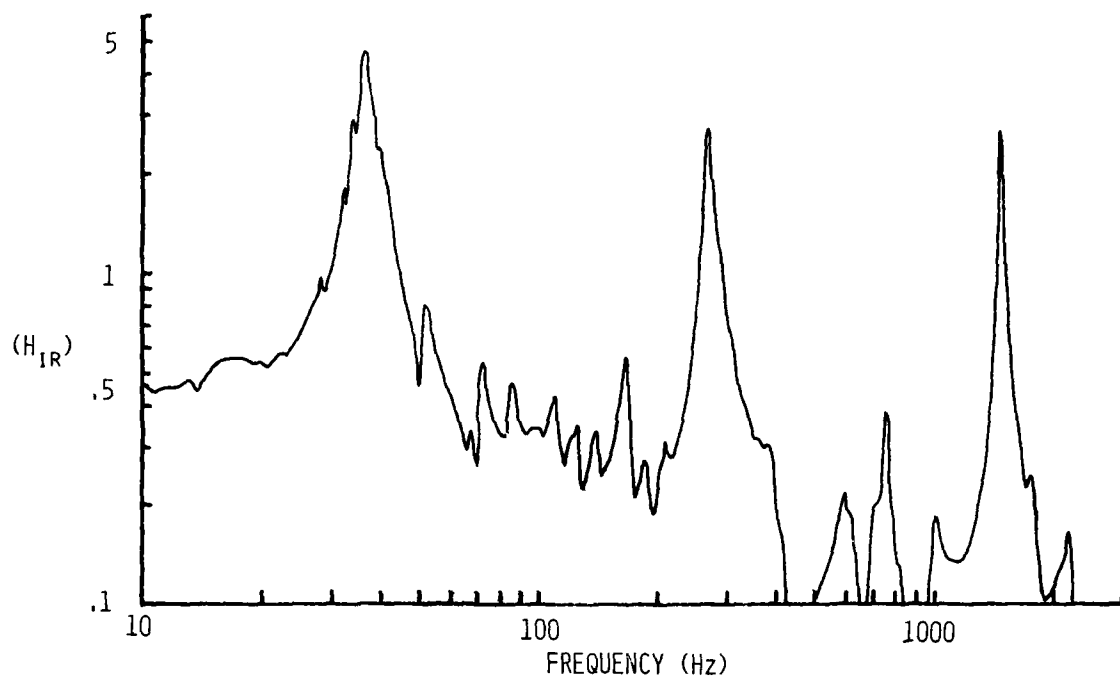


Fig. 17 - Test specimen transfer function

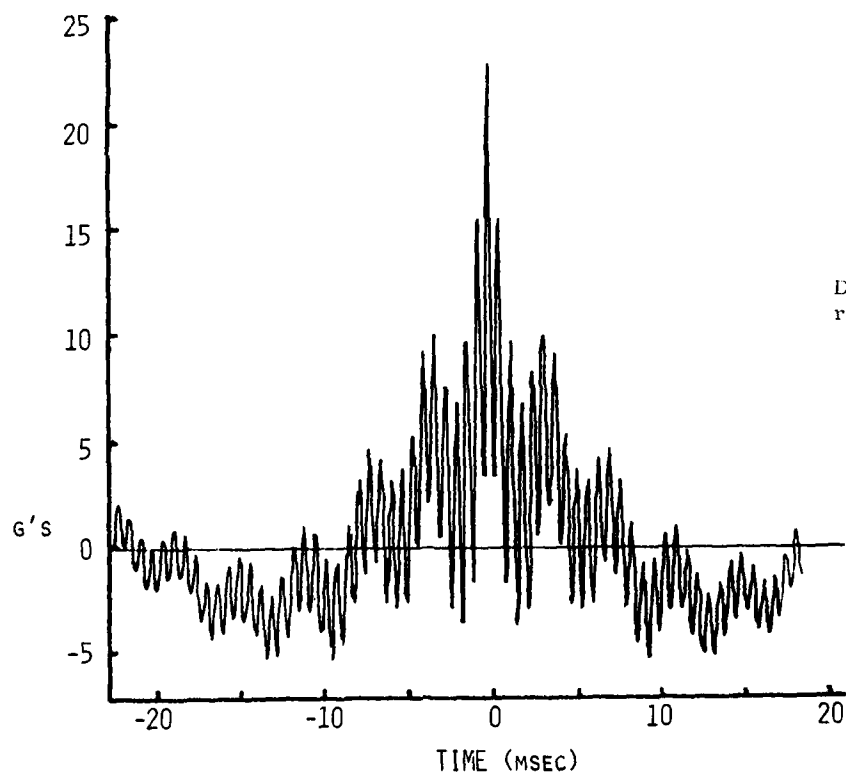


Fig. 18
Desired least favorable
response

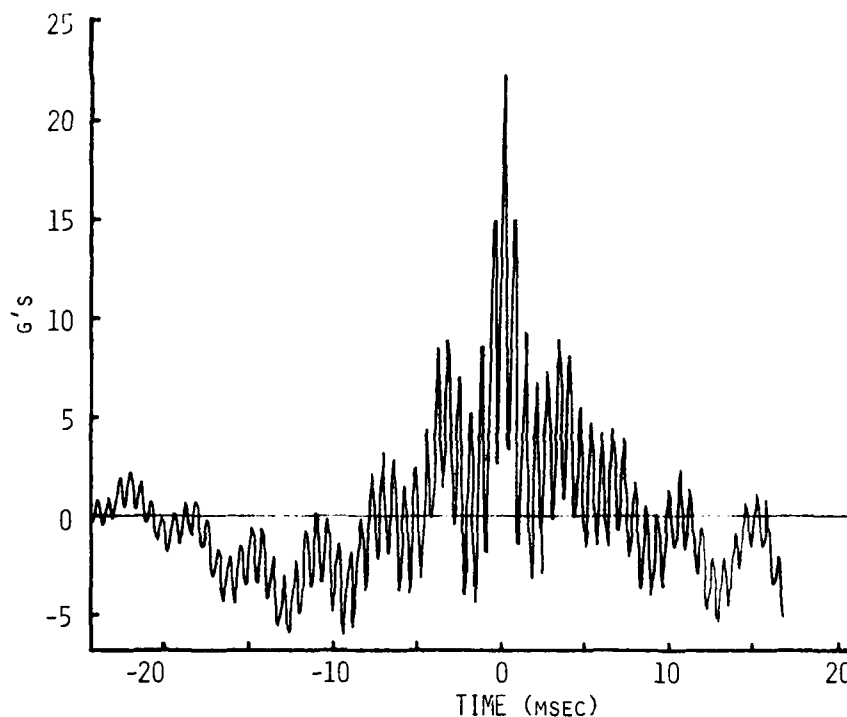


Fig. 19
Actual specimen
response

4. The technique can be applied to generate a single test to simulate several environments.

The disadvantages include:

1. A greater burden is placed on the personnel responsible for specifying the test. Not only must the Fourier spectrum of the input be specified, but the point or points on the structure from which the least favorable input will be generated must be specified.
2. A knowledge of the Fourier spectrum of the environment is required. However, this knowledge can range from excellent to an estimation of the area under the curve; the less that is known the more conservative the resulting test.
3. The technique requires advanced testing equipment.
4. At the present the technique can only be applied on electrodynamic or hydraulic shaker systems, and the limitations of these systems must be considered.

REFERENCES

1. John V. Otts and Norman F. Hunter, "Shock Reproduction on Shakers," Proceedings of the 1969 Instrument Society of America Annual Conference.
2. Jay M. LeBrun and John Favour, "Feasibility and Conceptual Design Study—Vibration Generator Transient Waveform Control System," Final Report prepared for NASA June 1969, Contract NAS5-15171, Goddard Space Flight Center, Greenbelt, Maryland, by Aerospace Group, The Boeing Company, Kent, Washington. This report also released as Boeing document D2-114438-1.
3. Rudolf F. Drenich, "Model-Free Design of Aseismic Structures," Journal of the Engineering Mechanics Division, Proceedings of the American Society of Civil Engineers, pp 483-493, August 1970.
4. Masonobu Shinozuka, "Maximum Structural Response to Seismic Excitations," Journal of the Engineering Mechanics Division, Proceedings of the American Society of Civil Engineers, pp 729-738, October 1970.

REFERENCES (cont)

5. Masanobu Shinozuka, "On the Maximum Dynamic Response of Structures," Space Programs Summary 37-61, Vol. III, Jet Propulsion Laboratory, California Institute of Technology, Pasadena, California, February 1970.
6. D. O. Smallwood, "A Transient Vibration Test Technique Using Least Favorable Responses," SC-DR-71 0897, Sandia Laboratories, Albuquerque, New Mexico, February 1972.
7. D. O. Smallwood, "An Extension of a Transient Vibration Technique Using Least Favorable Responses," SC-RR-72 0735, Sandia Laboratories, Albuquerque, New Mexico, November 1972.
8. D. O. Smallwood and A. F. Witte, "The Use of Shaker Optimized Periodic Transients in Matching Shock Spectra," SC-RR-71 0911, Sandia Laboratories, Albuquerque, New Mexico, February 1972. Also to be published in Shock and Vibration Bulletin No. 43.

DISCUSSION

Mr. Gaberson (Naval Civil Engineering Laboratory): What is the envelope of a Fourier Spectrum?

Mr. Smallwood: The Fourier Spectrum is strictly speaking a complex quantity. All I am doing is calculating the magnitude of the Fourier Spectrum and forming an envelope. It is just like you form envelopes of power spectral densities for random vibration testing.

Mr. Gaberson: We plot a lot of Fourier transforms and we plot all amplitudes. Would you call the graph of the amplitudes versus the frequency the envelope?

Mr. Smallwood: Generally the envelope would be a smooth function. Usually the magnitude of the Fourier Spectrum is a very ragged function. By speaking of an envelope, I'm simply saying that you smooth this out by drawing some straight lines over the peaks. Your conservatism in drawing this envelope will influence the conservatism of your test.

Mr. Gaberson: We have done some tests where clearly during the test there was a heck of a response at a single frequency. When we do the Fourier transform we will see velocity levels at 1000 and 1300 inches per second. If you put an envelope on that and tried to test to 1000, you couldn't on an electrohydraulic or electrodynamic shaker. What would you do if you did a Fourier transform of a pulse and you saw 1400 inches per second?

Mr. Smallwood: We wouldn't be able to reproduce it using this technique, because we have to stay within the limitations of the electrohydraulic or electrodynamic shaker systems.

Mr. Gertel (Kinetic Systems): I find it very difficult to believe that enveloping Fourier spectra will only introduce a small degree of conservatism. I have a very strong feeling that such enveloping, if enough data are enveloped, will lead to considerable overtesting in some instances. You are inevitably apt to wind with the antiresonant type of situation where one component or other is going to catch a very difficult environmental ride by the test trying to force it up to a level that wouldn't exist in the real environment.

Mr. Smallwood: I agree with you wholeheartedly. In fact I discussed this business of how you form the envelope more fully in the written version of the paper where I suggest that perhaps you would not want to envelope all the peaks. Perhaps you would want to draw a mean envelope so that you are not trying to envelope either the peaks or the minimums. This might perhaps be a more realistic envelope.